CIVIL ENGINEERING STUDIES
Illinois Center for Transportation Series No. 15-017
UILU-ENG-2015-2023
ISSN: 0197-9191

Testing Protocols to Ensure Performance of High Asphalt Binder Replacement Mixes Using RAP and RAS

Prepared By
Imad L. Al-Qadi, Hasan Ozer, John Lambros
Ahmad El Khatib, Punit Singhvi, Tamim Khan,
José Rivera-Perez, and Berangere Doll
University of Illinois at Urbana-Champaign

Research Report No. FHWA-ICT-15-017

A report of the findings of

ICT Project R27-128

Testing Protocols to Ensure Performance of High Asphalt Binder Replacement Mixes Using RAP and RAS

Illinois Center for Transportation

December 2015

Technical Documentation Page

1. Report No.	2. Government Accession No.	3. Recipient's Catalog No.
FHWA-ICT-15-017		

4. Title and Subtitle	5. Report Date
Testing Protocols to Ensure Performance of High Asphalt Binder Replacement Mixes Using RAP and RAS	December 2015
	6. Performing Organization Code

7. Author(s)	8. Performing Organization Report No.
Imad Al-Qadi, Hasan Ozer, John Lambros, Ahmad El Khatib, Punit Singhvi, Tamim Khan, José Rivera, Berangere Doll	ICT-15-017 UILU-ENG-2015-2023

9. Performing Organization Name and Address	10. Work Unit No. (TRAIS)
Illinois Center for Transportation Department of Civil and Environmental Engineering University of Illinois at Urbana-Champaign 205 N. Mathews Ave. Urbana, IL 61801	11. Contract or Grant No. R27-128

12. Sponsoring Agency Name and Address	13. Type of Report and Period Covered
Illinois Department of Transportation (SPR) Bureau of Materials and Physical Research 120 E. Ash St. Springfield, IL 62704	Final Report, 1/1/13–12/31/15
	14. Sponsoring Agency Code FHWA

15. Supplementary Notes

Conducted in cooperation with the U.S. Department of Transportation, Federal Highway Administration.

16. Abstract

The use of reclaimed asphalt pavement (RAP) and recycled asphalt shingles (RAS) in AC mixtures can reduce demand for virgin aggregates and asphalt binder, bringing environmental and economic benefits. However, replacing virgin asphalt binder in asphalt concrete (AC) mixtures poses challenges in terms of mixture volumetrics and low-temperature cracking, fatigue cracking, and other deterioration related to cracking. To counter these effects, softer virgin asphalt binder grades or modifying agents are used to improve production consistency. The purpose of this study was to develop and evaluate protocols, procedures, and specifications for testing engineering properties and performance of AC mixtures with high amounts (up to 60%) of RAP and RAS. The criteria for selection of the test method were (1) statistically significant spread in test outcome, representing a mix's cracking resistance; (2) applicability and seamless implementation; (3) correlation to other independent test methods and engineering intuition; and (4) correlation to field performance. A practical test method, the Illinois modified semi-circular bending test (IL-SCB) was developed that can be readily implemented to quantify AC mixture's cracking potential. In addition, a flexibility index (FI) was introduced to determine cracking resistance in a consistent way. The IL-SCB showed consistent and repeatable trends for changes in AC mix design properties. The developed FI was shown to provide greater separation between AC mixes to capture some of the changes that could not be captured by fracture energy alone. This approach does not enforce any limits on any AC mixture design characteristics, such as RAP and RAS content, or other alternative materials or technologies. Instead, it categorizes AC mixes based on their performance index. Hence, this approach encourages innovation and sustainability at the same time.

17. Key Words	18. Distribution Statement
asphalt binder replacement, asphalt concrete, flexibility index, Illinois modified semi-circular bending test, pavement performance, reclaimed asphalt shingles, recycled asphalt pavement	No restrictions. This document is available to the public through the National Technical Information Service, Springfield, Virginia 22161

19. Security Classif. (of this report)	20. Security Classif. (of this page)	21. No. of Pages	22. Price
Unclassified	Unclassified	80 plus appendices	

Form DOT F 1700.7 (8-72) **Reproduction of completed page authorized**

ACKNOWLEDGMENT, DISCLAIMER, MANUFACTURERS' NAMES

This publication is based on the results of R27-128, Testing Protocols to Ensure Performance of High Asphalt Binder Replacement Mixes Using RAP and RAS. R27-128 was conducted in cooperation with the Illinois Center for Transportation; the Illinois Department of Transportation, Division of Highways; and the U.S. Department of Transportation, Federal Highway Administration.

Contributions of the following Technical Review Panel members are acknowledged:

Matt Mueller (TRP Chair), Illinois Department of Transportation

Kevin Burke, Illinois Asphalt Pavement Association (formerly with the Illinois Department of Transportation)

Abdul Dahhan, Illinois Department of Transportation

Steve Hefel, Illinois Department of Transportation

George Houston, Illinois Department of Transportation

John Lambros, University of Illinois at Urbana-Champaign

Brian Pfeifer, Federal Highway Administration

Bill Pine, Heritage Research Group

Vickie Prill, Illinois Department of Transportation

Jim Trepanier, Illinois Department of Transportation

Mark Vock, Illinois Department of Transportation

Tom Zehr, Illinois Department of Transportation

EXECUTIVE SUMMARY

Replacing virgin materials with recycled materials in the production of asphalt concrete (AC) mixtures has become a common means to reduce construction costs. The most commonly used recycled materials in AC mixtures are reclaimed asphalt pavement (RAP) and recycled asphalt shingles (RAS). The use of RAP and RAS can result in a reduction in the demand for virgin, quarried aggregates and, more importantly, asphalt binder. However, replacing virgin asphalt binder in AC mixtures with aged and stiffer binders poses numerous technical challenges in terms of mixture volumetrics and resistance to thermal (low-temperature) cracking, fatigue cracking, and other types of AC pavement deterioration.

A number of research studies have been conducted nationwide to investigate the effects of RAP and RAS on the performance of AC mixtures. In general, the consensus is that these materials can improve rutting resistance and increase stiffness of AC mixtures for properly designed mixes. However, increasing the stiffness of AC mixtures with RAP and/or RAS results in more brittle mixes, which may accelerate pavement deterioration through cracking and raveling. Therefore, a balanced mix design approach is vital in engineering AC mixtures to ensure sufficient rutting resistance for expected traffic and for the capacity to withstand potential fatigue and thermal cracking from traffic- and environment-related stresses.

The purpose of the current study was to identify, develop, and evaluate protocols, procedures, and specifications for testing engineering properties of AC mixtures with varying amounts of asphalt binder replacement (up to 60%) using RAP and RAS, as well as a number of other AC mixtures with various field performance and mixture volumetrics. One of the major outcomes of this study was the development of a test method and testing protocol that can rank AC mixtures based on their cracking resistance. *The criteria for selection of the test method were as follows: (1) a statistically significant and meaningful spread in test outcome, representing a mix's cracking resistance; (2) repeatability, practicality, low cost, and easy implementation by IDOT districts and contractors; (3) correlation to other independent test methods and engineering intuition; and (4) correlation to field performance.*

To accomplish the objectives of the study, various existing/conventional performance characterization tests were evaluated. The conventional performance tests evaluated included a low-temperature semi-circular bending test, a low temperature disc compact tension test, a Texas overlay test, a push-pull fatigue test, an indirect tensile strength test, and a complex modulus test. Three types of plant mixes with varying percentages of RAP and RAS were used in this part of the study. It was concluded that none of the conventional tests employed in this phase of the project was appropriate to accurately (and consistently) predict and rank an AC mix's cracking resistance with the established test methods' criteria. Therefore, an alternative fracture testing method was developed using the semi-circular bending (SCB) geometry.

The SCB test geometry was selected for further evaluation because of its potential low-cost implementation, ease of specimen preparation and testing, and off-the-shelf equipment availability. The effects of testing conditions that included a wide range of temperature and loading rates were explored *to ensure a high discrimination potential between test results.* As a result, new IL-SCB test procedures sugggested a testing temperature of 25°C (77°F) with a loading head displacement rate of 50 mm/min (2 in/min). The experiments were supported by finite element simulations and digital image correlation technique measurements as a means to understand the mechanisms of damage and to support development of the test method.

The flexibility index (FI) was introduced to capture cracking resistance of mixes in a more robust and consistent way. Derived from the load-displacement curves obtained from the IL-SCB test with parameters of fracture energy and slope at the post-peak inflection point, the FI describes the fundamental fracture processes consistent with the size of the crack tip process zone. It was shown that the FI has the ability to capture the effects caused by various changes in the materials and volumetric design of AC mixes. Plant-produced, laboratory-produced, and field core specimens were used in validating the potential of the IL-SCB test and the FI to predict cracking resistance among mixes. *The effects of increasing the RAP and RAS content were shown with a reduction in the FI demonstrating a more brittle behavior. The FI values varied from 15 to 1 for the best- and poorest-performing laboratory-produced mixtures.*

The IL-SCB test method was validated using two sets of field data. The first dataset was from FHWA's accelerated loading facility (ALF) sections; the second dataset was obtained from random field cores provided by each IDOT district. The ALF sections provided a great opportunity to correlate fracture energy and the FI obtained from the IL-SCB test because the sections were constructed for the sole purpose of evaluating AC mixture design characteristics on fatigue cracking performance, and all sections had similar structural properties. The FI proved to have a very good correlation with the performance rankings based on fatigue cracking measurements and structural analysis predictions for the sections with completed ALF and IL-SCB tests.

The FI and ALF performance measurement classifies the AC mixes into three categories based on performance. The mixes in the poorest-performing category had an FI less than 2, whereas the AC mixes in the best-performing category had an FI value greater than 6. Intermediate-performing mixes were between those FI numbers. The ALF test demonstrated that increasing the recycled content up to 40% ABR levels without adequate binder grade bumping, or introducing excessive amounts of RAS (6%), can have some detrimental effects on fatigue cracking performance. This finding is consistent with the results obtained from the laboratory-produced mixes designed in this study.

In addition, the results from the IL-SCB test method and the FI values obtained for field cores showed good correlation. FI values obtained from the field specimens ranged from approximately 1 to 25. Recently constructed, good-performing sections, with one exception, had FI values greater than 10. Sections with an FI less than 6 were generally the sections that exhibited premature cracking and had been identified as poor performing by the districts.

Finally, an approach to develop a more balanced and performance-related AC mixture design procedure was introduced with the use of two practical laboratory performance characterization tests. The balanced mix design approach consisted of integrating two laboratory performance–level tests to the AC mix design volumetric design process. This approach integrates the Hamburg wheel tracking and IL-SCB test methods to develop combined performance criteria that not only serve as indicators of cracking potential but also of the potential for fatigue and high-temperature rutting. The initial cracking thresholds were proposed based on the IL-SCB tests conducted for varying types of AC mixes and the correlation to field cracking performance. With this method, the combined field performance-related criteria will allow AC mixture designers and contractors to develop AC mixes that have the potential to resist cracking and rutting for various applications under varying traffic or environmental conditions. *This approach does not enforce any limits on any AC mixture design characteristics, such as RAP and RAS content, or other alternative materials or technologies. Instead, it categorizes AC mixes based on their performance index. Hence, this approach encourages innovation and sustainability at the same time.*

CONTENTS

LIST OF FIGURES

LIST OF TABLES

CHAPTER 1: INTRODUCTION

1.1 BACKGROUND

The pursuit of pavement sustainability has focused on recycling previously used materials into new pavements with a subsequent reduction in new mineral aggregates, barrels of oil (asphalt), and filling of landfill space. This has led to a reduction in first cost for asphalt concrete (AC) pavements.

A recent review of recycling practices in Illinois indicates that an average mile of construction in 2013 contained nearly four times more recycled content than an average mile constructed in 2009 (Lippert et al. 2015). For AC, the increased specified allowances of reclaimed asphalt pavements (RAP) in the past few years and the introduction of recycled asphalt shingles (RAS) in 2011 have greatly contributed to the increase in the recycle tonnage used.

Using RAP and RAS to replace virgin asphalt binder and aggregates may result in paving projects that have lower initial costs or life-cycle costs. However, true overall savings hinge upon a pavement's ability to perform equally or better than pavements produced with traditional AC mixes.

Owing to budgetary constraints for transportation projects, the use of increasing amounts of recycled materials content is promoted because of the initial cost savings—in spite of the uncertainty about long-term performance of such pavements. To reduce those risks, the use of RAP and RAS has commonly been controlled by specifications that limit the amount of recycled materials in pavements. The resulting typical specification limits the use of recycled materials, especially the asphalt binder replacement (ABR), thus reducing the risk of performance problems. ABR refers to asphalt binder replaced with recycled binder, usually expressed as a percentage, and assumes 100% contribution of asphalt binder in RAP and RAS. On the other hand, improved specification methods such as performance-based specifications could allow contractors to use a number of recycled material combinations, while employing new methods and modifiers to counteract the introduction of harder/stiffer asphalt binders from recycled materials. The improved specification methods must be based on sound engineering approaches that would allow optimizing the use of recycled materials while providing desired pavement performance.

The increasing use of recycled materials requires a comprehensive understanding of the effects of recycled content on pavement performance. Generally, mixes prepared with RAP and/or RAS have high-temperature rutting resistance that is equivalent or better than that of well-designed virgin AC mixes. According to the literature findings for AC mix-level laboratory tests, a consensus exists regarding the ability of RAP and RAS to increase rutting resistance and stiffness of AC. However, thermal (low-temperature) cracking and intermediate-temperature fatigue cracking resistance of AC with high ABR achieved by adding RAP and/or RAS into the AC could be compromised.

With the introduction a few years ago of a rutting performance test for AC acceptance, cracking of AC pavements is now driving the Illinois Department of Transportation's (IDOT) rehabilitation cycle. With existing pavement structures continuing to deteriorate and the occasional cold spikes in winter temperatures (–27°C [–16.6°F] in January 2014), fatigue, reflective, and thermal cracking resistance of AC are of paramount concern. Changing the material sources, especially stemming from the desire to be more sustainable, could increase the uncertainty in the value of historical performance, thereby hindering the accurate estimation of future pavement life cycles.

Therefore, a distinct need exists for a comprehensive study to assess the impact of high RAP and/or RAS contents on critical AC performance criteria, such as thermal and fatigue cracking. In addition, a practical test suite and proven procedures are needed for screening AC prepared with increased amounts of RAP and/or RAS to ensure that performance expectations are met.

1.2 CURRENT STATUS OF RECYCLING EFFORTS IN THE U.S. AND ILLINOIS

Recent nationwide statistics indicate that the amount of RAP used in AC was about 70 million tons in 2013 (according to a NAPA survey of U.S. asphalt producers) which is approximately 10% of the total AC produced in the U.S. At the same time, approximately 11 million tons of roof shingles are disposed of in U.S. landfills every year (Goh and You 2011). According to recent statistics, approximately 1.6 million tons of shingles are used in pavements (Hansen and Copeland 2014).

In Illinois, reclaimed and recycled materials, totaling 1,643,948 tons, were used in highway construction. The recycled materials include slags used as aggregate, crumb rubber, RAP, and RAS. RAP use in AC constitutes a significant portion, with approximately 0.782 million tons. Other materials, such as RAS, have a much shorter history of use in paving practices in Illinois until recently. The State of Illinois desires to move forward with implementation of more sustainable pavements, including the use of recycled and reclaimed products, provided that the durability of AC mixes is not jeopardized.

1.3 CHALLENGES AND ISSUES

The challenges with the inclusion of RAP and RAS in AC stem from the fact that these materials contain binder that is harder and staffer than the prescribed performance grade. Unknown degrees of blending of recycled binder with virgin binder is another challenge that may affect final volumetrics and performance characteristics of AC. Difficulties in achieving desired mix volumetrics in the laboratory and in the field with recycled materials have prevented state highway agencies from increasing the amount of recycled material in AC. Despite the initial economic advantages of adding RAS due to high percentages of asphalt binder (18%–35%), a new set of challenges is posed to mix designers. The variability in the type, composition (organic fibers vs. fiberglass fibers), and processing of RAS material; presence of deleterious material such as wood, plywood, nails, and tar paper; high amount of mineral filler; and very stiff binder are a few of the challenges linked to introducing RAS in AC.

Numerous studies on laboratory performance of AC with RAP have reported changes in the physical behavior of AC. An increase in the complex moduli, decrease in rutting potential, and increase in low-temperature cracking potential are some of the commonly observed effects described in the literature (Al-Qadi et al. 2009, 2012; Daniel and Lachance 2005; Shah et al. 2007; Li et al. 2008; Stroup-Gardiner and Wagner 1999). The stiffness of AC with RAS was likewise shown to increase and could result in higher rut resistance although thermal and fatigue cracking resistance was decreasing (Stroup-Gardiner and Wagner 1999). Those studies, discussed in detail in Chapter 2 of this report, exhibit some inconsistencies and variability, especially in cracking resistance of AC containing high recycled content. In addition, these studies were often conducted as part of complex experimental programs such as fatigue and modulus tests requiring advanced test equipment that cannot be streamlined for widespread implementation.

Therefore, there is a gap in the literature to guide the asphalt industry to reliably and cost effectively measure the changes in AC critical performance indicators when using recycled and reclaimed

materials. This project addresses those challenges and develops a testing protocol to be used as part of the mix design acceptance specifications and production testing.

1.4 OBJECTIVES AND RESEARCH SCOPE

The purpose of this study was to identify/develop and evaluate protocols, procedures, and specifications for testing the engineering properties of AC with high amounts of asphalt binder replacement from RAP and/or RAS and a number of other mixtures with varying field performance and mixture volumetrics. This study aimed to develop a practical and cost-effective cracking test method that can be readily implemented by IDOT districts, consulting laboratories, and contractors.

In addition, the study addresses the following research and practical concerns and questions regarding the use of RAP and RAS in AC:

- How do RAP and RAS in combination or alone affect the critical performance indicators such as modulus, cracking, and rut resistance?
- How does source variability affect these critical performance indicators?
- How is cracking resistance affected by the addition of RAS alone and RAS and RAP together?
- How does cracking resistance of AC vary with temperature and testing rate, and what are the underlying fundamental fracture mechanisms?
- Are there any test method(s) that can reliably distinguish overall cracking performance with changes in mix design characteristics?

To achieve these goals, an experimental program was designed for a variety of plant and laboratory mixes and field cores with distinct mix design characteristics. The scope of the experimental program included characterization of AC with varying percentages of RAP and RAS. Experimental AC characterization included modulus, fatigue, fracture, and rutting resistance determination. The study then focused on developing a test method to distinguish the overall cracking resistance of AC.

1.5 REPORT ORGANIZATION

The scope of the research study included AC laboratory testing of plant- and laboratory-mixed AC prepared in the laboratory along with pavement field cores. The outcome of the experimental procedures, as well the field correlation of the results, are presented in this report. A flexibility index (FI) is introduced to characterize the cracking behavior of the ACs. Chapters are organized as follows:

Chapter 2 presents a summary of the literature on the tests used to characterize the behavior of ACs. Several of these tests were performed during this project.

Chapter 3 introduces materials, experimental methods, and the program followed during this study. Results from the standard-performance characterization tests are also introduced in this chapter.

Chapter 4 discusses the development of the Illinois semi-circle bending (IL-SCB) fracture test that can be used to identify ACs' cracking resistance. Fundamental fracture mechanisms, and temperature and rate dependency of AC are discussed relative to optimizing the testing conditions of the IL-SCB test method.

Chapter 5 introduces the flexibility index (FI) to characterize the ACs based on fracture energy and shape of load vs. displacement curve during crack propagation (using the IL-SCB test).

Chapter 6 discusses the validation approach and results of the use of the IL-SCB and FI. Field cores and performance information obtained for all IDOT districts, along with accelerated pavement testing results, are used to validate the method and develop thresholds.

Chapter 7 introduces the balanced mix design to optimize the overall performance of mixes, considering volumetrics along with resistance to rutting and cracking. The concept of interaction plots combining the two acceptance tests is presented combining the Hamburg wheel tracking test for rutting performance and IL-SCB for overall damage related to cracking.

Chapter 8 summarizes the main conclusions and recommendations of this study.

CHAPTER 2: SUMMARY OF LITERATURE ON PERFORMANCE CHARACTERIZATION OF ASPHALT MIXTURES WITH RECYCLED CONTENT

This chapter summarizes and discusses the literature compiled from other studies conducted to characterize laboratory performance of AC with recycled materials. This chapter presents the conventional test methods used in characterizing AC that are commonly used for evaluating the effect of RAP and RAS and discusses significant outcomes and changes in AC performance when RAP and/or RAS was added.

2.1 MODULUS AND STIFFNESS

Complex modulus, a primary input in the *Mechanistic Empirical Pavement Design Guide* (MEPDG), is increasingly recommended for comprehensive characterization of AC because of its effectiveness in comparing different mixtures (Witczak et al. 2002; Bonaquist et al. 2003; Carpenter 2007; Vavrik et al. 2008; Ye et al. 2009; Braham et al. 2011; Ozer et al. 2012).

The complex modulus test is conducted in accordance with AASHTO TP62-03. Specimens are tested at temperature and frequency sweeps under stress-controlled loading. Testing is conducted on cylindrical specimens of 100-mm (3.94-in) diameter (cored from a 150-mm [5.91-in] diameter cylinder) and 150 mm (5.91-in) height. Microstrain values are limited between 50 to 150 microstrains. Measured strains are collected using strain gauges placed around the specimen's circumference. Testing is conducted at temperatures of –10°C (14°F), 4°C (39°F), 21°C (70°F), 37°C (99°F), and 55°C (131°F) and at frequencies of 25, 10, 5, 1, 0.5, and 0.1 Hz. Obtained modulus values are used to produce a complex modulus master curve.

Research shows that the addition of RAS and RAP significantly impacts the complex modulus of asphalt materials. Ozer et al. (2012) evaluated plant AC with varying amounts of RAP and RAS and found that modulus increases with increasing RAS content at high testing temperatures and low frequencies. AC with high RAS content also exhibited flatter master curve slopes, an indication of deteriorating relaxation properties resulting in mixes with greater risk of cracking.

Additional research conducted by Swamy et al. (2011) and Al-Qadi et al. (2012) showed that the addition of RAP to AC increases complex modulus values. Asphalt concrete with varying amounts of RAP from 0% to 50% were tested, and AC with high RAP showed higher complex modulus, indicating the presence of aged asphalt binder.

2.2 PERMANENT DEFORMATION

Two primary performance characterization tests are used to indicate a mixture's susceptibility to permanent deformation or rutting: the Hamburg wheel tracking test (WTT) (AASHTO T324) and the uniaxial flow test (AASHTO TP 79). Loading in both test setups is intended to simulate permanent deformation accumulation as a result of cyclic loading (Figure 2.1).

The WTT is conducted by repeatedly applying a steel wheel in a linear path over asphalt specimens. The steel wheel is 203.2 mm (8.0 in) in diameter, 47.0 mm (1.85 in) wide, and applies a load of 705.0 ± 4.5 N (158.0 ± 1.0 lb). Wheel speed is 0.305 m/s (1 ft/sec), and the specimens experience 52 ± 2 passes/min. Thinner specimens are fixed with gypsum into molds and tested in a water bath at a temperature of 50°C (122°F) in accordance with AASHTO T324-11.

Al-Qadi et al. (2012) showed, through testing a variety of N90 AC with RAP between 0% and 50% under the WTT, that the addition of RAP increases resistance to rutting. Similar results were reported by Xiao et al. (2007) for rubberized AC with RAP under a loaded wheel tester. Similarly, the use of RAS in asphalt mixtures was shown to improve the mixture's resistance to rutting or permanent deformation at intermediate and higher pavement temperatures (Goh and You 2011 and Mogawer et al. 2011).

The uniaxial flow test is run on a cylindrical AC specimen 100 mm (3.94 in) in diameter (cored from a 150-mm [5.91-in] diameter cylinder) and is 150 mm (5.91 in) high. Haversine loading is applied for 0.1 sec, and the specimen is allowed to rest for 0.9 sec. Strain is measured at the end of every rest period by measuring axial deformation from attached strain gauges. The flow number, the primary parameter of interest in this test, is considered to be the minimum rate of change in the axial strain for the duration of the test.

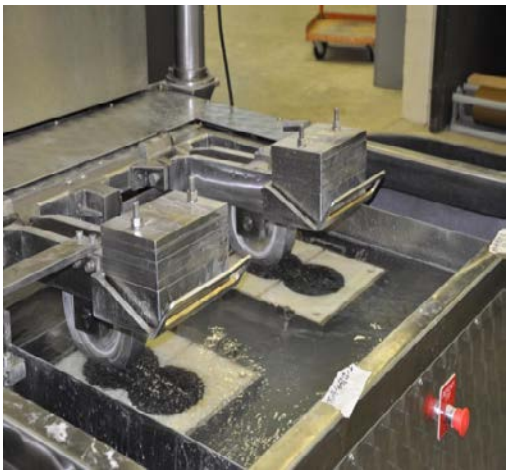

Figure 2.1 Laboratory tests used in AC rutting evaluation. Hamburg wheel tracker (left) and flow number test (right)

Apeagyei et al. (2011) tested AC with varying amounts of RAP under the flow test setup. Mixtures tested were designed with 0% to 25% RAP. Researchers found that the addition of RAP to AC decreased the rutting resistance. However, this finding may have been the result of binder grade bumping in AC with higher RAP content. Williams (2010) prepared and placed in the field various mixtures of varying levels of both RAP and RAS. Laboratory data and field performance were collected and showed that higher amounts of recycled (RAP and RAS) content would potentially decrease rutting.

2.3 FATIGUE CRACKING

Fatigue cracking is a primary concern with the use of recycled content in AC. It is presumed that the addition of recycled content may have adverse impacts on the fatigue performance of AC. This hypothesis suggests that high stiffness and poor relaxation properties of mixes with RAP and/or RAS caused by stiff oxidized binder and a deficiency of virgin binder can cause faster crack initiation and propagation.

The Texas overlay test (TOL) is a fatigue test intended to indicate the reflective cracking potential of AC, as shown in Figure 2.2a. Developed by Robert Lytton in the 1970s, this test simulates the opening and closing of joints or cracks to determine crack initiation and propagation potential (Zhou and Scullion 2005). Specimens are subjected to displacement-controlled cyclic loading at 25°C (77°F) with an opening displacement of 0.635 mm (0.025 in) at a loading frequency of 1 Hz. The primary parameter of interest is the number of cycles to failure.

The push-pull test has also been used to characterize fatigue cracking resistance of various materials. Developed by Richard Kim and coworkers at North Carolina State University, the test loads specimens (same geometry as those for complex modulus test) in cyclic tension and compression (Kim et al. 1997; Underwood et al. 2012). Testing is conducted at 21°C (70°F). A specimen is fixed to steel plates at the top and bottom as shown in Figure 2.2b. Loading is applied at a frequency of 10 Hz. Strain levels are varied from 200 to 300 microstrains. Three axial linear variable differential transformers (LVDTs) are located 120° apart around the radius of the specimen. Various criteria such as a 50% reduction in modulus have been used to determine specimen failure. Crack initiation is desired toward the midway point of specimen height. The primary parameter of interest is number of cycles experienced until failure.

McDaniel et al. (2012) tested mixtures of 0%, 15%, 25%, and 40% RAP under the push-pull configuration and obtained results contrary to their expectations. It was shown that 40% RAP mixes exhibited higher fatigue resistance followed by control mix. The mixes with 15% and 25% RAP had similar fatigue lives. Binder grade changes did not result in consistent changes in the fatigue live. In contrast, Ozer et al. (2012) tested AC with RAS content varying from 2.5% to 7% under the same push-pull setup and concluded that the addition of RAS significantly decreases the mixture fatigue life. Slight improvement in the fatigue life of those mixtures was observed when using a softer asphalt binder grade as opposed to a stiffer asphalt binder grade in the mixture with high levels of recycled content.

The flexural beam fatigue test is a four-point bending test to simulate the fatigue performance of asphalt pavements under repeated traffic loading. A rectangular asphalt specimen with a dimension of 15 x 2 x 2.5 mm (380 x 50 x 63 in), clamped at four points along its length, is subjected to repeated loading at a loading frequency of 0.1 to 10 Hz at a fixed strain level, as shown in Figure 2.2c. Primary parameters of interest are number of cycles to failure (which usually occurs at the middle of the beam), dissipated energy resulting from mechanical loading, and damage accumulation.

Aurangzeb et al. (2014) and Al-Qadi et al. (2012) concluded that the addition of RAP to mixtures slightly improved fatigue life when tested under the flexural beam fatigue setup. Mixtures tested ranged from 0% to 50% RAP content. The same trend was observed by Tabaković et al. (2010) when testing mixtures with RAP content ranging from 10% to 30%. However, Xiao et al. (2013) and Williams et al. (2011) tested mixtures with varying amounts of recycled content and could not discern an obvious trend in fatigue life with the increase of recycled content.

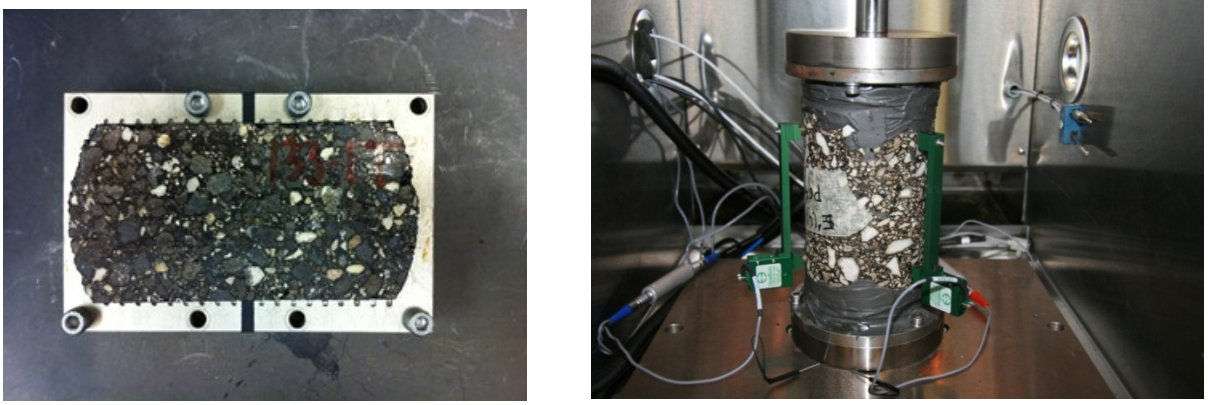

(a) (b)

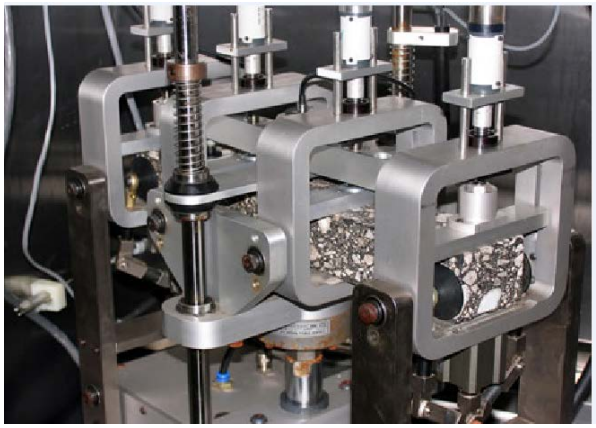

(c)

Figure 2.2 Fatigue test setups commonly used in fatigue performance evaluation of AC: (a) Texas overlay test specimen (courtesy of Tom Zehr, Illinois Department of Transportation), (b) push-pull test, (c) four-point beam fatigue apparatus

2.4 THERMAL CRACKING

The replacement of virgin binder with oxidized or aged recycled binder is believed to significantly increase the thermal cracking potential of AC. The semi-circular bending beam (SCB) test and the disc compact tension (DCT) test have been commonly used to characterize AC thermal cracking potential (Wagoner et al. 2005; Wagoner 2006).

The classical SCB test method is a three-point bending test typically run at low temperatures (PG lower limit + 10°C). The specimen has a 75-mm (3-in) radius and is 50 mm (2 in) thick. A 1.5-mm (0.06 in) notch is machined in the bottom center of the specimen, extending 15 mm (0.59 in) upward. The primary parameters extracted from this test are the fracture energy (G_f) and peak load. The fracture energy is defined as the amount of energy required to propagate a crack for a unit area and is typically expressed in J/m^2. Displacements are measured through crack mouth opening displacement (CMOD) using a clip-gauge extensometer or an extensometer measuring the load-line displacement. Stable crack growth condition is ensured during the test.

The SCB fixture is illustrated in Figure 2.3. In general, the SCB test is simple, low cost, and can easily be performed on the cylindrical samples (cores prepared in the Superpave gyratory compactor [SGC]

or cores obtained from the field). The test method was recently published in an AASHTO provisional specification (AASHTO TP 105-13). This test method requires a displacement control in two phases after the application of a 0.3 ± 0.02 kN (67.5 ± 4.5 lb) seating load: first, the specimen is loaded to 1 ± 0.1 kN (224.8 ± 22.5 lb) in stroke displacement control at a displacement rate of 0.06 mm/min (0.002 in/min). Second, the test switches to CMOD displacement control and the specimen is loaded at a displacement rate of 0.03 mm/min (0.001 in/min) to failure, which is defined as a drop to 0.5 kN (112 lb) or a specified CMOD opening.

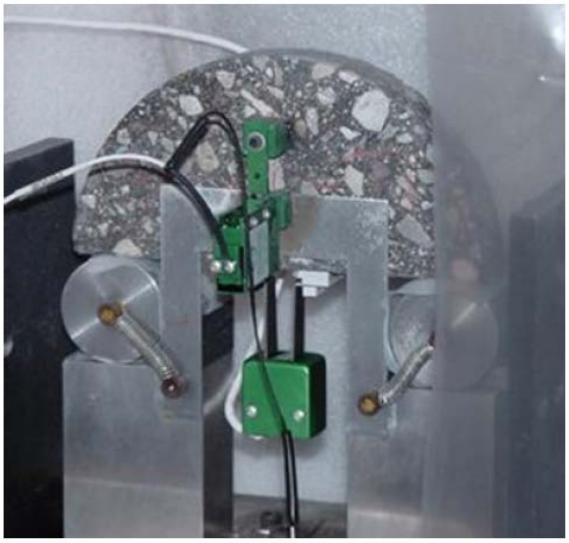

Figure 2.3 Semi-circular bending beam test fixture and typical outcome from this test to calculate fracture energy (Marasteanu et al. 2012).

Research conducted by Li et al. (2008) and Williams (2010), using the SCB test, concluded that fracture energy decreases with an increase in recycled (RAP or RAS) content. However, Williams. (2010) also showed that AC with both RAP and RAS displayed higher fracture energy than AC with only RAS.

Similar to the SCB test, the DCT test is conducted by propagating a crack through a notched specimen under displacement-controlled tensile loading, as shown with a fracture specimen in Figure 2.4. Arms are inserted into dual openings cored into the circular specimen. These openings are pulled apart at a rate of 1.00 mm/min (0.04 in/min) measured through CMOD displacement. Unlike the SCB test, loading is applied in the vertical direction while the crack propagates horizontally into the specimen. Data are collected in the same method as those from the SCB, and the primary parameters of interest are identical (G_f and peak load). Behnia et al. (2011) showed that fracture energy decreases when there is a significant increase in the RAP content.

Figure 2.4 DCT specimen after the completion of a test.

The indirect tensile (IDT) test is also used to characterize fracture properties of AC (Roque et al. 2004). The 150-mm (6-in) diameter gyratory specimens are cut to a thickness of 1 in (25.4 mm). A circular hole with an 8 mm (0.32 in) diameter at the center of the specimen is drilled from which cracks will initiate and propagate. Typical IDT setup requires a servo-hydraulic closed-loop testing machine applying axial compression.

The specimen is typically loaded diametrically in compression, which indirectly induces horizontal tensile stresses in the middle zone of the specimen that ultimately causes cracking. For evaluation of the tensile properties of the AC, the permanent deformation under the loading strip is undesirable (Huang et al. 2005). Therefore, the compressive load is distributed using loading strips, which are curved at the interface to fit the radius of curvature of the specimen. Typical test temperatures range from –20°C (4°F) to 25°C (77°F) (Huang et al. 2005). The data captured during IDT testing include time, applied load, and horizontal and vertical specimen deformation.

McDaniel et al. (2012) tested AC with 0% and 40% RAP content under the IDT test. Even with binder grade bumping to accommodate the additional 40% RAP, they concluded that strength and stiffness increased with the addition of recycled content.

2.5 SUMMARY

A summary is presented for standard and non-standard AC test methods commonly used for characterizing the effects of RAP and/or RAS. Table 2.1 (at the end of this chapter) presents an overview of commonly used performance tests for AC. Literature findings are summarized as follows:

- The use of RAS and/or RAP in AC generally increases the AC resistance to rutting and permanent deformation. In addition, the AC stiffness and complex modulus values increase.
- Fatigue tests, including beam fatigue and push-pull, do not show a consistent trend for AC with high amounts of RAP and/or RAS. This could be the result of inconsistencies in the mix volumetrics and/or testing mode. Stress-controlled or strain-controlled tests tend to yield contradicting results for mixes with varying stiffness.

- SCB and DCT tests are two of the most commonly used AC fracture tests. In general, a slight decrease in fracture energy was noted with increasing ABR. For mixes with increasing ABR, however, this finding cannot be generalized because it was not the case for all of the studies examined in the literature review.
- A set of criteria was formulated for the selection of a suitable cracking test that is consistent with the objectives of the study. Accordingly, the following criteria are considered:
    1. Feasibility and cost effectiveness
    2. Meaningful and significant spread of test results for widely varying mixtures
    3. Correlation to independent tests
    4. Correlation to field performance

An experimental program was developed that included some of the standard-performance tests cited in this chapter.

Table 2.1 Laboratory Cracking Test Methods

Test Type		Purpose	Specimen Dimensions	Specimen Preparation	Test Output	*Pros*/Cons
Semi-circular bending (SCB)		Cracking resistance	6 in (Ø) 3 in (H) 2 in (T)	Notching required = 0.6 in; external LVDTs optional	Fracture energy from load-displacement curve, peak load, critical displacement	*Inexpensive device* *Relatively easy specimen fabrication* *Easily obtained field specimens* *Two specimens per core or slice* *Simple three-point bending load representing field bending* Smaller ligament area
Disc compact tension (DCT)		Cracking resistance	6 in (Ø) 5.7 in (H) 2 in (T)	Notching required = 2.46 in; extensometer required	Fracture energy from load-displacement curve, peak load, critical displacement	*Direct tensile mode* *Easily obtained field specimens* Possible breakage close to loading holes at intermediate-temperature application Moderately expensive device
Texas overlay (TOL)		Cracking (reflective) potential	6 in (L) 3 in (W) 1.5 in (T)	Gluing required; curing time needed; external LVDTs optional	Number of cycles used as measure of crack resistance	*Cyclic loading application* High variability No fundamental property related Moderately expensive device
Direct tension (DT)		Tensile strength, cracking resistance, and ductility potential	4 in (Ø) 4 in (H)	Gluing required; overnight curing time; external LVDTs required	Tensile strain at max load used as indicator of ductility and cracking resistance potential	*Simple stress state* Possibility of load eccentricity because of end fixtures Difficult to obtain field specimens Closed-loop displacement control is difficult High variability Moderately expensive device
Indirect tension test (IDT)		Tensile strength (indirect)	6 in (Ø) 2 in (T)	External LVDTs required	Max horizontal strain at max load and strength used as indicator of ductility and cracking resistance potential	*Relatively easy specimen fabrication* *Easily obtained field specimens* *Tensile strength potentially related to cracking resistance* No fundamental property related

CHAPTER 3: EXPERIMENTAL METHODS, TESTING PROGRAM, AND MATERIALS

On the basis of the objectives of the study and the literature survey, an experimental program was developed. The scope of the experimental program contains mixture-level testing of laboratory-produced and laboratory-compacted specimens, plant-produced and laboratory-compacted specimens, and specimens obtained from field cores with varying contents of RAP and RAS. This chapter introduces the AC mixtures used in the study and the testing program and methods selected to characterize these mixtures.

3.1 RESEARCH METHODOLOGY

The research methodology focused on developing a reliable, yet practical, test method based on fracture mechanics principles. The research approach for developing the practical testing method and thresholds included the following:

- Assessment of plant and laboratory AC mixtures for modulus, fatigue, and fracture characterization at various temperatures and loading rates
- Development of a database of AC mixtures with different N-design, nominal maximum aggregate size (NMAS), RAP and/or RAS content, and binder type
- Correlation to field performance with testing field cores and cores form accelerated pavement testing sections
- Theoretical development and numerical models based on fracture mechanics principles
- Digital image correlation to evaluate the impact of recycled materials on cracking of AC to understand the mechanisms of loading rate and temperature on AC fracture

Figure 3.1 illustrates the experimental approach developed for this study. Chemistry and composition is covered under the ongoing project, “Modeling the Performance Properties of RAS-Blended Asphalt Mixes through Chemical Compositional Information” (ICT R27-162).

The test methods used in this study were chosen on the basis of the rationale discussed in Chapter 2. The following test methods were used to evaluate the effects of various levels and types of ABR and to develop the desired testing protocol. Complex modulus testing was conducted to characterize the modulus properties of the materials. Push-pull and Texas overlay (TOL) testing was conducted to provide insight into the fatigue-fracture resistance of materials and correlate results to those of the monotonic fracture test results. The traditional SCB and DCT tests were conducted to characterize the fracture potential of materials. Indirect tensile testing was conducted to characterize the strength capacity of selected mix designs. Apart from the conventional and standard test methods, different versions of fracture tests were conducted in accordance with the study objectives to develop a practical, cost-effective, and yet reliable test method that can correlate well with well-known and trusted but time consuming and complicated fatigue tests and field performance.

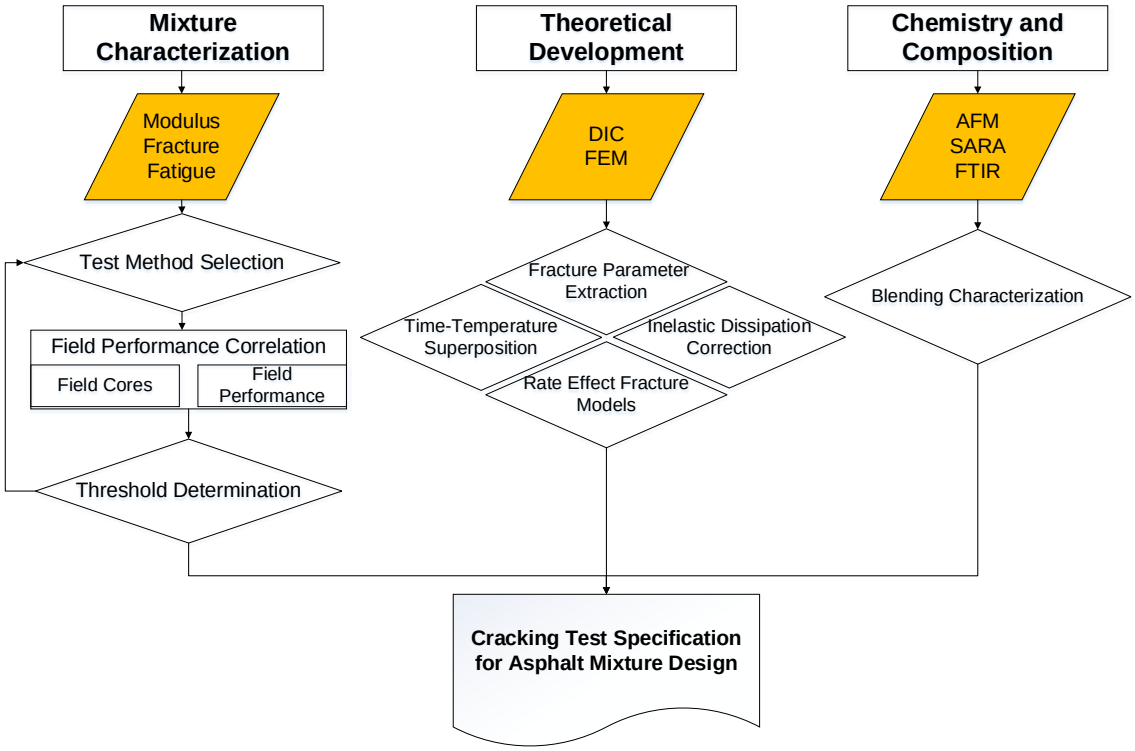

Figure 3.1 Integrated approach to develop a practical cracking potential test.

Furthermore, testing was conducted at the fine aggregate mixture (FAM) level on a variety of materials using the dynamic shear rheometer (DSR) machine. Shear strength and fatigue characterization of FAM with varying RAS levels and binder grades were conducted using the DSR tests. FAM-level testing was used to initially screen potential effects of RAS on fatigue and strength characteristics.

3.2 ASPHALT MIXTURES

Eleven laboratory-designed mixes, more than 15 plant mixes, and numerous field cores from the nine districts in Illinois, taken from various sections, were part of the developed testing program. The AC's used constitute a wide spectrum of mixes. The importance of each mix type and its constituents are discussed below.

3.2.1 Materials Used

3.2.1.1 Binder

Various binders were used in the study, based on different ABR content. The binders used were PG 70-22 SBS, PG 64-22, PG 58-28, and PG 52-34. In addition, 1% of Pavegrip 550 anti-strip was added to the total binder weight for some of the mixes to reduce stripping potential and meet the tensile strength minimums and ratio requirements.

3.2.1.2 Aggregate

Table 3.1 shows the details of the aggregate materials used in the mix designs.

Table 3.1 Type and Source of Aggregate Stockpiles Used in the Mix Designs

Material ID	032CM16	038FM20	037FM02	004MF01
Producer name (on mix design)	Quarry Materials	Quarry Materials	Quarry Materials	Hanson (Thornton)
Producer number (on mix design)	2298-06	2298-06	2298-06	
Plant location	Hodgkins, IL	Hodgkins, IL	Hodgkins, IL	Thornton, IL
Source no.	50312-78	50312-78	50970-02	50312-04
Source name	Vulcan	Vulcan	Thelan	Hanson
Source location	McCook	McCook	Antioch	Thornton, IL
Type of material	Dolomite	Crushed dolomite sand	Natural sand	Mineral Filler

3.2.1.3 RAS and RAP

The RAS samples were obtained from Southwind RAS, LLC. RAS materials were acquired on different dates during the duration of the project and were identified as sources 1 and 2 to differentiate between them in this report. Aggregate and asphalt binder were extracted from samples of both sources. The results show that the gradation and the asphalt binder content were comparable. Differences between both sources were taken into consideration during the mix design process. The RAP incorporated into the laboratory mixtures was sampled from District 5 (Open Road Paving in Urbana). Two fractionated RAP gradations of 1/2-in nominal maximum aggregate size (NMAS), +9.5 mm (+3/8 in), and -9.5 mm (–3/8 in) were provided. Appendix A provides details on the extracted gradations of the two RAP sources.

3.2.2 Laboratory-Designed Mixes

To better understand the effect of ABR on AC performance, the mixes were designed per Illinois modified AASHTO M 323 specifications. The Bailey method was used to produce mix design trials. Target voids in mineral aggregates (VMA) were kept constant for all mixes; the design air voids were 4%, and total binder content was constant. To evaluate the effect of ABR, the total binder used in each mix was kept constant at 6% (including both virgin and ABR binder). However, there were a few mixes in which total binder content was increased by 0.1% in order to maintain constant VMA at 15.3 ± 0.1%.

The specification requirements for dust to binder ratio were violated because of the limited availability of aggregate stockpiles to counter the increasing amounts of high ABR, which ultimately increased the fines content. The viscosity of 0.17 + 0.02 Pa-s was used to determine mixing temperature and 0.28 + 0.03 Pa-s to determine compaction temperature. Viscosity was determined in accordance with AASHTO T 316.

During the laboratory mix design process, RAS was batched separately from the virgin aggregates. The mixing process was performed in accordance with the specifications, but a modification was made to incorporate RAS into the AC mixture. The virgin aggregate and RAP were heated with the binder at the required mixing temperature. RAS material was heated in a separate oven at 110°C (230°F) for 30 min before the virgin binder reached the required mixing temperature. The virgin aggregate, RAP, and RAS were dry-mixed in a bowl and put back into the oven at the mixing temperature for an additional 30 min. The virgin binder was added to the bowl and mixed following the Illinois modified specification.

The AC mixes were prepared with utmost control of the volumetric properties by changing only one single variable at a time. This procedure made it possible to evaluate the effects of different mix parameters that may have been influencing fracture properties. A matrix for laboratory mixes was developed as shown in Table 3.2. The effect of ABR content (including a combination of RAP, RAS, RAS source, RAP source, and binder grade bumping) on the AC mixes was taken into consideration. These mixes will be referred to as "L#" hereafter.

Table 3.2 Major Characteristics of Laboratory-Designed Mixtures

Mix ID	Mix Name	Binder Grade	RAP (%)	RAS (%)	ABR (%)	AC (%)	VMA (%)
L3	N90-0[1] CG[2]	70-22	—	—	—	6.0	15.3
L4	N90-0 CG	64-22	—	—	—	6.0	15.3
L5	N90-30 CG S1[3]	70-22	—	7	29.8	6.0	15.3
L6	N90-30 CG S1	58-28	—	7	29.8	6.0	15.3
L7	N90-20 CG S1	58-28	—	5	21.2	6.0	15.3
L8	N90-10 CG S1	64-22	—	2.5	10.5	6.0	15.3
L9	N90-30 CG S2[4] AS[5]	58-28	11	5	30.5	6.0	15.2
L10	N90-60 CG S2 AS	52-34	40	7	60.8	6.1	15.2
L11	N90-0 CG AS	64-22	—	—	—	6.0	15.3
L12	N90-30 CG S2[4] AS[1]	58-28	—	7	30.6	6.0	15.2
L13	N90-30 CG S1[3] AS[1]	58-28	—	7	29.8	6.0	15.3

[1] N90-0, N90-20, N90-30, and N90-60 indicate N-design and ABR percentage

[2] CG: Coarse graded

[3] S1: RAS source

[4] S2: RAS source

[5] AS: Mixture with 1% anti-strip added to virgin binder

The mix designs were validated by conducting Hamburg WTT and IDT tests. The IDT tests were performed to obtain the tensile stress ratio (TSR) per the IDOT modified moisture susceptibility test specifications. The Hamburg WTT results were conducted for selected mix designs and are presented in Table 3.3. The results of the TSR suggested the use of anti-striping agents to avoid failure due to moisture damage. Hence, anti-stripping agent was added to the L9–L13 mixes. This resulted in these mixes passing the TSR criteria.

Table 3.3 Hamburg Wheel Tracking Test Results for Laboratory-Designed Mixes

Mix ID	Mix Name	Rut Depth (mm)	Total Passes at Rut Depth	Minimum Passes	Result
L3	N90 4 CG	12.5	11520	7500	Pass
L7	N90 20 CG	12.5	7000	5000	Pass
L9	N90 30 CG AS S2	6.1	20000	5000	Pass
L10	N90 60 CG AS S2	3.1	20000	5000	Pass
L12	N90 30 CG AS S2	5.0	20000	5000	Pass

3.2.3 Plant-Produced Mixes

In the initial phases of the study, a total of 16 plant-produced mixes were sampled. These mixes were used in the development of the test method and testing condition because they had distinct mix design characteristics, which enabled the effect of various types and levels of ABR and N-design to be evaluated. In the later stages of the study, more plant mixes were added to the database. Later in the study, additional plant mixes were tested to provide more data for fine-tuning the testing protocols and finalizing the specifications. The major characteristics of these mixes are shown in Table 3.4 and Table 3.5. These mixes will be referred to as "P#" hereafter. Other details of the laboratory and plant-produced mixes are provided in Appendices B and D.

Table 3.4 Major Characteristics of Plant-Produced Mix Designs Used in the Initial Test Development

Mix ID	Mix Name	Binder Grade	RAP (%)	RAS (%)	ABR (%)	AC (%)	VMA (%)
P1[1]	N50 SC[3]	52-28	50	3.5	60	6.7	15.0
P2[1]	N50 SC[3]	58-28	27	—	29	5.8	14.7
P3	N70 BC[4]	58-28	26	—	29	4.8	13.4
P4	N30 BC[4]	58-28	46.5	—	37	4.8	13.6
P5	N70 SC[3]	64-22	10	—	6	6.1	15.8
P6	N90 SC[3]	76-22	10	—	6	5.6	14.1
P7	N50 SC[3]	64-22	—	—	—	5.9	16.7
P8	N50-50	58-28	42	4	49	5.5	13.0
P9	N50-60	52-28	42	6	59	5.6	13.0
P10	N70-25	58-28	29	—	25	6	14.5
P11	N70-50	58-28	30	5	48	6	14.5
P12	N80-25	70-28	8	5	26	6.1	16.1
P13	N80-50	70-28	10	8	50	6	15.8
P14[1]	N50-Joliet	58-28	30	—	34	5.4	15.3
P15[1,2]	N50-Sandeno	52-28	52	4	60	6.7	15.1
P16[1,2]	N50-K5	52-28	53	5	57	6.5	14.9

[1] AC contains steel slag

[2] AC contains recycled concrete aggregate (RCA)

[3] SC: AC wearing surface

[4] BC: AC base course

Table 3.5 Major Characteristics of Plant-Produced Mix Designs Used in the Later Stages of the Study (Lippert et al. 2015)

Mix ID	Mix Name	Binder Grade	RAP (%)	RAS (%)	ABR (%)	AC (%)	VMA (%)
P17	147 M	70-28	34	4	35	7.7	18.5
P18	156 M	64-22	5	2	15	5.7	15.1
P19	157 M	58-28	10	4	30	5.8	15.0
P20	141 M	70-28	30	4	35	7.8	18.8
P21	140 M	58-28	20	2.5	30	5.8	15.1
P22	159 M	58-28	34	—	30	6	15.0

3.2.4 Field Cores

Field cores from 37 different sections from all nine IDOT districts were collected. Historical pavement data were also requested from the aforementioned districts. The field cores were used to validate the selected testing protocol and establish test threshold values. Details of the field cores are presented in Table 3.6.

Table 3.6 Field Core Information Collected from IDOT Districts

District	Lab Name	Mix Type	N-Design	NMAS	Year of Construction	AC Grade	AC (%)	RAP (%)	RAS (%)	ABR (%)
1	1-1	SMA-SC	80	12.5	2008	PG 76-22	5.8	0	0	0
	1-2	SMA-SC	80	12.5	2008	PG 76-22	5.7	0	0	0
	1-3	SMA-SC	80	12.5	2009	—	6	0	0	0
	1-4	SMA-SC	80	12.5	2013	PG 70-28	5.8	14.2	3	28.2
	1-5	F-SC	90	9.5	2013	PG 70-28	5.5	8	5	29.6
	1-6	F-SC	90	9.5	2013	PG 76-22	5.2	14	2.5	30.4
	1-7	F-SC	90	9.5	2009	—	5.3	10	0	10
	1-8	D-SC	70	9.5	2010	—	5.8	20	0	14.4
	1-9	D-SC	70	9.5	2013	PG 58-28	5.9	30	0	20.2
	1-10	D-SC	50	9.5	2013	PG 52-28	6.5	53	6	67.1
	1-11	D-SC	70	NA	2009	PG 64-22	5.9	10	0	7.5
	1-12	D-SC	70	9.5	2013	PG 58-28	5.7	17.5	2.5	30.3
	1-13	F-SC	90	9.5	2013	PG 70-22	5.8	10	0	10.2
2	2RT26	SMA-SC	—	—	2004	PG 76-28	6.2	0	0	0
	22RT2	D-SC	50	—	2003	PG 70-22	5.3	0	0	0
	22SRT2	C-SC	70	—	2004	PG 58-28	5.2	15	0	0
3	3-6E	D-SC	70	9.5	2012	PG 64-22	6.2	10	0	7
	3-6W	F-SC	50	9.5	2013	PG 64-22	6	40	0	27
	3-LB-E	LB	50	4.75	2012	PG 64-28	8.1	20	0	16.3
	3-LB-W	LB	50	4.75	2013	PG 64-22	5.7	40	0	—
4	D4-IL78	E-SC	90	9.5	2012	PG 70-22	5.8	10	5	—
	D4-IL9	D-SC	50	9.5	2013	PG 64-22	5.8	16	3.2	33.5
	D4-IL55	E-SC	90	9.5	2012	PG 76-22	6	10	0	10.3
5	5-US136-1	C-SC	50	—	2013	PG 58-28	5.9	30	0	22
	5-US136-2	D-SC	90	—	2014	PG 70-22	5.9	10	0	9
	5-I39	D-SC	90	—	2013	PG 70-28	6.2	12	0	10
	5-I57	D-SC	90	—	2013	PG 70-28	5.9	10	0	9
	5-IL47	D-SC	70	—	2012	PG 64-22	6.1	10	0	8
	5-IL6	—	50	—	2012	PG 64-22	5.7	14	0	13
6	6G2	D-SC	70	9.5	2013	—	6	Yes[2]	0	8.5
	6P	D-SC	70	9.5	2013	—	6	Yes[2]	0	16
7[1]	7-I130	—	—	—	—	—	—	—	—	—
	7-I121	—	—	—	—	—	—	—	—	—
8	8JVS2	C-SC	70	9.5	2013	PG 64-22	5.6	15	0	14.5
	867S1	D-SC	70	9.5	2013	PG 64-22	6.2	15	0	14.5
9	9-I4	D-SC	90	NA	2013	PG 64-22	5.3	0	0	0
	9-I54	C-SC	90	NA	2013	PG 64-22	N/A	20	0	—

[1] No information was provided by the district at the time of preparation of this report.

[2] RAP content was not provided by the district.

3.3 MIXTURE PERFORMANCE CHARACTERIZATION

3.3.1 Complex Modulus

Complex modulus testing was conducted in accordance with the AASHTO TP 79-15 to characterize linear viscoelastic properties of selected laboratory-produced and plant-produced mixes using the Interlaken hydraulic testing machine. A Superpave gyratory compactor was used to produce cylindrical samples of 150 mm (6 in) diameter and 180 mm (7.1 in) height. The asphalt cylinders were cored and cut to a diameter between 100 and 104 mm (4 in) and a height between 147.5 and 152.5 mm (6 in). The air void content for the gyratory-compacted specimens was targeted at 7 ± 0.5%.

To measure the axial displacement of these specimens, three extensometers were glued to the surface of the specimens at 120° radial intervals with a 70 mm (2.75 in) gauge. The standard protocols were followed for specimen conditioning, at testing temperatures of –10°C, 4°C, 21°C, 37°C, and 51°C (14°F, 40°F, 70°F, 100°F, and 130°F). At each temperature, modulus testing was completed at frequencies of 25, 10, 5, 1, 0.5, and 0.1Hz in the same order. The average microstrain at each temperature and frequency was kept between 50 and 75.

Viscoelastic characterization results for laboratory-produced AC are presented and discussed in Appendix E. In general, complex modulus can capture changes in the major mix design characteristics. AC mixes displayed a wide range of viscoelastic characteristics depending on the mix design and volumetrics (binder content and type, VMA, aggregate size and gradation, and ABR). In this case, the effects of RAS and binder grade bumping can be seen in the results—specifically, noticeable changes in the major viscoelastic characteristics.

In addition to performance characterization of AC mixtures, complex modulus tests are commonly used as part of advanced structural analysis protocols such as in MEPDG and numerical finite element simulations. The complex modulus test provides fundamental modulus characteristics of an AC mix. Although the modulus test may provide insight about the effect of ABR on AC characteristics that may affect cracking potential, it is very time consuming, requires complex analyses, and lacks the accuracy required for the purpose of this study. Hence, it has not been further considered in this study.

3.3.2 Push-Pull Fatigue Testing

Push-pull testing was conducted using the UTM-100 device for selected plant-produced mixes. A series of three strain gauges was placed around the specimen at a spacing of 120° apart. Specimens were fixed to the top and bottom steel plates of the device using Devcon 10110 epoxy. The epoxy was distributed evenly on the top and bottom to ensure failure toward the center of the specimen.

Specimens were subjected to a fingerprint modulus test to determine the complex modulus prior to loading in order to accurately apply the microstrain levels desired. After the specimen was allowed to rest for 15 min, cyclic loading was applied at a loading rate of 10 Hz until visible failure occurred. Testing was conducted at 20°C (68°F) at strain values of both 200 and 300 microstrains. The following failure criteria were considered to determine failure point for each test:

- 50% reduction in the initial complex modulus
- Abrupt change in the phase angle
- Abrupt change in the dissipated strain energy (W_N)
- Abrupt change in the energy ratio (R) defined by the ratio of initial dissipated energy and dissipated energy at the Nth cycle

- Abrupt change in the dissipated energy ratio (DER), which is defined as the ratio of the cumulative dissipated energy up to cycle N (W_i) and the dissipated energy for cycle N (W_N) multiplied by N (Ghuzlan and Carpenter 2000)
- Abrupt change in the incremental dissipated energy ratio (∆DER). This is calculated as the change in dissipated energy (∆DER) between cycles N and N-1 divided by the total dissipated energy up to cycle N-1.

The number of cycles to failure for the respective mixtures using the studied parameters is provided in Table 3.7.

Table 3.7 Number of Cycles to Failure Using Different Fatigue Parameters for Plant and Laboratory Mixtures (based on the tests conducted at 300 microstrain level)

Mix	50% E*	Phase Angle	W_N	R	DER	∆DER
P14	11324	17666	17820	17820	18125	18537
P15	6640	17160	16000	16252	—	—
P8	3221	13172	13000	13000	13100	13160
P9	1260	2330	2350	2350	—	—
P10	8526	17234	17163	17163	—	—
P11	823	1432	1497	1525	1510	1542
P12	3122	17122	17012	16952	—	—
P13	362	683	665	672	650	653
L4	15980	15980	12250	12223	12764	12855
L7	19720	20567	9076	9224	10143	10223
L6	14122	12375	10453	11589	10032	11343

Some reduction was noted in the fatigue life with increasing ABR for the plant-produced AC N50, N70 and N80. However, the same trend was not observed with the laboratory-produced AC mixes with increasing ABR (with RAS only). General observations for the push-pull tests were the lack of repeatability and the time-consuming specimen preparation and testing. Hence, it was determined that this test should not be used to identify the impact of ABR on AC mixtures nor it is consistent with the set of criteria developed for the purposes of this study.

3.3.3 Texas Overlay Test

The TOL was conducted at the IDOT's Bureau of Materials and Physical Research (BMPR) Hot-Mix Asphalt Lab. Specimens were mounted to base plates with the use of a mounting jig and a two-part epoxy. The epoxy was allowed to cure, typically for 8 hr, per manufacturer recommendations. Base plates were then bolted to the loading setup. Testing was displacement-controlled cyclic loading applied at 25°C ± 0.5°C (77°F± 1°F). Specimens were repeatedly displaced in tension to a displacement of 0.6 mm (0.025 in) and then released. The test is considered complete when a 93% reduction in the first cycle's recorded maximum load is noted or when 1,000 cycles are reached. All of the TOL tests were conducted using the first generation test fixture built by the manufacturer.

Texas overlay test results are shown in Figure 3.2, with number of cycles to failure and initial load at the beginning of the test. P6 and P7 showed better performance in terms of cycles to failure, while P2 and P5 showed low performance. There is a clear trend between the peak load and cycles to failure

that AC experiences. P7, an excellent-performing AC, had the lowest peak load value while P6, also an excellent performance AC, displayed the highest peak load value.

The TOL is a good qualitative test that can identify good and bad mixtures; however, its error percentage is relatively high, specimen preparation is cumbersome, and testing duration is relatively long. Hence, this test was not pursued further, although it can still be used as a qualitative test.

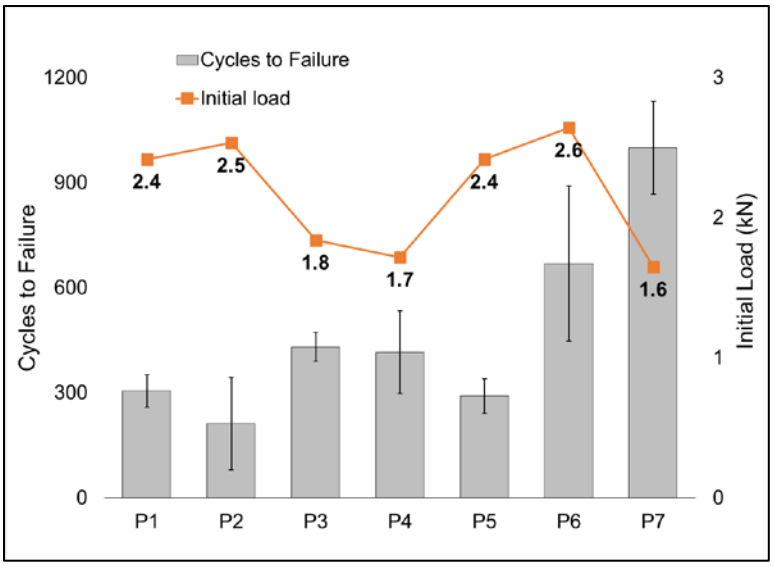

Figure 3.2 Texas overlay results for selected plant AC mixtures.

3.3.4 Low-Temperature DCT Fracture

Disk-compact tension (DCT) tests were conducted on an Instron servo-hydraulic load frame at ICT facilities. Test specimens were fabricated to be 50 mm (2 in) thick and 150 mm (6 in) in diameter. Bore holes 25 mm (1 in) in diameter were fabricated into which the loading rods were inserted. Specimens were conditioned prior to testing in refrigerated chambers. Temperature was verified by temperature gauges, and specimens were tested within 1°C (1.5°F) of the desired temperature.

Upon reaching the desired testing temperature, the two loading rods were first moved apart until a seating load of approximately 0.2 kN (45 lb) was experienced by the specimen. Then, a constant CMOD rate of 1.02 mm/min (0.04 in/min) (controlled by measuring displacement using knife points) was applied until the induced load on the specimen was reduced to approximately 0.1 kN (22.5 lb).

The fracture energy is calculated by dividing the work of fracture (the area under the load vs. the average load-line displacement curve) by the ligament area (the product of the ligament length and the thickness of the specimen) of the test specimen prior to testing. The same fracture energy equation can be used for all types of fracture tests, including SCB and DCT, conducted at different temperatures.

$$G_f = \frac{W_f}{Area_{lig}} \tag{3.1}$$

where G_f = fracture energy (usually expressed in J/m^2); W_f = work of fracture calculated by finding the area under the load-displacement curve; $Area_{lig}$ = ligament area calculated by ligament length × thickness of specimen (ligament length describes the portion of the specimen ahead of the pre-cut notch).

Results from the DCT tests are presented in Figure 3.3. The results showed inconsistent trends and no clear relationship was observed between the fracture energy and amount of recycled content or mixture characteristics. For example, P8 and P9 displayed a trend of decreasing fracture energy with increasing ABR, but P12 and P13 contradicted that trend. The fracture energy values in the DCT test setup showed a range of fracture energy values of 83 J/m^2 (a relatively small range for a wide range of ABR levels and types).

In recently completed ICT-sponsored projects, DCT tests were used for fracture characterization and resulted in similar conclusions. The DCT fracture test was employed to evaluate coarse- and fine-graded AC mixtures (Buttlar et al. 2015). According to the DCT cracking test results at three temperatures below 0°C (32°F), no differences were observed for mixes with similar binder content and VMA but with distinct aggregate gradation characteristics. In 2008, a study on RAP effect on HMA was conducted at ICT and showed that data spread and ability to quantify the impact of RAP on AC diminish as testing temperature decreases for both SCB or DCT (Al-Qadi, et al. 2009). Hence, the DCT was found to be incapable of reasonably distinguishing between various mixes at low temperature.

Given the results in this study as well as recent studies cited herein, DCT testing was not pursued any further.

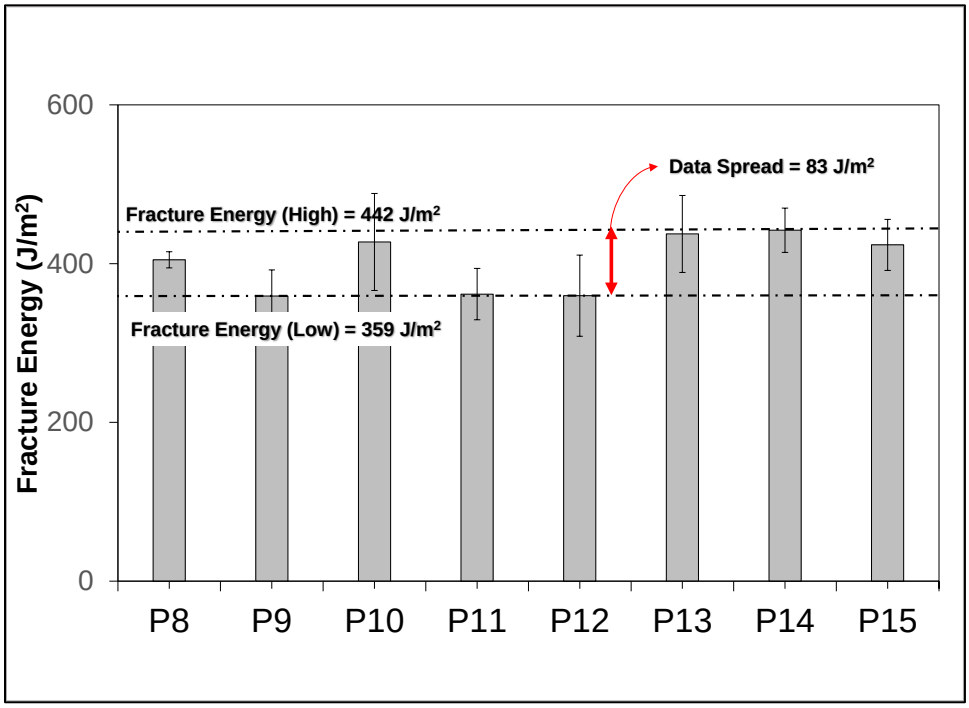

Figure 3.3 DCT results for AC fracture testing in CMOD control at –12°C (10.4°F).

3.3.5 Low-Temperature SCB Fracture

Low-temperature SCB tests were conducted using the servo-hydraulic Interlaken load frame at a temperature of –12°C (10.4°F) for all mixes. Specimens were conditioned prior to testing in refrigerated chambers. Temperature was verified by temperature gauges, and specimens were tested within 1°C (1.5°F) of the desired temperature. To avoid impact loading, the specimen was first loaded with a sitting load of 0.2 kN (45 lb). Displacement was controlled by a crack mouth opening displacement (CMOD) measured at the bottom of the specimen using two knife points. Displacement rate was 0.7 mm/min (0.027 in/min).

The results for plant-produced mixtures are shown in Figure 3.4. Fracture energy values for the 15 plant AC mixes ranged between 436 and 689 J/m^2. Despite a greater range of values (more than double that of DCT), the low-temperature fracture energy results produced a limited range of fracture energy even though the mixes have distinctive mix design characteristics, including N-design, binder type and content, ABR level, and aggregate gradation and sources.

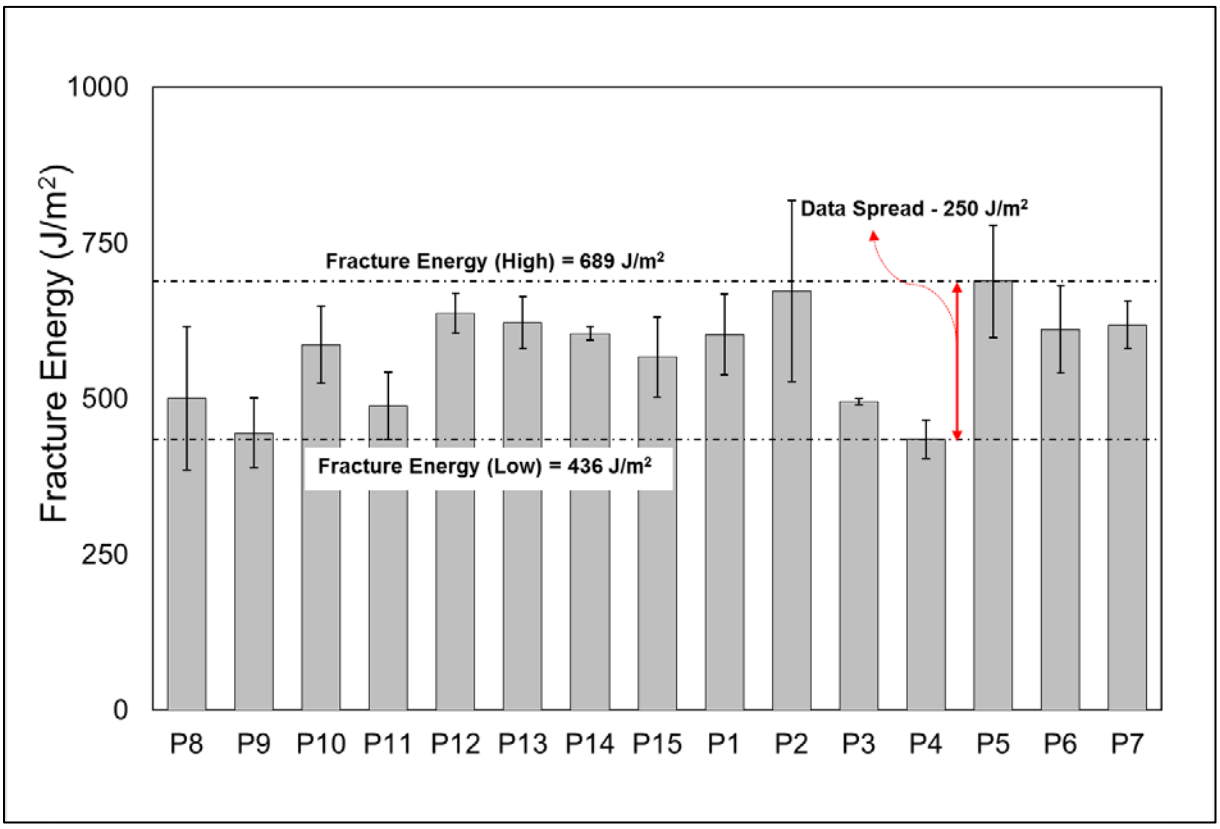

Figure 3.4 SCB plant mixture results for fracture testing in CMOD control at –12°C (10.4°F).

Similar results were obtained for the laboratory-produced materials. Laboratory-produced mixes were derived from the same parent mix by adding RAP/RAS and changing binder grade, which resulted in mixes with potentially distinct performance characteristics. However, as shown in Figure 3.5, except for mix L10 with 60% ABR, there was no significant difference in the fracture energy results at low temperature. Similarly, the tests conducted as part of a previous study by ICT showed that low-temperature SCB tests did not capture any differences in the fracture energy of various AC mixes with RAP contents varying between 30% and 50% (Aurangzeb 2012; Aurangzeb et al. 2014).

Therefore, it was concluded that changes in the AC design for the fracture test results of either DCT or SCB are masked at low temperature. Hence, for the purpose of the current study, neither test at low temperature could provide results reliable enough to distinguish between the AC mixes.

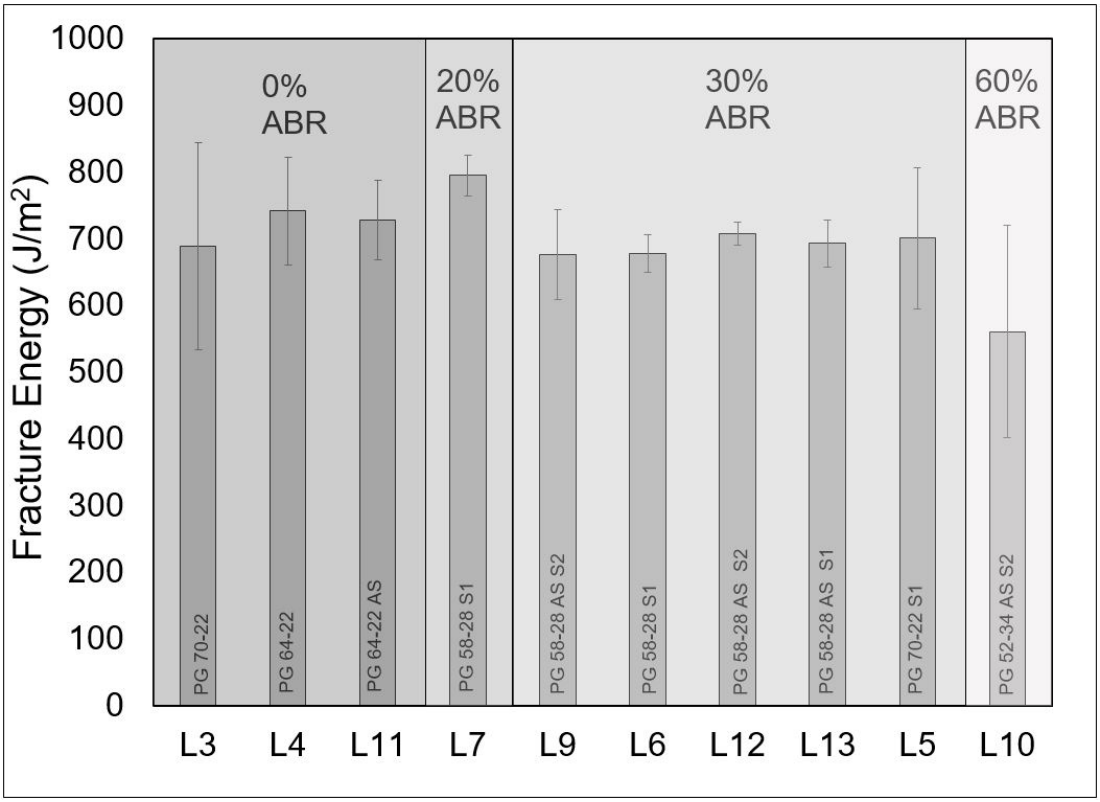

Figure 3.5 SCB laboratory AC mixture results for fracture testing in CMOD control at –12°C (10.4°F).

As discussed previously in relation to the TOL qualitative results, statistical analysis was conducted to analyze low-temperature SCB and TOL test results and quantify the statistical distinction that those two tests provide between different mixtures. In addition, correlation between a commonly used fatigue test and a fracture test was explored by ranking the mixtures using statistical analysis.

Table 3.8 presents the results from the statistical analysis. The t-test results indicated that there is no statistical difference between mixtures at low-temperature for traditional SCB test setup; most of the mixes placed in the similar statistical subsets. The TOL test seemed to separate P6 and P7 into their own statistical subset, with the remaining mixtures in a second subset. However, low-temperature and TOL tests showed contradictory results pertaining to the performance of P5. According to the SCB test, P5 was determined as one of the good-performing mixes, whereas P5 was in the “B” category (poor performing) with the lowest number of cycles to failure by the TOL.

Table 3.8 Statistical Classification for Low-Temperature SCB and Texas Overlay Results

	Texas Overlay		Low-Temperature SCB	
Mix #	**Statistical Grouping at α = 0.10**	**Average # of Cycles to Failure (COV)**	**Grouping at α = 0.10**	**Average Fracture Energy (COV) (J/m^2)**
P1	B	305 (14.65%)	A/B/C	604 (10.74%)
P2	B	212 (43.47%)	A/B	673 (21.63%)
P3	B	431 (10.05%)	B/C	495 (0.90%)
P4	B	416 (23.69%)	C	436 (7.04%)
P5	B	291 (16.67%)	A	689 (13.12%)
P6	A	669 (29.72%)	A/B/C	611 (11.42%)
P7	A	1000 (14.31%)	A/B/C	619 (6.13%)

Despite its ability to distinguish between mixtures, the TOL displayed a high coefficient of variation (COV) in the range of 10.05% to 43.47%. The COV of the SCB fracture energy, on the other hand, was around 8.2% when not considering the one exception of P2.

3.4 FINE AGGREGATE MIXTURE–LEVEL TESTING

The objective of fine aggregate mixture (FAM)–level characterization is to characterize the inherent effect of RAS on AC. A fine aggregate scale was selected for use based on its convenience in specimen preparation without the need for mix design. The characteristics determined were linear viscoelastic modulus, shear strength, and fatigue resistance. FAM-level specimens were prepared using one fine aggregate stockpile (FM-20 type), virgin binder, and various levels of RAS content. This could be a potential test for initial screening the effects of RAS on AC mixture performance.

Samples were mixed and compacted, using the gyratory compactor, at a temperature of 155°C (311°F). Short-term conditioning of mixes was done similar to that of the conventional AC mixtures. Each mixture was subjected to 150 gyrations—a number chosen in order to obtain mixes with consistent air void content. The FAM samples were then cored from the gyratory-compacted samples to the desired diameter of 12.45 mm (0.490 in) and length of 50 to 60 mm (1.96 to 2.36 in). Samples were then glued at the top and the bottom to special circular steel caps to hold them in the DSR fixture. Figure 3.6 illustrates the sample preparation process and testing fixture for holding solid samples. The solid-testing fixture in the Malvern Gemini-2 type of DSR equipment was used to tests the specimens. Additional details of FAM specimen preparation is provided in Appendix J.

Figure 3.6 Specimen preparation process for FAM specimens including cutting, coring, and test setup.

The DSR-based test method was successfully used to identify critical changes in mix performance with the addition of RAS. Specimen preparation protocols provided consistent volumetric and test results to statistically isolate the effect of RAS on the test outcome as well as the effect of changing the RAS source. The FAM results identified distinct changes in the viscoelastic characteristics of the materials with RAS—similar to those usually observed in mixture-level testing.

It was shown that with different types of tests and at different scales (mix, FAM, and binder), FAM testing can be used to quantify the effects of RAS on asphalt mixtures and to address RAS source variability. FAM testing is a rapid way to evaluate a large array of test parameters and to narrow the choices for mixture-level testing. The proposed test can be used for characterization and screening of other recycled materials, by-products, binder additives, and rejuvenators.

3.5 THEORETICAL STUDY

The effects of displacement rate and temperature are discussed in Chapter 4. In addition, analyses using digital images are presented in that chapter. Finite element simulations for the SCB test geometry were also conducted. The primary purpose of those simulations was to investigate the effects of dissipation mechanisms that are not related to crack initiation and propagation. Additional dissipation of energy, referred to as spurious dissipation of energy, is not related to cracking and can occur in a zone far away from the crack tip and under the loading head. Such additional mechanisms of energy dissipation may affect total energy calculated in a fracture test. Details of the finite element simulations and results are discussed in Appendix H.

3.6 SUMMARY

While the spread in the SCB data was more than double the spread for the DCT, neither test was able to properly distinguish between AC mixes, even though the AC mixes had distinct characteristics.

Therefore, it was determined that low-temperature fracture energy tests conducted at opening displacement rates of around 0.7 to 1.0 mm/min (0.028 to 0.039 in/min) are not sufficient to screen AC mixtures with respect to their potential cracking resistance. Monotonic low-temperature fracture tests are relatively easy to conduct; however, they require an environmental chamber, which makes the tests expensive.

Although complex modulus tests present a comprehensive viscoelastic characterization of AC mixtures and can trace the significant changes in the mix designs such as ABR, binder grade, and content, the test results cannot be used alone to evaluate cracking potential. In addition, the test complexity and cost of equipment could be prohibitive.

Push-pull fatigue tests conducted on plant- and laboratory-produced mixtures followed a weak trend with a decreasing number of cycles to failure with increasing ABR. In addition to test duration and level of difficulty, repeatability of this test is low; hence, it may not be able to distinguish between mixes. On the other hand, the TOL test showed some qualitative success in distinguishing mixes with respect to their significant mix design characteristics. However, results suffered from lack of repeatability. In addition, specimen preparation and cost may hinder seamless application of that system.

On the basis of the shortcomings of the aforementioned tests, it is evident that an alternative testing protocol needs to be developed that meets the test method selection criteria introduced in Chapter 2.

CHAPTER 4: CHARACTERIZATION OF ASPHALT MIXES TO DISCRIMINATE PERFORMANCE

Having concluded that low-temperature fracture tests (both SCB and DCT) are insufficient at distinguishing between various AC mixtures of the same category and that fatigue-type tests suffer from repeatability problems and difficulties in specimen preparation and actual testing, monotonic fracture tests at various temperatures and loading rates were explored. The SCB test geometry was selected for further evaluation because of its potential low-cost implementation and ease of specimen preparation and testing.

A testing temperature and loading rate were identified that can discriminate mixes' cracking potential. The SCB test conducted at room temperature (25°C [77°F]) was chosen as a point of focus primarily for its practicality, repeatability, and low-cost implementation (i.e., room-temperature testing without the need for a temperature-control chamber, possible adaptability to existing equipment, and easy specimen preparation).

This chapter presents the results of fracture tests conducted at various temperatures and displacement rates along with a fundamental discussion about the fracture processes and how the displacement rate and temperature combination was selected for the testing protocol.

4.1 SELECTION OF DISPLACEMENT RATE AND TEMPERATURE FOR TESTING

Fracture processes and energy of AC have been shown to be dependent on temperature and the loading rate of testing. Because AC is subjected to varying loading rates and temperatures in the field, it is important to understand the effects of loading rate and temperature on the fracture behavior of AC.

4.1.1 Testing Program and Materials Used

The testing program was divided into two main stages. The first stage consisted of evaluation of loading rate and temperature on fracture parameters with an objective to determine the testing temperature with the highest potential for discrimination. The second stage explored displacement rates (at fixed temperature) to determine the displacement rate for testing. The testing program was applied to selected plant- and laboratory-produced mixtures.

In the first stage, fracture testing was conducted over several displacement rates and temperatures. The rates were then adjusted, using shift factors determined from an independent complex modulus test. This was done to compare the results of varying displacement rates and temperatures with respect to a single intermediate temperature (T_R = 25°C [77°F]). The equivalent time concept that was introduced by Nguyen et al. (2013) was used in this study. According to this concept, equivalent time is as follows:

$$t_{eq} = \frac{t}{a_T} \tag{4.1}$$

where a_T is a shift factor obtained from the complex modulus test.

The P10 and P11 mixtures were run using CMOD control, and the P12 and P13 mixtures were tested using LVDT control.

The calculations for the reduced rate were performed as follows:

$$V(T_i) = V(T_R) * \frac{a_T(T_R)}{a_T(T_i)} \quad (4.2)$$

where $V(T_i)$ is the rate of testing at temperature T_i and $a_T(T_R) = 1$ as a reference temperature; for other temperatures, a shift factor was calculated using the Williams-Landel-Ferry equation and coefficients. For example, if the rate of loading displacement at –12°C (10.4°F) is 0.7 mm/min (0.028 in/min), equivalent rates at 0°C (32°F) and 12°C (53.6°F) are 45 mm/min (1.8 in/min) and 1990 mm/min (78.4 in/min). Fracture energy was calculated using the Equation 3.1 introduced in Chapter 3.

4.1.2 Rate and Temperature Effects on Fracture Energy

Owing to various inelasticity mechanisms, including viscoelasticity, viscoplasticity, and damage, AC fracture behavior is time and temperature dependent. To properly select test methods and protocols, a representative combination of displacement rate (indicating time effect) and temperature should be identified to capture the overall crack potential of AC. Therefore, selected plant- and laboratory-produced mixes were tested under a wide range of temperatures and displacement rates using the SCB test geometry. This provides an understanding of the effects of time and temperature on AC cracking behavior and can be used to verify the applicability of the time–temperature superposition rule.

Figure 4.1 illustrates the fracture energy results obtained for selected plant mixtures. Fracture energy values obtained at temperatures from –30°C to 30°C (–22°F to 86°F) at varying displacement rates were plotted with respect to a common x-axis of reduced rate. Several observations can be made from the charts in the figure. First, fracture energy behavior over a wide range of temperatures and displacement rates approach a plateau value at high rates (low temperatures) and has a peak value near a displacement rate of approximately 5 to 100 mm/min (0.197 and 3.94 in/min). Peak values were always obtained around 25°C (77°F). Therefore, it can be concluded that selecting an intermediate temperature with a rate of loading between 5 and 100 mm/min (0.197 and 3.94 in/min) can produce the highest degree of separation for the purpose of distinguishing AC mixes.

A second observation regards the validity of the time–temperature superposition. In Figure 4.1, it can be seen that time–temperature superposition may not be valid when reduced rates are less than 1000 mm/min (39.370 in/min) corresponding to tests conducted at 0°C (32°F) and above. However, at higher reduced rates (corresponding to generally low temperatures), points are well separated from each other without any overlap. This suggests that time–temperature superposition, with the coefficients obtained from complex modulus test, may have limited applications for fracture energy. Time–temperature superposition for fracture energy can be valid only for a certain range of temperatures and testing rates at lower temperatures or high displacement rates.

Alternately, the effects of temperature and displacement rate on fracture energy are demonstrated in Figure 4.2. At each temperature, fracture energy was obtained at two rates, identified as slow and fast. These two rates varied at each temperature with increasing order as temperature increases. For example, at –25°C (–13°F), the slow and fast rates were 0.07 mm/min (0.0028 in/min) and 0.3125 mm/min (0.012 in/min), respectively. At –6°C (–0.4°F), the slow and fast rates became 0.7 mm/min (0.028 in/min) and 3.125 mm/min (0.12 in/min), respectively. As temperature increased, rates also increased. At 25°C (77°F), the slow and fast rates were 6.25 mm/min (0.25 in/min) and 50 mm/min (2 in/min), respectively. In general, it was observed that fracture energy increases with increasing temperature up to room temperature. Fracture energy appears to be less rate dependent at lower

temperatures than at intermediate temperatures. At temperatures less than 0°C (32°F), the effect of rate on fracture energy is not generally consistent with an increase in fracture energy at slow rates or similar values for both rates. However, at the same intermediate temperatures, the higher the rate, the consistently higher the fracture energy. Once again, Figure 4.2 shows that fracture energy reaches a peak value at the intermediate temperatures, amplifying the difference between mixes.

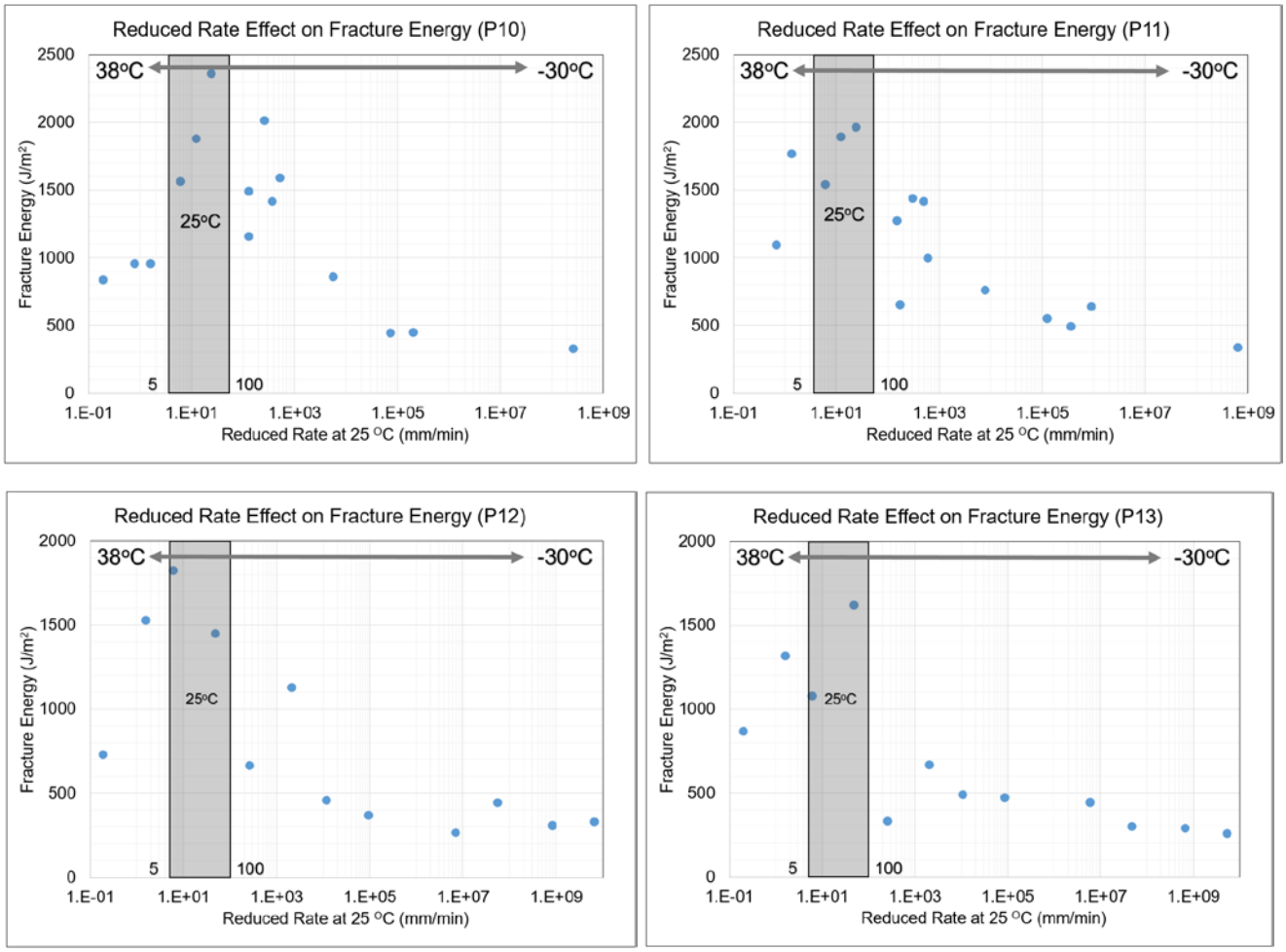

Figure 4.1 Reduced rate effect on fracture energy of P10, P11, P12, and P13 AC mixtures.

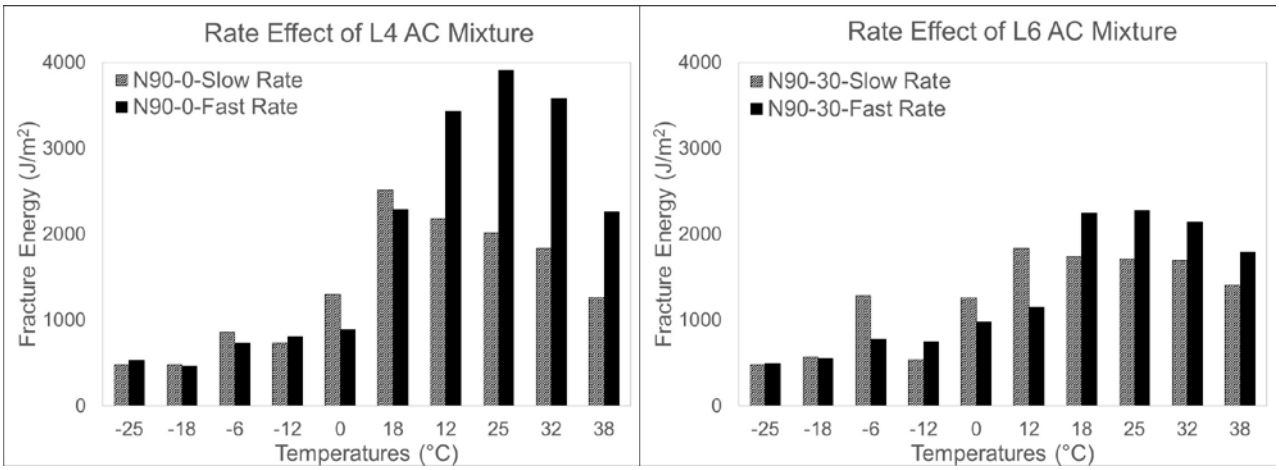

Figure 4.2 Temperature and displacement rate effect on fracture energy of laboratory-produced AC mixtures (Khan 2015).

4.1.3 Fundamental Fracture Mechanisms

To investigate the mechanisms associated with rate and temperature, a high-resolution charge-coupled device (CCD) camera system was used. Pictures were taken during SCB fracture tests to allow further analysis of the tests with the digital image correlation (DIC) technique. DIC is an imaging technique that enables measurement of displacements, strains, and stresses (the latter through appropriate constitutive equations) on the entire surface of a specimen, for the instant corresponding to each picture taken (Sutton et al. 2009). DIC has the advantage of being a non-contact full-field measurement technique and has been used for fracture or material characterization in many situations. For example, DIC has been used to study the mechanical and fracture properties of composites (Leclerc et al. 2009), metals (Carroll et al. 2013), functionally graded materials (Abanto-Bueno and Lambros 2002), concrete (Skarżyński et al. 2013; Wu et al. 2011), and AC (Seo et al. 2002).

To obtain the displacement field on the surface of a specimen, a reference picture is taken (usually at the unloaded state) of a random speckle pattern on the surface, and the pixels in a zone of interest are selected. Then, subsets of pixels are compared with a deformed picture (taken at a loaded state) to find a best match and thus compute the deformation of the subset (i.e., the displacement and the displacement gradients corresponding to the center of the subset). Figure 4.3 shows an image of an SCB specimen painted for DIC analysis.

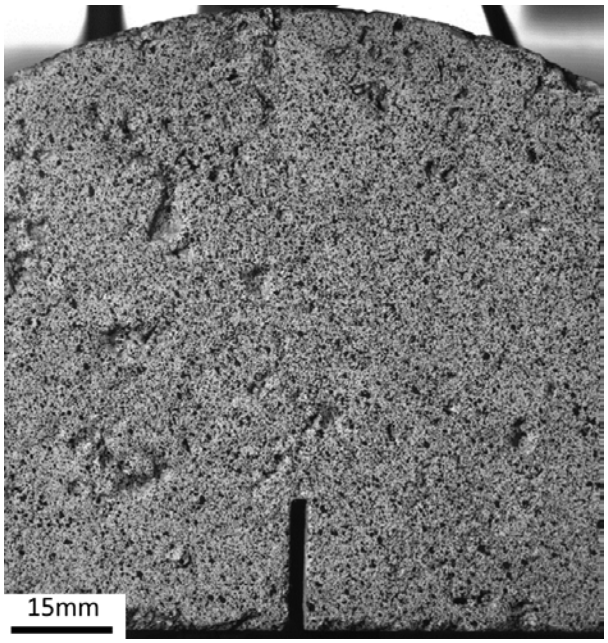

Figure 4.3 SCB specimen painted for DIC analysis.

Two different CCD cameras were used for the experiments: a Point Grey Gazelle 4.1MP Mono (2048 x 2048 pixels, 150 FPS) and an Allied Vision Prosilica GX6600 (6576 x 4384 pixels, 4 FPS) with a Tokina AT-X Pro Macro 100 2.8D lens. The Gazelle camera has a faster acquisition rate than the Prosilica, but the Gazelle has a lower pixel count. The choice of camera to use for a particular experiment depended on the acquisition rate and spatio-temporal resolution required. The software used for picture acquisition was Vic-Snap, which was provided by Correlated Solutions with the cameras.

The DIC technique was used in this study to perform the following:

- Evaluation of the fracture process zone before and after crack initiation to understand mechanisms of damage and cracking in AC at varying temperatures and displacement rates in addition to desired mix design characteristics.
- Calculation of strains and damage in the entire specimen (under the loading head, supports, and elsewhere).
- Calculation of viscoelastic crack front parameters driving crack propagation.

Figure 4.4 shows the horizontal (i.e., opening) strain field (primarily responsible for crack initiation and propagation in the SCB test) at peak load for the two testing conditions of –12°C (10.4°F) at a rate of 0.7 mm/min (0.027 in/min) and 25°C (77°F) at a rate of 50 mm/min (2 in/min) for a control laboratory design mix (L3) and a mix with 7% RAS (L6), respectively. The color contours, plotted on different scales for low and intermediate temperatures denoting the measured opening strain, were superimposed onto a micrograph of the aggregate structure for the specific specimen in each case (light color is aggregate and the dark color is binder).

The images in Figure 4.4 show the difference in crack front damage mechanisms with changing temperatures, loading rates, and RAS content levels. It is apparent from these images that the

damage develops in the mastic (as might be expected in the field), while the strains in the aggregates are very small. Damage is more widely distributed with the increase of temperature, which explains the increase in fracture energy values calculated at 25°C (77°F).

When the strain distribution becomes more localized, as in the case of low-temperature testing, more brittle failure occurs. Note that the contour scale in the low-temperature case is ten time smaller than the room-temperature ones. The same transition can also be observed in the specimens with 7% RAS. Damage localization is more pronounced for specimens with 7% RAS (L6) at all testing conditions, indicating a more brittle failure and AC embrittlement. Because damage is distributed over a wider area, other AC mix design characteristics, such as volumetric properties, mastic properties, and aggregate size and distribution, may play a more significant role in the behavior of the specimens (Figure 4.4).

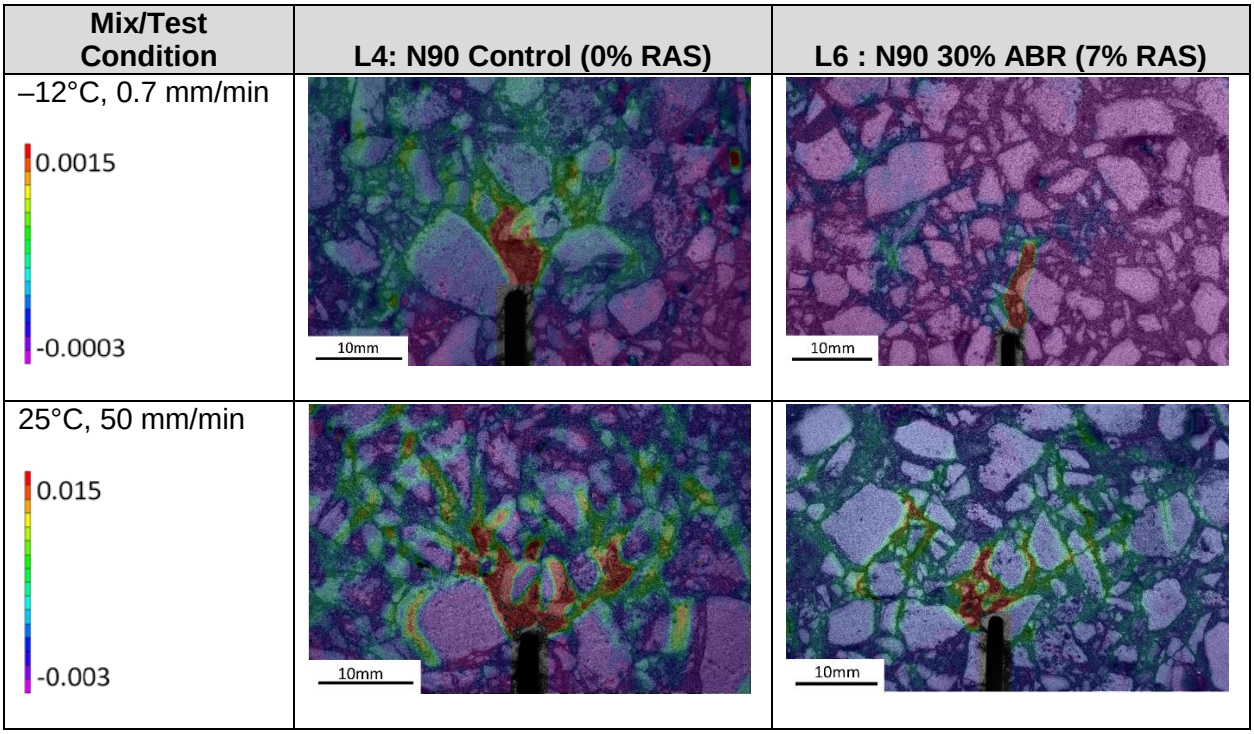

Figure 4.4 Horizontal strain field at specimen's surface (at peak load) for two AC mixes and two test conditions.

To better explain fracture energy results obtained at various temperatures and displacement rates, a review of viscoelastic fracture mechanisms is provided. According to Bazant and Planas (1997), for quasi-brittle materials with small plastic (or viscoplastic) zone, three possibilities can lead to time- and temperature-dependent fracture properties:

1. The outer zone (far-field region from the crack) is linear elastic (time independent) and the fracture process is time dependent.
2. The outer zone is linear viscoelastic (time dependent) and the fracture process zone is time independent.
3. The outer zone and the fracture process zone are both time dependent.

These mechanisms have been investigated with concrete primarily to determine the effect of loading rate and temperature. Viscoelastic fracture models were developed taking into consideration the viscoelastic coupling of the regions surrounding the crack and crack front (Bazant and Li 1997; Li and Bazant 1997). Even though the material time scale of concrete is significantly different than that of AC, such models may shed light on the discussion and results presented in this report. Fracture mechanisms in AC may be assumed to follow the third possibility in which both the fracture process and the surrounding regions are strongly viscoelastic with the addition of a sizeable viscoplastic zone.

4.2 INTERMEDIATE-TEMPERATURE SCB TEST METHOD

On the basis of the results from the tests conducted at different temperatures and displacement rates, it was shown that intermediate-temperature testing at 25°C (77°F) can provide an opportunity to accomplish the objectives of the study to develop a practical and yet reliable test method to distinguish a mixture's cracking resistance. The study focused on testing at this temperature with varying displacement rates to identify a rate that provides the highest degree of meaningful separation, along with acceptable repeatability.

The intermediate-temperature SCB test is a modification of the low-temperature SCB test. For testing herein, specimen geometry and testing fixture setup are identical. A linear variable displacement transducer (LVDT) was added to the fixture (Figure 4.5). The procedure to calculate the fracture energy is identical to that of the low-temperature SCB test except for the use of LVDT displacement values instead of CMOD displacement values. Based on the aforementioned results and discussions, displacement rates of 6.25, 25, and 50 mm/min (0.25, 1, and 2 in/min) were explored.

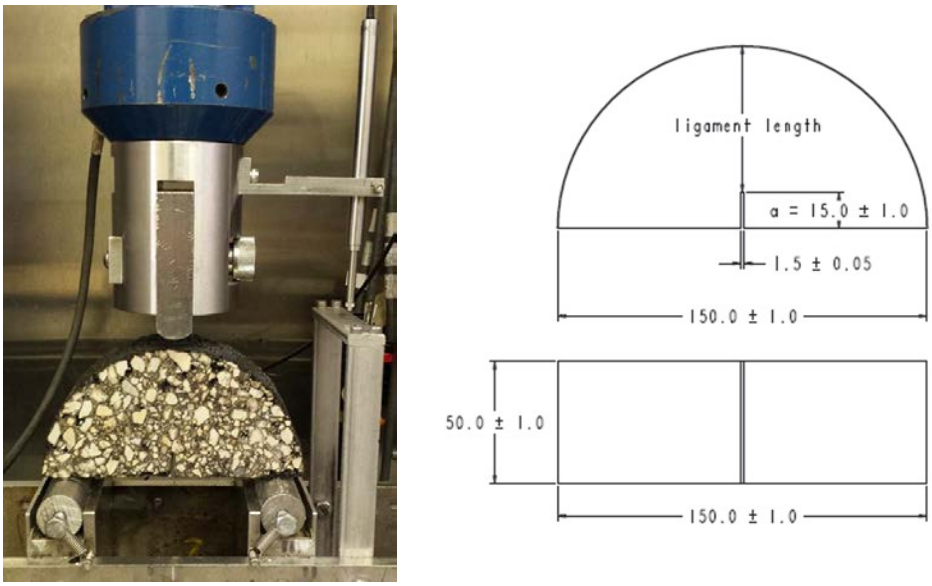

Figure 4.5 Semi-circular bending beam test fixture and specimen configuration.

Typical results from the intermediate-temperature testing are shown in Figure 4.6 and Figure 4.7. These figures illustrate the effect of displacement rate and ABR using a low and high rate of testing for mixtures with no ABR and with 30% ABR. The lower displacement rate of 6.25 mm/min (0.25

in/min) produced more ductile behavior and displayed a lower peak load and softer post-peak tail. The higher displacement rate of 50 mm/min (2 in/min) produced a load-displacement curve indicating a more brittle mixture behavior with higher peak loads and sharper post-peak unloading. Similar results were obtained for the AC mix containing 30% ABR (L6). However, in that case, it is clear the response is much more brittle with increasing peak loads and a reduction in the displacement to initiate and complete crack propagation.

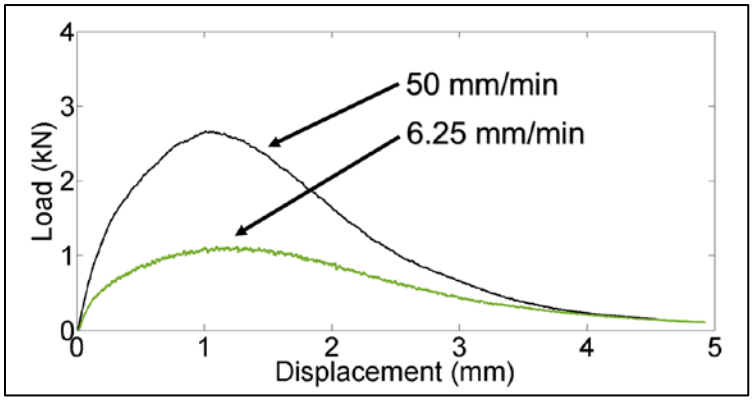

Figure 4.6 Typical load-displacement curve for a control AC mixture with 0% ABR at 25°C (77°F).

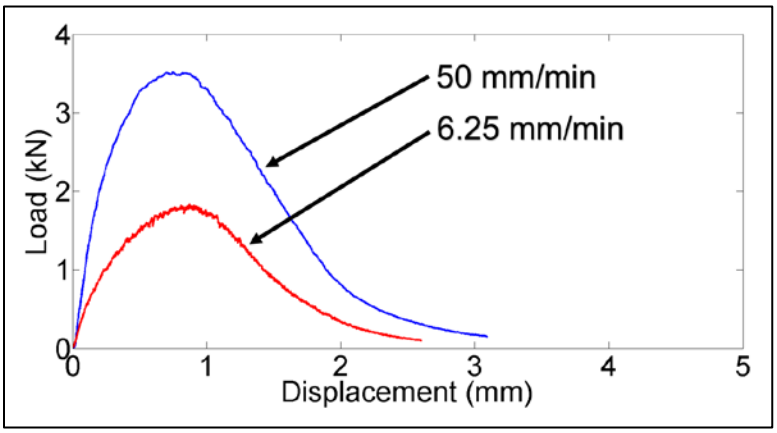

Figure 4.7 Typical load-displacement curve for a control AC mixture with 30% ABR at 25°C (77°F).

Figure 4.8 illustrates typical results for some laboratory AC mixtures with varying ABR percentages and binder grades. Tests were conducted at 50 mm/min. The separation between the AC mixtures is evident from the load-displacement curve patterns. As the ABR increases, curves appear to become more brittle with increasing peak, smaller displacement range, and higher slope in the post-peak segment of the load-displacement curves.

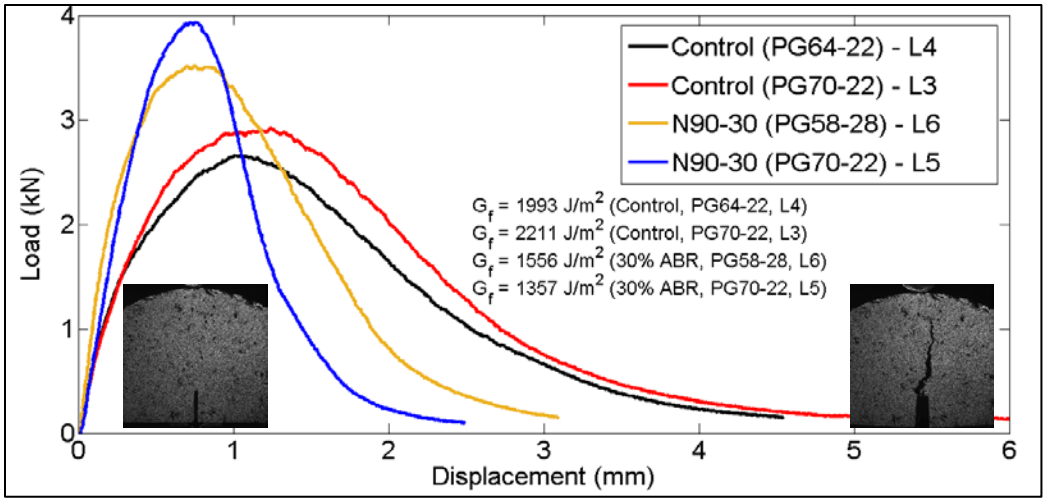

Figure 4.8 Typical load-displacement curves for laboratory N90 AC mixes (L3–L6) and corresponding fracture energy calculated from the IL-SCB tests conducted at a loading rate of 50 mm/min (2 in/min) and temperature of 25°C (77°F).

Typical load-displacement curves illustrate that, at intermediate-temperature testing, separation of AC mixes results due to changes in the mix design characteristics is possible. Hence, the next step was to optimize the displacement rate.

4.2.1 Results at Various Displacement Rates

Figure 4.9 presents intermediate-temperature SCB fracture energy results for plant AC mixtures tested at 50 mm/min (2 in/min). The range of fracture energy varied from 877 to 2148 J/m^2 for the tests conducted at 50 mm/min (2 in/min). This produces a fracture energy value range of 1271 J/m^2, as compared to the previous 253 J/m^2 observed under classical low-temperature SCB testing for plant AC mixes.

Similarly, Figure 4.10 presents fracture energy results for laboratory mixtures. The effect of increasing ABR on the fracture energy is clearly evident for these mixtures. Fracture energy drops as ABR increases up to 60%. Fracture energy values ranged from 967 to 2226 J/m^2, a range of 1253 J/m^2. This can be compared with the corresponding fracture energy range of 250 J/m^2 for the classical low-temperature SCB test setup for the same mixtures.

In general, these results provide a better distinction between AC mixes. On the other hand, Figures 4.11 and 4.12 present the results from a low-rate fracture test conducted at 6.25 mm/min (0.25 in/min). At that displacement rate, no clear trend was observed. It was generally observed that the fracture energy values at higher displacement rates produced higher fracture energy for all mixes at 25°C (77°F) and the results obtained at higher rates appeared to be more consistent when the changes in mix design characteristics were considered.

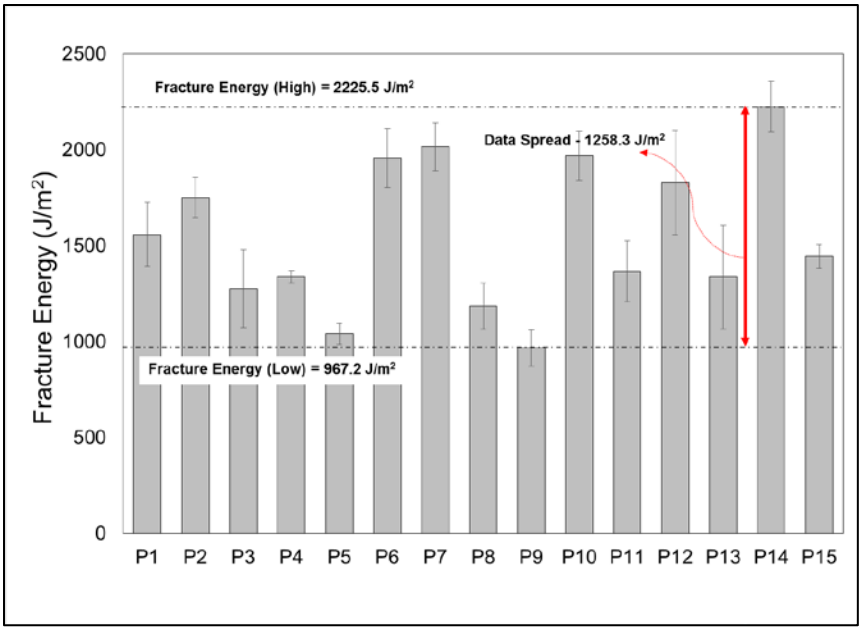

Figure 4.9 Intermediate-temperature (25°C [77°F]) SCB results for plant AC mixtures tested at a 50 mm/min (2 in/min) displacement rate.

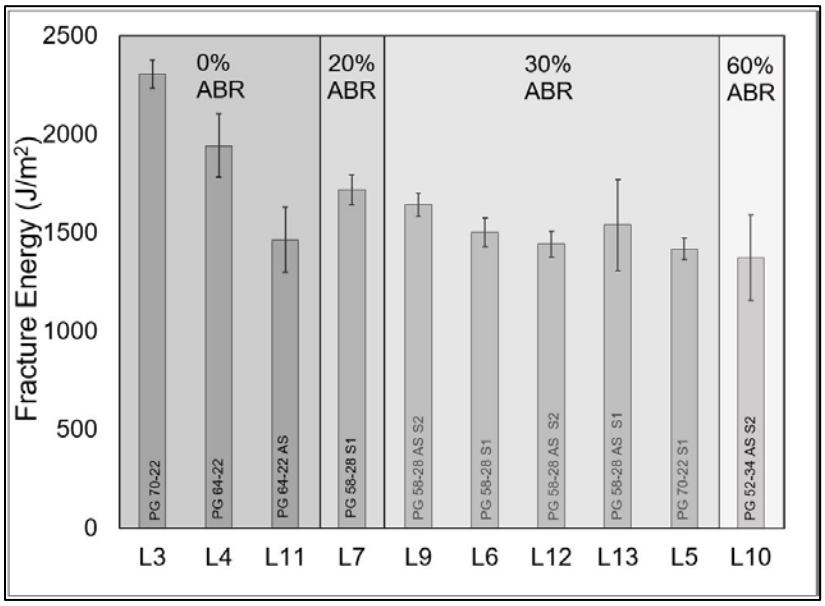

Figure 4.10 Intermediate-temperature (25°C [77°F]) SCB results for laboratory mixtures tested at a 50 mm/min (2 in/min) displacement rate.

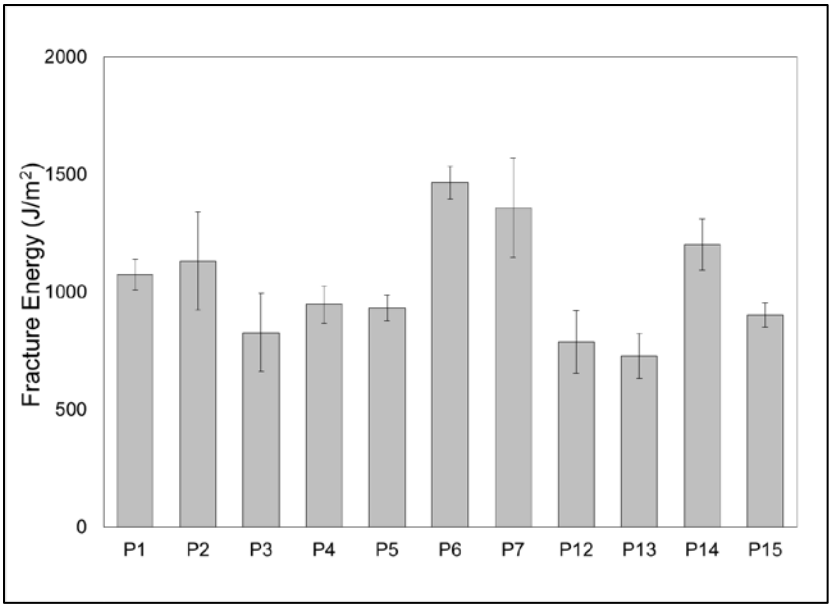

Figure 4.11 Intermediate-temperature (25°C [77°F]) SCB results for plant mixtures tested at a 6.25 mm/min (0.25 in/min) displacement rate.

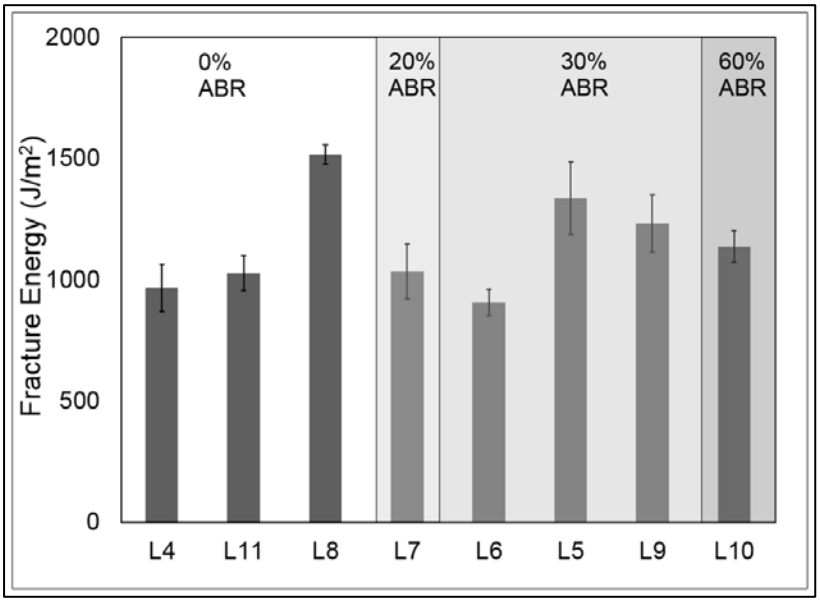

Figure 4.12 Intermediate-temperature (25°C [77°F]) SCB results for laboratory mixtures tested at a 6.25 mm/min (0.25 in/min) rate.

Table 4.1 presents a summary of fracture tests conducted at multiple displacement rates for laboratory mixes. In general, fracture energy increased with increased loading rate, although the level of increase is mixture dependent. Plant AC mixtures showed the same behavior (Appendix G). The coefficient of variation (COV) was generally less than 10% at all rates for each fracture energy and strength demonstrating that very good repeatable results could be obtained using the IL-SCB test method. Statistics presented here for the SCB tests were calculated using minimum three replicates of SCB test specimens.

Table 4.1 Summary of SCB Fracture Test Results Conducted at Intermediate Temperature (25°C [77°F]) at Two Loading Rates

Mix #	Intermediate-Temperature SCB (25°C) at 6.25 mm/min				Intermediate-Temperature SCB (25°C) at 50 mm/min			
	G_{fa} (J/m^2)	COV (%)	f_t (MPa)	COV (%)	G_{fa} (J/m^2)	COV (%)	f_t (MPa)	COV (%)
L3	—	—	—	—	2307	3	0.37	1.79
L4	966	2	0.16	6	1944	8	0.37	16.40
L5	—	—	—	—	1418	4	0.48	7.23
L6	908	13	0.25	3	1503	5	0.51	18.90
L7	1034	13	0.18	2	1718	4	0.36	4.58
L8	1518	8	0.29	7	2019	6	0.50	1.37
L9	1233	4	0.26	2	1642	4	0.44	4.29
L10	1138	6	0.35	4	1374	16	0.56	12.03
L11	1027	6	0.15	1	1465	11	0.33	27.29
L12	944	3	0.24	5	1442	5	0.39	3.78
L13	991	16	0.27	8	1541	15	0.50	7.59

[1] Tensile strength (f_f) is calculated using the equation: $f_t = {}^{P}/_{2rt}$ (P: load, r: radius, t: thickness)

4.3 CORRELATION TO FATIGUE RESULTS AND STATISTICAL ANALYSIS TO DISCRIMINATE PERFORMANCE

Among the criteria considered in the selection of the SCB test method and parameters is correlation to other independent tests and engineering intuition. To determine whether these criteria are satisfied, a group of AC mixes was selected to compare fatigue performance using the TOL and SCB fracture test results. Statistical analysis was conducted to evaluate the capability of each test and establish an independent ranking.

The results, shown in Table 4.2, indicate a positive correlation between intermediate-temperature (25°C [77°C]) SCB fracture tests and TOL in identifying the material demonstrating the best and worst performance (A and B). Because of the spread in test data, the SCB fracture test resulted in three groups (A, B, and C) with statistically significant differences when loaded at 6.25 mm/min (0.25 in/min) and four groups (A, B, C, and D) when loaded at 50 mm/min (2 in/min).

From Table 4.2 it can be seen that the intermediate-temperature SCB test method and the TOL test are correlated at their performance extremes. P6 and P7, the better-performing AC mixtures, are placed in the higher-performance subsets in both testing methods. Additionally, the lower-performing

AC mixtures, such as P5, are consistently placed in the lower-performance subsets in both test methods.

Table 4.2 Summary of Statistical Ranking Results for the Texas Overlay and SCB Test at Two Displacement Rates at a Significance Level of 0.10

Mix #	RAP/RAS (%)	Texas Overlay		SCB at 25°C and 6.25 mm/min		SCB at 25°C and 50 mm/min	
		Grouping at α = 0.10*	Cycles to Failure	Grouping at α = 0.10	Avg. G_{fa} (J/m^2)	Grouping at α = 0.10	Avg. G_{fa} (J/m^2)
P1	50/3.5	B	305	B/C	1073	B/C	1473
P2	27/0	B	212	A/B/C	1131	A/B/C	1576
P3	26/0	B	431	C	827	C/D	1209
P4	46.5/0	B	416	C	946	C/D	1314
P5	10/0	B	291	C	933	D	952
P6	10/0	A	669	A	1466	A/B	1852
P7	0/0	A	1000	A/B	1359	A	1948

* α = 0.10, means the rejection region comprises 10% of the sampling distribution

In light of the larger and more meaningful data spread presented by the intermediate-temperature SCB test method, its correlation to qualitative fatigue tests, and its applicability, it was concluded that this test method can be used to distinguish AC mixes for their cracking potential. However, additional analysis of SCB test results could further improve its reliability and prediction accuracy.

4.4 FINE-TUNING THE IL-SCB TEST

The IL-SCB test method was developed to calculate significant parameters from the SCB test method and later drafted as a provisional AASHTO specification. The same calculation method was applied for all tests conducted at intermediate temperatures. Appendix K presents the AASHTO test method specifications and the calculation procedures for fracture energy and other significant parameters.

In the development of the test method, the following additional considerations were taken into account.

- Robustness of fixture and compliance in recording actual specimen deformations
- Existence of other dissipation mechanisms that might affect calculated fracture energy (discussed in Appendix H)
- Effect of specimen geometry on the load-displacement curve (discussed in Appendix I)
- Specimen conditioning method
- Repeatability of the selected displacement rate

4.4.1 Effect of Fixture and Machine Compliance

The displacement measurements used for the IL-SCB fracture tests conducted in this project differ from the method described in the AASHTO TP 105-13 specification for the computation of fracture

energy. The specification recommends measuring displacements with two load-line displacement (LLD) gauges attached to gauge points on the front and the back of the specimen, with the gauges being aligned with the notch and placed 44.5 mm (1.75 in) from the bottom of the specimen. In the remainder of this section of the report, this measurement will be referred to as the AASHTO displacement. The measurements of the loading head displacement relative to the load frame with LLD gauges, will be referred to as loading head displacement.

The DIC technique was used to compare the two methods by measuring the displacement of DIC gauges at the surface of the specimen. The digital DIC gauges are representing the zones at the surface of the specimen where the displacement is averaged. The DIC gauge measuring the AASHTO displacement is positioned where the gauge point should be for this method, while the DIC gauge for the loading head displacement is positioned directly under the loading head (Figure 4.13). The displacements measured through DIC were used to obtain the load-displacement curves and compare them to a load displacement obtained directly from the machine (Figure 4.14).

The curves in Figure 4.14 show that the two measurements with the DIC are almost exactly the same. There are some minor differences from the measurements recorded with the load frame; those differences were probably due to the compliance of the machine. The results show that the loading head displacement method provides results similar to the AASHTO method. However, the AASHTO method has some drawbacks: it requires gauge points that can be on the crack path and cause measurement issues, which are problems that do not occur with loading head measurements.

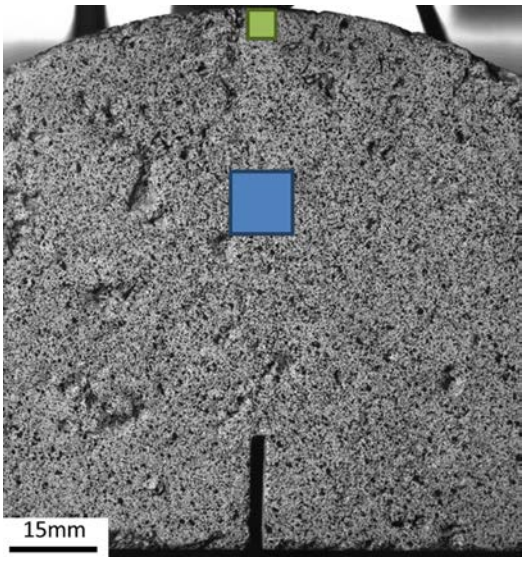

Figure 4.13 Location of the DIC gauges on the IL-SCB specimen (green box = loading head displacement; blue box = AASHTO displacement).

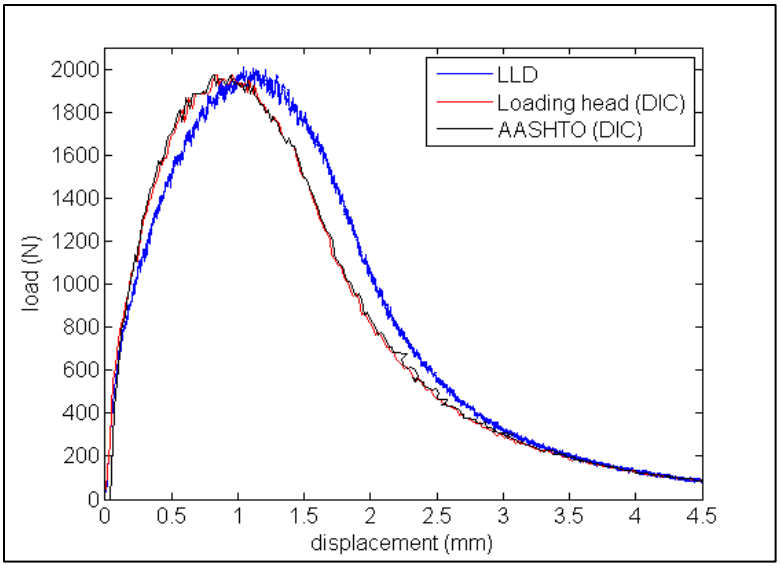

Figure 4.14 Comparison of load-displacement measurements (blue line = loading head displacement measured by the load frame; red line = DIC loading head measurements; black line = DIC AASHTO measurements).

4.4.2 Other Dissipation Mechanisms

Asphalt concrete mixture is a viscoelastic and sometimes viscoplastic material producing displacements that cannot be recovered permanently or during the testing period. This may result in energy dissipation other than in the actual fracture processes. Therefore, energy dissipation related to the viscoelastic mechanism away from the fracture process (bulk dissipation in the far-field zones) and under the loading head was explored. The effects of the two mechanisms of energy dissipation on total fracture energy are discussed in Appendix H. Numerical simulations and DIC measurements suggest that far-field zones and zones under the loading head do not have a significant contribution to the total energy calculated as fracture energy.

4.4.3 Selection of Temperature Conditioning Method

Even at the proposed temperature of 25°C (77°F), there is still a need for a conditioning method to ensure a consistent testing temperature. A study was conducted to examine various methods of temperature conditioning. Three methods were explored: water-bath conditioning, oven conditioning, and chamber conditioning.

Water-bath conditioning was conducted in accordance with (AASHTO T 283). Specimens were submerged in a water bath at a specified temperature of 25°C (77°F) for 2 hr and then tested under the intermediate-temperature IL-SCB fracture test. Oven conditioning was conducted by placing specimens on trays into AC mixing ovens set to a temperature of 25°C (77°F). Specimens were monitored with temperature gauges until the gauges indicated that the desired temperature of 25°C (77°F) had been reached. The specimens were then tested under the intermediate IL-SCB fracture test. Test chamber conditioning was conducted by conditioning the specimens in an Interlaken environmental chamber. The test chamber temperature was set to 25°C (77°F), and specimens were conditioned until a temperature gauge reached a temperature of 25°C (77°F). Specimens were then tested under the intermediate-temperature IL-SCB test method. Test results are shown in Figure 4.15 and statistically analyzed in Table 4.3. No significant difference seems to be apparent between the

three different conditioning methods. Most of the load-displacement curves fall on top of each other, and any deviations can be attributed to test variability.

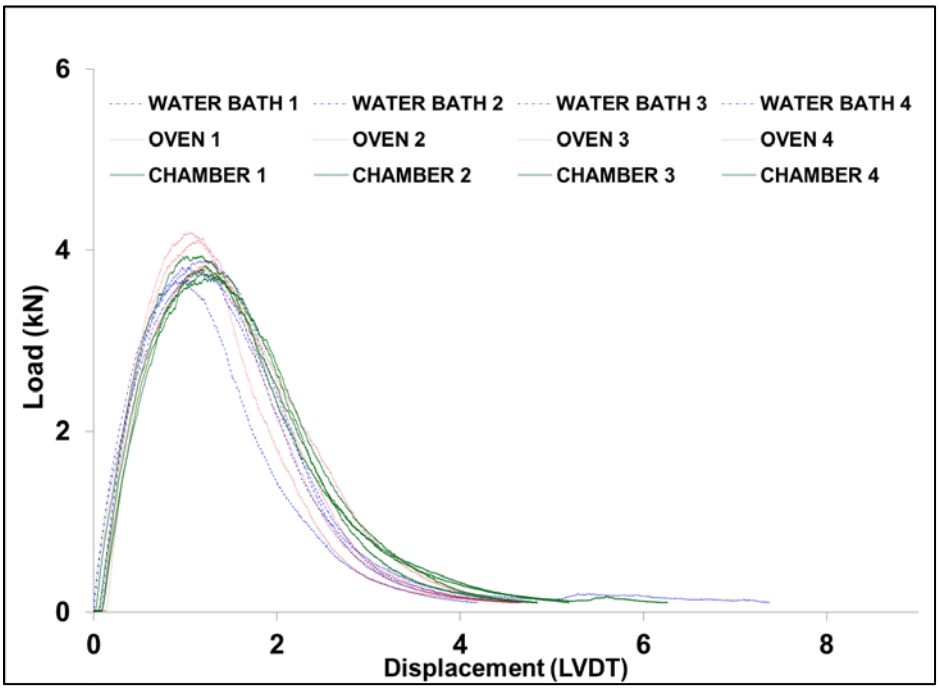

Figure 4.15 Load-displacement curves for specimens tested after three different conditioning methods.

Table 4.3 Statistical Summary for Various Temperature Conditioning Methods Explored Prior to Intermediate-Temperature IL-SCB Testing

Conditioning Method	Replicate ID	COV of Fracture Energy (%)	COV of Strength (%)
Water Bath	T4-B-1	7.8	13.3
	T4-B-2		
	T4-T-1		
	T4-T-2		
Oven	T2-B-1	4.8	6.2
	T2-B-2		
	T2-T-1		
	T2-T-2		
Chamber	T1-B-1	3.3	2.4
	T1-B-2		
	T1-T-1		
	T1-T-2		

4.4.4 Repeatability

Repeatability of the test methods for the fracture energy was explored at varying rates. One of the criteria for the selection of rate is repeatability. According to the results of AC mixes tested at multiple rates, average coefficients of variation are 11.3%, 8.6%, and 9.2% for 6.25, 25, and 50 mm/min (0.25, 1, and 2 in/min) rate tests, respectively, as shown in Figure 4.16. Accordingly, it was concluded that low and high displacement would result in comparable repeatability for the fracture energy. It must be noted that these tests were conducted before the IL-SCB was completely fine-tuned. In addition, some of the mixtures with relatively high COV could not be repeated due to material unavailability.

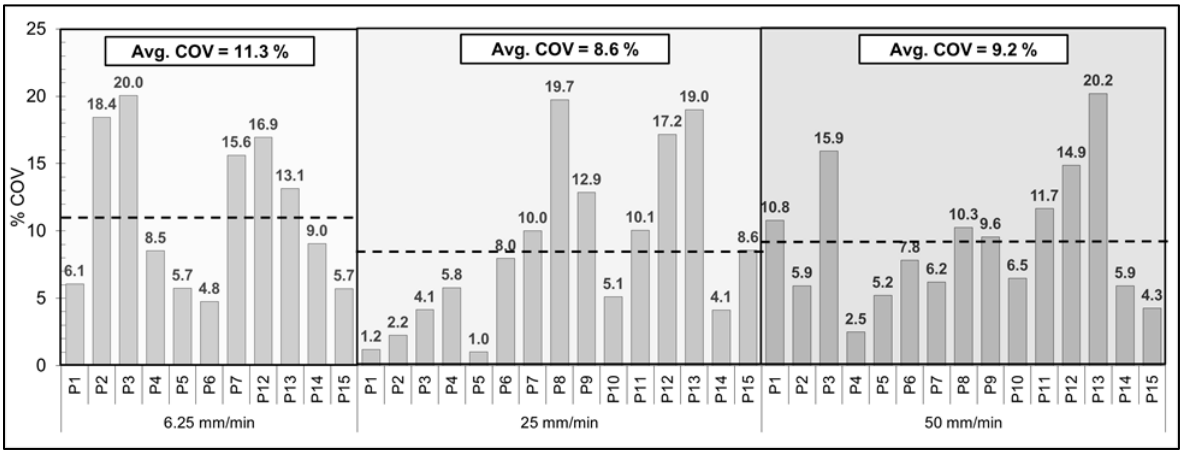

Figure 4.16 Average coefficient of variation for fracture energy using IL-SCB test at testing rates of 6.25, 25, and 50 mm/min (0.25, 1, and 2 in/min).

Figure 4.17 illustrates the coefficient of variation for fracture energy of plant- and laboratory-produced AC mixtures that were introduced in the latter stages of the project. These tests were conducted at a displacement rate of 50 mm/min (2 in/min). It can be seen that there is a significant reduction in the coefficient of variation for both plant- and laboratory-produced mixtures as the test method became more streamlined. Average coefficient of variation for fracture is less than 10% confirming that the displacement rate of 50 mm/min (2 in/min) could produce repeatable test results.

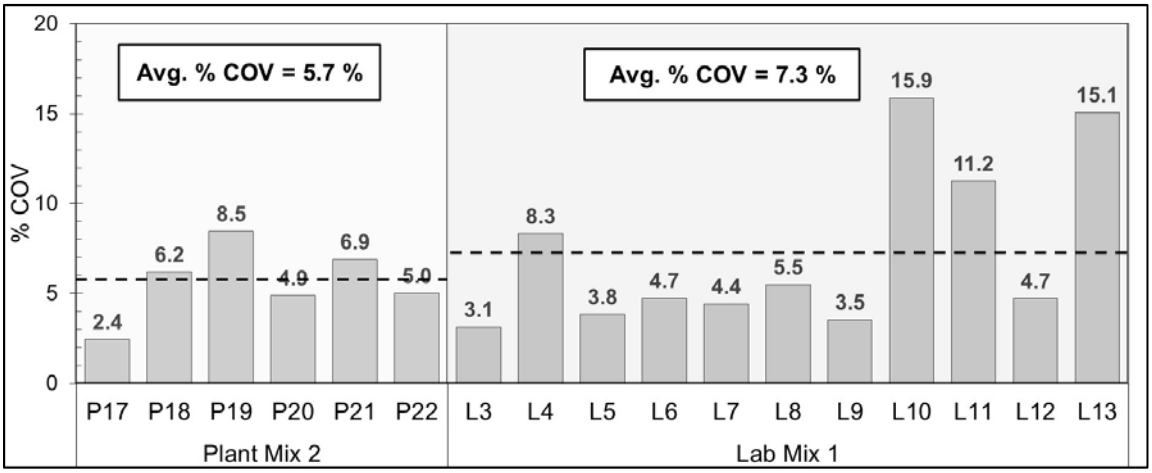

Figure 4.17 Average coefficient of variation for fracture energy of plant- and laboratory-produced AC mixes using IL-SCB test at 50 mm/min (2 in/min).

4.5 SELECTION OF FINAL TEST METHOD DISPLACEMENT RATE

Based on multi-temperature and rate testing conducted using the SCB test geometry, it was concluded that 25°C (77°F) is the testing temperature most consistent with the objectives of the study.

The second issue to address was selection of displacement rate. Selection of a specific displacement rate must accomplish the following:

- Sufficient repeatability with acceptable coefficient of variation
- Future potential for running on a standard, commonly available load frame with some hardware and software modifications
- Accommodation of a wide spectrum of AC mixtures with varying stiffness
- Proper distinction between different AC mixtures
- Minimized testing time

The selected displacement rate must contribute to distinguishing between various AC mixtures because that is the ultimate objective of the testing specification. The higher the displacement rate, the more brittle the behavior of the material. Low displacement rates might not initiate cracks for some ductile materials exhibiting excessive creep and relaxation. Hence, the selected displacement must not cause the material to fail catastrophically but still allow crack initiation and propagation. Because the brittleness of AC materials can differ, the selected displacement rate must provide a sufficient soft failure to allow stability during failure. At a testing temperature of 25°C (77°F), the displacement rate of 50 mm/min (2 in/min) was determined to be appropriate when testing, wide variety of mixtures in this project.

On the basis of the results presented in Section 4.2, the displacement rate of 50 mm/min (2 in/min) was shown to produce a higher data spread between different AC mixtures. It was also shown that adequate repeatability could be achieved for the rate of 50 mm/min (2 in/min). Additionally, the selected displacement rate must be as fast as possible to ensure reasonable testing time but also to help avoid excessive creep and relaxation during the load application. Because the final objective is to run the developed test on a standard load frame, any displacement rate selected must be accommodated by an existing load frame. A standard tensile strength ratio (TSR) load frame operates at 50 mm/min (2 in/min). Thus, the SCB test can be performed using existing equipment. It is clear that the 50 mm/min (2 in/min) displacement rate is best suited for the purposes of this project.

4.6 SUMMARY

It was determined that low-temperature fracture testing was not sufficient for distinguishing between AC mixtures; hence, testing at 25°C (77°F) was explored. Test results at this temperature are capable of distinguishing between different AC mix designs and identifying potential performance. Multiple displacement rates were explored at 25°C (77°F). A displacement rate of 50 mm/min (2 in/min) was found to be the optimum and was selected to maximize distinction between AC mixtures, accommodate common load frames, and expedite testing time.

Finally, the validity of the IL-SCB test method was verified showing that loading head displacement control could be used and produce repeatable test results. No sign of loading head damage was observed. The test method yielded fracture energy results discriminating the performance of laboratory- and plant-produced mixes. In addition, the fracture energy obtained from the IL-SCB test method showed good correlation with a qualitative fatigue test (TOL).

CHAPTER 5: DEVELOPMENT OF IL-SCB TEST METHOD AND FLEXIBILITY INDEX

5.1 INTRODUCTION

It was shown in Chapter 4 that low-temperature fracture testing is unreliable for distinguishing between different AC mixtures. However, fracture testing at an intermediate temperature (25°C [77°F]) provides the desired distinction.

The intermediate-temperature IL-SCB testing was conducted at a displacement rate of 50 mm/min (2 in/min), although in some cases, fracture energy was not sufficient as the sole parameter to distinguish between AC mixtures. For example, Figure 5.1 illustrates a comparison of two mixes (control with no recycled materials and the same mix with 30% ABR using 7% RAS) tested at 50 mm/min (2 in/min) at a temperature of 25°C (77°F). The fracture energy values of the two AC mixes were nearly identical; however, the mixes had distinctive load-displacement characteristics that may significantly differentiate their cracking response. Hence, it was evident that fracture energy alone cannot be used to discriminate between the two AC mixes.

This conclusion can be attributed to the nature of the fracture energy parameter. Depending directly on the shape of the load-displacement curve, the fracture energy is a function of both the strength (defined by peak load) and ductility (defined as the maximum displacement at the end of the test) of the material. If the material displays a high peak load, it may compensate its fracture energy for the lack of ductility in the post-peak region of the load-displacement curve. This is a potential explanation for why brittle AC mixtures with high amounts of recycled content may display similar or sometimes higher fracture energy values than their counterparts with no recycled materials.

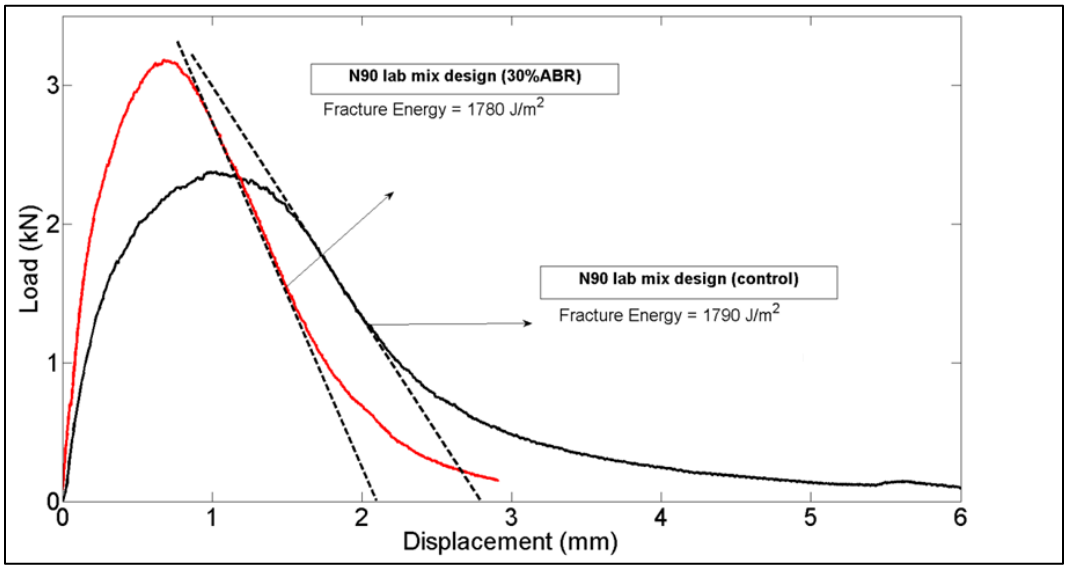

Figure 5.1 Major characteristics derived from load-displacement curves from IL-SCB tests conducted at 25°C (77°F) and at 50 mm/min (2 in/min) displacement rate illustrating the potential effects of ABR.

5.2 DEVELOPMENT OF A FLEXIBILITY INDEX

There is a need to develop a parameter that can describe the fundamental fracture processes and overall patterns of load-displacement curves (Figure 5.2) and can determine the cracking potential of AC mixes. The primary underlying mechanism that causes changes in the load-displacement curve in a fracture test can be attributed to the size of fracture process zone. The size of the fracture process zone in which microcracking and/or void formation takes place is a characteristic of the material and is determined by the inhomogeneities in the microstructure (maximum aggregate size, shape, distribution of aggregates, matrix volume, and properties). In general, the size of this zone is correlated to the brittleness of material and strongly governs fracture behavior. As the zone grows, the load-displacement curve becomes “bulkier”—reflecting an increase in fracture energy.

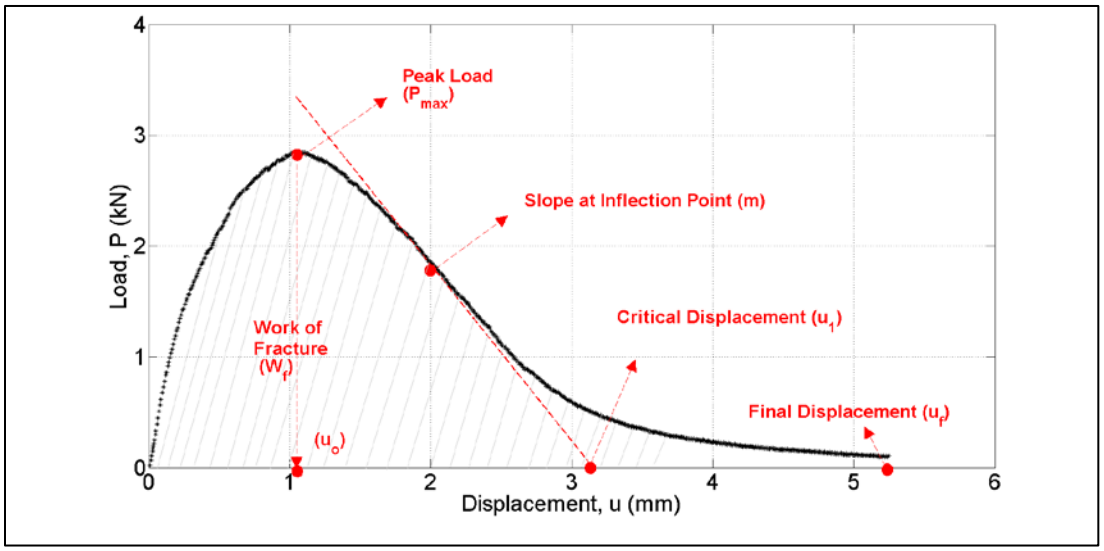

Figure 5.2 A typical outcome of the IL-SCB test illustrating the parameters derived from the load-displacement curve, including peak load (could be related to tensile strength), critical displacement, slope at inflection point, displacement at peak load, and fracture energy.

In addition, it can be hypothesized that the process zone and, consequently, any index parameter derived from it, will have an impact on crack propagation speed. As the material becomes more brittle, the speed of crack propagation increases. Therefore, the parameters that might have an influence on the formation of the fracture process zone were considered in the development of the flexibility index (FI).

From the load and displacement history recorded from the IL-SCB test, the following parameters of interest can be extracted:

- Fracture energy (G_f) calculated from work of fracture (W_f) using the Equation 3.1 introduced in Chapter 3
- Peak load (P_{max})
- Critical displacement (u_1)
- Displacement at the peak load (u_o)
- Displacement at the end of test (u_{final})
- Slope at inflection point (m)

The fracture energy is calculated as the area under the load-displacement curve divided by the area of crack propagated during the SCB test. The critical displacement-related parameters are calculated using the following procedure: the inflection point is determined on the curve after the peak point, and the tangential slope is drawn at the inflection point. The intersection of the tangential slope with the x-axis yields the critical displacement value. Critical displacement and slope are related to the ability of the mix to resist crack propagation. For example, the higher the value of critical displacement, the more ductile the AC mix.

Empirical correlations between candidate indices and the speed of crack propagation (or approximate crack propagation velocity) were obtained from the IL-SCB experiments. The form of the index parameter was inspired by the rate of crack growth definition provided by Bazant and Prat (1988) for concrete materials to explain the effect of temperature and humidity on crack growth at a reference temperature.

$$\dot{a} = v_c(\frac{G}{G_f})^{n/2} \tag{5.1}$$

where v_c is a constant, G is energy release rate ($G = K_I^2/E$, where K_I is stress intensity factor), and *n* is a constant. Substituting:

$$\dot{a} = v_c \frac{1}{(EG_f)^{n/2}} (K_I)^{n/2} \tag{5.2}$$

The stress intensity factor is related to the geometry and loading, which can be assumed to be constant for the IL-SCB geometry; the other factors are proportional to material properties that can accelerate or decelerate crack growth. As fracture energy and modulus decrease or applied stress intensity increases, crack growth accelerates. An empirical correlation between brittleness (the inverse of flexibility) and crack growth is exploited to formulate the index parameter. Therefore, Equation 5.2 is generalized as follows and includes a function for the FI:

$$\dot{a} = \frac{1}{FI_o} (K_I)^{n/2} \tag{5.3}$$

where three versions of FI were considered in this study:

$$FI_I = {G_f}\Big/{abs(m)} \tag{5.4a}$$

$$FI_{II} = {G_f E}\Big/{(abs(m) f_t^2)} \tag{5.4b}$$

$$FI_{III} = G_f \tag{5.4c}$$

The FI could be a parameter representing process zone size or other property combinations with a good correlation to crack growth speed. In this study, because the test specimen geometry is kept fixed, the stress intensity factor is also assumed to be similar at least up to crack initiation as long as the changes in the crack front stress field are not dramatic between different materials.

5.3 CRACK VELOCITY CORRELATION

An approximate crack velocity is used as proxy for the speed of crack propagation in Equation 5.3. The approximate crack velocity was calculated directly from the experimental data by assuming a constant crack propagation speed. A comparison of the approximate crack velocity to the true velocity profile was done using the high-resolution CCD camera system, as shown in Figure 5.3.

The true crack velocity is calculated by tracking the crack position while it propagates for the first 20 to 25 mm (0.8 to 1 in) from its original position. It was observed that the true crack velocity obtained at the crack front increased with time and as the crack propagated. Among the materials compared (L4 and L5), acceleration of the crack was more significant as the material became more brittle.

Constant velocity profiles obtained directly from the specimen loading can be considered as a first order approximation for the true crack speed profile (Figure 5.3b). As expected, deviation from the true velocity profile becomes more significant for brittle materials with non-linear crack velocity profiles, as demonstrated in the case of L5 (N90-30). Approximate crack velocity is doubled as material becomes more brittle (L5).

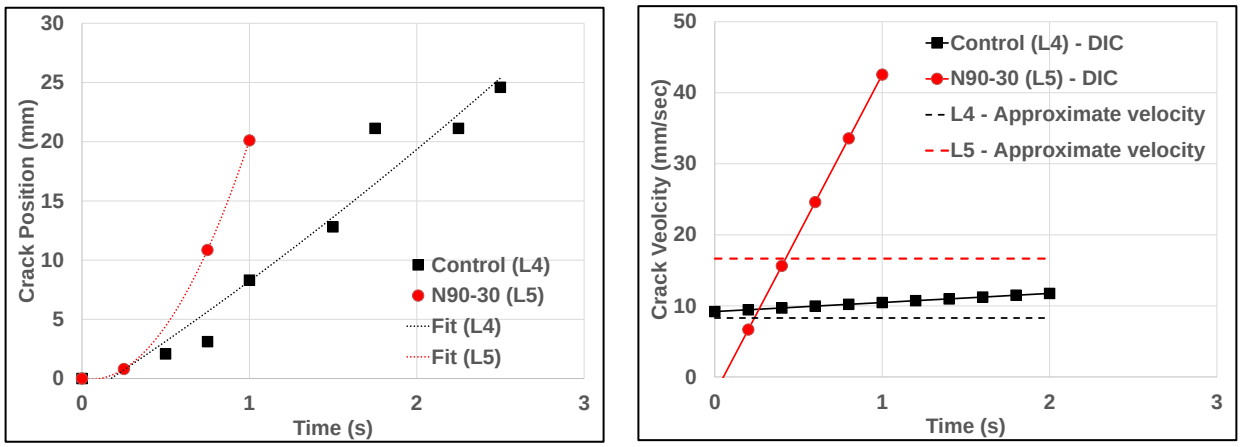

(a) (b)

Figure 5.3 A comparison of true crack profile of crack velocity (obtained from the DIC system) with the approximate crack velocity for tests conducted at 25°C (77°F) and 50 mm/min (2 in/min) and two different specimens (L4 and L5): (a) crack position obtained from the DIC system and polynomial fit; (b) true crack velocity obtained from crack position from DIC and approximate crack velocity directly obtained from the experimental data.

An empirical correlation between the approximate crack velocity and candidate FI parameters is shown in Figure 5.4. Among the parameters derived from the load-displacement curve, post-peak slope (m) appeared to be most sensitive to changes in testing conditions (loading rate and

temperature) and material characteristics and in good correlation with crack growth speed. Therefore, it is clear that correlation improved when slope (m) was used in the definition of the FI. In addition, this slope physically is an indication of how brittle a material is because a rapid unloading after crack initiation is related to a brittle response, while a gradual unloading indicates material ductility.

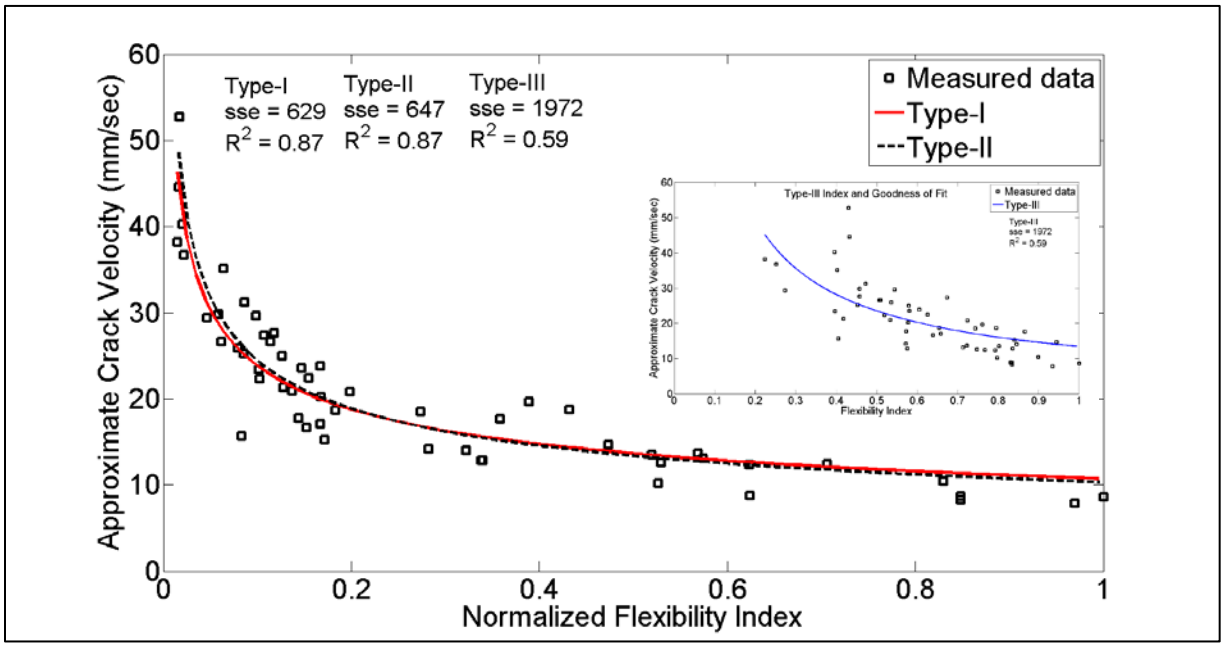

Figure 5.4 Correlation between normalized FI parameters (Types I, II, and III, corresponding to Equations 5.4a through c, respectively) and approximate crack velocity derived from IL-SCB tests conducted at 25°C (77°F) at 50 mm/min (2 in/min).

The form of the FI with fracture energy and post-peak slope (Type I in Figure 5.4) was chosen as the final form because of its simplicity, its physical relevance, and its good correlation to crack propagation growth. The final form of the FI proposed is presented in Equation 5.5. Coefficient A is a calibration coefficient for unit conversions and possibly field aging shift. Coefficient A was 0.01 for the plant- and laboratory-compacted AC mixes used in this study. However, that value may change for field specimens when aging and field compaction are considered.

$$FI = A \times {G_f}\Big/_{abs(m)} \tag{5.5}$$

The FI, along with fracture energy and crack propagation speed for the laboratory design AC mixes, is shown in Figure 5.5, with the index normalized with respect to the control AC with PG 70-22. For example, when L4 is modified to L8 with the addition of 2.5% RAS, the FI can capture this modification, with a decrease in the index indicating brittleness. When L7 is modified to L6 with the addition of another 2.5% RAS, the index again captures this change. Similarly, when softer binder was used for AC mixes with 30% ABR, FI captured that change (L5 and L6)

The evolution of the FI with critical changes in the AC mix design characteristics is consistent and reflects the brittleness of the material observed in the load-displacement curves as well as the increase in crack propagation speed. A strong inverse correlation between crack velocity and the FI exists. Such a strong correlation does not exist with fracture energy which would, for example, rank

L6, L7, and L8 similar to—or even better than—L4, although the latter exhibits slower crack propagation speeds.

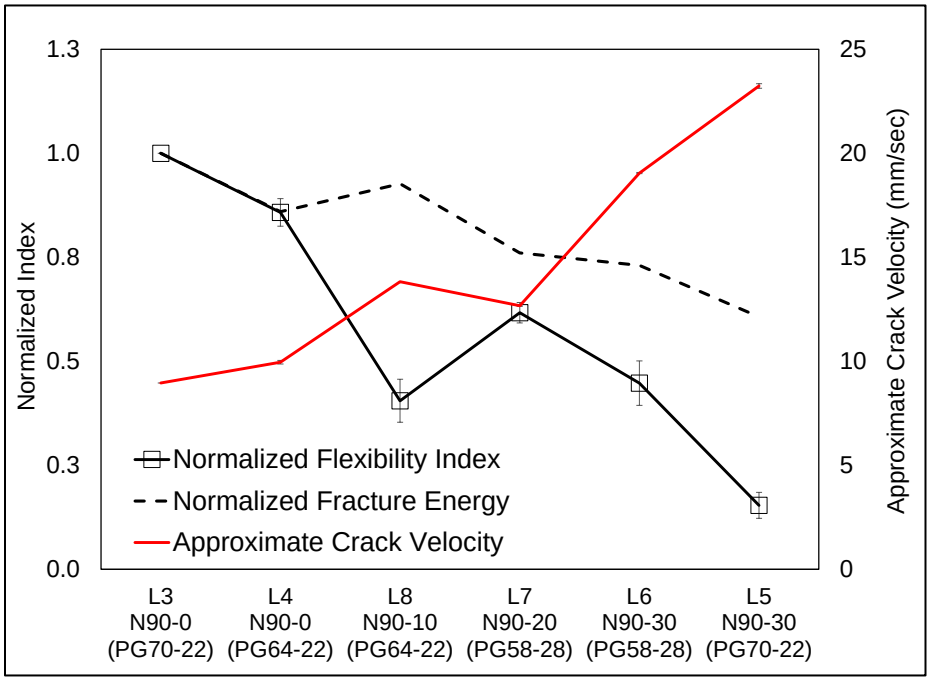

Figure 5.5 Normalized FI for laboratory design mixes (L3–L7) calculated at 25°C (77°F), illustrating the reduction in flexibility with changes in mix design characteristics and compared with approximate crack velocity and normalized fracture energy.

5.4 FLEXIBILITY INDEX TO DISCRIMINATE PERFORMANCE

This section presents results from various mixes to demonstrate how the FI can discriminate among mixes and as a means to discuss discrimination performance by comparing the FI and other test parameters using a statistical approach. The mixes presented in this section are as follows:

- Laboratory-produced mixes designed in this study (refer to Table 3.2 for mix design properties)
- Plant-produced mixes sampled in this study (refer to Tables 3.4 and 3.5 for mix design properties)
- Plant-produced mixes sampled as part of ICT Project R27-161 (refer to Table 3.6 for mix design properties)

5.4.1 Laboratory-Produced Mixes

The FI and fracture energy values are shown in Figure 5.6 for all of the laboratory mixes. The values are normalized with respect to the control mix with PG 70-22. The overall pattern seen with the FI is a consistent reduction trend with increasing ABR. The reduction is much more pronounced when it is compared with fracture energy values obtained at the same temperature. Some of the key findings from the comparison of FI values for various AC mixes are as follows (see Table 5.1 for details):

- The worst FI values belonged to L5 (N90, 30% ABR with PG 70-22) and L10 (N90, 60% ABR with PG 52-34).

- Mixes with similar ABR content and same binder type but different proportions of RAP and RAS (L6, L9, L12, and L13) had similar index values, also indicating that RAS source does not have a significant impact.
- The changes in the binder grade had clear impact on the FI values. For example, mixes with the same ABR and the stiffer binder [L5 (N90, 30% ABR with PG 70-22)] had significantly lower FI values compared with mixes having a softer binder [L6 (N90, 30% ABR with PG 58-22)].

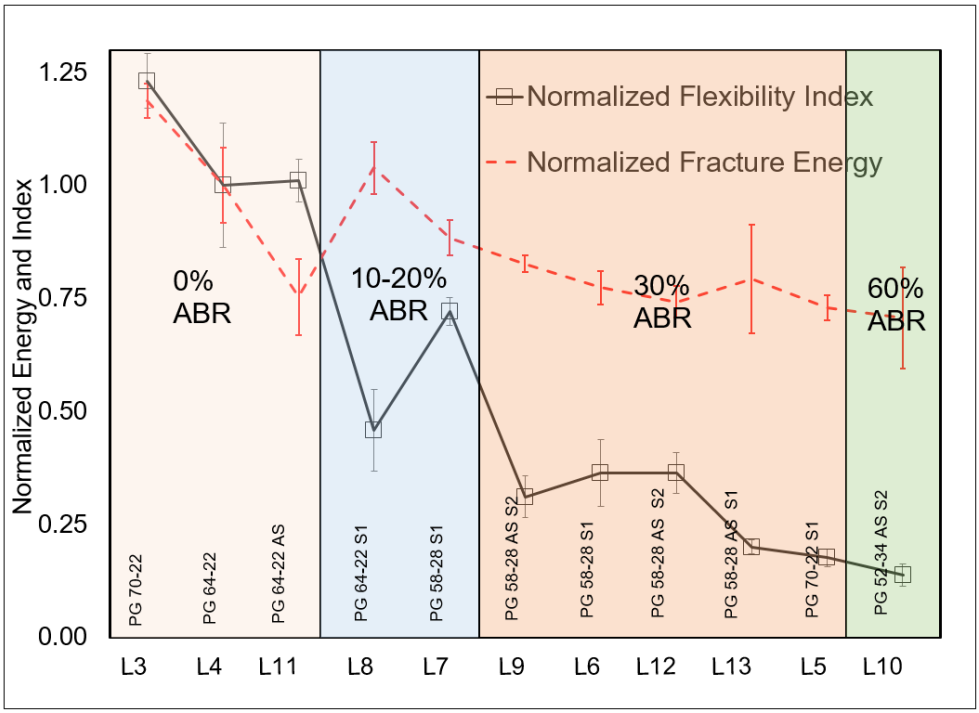

Figure 5.6 Normalized IL-SCB fracture energy and FI for AC laboratory mixes illustrating the changes in the FI and fracture energy as changes are applied to a parent mix design.

Table 5.1 Flexibility Index and Fracture Energy for the Laboratory-Produced AC Mixtures, Illustrating the Effect of ABR

	Binder Grade	ABR %	RAP %	RAS %	G_{fa} (J/m^2)	COV (%)	FI	COV
L3	70-22	—	—	—	2307	3	16	5
L4	64-22	—	—	—	1944	8	13	14
L5	70-22	29.8	—	7	1418	4	2	11
L6	58-28	29.8	—	7	1503	5	5	20
L7	58-28	21.2	—	5	1718	4	9	4
L8	64-22	10.5	—	2.5	2019	6	6	20
L9	58-28	30.5	11	5	1642	4	4	15
L10	52-34	60.8	40	7	1374	16	2	18
L11	64-22	—	—	—	1465	11	13	5
L12	58-28	30.6	—	7	1442	5	5	12
L13	58-28	29.8	—	7	1541	15	3	8

5.4.2 Plant-Produced Mixes

Figure 5.7 illustrates the results for some of the mixes evaluated using the FI. Mix P7 has no recycled content and has polymer-modified binder, whereas mixes P1 through P4 contain high levels of recycled binder. Mix P5 does not have significant recycled content; however, it ranked as the worst-performing material in the TOL and IL-SCB tests. According to the results obtained from these plant mixes, the proposed FI appears to rank mixes consistently and generates a greater separation between mixes to allow capturing nuances between mixes.

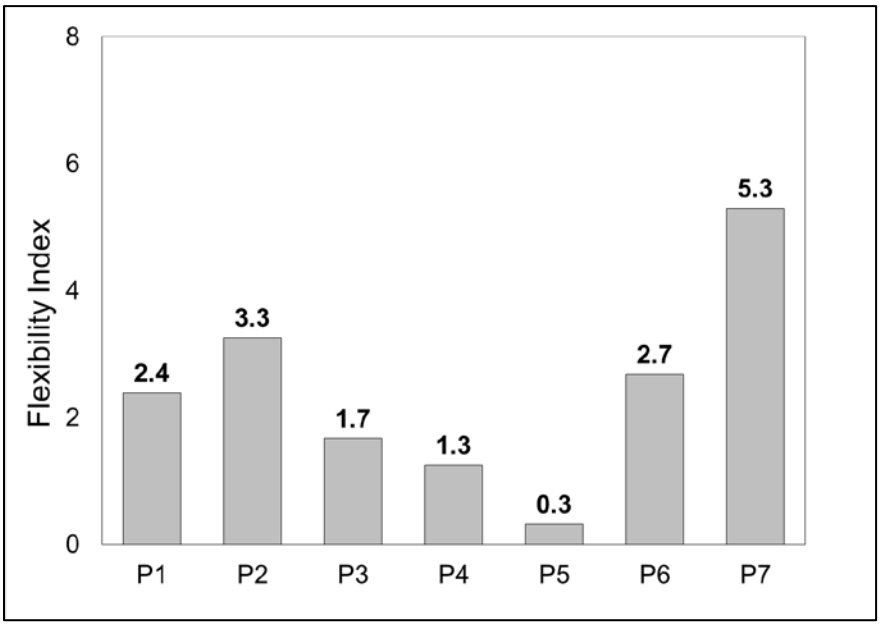

Figure 5.7 Flexibility index calculated for selected plant AC mixes.

5.4.3 Statistical Analysis to Evaluate Discrimination Potential

Statistical analyses were performed to evaluate the discrimination potential for the FI compared with other fracture parameters commonly used in the literature and discussed earlier in this chapter. Probability distribution curves were plotted to compare mixes with distinct characteristics being distinguished from each other using low- and intermediate-temperature fracture energy and the FI. This approach considers both the mean values and standard deviation of the selected fracture parameter.

5.4.3.1 Low-Temperature Fracture Energy (from the SCB and DCT)

The values obtained from the low-temperature fracture energy tests using the SCB and DCT geometries are used. Plant-produced mixes P8 through P15 were tested using both fracture test geometries. The probability distribution curves are shown in Figure 5.8 and illustrate how mean values are distributed, along with the standard deviation obtained from each mix. Although the SCB results show better distribution, the plots show a significant amount of overlap between AC mixes, indicating that they have similar cracking resistance (i.e., a very high probability).

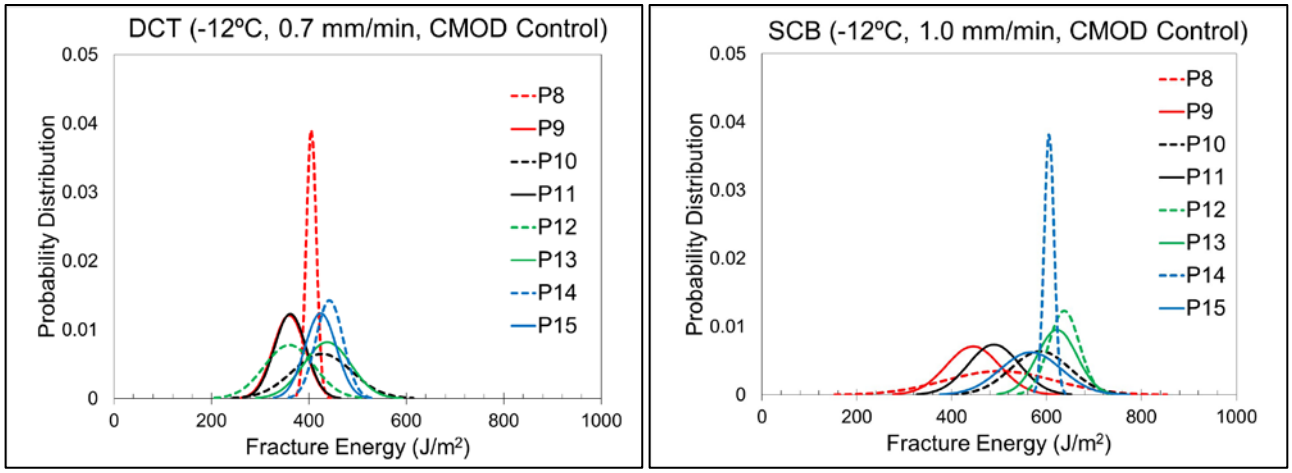

Figure 5.8 Comparison of probability distribution curves between low-temperature fracture tests.

5.4.3.2 Low-Temperature Fracture (DCT) and SCB Intermediate-Temperature Fracture Energy

A second comparison is shown for the low-temperature fracture energy obtained from the DCT and the intermediate fracture energy from the IL-SCB test. The same plant-produced mixes were used in the probability comparison (Figure 5.9). The plots indicate that the IL-SCB test has greater potential and likelihood for distinguishing these plant-produced AC mixes.

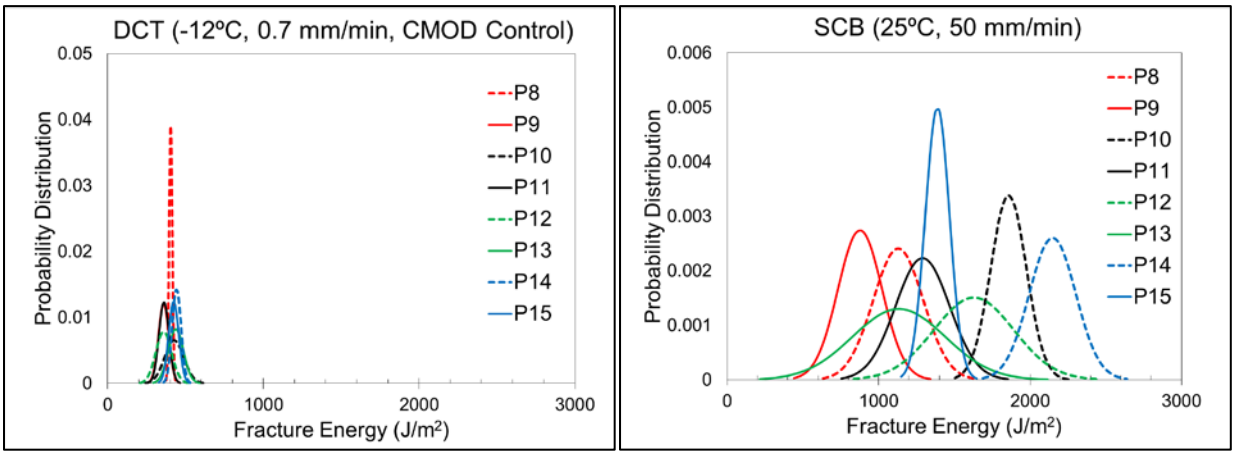

Figure 5.9 Comparison of probability distribution curves between low-temperature fracture DCT and IL-SCB fracture energy.

5.4.3.3 IL-SCB Parameters Including Flexibility Index and Fracture Energy

The discrimination potential of the FI is shown in Figure 5.10, which illustrates the results of comparisons with the fracture test parameters obtained from the SCB tests. Laboratory-produced AC mixes were used in the comparison of low-temperature fracture energy, intermediate-temperature fracture energy, and FI. The differences in each fracture parameter's discrimination potential is clearly shown by the contrasts in the overlap between each probability curve. Accordingly, it can be concluded that the FI has the greatest discrimination potential between the laboratory-produced AC mixes with increasing ABR and changing binder grade. There is low to no overlap between the AC mixes illustrated in the figure.

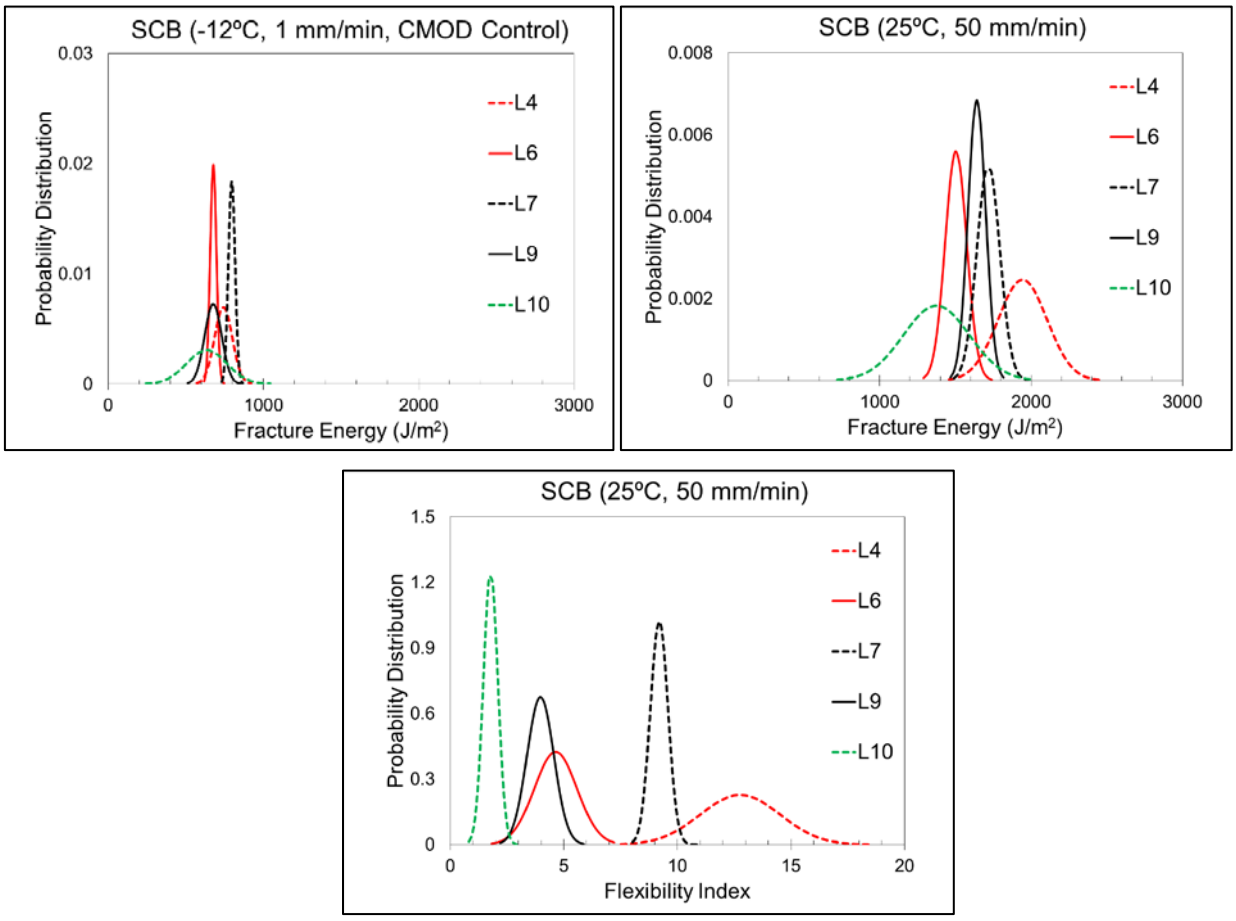

Figure 5.10 Comparison of SCB fracture energy parameters for discrimination potential.

Another important consideration is the coefficient of variation (COV) with the FI. Figure 5.11 shows the COV values for the FI. It was observed that the FI generally has a somewhat higher COV, which is expected because the FI is derived from the shape of the post-peak segment of the load-displacement curve characteristics, whereas fracture energy represents an average value derived from the same area under the same curve (e.g., an average integrated quantity). It is expected that the FI would be very sensitive to density changes in the specimen, operator variability, and other random material or equipment variability. According to the results presented in Figure 5.1, except for a few mixes, the COV values for FI are within the range of 10% to 20% at an average of 8.8% for the plant-produced mixes and 12% for the laboratory-produced mixes.

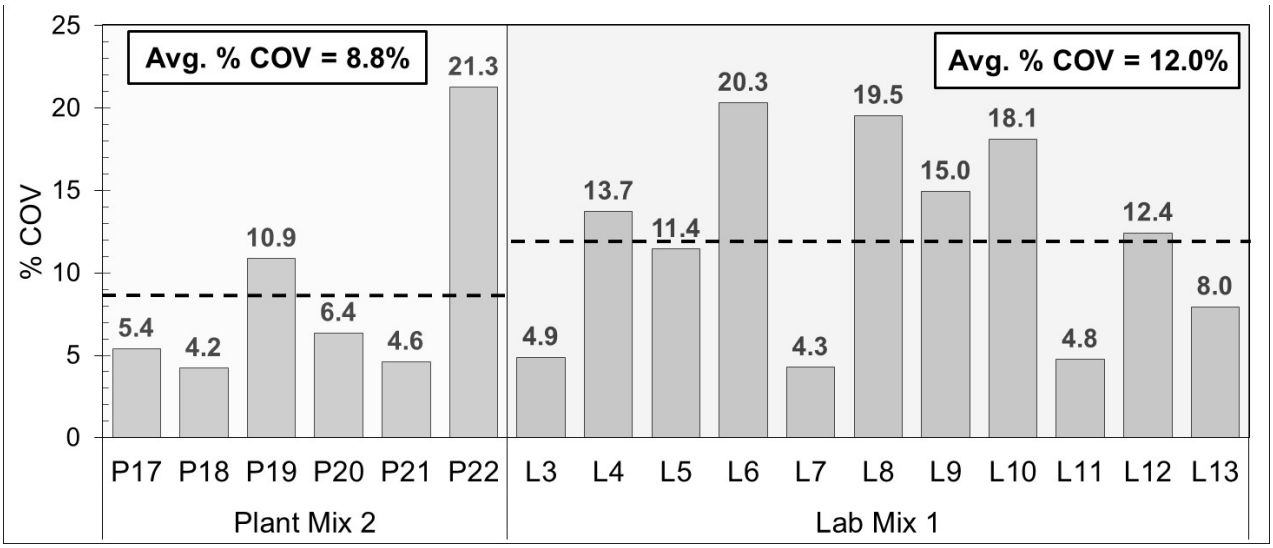

Figure 5.11 Coefficient of variation for the flexibility index obtained from various plant- and laboratory-produced AC mixes.

The results presented so far were calculated based on a minimum of three replicates and on occasion using IL-SCB specimens from two gyratory-compacted specimens that yielded more than four replicates. The current test method draft specification requires four specimens be obtained from one gyratory specimen. The COV can certainly be improved further by using additional test replicates that can be prepared from at least two gyratory-compacted specimens. Apart from improving repeatability, preparing more than one gyratory-compacted specimen would better represent the AC mixture characteristics. Air voids were measured for the gyratory-compacted specimens or individual slices (prior to preparing the IL-SCB test specimen) for the results presented so far. Another option to improve repeatability is to ensure target air voids for the test specimen. The IL-SCB specimens can be prepared using multiple gyratory-compacted specimens (minimum two), and a minimum of eight IL-SCB specimens can be obtained. After removing the outliers caused by air void variation, fracture energy, strength, and FI values can be calculated using a minimum of six IL-SCB specimens at the target air void.

5.5 SPECIMEN THICKNESS EFFECT

Fracture energy is a size-dependent property that changes with specimen geometry and with changing thickness, notch size, or radius for geometry. Hence, recommended specimen geometry and thickness should be followed. The effect of thickness variations on the IL-SCB test outcome was preliminarily investigated. Specimen thickness varied from 25 mm (1 in) to 62.5 mm (2.5 in). Figure 5.12 illustrates FI variation with thickness. The figure shows a decreasing trend when specimen thickness increased. Fracture energy also varied with thickness; however, the change was not statistically significant and/or as clear as the FI to establish a correction factor. Therefore, a simple correction factor for FI was developed; details are discussed in Appendix I.

$$FI_{50} = FI_t \times {}^{t}/_{50} \quad (5.6)$$

where FI_{50} is the corrected index using 50 mm (2 in) as reference thickness, FI_t is the index calculated for a specimen with average thickness I. Additional adjustments, which are the subject of an ongoing study, are needed to find the relationship between laboratory-produced, plant-produced and field core specimens.

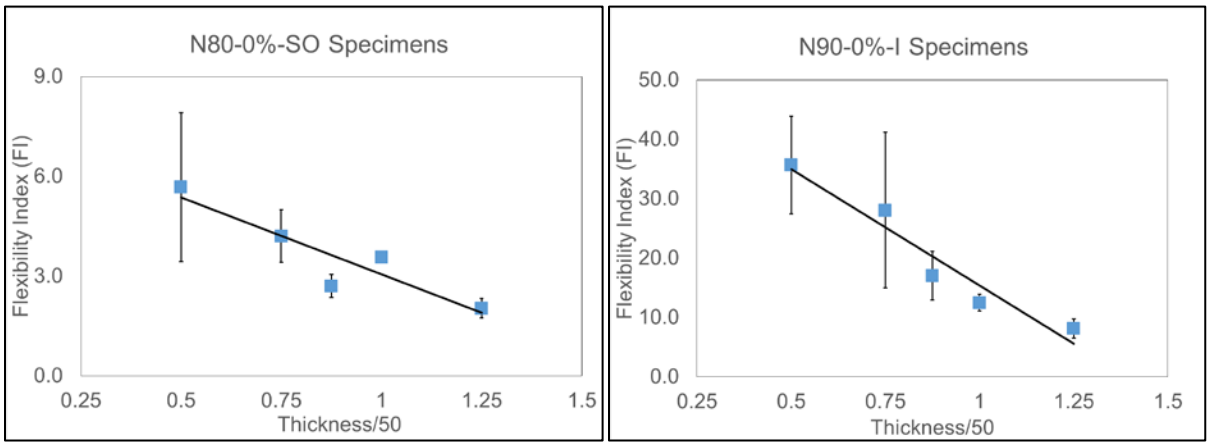

Figure 5.12 Flexibility index calculated for varying thicknesses of plant- and laboratory-produced AC mixtures.

5.6 AASHTO IL-SCB TEST METHOD SPECIFICATIONS

The outcome of this study was documented as a draft test method specification to enable characterization of an AC material's potential for overall damage caused by the mixture's increasing brittleness. An AASHTO provisional test specification was submitted to the AASHTO committee for consideration. Based on the votes of the members of the relevant committee, the ballot for the IL-SCB test method and FI was submitted to AASHTO for consideration as a provisional test specification. The AASHTO test specification is provided in Appendix K.

5.7 SUMMARY

This study introduced a practical test method and developed an index parameter to characterize fracture potential of AC mixes. The FI was introduced to identify the potential of AC mixes for development of cracking-related damage in the field. The formulation of the FI is consistent with fundamental fracture mechanics principles and displays a strong correlation to crack velocity.

The results of the tests using plant- and laboratory-produced AC mixes show that the FI captures changes in the AC mixtures better than a single fracture energy parameter. The ranking obtained using the FI is consistent with changes in mix volumetrics and independent test outcomes.

The variation in FI results is higher than that based on fracture energy alone. The average COV for fracture energy is 4.6% and that of the FI is an average of 10% to 15% for both the laboratory- and plant-produced AC mixtures.

A preliminary specimen thickness correction factor is proposed for the FI to adjust index values obtained from field core or laboratory-compacted specimens with thickness outside the acceptable range. An adjustment factor to relate laboratory-produced to plant-produced and field core specimens

will be developed in a future research project. This is a critical correction factor to determine corresponding thresholds for poor- and good-performing mix categories. Another adjustment that may be considered in the future is a correction factor for machine compliance because the IL-SCB tests may be conducted in different fixtures.

CHAPTER 6: IL-SCB VALIDATION USING FIELD PAVEMENT PERFORMANCE DATA

6.1 INTRODUCTION

This chapter presents data and analysis that correlate IL-SCB test results with field performance. The objective is to validate the concept of the FI to predict AC cracking and determine thresholds. Field validation was conducted using two types of data. These includes the correlation of the IL-SCB fracture energy and FI with the field performance of various pavement sections from nine IDOT districts using field cores. In addition, a correlation was established with pavement section performance under accelerated loading testing conducted at the FHWA Turner Fairbanks' Accelerated Loading Facility (ALF) in McLean, Virginia. Loose plant AC mixes were obtained and tested, and the resulting FIs were correlated to cracking in each section.

6.2 CORRELATION TO THE ACCELERATED PAVEMENT TESTING RESULTS

Results from the accelerated pavement test sections built at the ALF were correlated with the IL-SCB's FI values. The sections were built in 2013 to evaluate the impacts of recycled materials and warm-mix asphalt (WMA) production on fatigue cracking. All sections have the same structural design and base materials; only the AC layer differs. The specific objectives of the ALF experiment were to establish realistic boundaries for AC mixes with ABR content (RAP and RAS) and employ different WMA technologies. This experiment provides an opportunity to seek correlations with a mixture design test such as IL-SCB.

The sections were built with a 200 mm (8 in) granular aggregate base reconditioned from a previous experiment. The AC layers were constructed with two lifts: 50 mm (2 in) thick each, with a target total asphalt layer thickness of 100 mm (4 in). The AC mixes were 12.5 mm NMAS designed for 65 gyrations with a target asphalt binder content of 5%. Production mixes were sampled during construction to ensure air voids (4.0 ± 1%), VMA (between 14% and 16%), and in-place density between 92% and 94% of maximum theoretical density. Details of the pavement sections are presented in Table 6.1.

Table 6.1 Summary of the AC Mixture Designs from the FHWA's ALF Sections and Production Mixture Volumetrics (Carvalho et al. 2015)

	Mixture Design Properties					Production Volumetrics		
	Binder Grade	ABR (%)	RAP (%)	RAS (%)	WMA Technology	Production VMA (%)	Production Air Voids (%)	Average Layer Thickness (in)
Lane 1	PG 64-22	—	—	—	—	16.1	4.3	5.0
Lane 2	PG 58-28	40	44	—	Foaming	16.1	4.3	4.8
Lane 3	PG 64-22	20	—	6.3	None	14.6	3.3	4.5
Lane 4	PG 64-22	20	23	—	Chemical	15.6	4.4	4.9
Lane 5	PG 64-22	40	44	—	—	15.9	5.2	3.9
Lane 6	PG 64-22	20	23	—	—	14.9	3.6	5.0
Lane 7	PG 58-28	20	—	6.3	—	15.3	4.1	4.3
Lane 8	PG 58-28	40	44	—	—	16.4	4.9	4.6
Lane 9	PG 64-22	20	23	—	Foaming	15.1	3.7	4.0
Lane 11	PG 58-28	40	44	—	Chemical	16.5	4.9	3.9

Accelerated pavement testing was conducted in a temperature-controlled environment. The temperature was set to 20°C (69°F). A 425 super-single wide-base tire was inflated to 100 psi (689 kPa), and the wheel load was 14,200 lb (63 kN) traveling at a speed of 11 mph (18 km/h). Fatigue cracking was measured manually and periodically. Total crack length was recorded to measure the percentage of fatigue cracking in each lane. In addition, falling weight deflectometer (FWD) tests were conducted to backcalculate layer moduli to account for variability introduced by subgrade and/or base layers.

6.2.1 Laboratory AC Mixture Characterization

Loose mix samples were obtained from each section and tested using the IL-SCB test method. The objective of the tests was to validate the ability of IL-SCB's FI in predicting field performance. Standard procedures were followed to conduct the IL-SCB test. The results are shown in Table 6.2.

The AC mixes used in Lanes 3, 5, and 7 have the lowest fracture energy values (less than 2000 J/m^2). The next range of fracture energy values are within 2000 to 2300 J/m^2, for the materials collected from Lanes 4 and 8. The AC mixes collected from Lanes 1, 8, and 9 had the highest fracture energy values, in the range of 2300 to 2600 J/m^2. A similar but much clearer grouping can be observed based on the FI results. Lane 1 (control section) has the highest FI followed by Lanes 9, 4, and 8 in descending order. The FI for those three AC mixes ranges between 6.5 and 10.0. The results obtained from Lanes 3, 5, and 7 (FI < 2) show a clear separation of those AC mixes from the high-performing AC mixes. Lane 11 can be considered in an intermediate range, with am FI of 4.7.

Table 6.2 Summary of the IL-SCB Tests Performed for the Plant-Produced AC Mixtures Collected from the ALF Experiment Sections

Lane No.	G_f (J/m^2)	COV (%)	Strength (MPa)	COV (%)	FI	COV (%)
Lane 1	2394	4	0.44	11	9.9	18
Lane 2[1]	—	—	—	—	—	—
Lane 3	1861	12	0.68	11	1.5	19
Lane 4	2284	5	0.55	8	6.7	18
Lane 5	1967	8	0.83	7	1.4	8
Lane 6[1]	—	—	—	—	—	—
Lane 7	1425	12	0.55	10	1.8	14
Lane 8	2279	5	0.50	5	6.5	12
Lane 9	2435	11	0.58	1	7.3	6
Lane 11	2300	10	0.62	7	5.3	20

[1] Testing has not yet been completed for Lanes 2 and 6.

6.2.2 ALF Pavement Section Performance and Correlation to IL-SCB Test Results

Three major categories of performance could be established: Lanes 1 and 9 as the best-performing category, with cycles to failure greater than 250,000. Lanes 3, 5, and 7 are in the poor-performing category, with cycles to failure less than 40,000. It is clear from the ALF measurements that AC mixes with RAS (Lanes 3 and 7) have the worst performance along with the mix containing 40% ABR and PG 64-22 produced without binder grade bumping (Lane 5). The best-performing mixes are the control (Lane 1) and AC mixes with 20% ABR and WMA technologies and PG 64-22 binder (Lanes 9

and 4). The intermediate-performing group consists of the AC mixes with 40% ABR and PG 58-28 (Lanes 2, 8, and 11), which illustrates the significance of the binder grade bumping that improved the AC mixes' performance from poor to intermediate. Based on the structural analysis calculations, the AC mix with 20% ABR and PG 64-22 without any WMA technology (Lane 6) is predicted to be in that category.

Table 6.3 and Figure 6.1 show that the FI demonstrates very good correlation with the ALF performance measurements as well as the ranking predictions. The AC mixes that belong to the best-performing category (based on the number of measured cycles) have FI values greater than 6.7. Poor-performing AC mixes are clearly distinguished from the rest of the groups, with FI values of less than 2.0. The AC mixes in the intermediate-performing category have FI values of 4.7 (Lane 11) and 6.5 (Lane 8). There is clearly an overlap between the AC mixes, especially if they are at the lower end of the best-performing category or upper end of the intermediate-performing category.

It is important to note that IL-SCB's FI provides ranking solely based on AC mixture design characteristics. Although those sections were constructed to have similar structural capacity and AC mix characteristics, variability in construction was documented and may have affected the accelerated test performance. However, it is clearly shown by the good correlation between the IL-SCB test and ALF section performance rankings by FHWA that the IL-SCB is capable of distinguishing AC mixes' cracking performance and tracing the changes in the mixture design characteristics (the effect of ABR, RAP vs. RAS, binder grade bumping, and presence of WMA technology). These conclusions are consistent with the results obtained from the laboratory-produced mixes designed in this study and discussed in Chapter 5. These findings show that the IL-SCB's FI parameter has excellent prediction capabilities.

Table 6.3 Summary of ALF Performance Evaluation and Correlation to IL-SCB Results

Lane No.	G_f (J/m^2)	FI	Measured ALF Performance (Cycles to Fatigue Threshold)
Lane 1	2394	9.9	368,254
Lane 9	2435	7.3	270,058
Lane 4	2284	6.7	88,740
Lane 8[1]	2279	6.5	—
Lane 11	2300	5.3	81,044
Lane 2[1]	—	—	—
Lane 6[1]			—
Lane 7	1425	1.8	23,005
Lane 5	1967	1.4	36,946
Lane 3	1861	1.5	42,399

[1] Performance measurements for the ALF lanes were not available at the time of publication of this report.

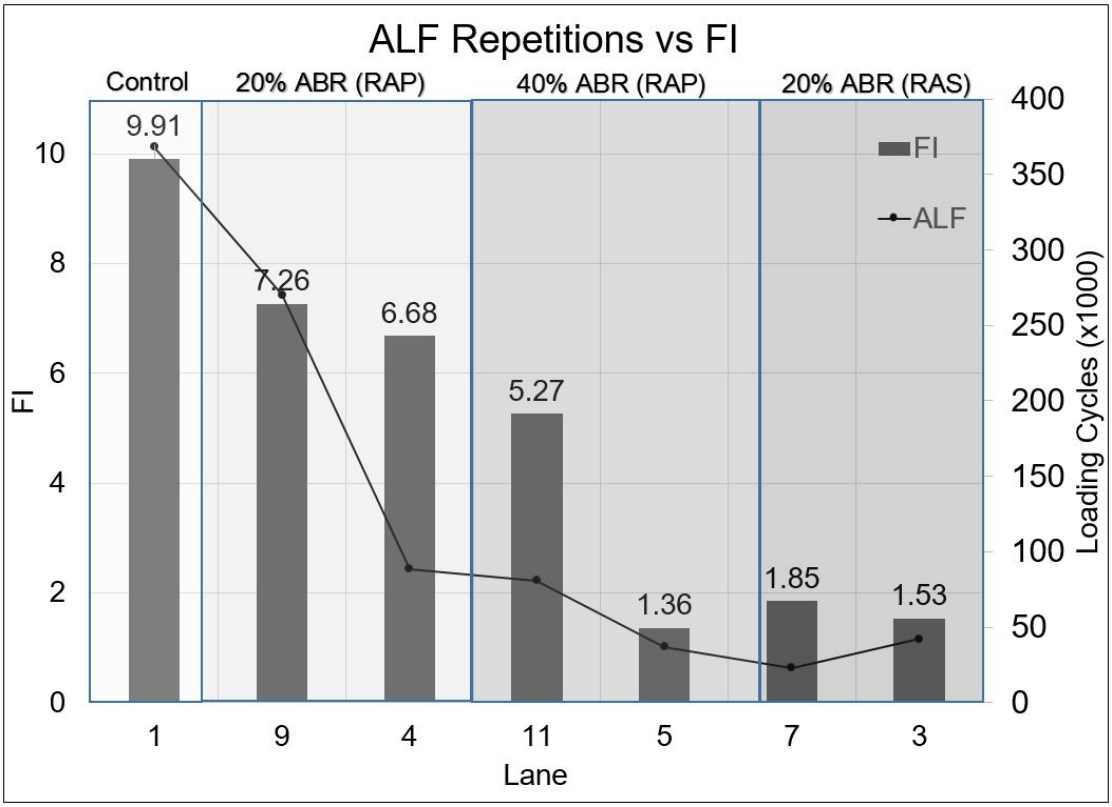

Figure 6.1 Correlation of the FI with accelerated testing fatigue cracking measurements recorded at FHWA's ALF facility.

6.3 FIELD PERFORMANCE AND FIELD CORE IL-SCB RESULTS

The field cores were acquired from 35 sections from nine IDOT districts. Six to eight cores were extracted from each section for this study. The top layer of each field core was carefully trimmed and fabricated to obtain the IL-SCB test geometry. The diameter of the field cores ranged from 143 to 147 mm (5.63 to 5.79 in), and the thickness ranged from 30 to 50 mm (1.2 to 2 in), the result of variation in section surface layer thickness. The notch length was 14 ± 1 mm (0.55 ± 0.04 in) to match the 0.1 diameter-to-notch ratio of the laboratory specimens.

The following pavement system information for each section was obtained from the districts: mix type, N-design, NMAS, construction year, mixture volumetric, recycled material content, binder type, binder content, and base layer and subbase layer. In addition, pavement condition, CRS value, and a brief description of the condition of the pavement was provided. The IL-SCB test was conducted for the prepared field specimens to calculate their fracture energy and FI. For detailed information on each section, please refer to Appendix C.

The following section presents the results from the IL-SCB test and correlation to the pavement section information provided by the districts.

6.4 LABORATORY TO FIELD CORRELATION

Field cores from a total of 35 sections in nine districts were obtained; the results are summarized in Table 6.4 and in Figure 6.2. The FI was used to correlate field performance with laboratory testing results. The following observations were made and will be discussed separately.

6.4.1 Effect of RAS and RAP on Flexibility Index

A comparison was made of sections constructed in 2012–2013 and having RAS. The results from fracture tests showed that all sections have an FI of 4 or less, except section D4-IL9, as shown in Figure 6.3. The FI value correlated well with the performance of the sections containing RAS; that is, generally low FI values corresponded to AC containing RAS. However, when AC mixtures constructed during 2012–2013 with varying amounts of only RAP (ranging from 10% to 40%) were compared, the value of the FI showed no direct correlation, as illustrated in Figure 6.4.

6.4.2 Effect of Construction Year on Flexibility Index

It is well established that with age, asphalt pavements undergo the phenomenon of oxidation. This results in stiffer and more brittle pavement sections. Such sections have a tendency to fail as a result of cracking. Test results of field cores correlated aging effect with FI: as the age of the pavement increased, the FI value decreased. As shown in Figure 6.5, the sections constructed in 2013–14 showed greater FI values than sections constructed in 2008–09 and 2003–04. The sections constructed in 2003–04 had the lowest FI values. Hence, IL-SCB may be performed on aged and unaged specimens. However, an aging protocol must be identified.

Table 6.4 Results of IL-SCB Fracture Energy and FI with Field Core Information

District	Lab ID	Mix Type	Construction Year	AC Grade	RAP	RAS	% ABR	Distress Type	Fracture Energy (J/m^2)	FI
1	1-1	SMA-SC	2008	PG 76-22	0	0	0	D1-Good	2528	5.0
	1-2	SMA-SC	2008	PG 76-22	0	0	0	D1-Bad	2303	3.1
	1-3	SMA-SC	2009	—	0	0	0	BMPR Good	2262	4.9
	1-4	SMA-SC	2013	PG 70-28	14.2	3	28.2	BMPR Bad	2285	1.8
	1-5	F-SC	2013	PG 70-28	8	5	29.6	BMPR Bad	1231	1.3
	1-6	F-SC	2013	PG 76-22	14	2.5	30.4	BMPR Bad	1711	2.9
	1-7	F-SC	2009	—	10	0	10	Good	1556	2.3
	1-8	D-SC	2010	—	20	0	14.4	Good	2515	6.0
	1-9	D-SC	2013	PG 58-28	30	0	20.2	Good	2937	10.9
	1-10	D-SC	2013	PG 52-28	53	6	67.1	Bad	1798	1.4

District	Lab ID	Mix Type	Construction Year	AC Grade	RAP	RAS	% ABR	Distress Type	Fracture Energy (J/m^2)	FI
	1-11	D-SC	2009	PG 64-22	10	0	7.5	Good	1852	3.4
	1-12	D-SC	2013	PG 58-28	17.5	2.5	30.3	BMPR Bad	2714	3.9
	1-13	F-SC	2013	PG 70-22	10	0	10.2	Bad	2608	10.4
2	2RT26	SMA-SC	2004	PG 76-28	0	0	0	An example of HMA pavement that has withstood weathering and traffic in good condition	1237	1.2
	22RT2	D-SC	2003	PG 70-22	0	0	0	Close-spaced cracking and cracking from gear box segregation	1536	1.3
	22SRT2	C-SC	2004	PG 58-28	15	0	0	Thermal cracking	1156	0.7
3	3-6E	D-SC	2012	PG 64-22	10	0	7	Good	2527	10.1
	3-6W	F-SC	2013	PG 64-22	40	0	27	Bad	1721	2.4
4	D4-IL78	E-SC	2012	PG 70-22	10	5	—	Subjective to the viewer; has transverse cracking (reflective?) of a pavement rehab of similar age	1843	4.0
	D4-IL9	D-SC	2013	PG 64-22	16	3.2	33.5	Subjective to the viewer; has transvers cracking (reflective?) of a pavement rehab of similar age	2664	11.1
	D4-IL55	E-SC	2012	PG 76-22	10	0	10.3		808	1.3
5	5-US136-1	C-SC	2013	PG 58-28	30	0	22	Good—no visible distress	2267	3.7
	5-US136-2	D-SC	2014	PG 70-22	10	0	9	Very good condition—new construction, no visible distress	2959	23.6
	5-I39	D-SC	2013	PG 70-28	12	0	10	Very good condition—new construction, no visible distress	3394	19.8
	5-I57	D-SC	2013	PG 70-28	10	0	9	Good—no visible distress	1997	6.0
	5-IL47	D-SC	2012	PG 64-22	10	0	8	Good—reflective cracks have appeared	2096	4.8
	5-IL6	—	2012	PG 64-22	14	0	13	Good—no visible distress	2090	3.7
6	6G2	D-SC	2013	—	—	0	8.5	No cracking was observed within the project limits	3068	25.1
	6P	D-SC	2013	—	—	0	16	Transverse cracking observed at approximately 100- to 500- ft intervals	2029	2.1
7	7-I130	—	—	—	—	—	—	—	1051	1.3

District	Lab ID	Mix Type	Construction Year	AC Grade	RAP	RAS	% ABR	Distress Type	Fracture Energy (J/m^2)	FI
	7-I121	—	—	—	—	—	—	—	2220	6.1
8	8JVS2	C-SC	2013	PG 64-22	15	0	—	—	2987	15.0
	867S1	D-SC	2013	PG 64-22	15	0	14.5	Longitudinal cracking exists at centerline, edges, and wheel paths along with transverse cracking periodically throughout project; cracking developed the year following construction immediately after winter	2385	11.3
9	9-I4	D-SC	2013	PG 64-22	0	0	0	O1, S1 O: Transverse cracking/joint reflection cracks S: Centerline deterioration	2008	7.2
	9-I54	C-SC	2013	PG 64-22	20	0	—	2012 L3, M2,O4, Q1, S3 2014 No distress L: Alligator cracking M: Block cracking Q: Longitudinal/center of lane cracking S: Centerline deterioration	2062	4.6

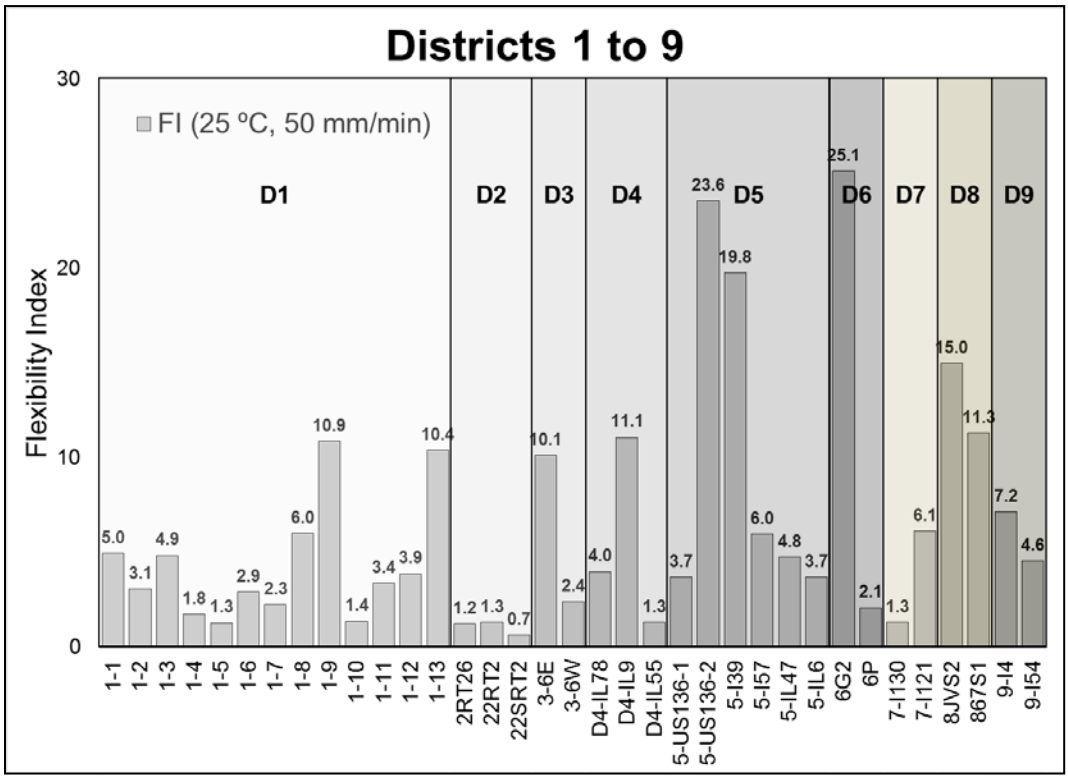

Figure 6.2 Flexibility index for all tested sections from the districts.

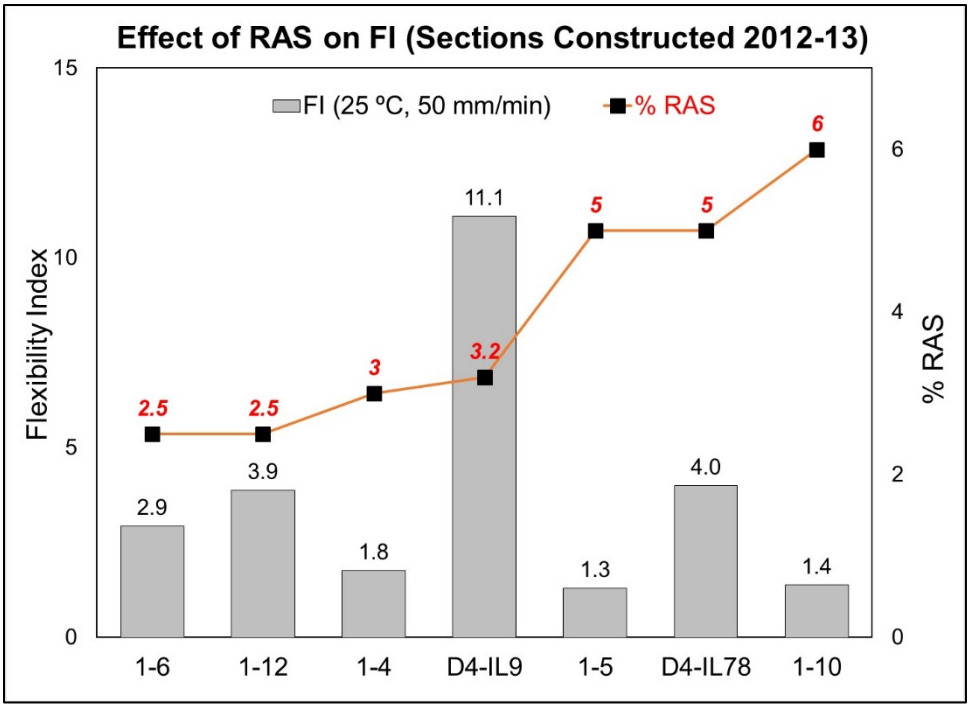

Figure 6.3 Effect of RAS on the FI for field cores.

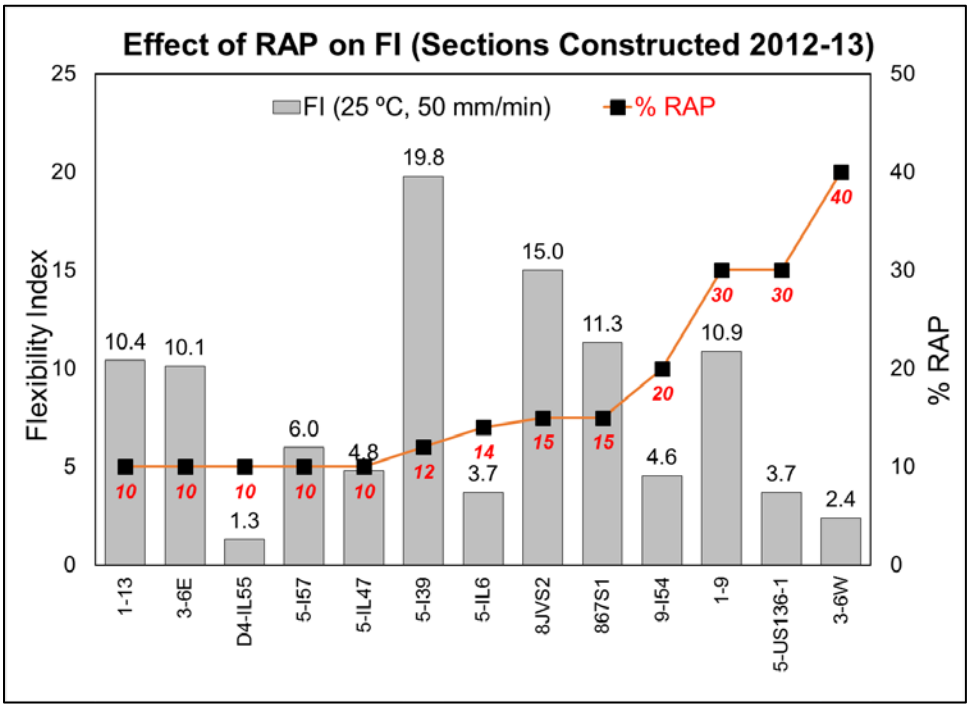

Figure 6.4 Effect of RAP on the FI for field cores.

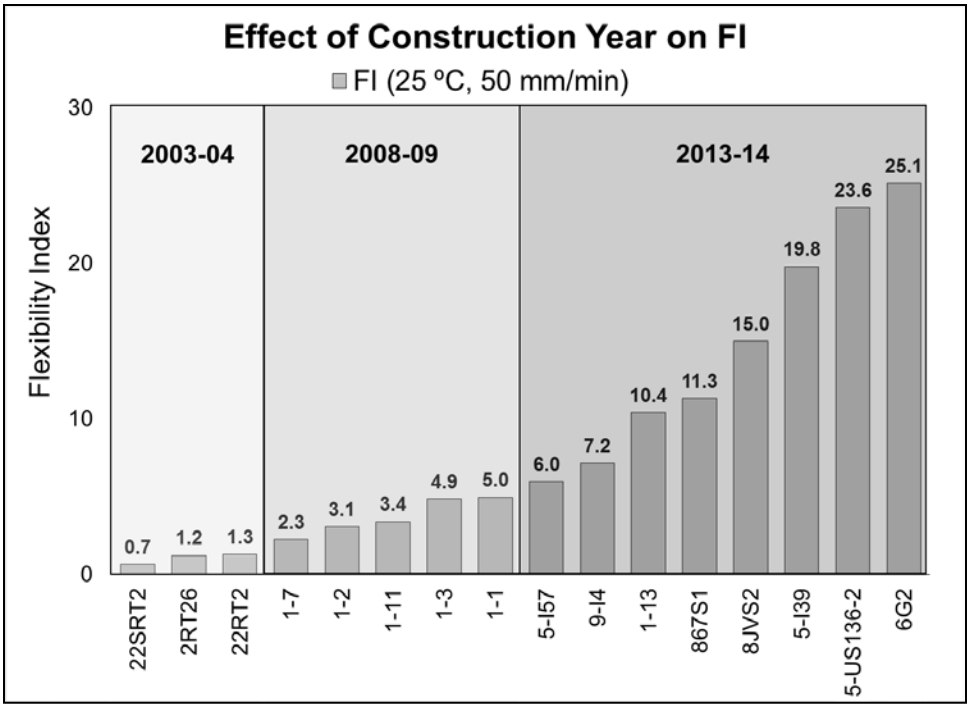

Figure 6.5 Effect of construction year on FI.

6.4.3 Correlation of AC Flexibility Index to Field Performance

A comparison was made between FI and observed field performance of the sections investigated. On the basis of the severity of distresses, CRS rating, and field observations, the pavement sections were subjectively divided into three categories: poor, fair, and good. The FI values corresponding to field performance data are presented in Figure 6.6 on the following page. To reduce the effect of age on performance, the sections compared are only the ones constructed in 2013–14. It was observed that the FI value of most of the sections correlated well with field performance except Section 1-13 (District 1), Section 867S1 (District 8), and Section 5US136-1 (District 5). In a later investigation, it was identified that Section 1-13 had moderate to severe frost heave that could have caused bad performance. The worst-performing sections had FI values ranging from 1.3 to 3.9, whereas good-performing sections generally had values greater than 10.

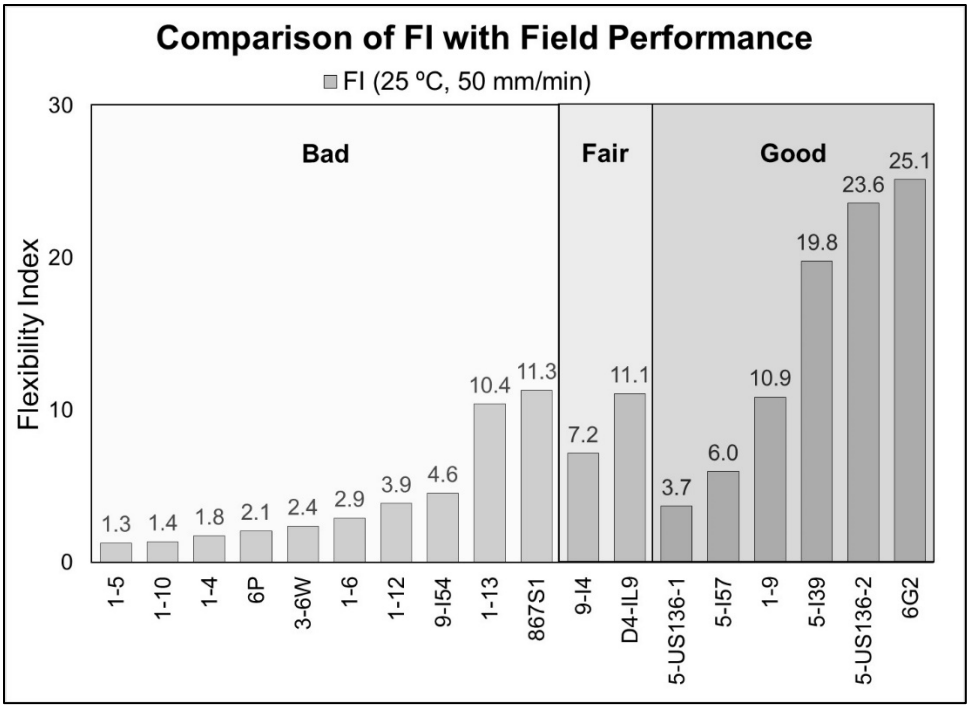

Figure 6.6 Correlation of FI with field performance.

6.5 SUMMARY

This chapter validated the IL-SCB test results with field performance in nine IDOT districts, as well as the performance of FHWA ALF's test sections. Pavement system information was provided by the districts to allow correlation between IL-SCB's FI and field performance. Correlation between field performance and the FI developed in this study is critical for validating the approach developed and for determining thresholds that can discriminate performance using a simple index parameter. On the basis of the results presented in this chapter, the following specific conclusions are offered:

- Performance measurement and predictions obtained from FHWA's accelerated loading facility show the ability of IL-SCB to identify the effect of ABR (RAP or RAS) as well as the presence of WMA technologies. The ALF sections were constructed to evaluate only mixture design characteristics with respect to fatigue cracking. Despite some construction variability that resulted in varying thicknesses of asphalt layers and differences in the modulus of base and subgrade layers, ALF sections results correlate well with IL-SCB's FI prediction of the AC mixture performance.
- The FI obtained from the IL-SCB tests is in very good agreement with performance rankings developed for the mixes, based on fatigue cracking measurements and structural analysis predictions. FI values of 2.0 and 6.0 appear to be cut-off values distinguishing poor- (less than 2.0), intermediate- (2.0 to 6.0), and good-performing (greater than 6.0) sections.
- Three performance categories were identified based on ALF performance and the FI. The cut-off FI value appears to be less than 2.0 for poor-performing sections, whereas the sections with an FI greater than approximately 6.0 were in the good-performing category.

- Field data and pavement characteristics obtained from districts illustrate a wide range of performance characteristics. Good correlation between FI and field performance and other pavement characteristics was observed.
- The random field data clearly show that aging can affect FI values. Results show the significant reduction in FI values of the sections constructed more than 10 years ago. None of the sections constructed between the years 2003–04 and 2008–09 had an FI greater than 1.3 and 5.0, respectively. On the other hand, relatively new sections constructed 2013–14 had FI values in a range of 6 to 25. This finding is consistent with the experiments conducted for the long-term-aged samples in the laboratory as part of ICT project R27-SP28 (Ozer et al. 2015). The reduction in FI is about 60% to 80% after long-term aging for the same mixes.
- FI values obtained for field specimens are in a range of approximately 1 to 25. Recently constructed, good-performing sections, with one exception, have FI values greater than 10. Sections with an FI less than 4 to 5 are generally the sections that exhibited premature cracking and were identified as poor-performing by the districts. A few exceptions disrupted this trend. Considering the variability in field performance that can be caused by many different reasons that were not controlled, this can be considered acceptable.
- Testing for field cores were obtained only for the wearing course material using the IL-SCB method. However, additional testing should be performed for rutting and stiffness characterization of field core specimens, and testing can be extended to the layers below the surface.

CHAPTER 7: SELECTION OF FLEXIBILITY INDEX THRESHOLDS FOR BALANCED MIX DESIGN

7.1 INTRODUCTION TO THE CONCEPT OF BALANCED MIX DESIGN

The FI is a measure of overall potential for cracking-related damage in AC mixtures. However, to more comprehensively evaluate AC mixture performance, it is necessary to have a performance measure criterion that includes not only indicators of cracking potential but also of the potential for fatigue and high-temperature rutting.

Progress has been made in developing a balanced mix design (BMD) approach by integrating several laboratory-level tests to control permanent deformations and cracking. The BMD approach often integrates performance-related laboratory tests such as Hamburg wheel tracking, Texas overlay, or a cracking test into the existing AC mixture volumetric design specifications with an ultimate goal of obtaining a balance between volumetrics and resistance to rutting and cracking.

The Hamburg wheel tracking test is a widely accepted test to evaluate rutting potential and is already part of the Illinois AC mixture design specifications. This chapter introduces an alternative approach that integrates the FI and Hamburg test results into the AC mix design specifications along with the preliminary thresholds determined.

7.2 DEVELOPMENT OF THRESHOLDS FOR BALANCED MIX DESIGNS

To initiate the concept of BMD, laboratory-designed mixes were used to establish FI thresholds for high-performance, acceptable, and unacceptable AC mixes. Because the AC mixtures were designed from a parent control mix with no ABR and gradually modified by changing ABR and binder grade, BMD principles were applied to these mixes. The FI thresholds are assumed based on engineering intuition and partial validation using the field cores, as summarized in Chapter 6.

The concept of an interaction plot is illustrated in Figure 7.1. The interaction plot can be used to evaluate overall resistance of rutting and cracking and to develop pass/fail regions for mix design quality. The interaction plot includes FI values on the y-axis and rut depth (in mm) on the x-axis, along with its thresholds. While the IL-SCB test provides the FI, rut depth values are obtained from the Hamburg WTT. Rut depth values correspond to the maximum allowable passes determined based on the binder grade per IDOT specifications. If an alteration to the mix requires the use of a softer binder, the mix should be assessed based on the targeted binder grade. For example, if a mix is designed using PG 64-22 and, because of adding RAP, a PG 58-22 is used, the number of cycles in the WTT should be based on PG 64-22.

Four quadrants define overall resistance of AC mixtures to rutting and cracking. The characteristics of AC mixes belonging to each quadrant determined with some preliminary thresholds can be explained as follows:

- *Stiff and Brittle:* Low cracking resistance (brittle) and high rutting resistance (stiff). Mixes with lower binder content, high ABR, or aging would typically be in this quadrant.
- *Stiff and Flexible:* Mixes with low cracking potential (flexible) and good rutting resistance (stiff). Acceptable AC mixes are expected to be in this quadrant (i.e., highest cracking and rutting resistance). This quadrant can be further subdivided into high-performance and standard-performance categories depending on the mix application requirements.

- *Soft and Flexible:* Mixes with sufficient cracking resistance (flexible) but with high rutting potential (soft). Leveling binders or crack-retardant mixes with very high binder content and polymer modifications are typically in this quadrant.
- *Soft and Unstable:* Extremely low cracking and rutting resistance with insufficient load-carrying capacity at all temperatures. The AC mixes found in this quadrant would generally have poor or unacceptable volumetric designs.

In the example shown in Figure 7.1, the base AC mix, N90-0 (64-22), was characterized as a high-performance mix, having a higher FI and relatively low rut depth. The addition of recycled material (up to 60%), along with lowering of the binder grade, resulted in lower-performing mixes. When the ABR content was increased up to 20% and the binder grade bumped to PG 58-28, the mix moved to the lower left quadrant of the interaction plot. This indicated that double binder grade bumping (from PG 64-22 to PG 58-28) for 20% ABR was not fully justified and could increase rutting potential of this mix while lowering its cracking resistance. Further reduction in the binder grade would move this mix to an unstable region. However, when ABR increased up to 30%, the mix moved to the lower right quadrant, toward becoming a stiffer and more brittle mix. With the addition of 60% recycled content, the mix migrated fully toward the lower left quadrant, indicating extremely stiff and brittle behavior.

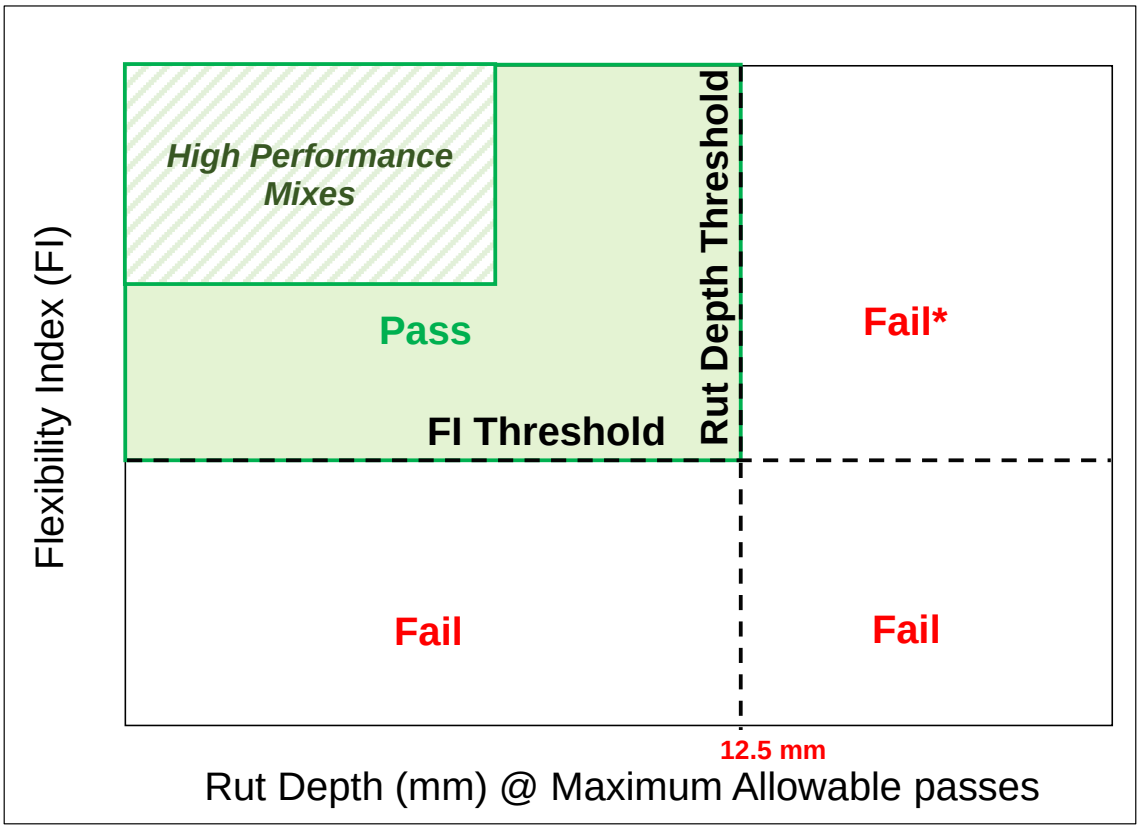

*This mix can be used as a thin, highly flexible interlayer to control reflective cracking

Figure 7.1 Interaction plot between FI and rut depth for balanced AC mix design (preliminary quadrants for concept illustration).

Figure 7.2 illustrates a typical implementation of the balanced mix design approach applied for laboratory AC mixtures. The thresholds can be defined based on the laboratory AC mixtures and should be used to differentiate mixes subjected to similar loading, environmental conditions, and structural design. This example presents the acceptability/unacceptability of AC mixes based on predefined FI and rut depth thresholds. Rut depth is measured for the maximum number of allowable passes depending on the type of virgin binder used in the mixture to be analyzed. Current IDOT specifications can be used to define the rut depth threshold for rutting resistance (i.e., 12.5 mm). The work for determining FI thresholds is under way. The FI threshold in Figure 7.2 is used only to demonstrate an example for the implementation of interaction plots. An AC mix is considered to pass when its FI is above and its rut depth is below the respective thresholds. A more nuanced selection process can be established if multiple threshold levels for each parameter are desired for application.

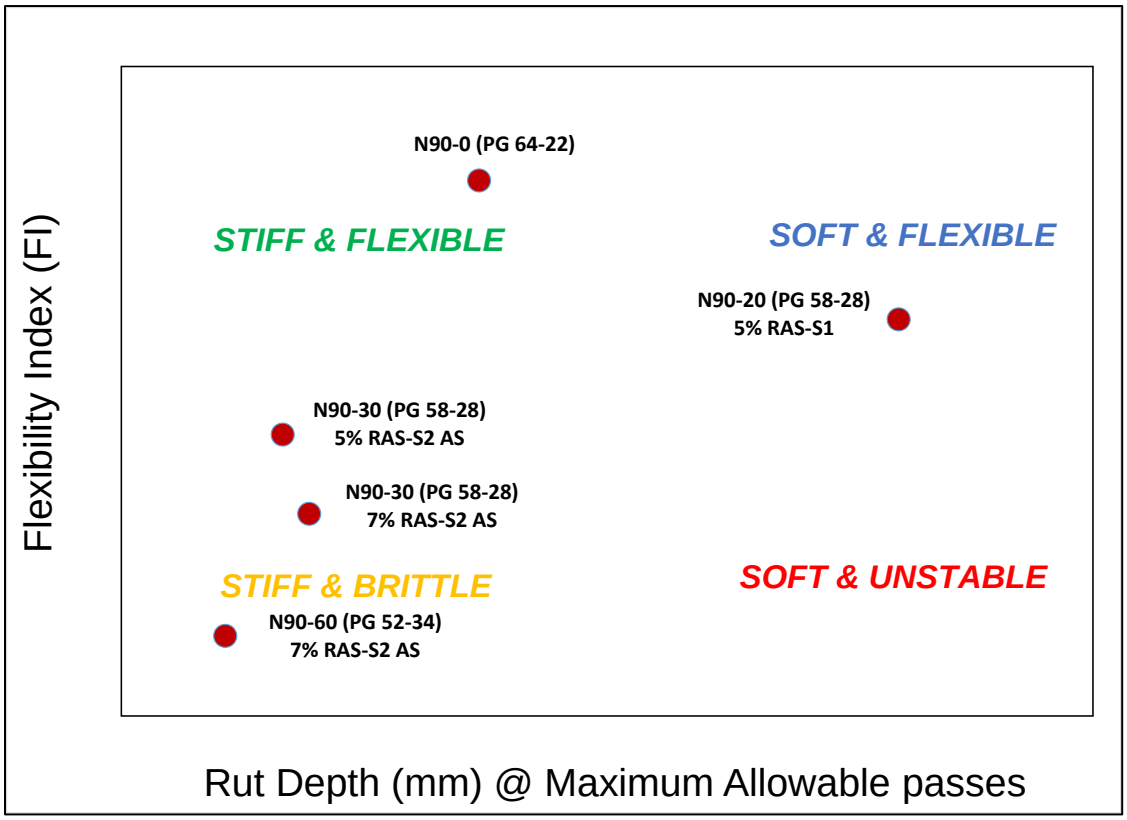

Figure 7.2 Example of an implementation of interaction plots as a pass/fail criterion applied to laboratory mixtures.

Efforts are under way to fine-tune the FI thresholds for Illinois. The FI threshold is affected by AC mix design and preparation (lab, plant, or core). For field cores, it is affected by loading, environmental conditions, and structural design. The thresholds could be adjusted as more field performance data become available. In addition, thresholds could be adjusted for local conditions that affect AC mix quality, environmental and traffic loading conditions, and applications. Threshold verification should include testing of a large set of lab-produced or plant-produced AC mixes used for various applications. A regional database can provide trends and an expected range of FI values. The ongoing research at the Illinois Center for Transportation and the department's Bureau of Materials and Physical Testing targets development of baseline thresholds using AC mixes from Illinois for different applications.

7.3 SUMMARY

The initial steps in developing a balanced AC mix design approach consisted of integrating two laboratory performance–level tests into the AC mix volumetric design process. Interaction plots were introduced to provide an overall and a more balanced evaluation of the performance of AC mixtures by combining rutting and cracking resistance and to aid in developing AC mixes with optimum resistance to cracking and rutting for various applications. Thresholds are a critical part of the development of the balanced AC mix design approach. The concept of interaction plots used in the development a balanced mix design procedures was introduced.

The remaining challenges in the development of the balanced mix design approach are (1) integrating the concept of interaction plots with AC mix design volumetrics and (2) developing and validating FI thresholds for different regions and pavement applications.

CHAPTER 8: CONCLUSION AND FUTURE WORK

A practical test method was developed that can be readily implemented to quantify an AC mixture's cracking potential. The IL-SCB test method ran at 25°C (77°F). A 50 mm/min (2 in/min) loading rate is proposed for screening AC mixtures to control potential premature cracking.

Test method development included various levels of performance characterization in the laboratory supported by a theoretical approach and a digital image correlation technique. Plant-produced and laboratory-compacted AC mixtures, laboratory-produced and laboratory-compacted AC mixtures, and field AC specimens were used at different stages of the study to validate the developed test. A large set of plant- and laboratory-produced AC mixtures was used in characterization and development of the test method.

During test development, several existing tests were evaluated—modulus, fatigue, and permanent deformation characterization—along with various cracking tests. Cracking characterization of AC mixtures was conducted using two test setups: disc compact tension and semi-circular bending. Tests were conducted at various temperatures and displacement rates to identify an optimum combination of temperature and displacement rate to allow a meaningful and consistent separation of the AC mixtures.

Ultimately, the introduced test method is coupled with an index parameter, the flexibility index (FI), to characterize the fracture potential of AC mixes. The FI is derived from the load-displacement response incorporating fracture energy and slope of the load-displacement curve after a crack begins to propagate. The FI was shown to correlate very well with the speed of crack propagation in the IL-SCB tests.

The following four criteria—along with simplicity, repeatability, efficiency, and cost effectiveness—were considered when selecting the test method:

1. *Significant spread in the test output* is necessary to develop a threshold and resolve differences in AC mixes that may cause premature cracking. The spread in the low-temperature (–12°C [10.4°F]) test output, especially for dense- and coarse-graded mixes without polymer-modified binders, can be easily masked by experimental variations, which is usually around 10%. On the other hand, at the intermediate temperature (25°C [77°F]), the IL-SCB test method provided significant spread of the AC mixes, thus allowing for clear distinction between the mixes.
2. *Correlation to independent tests and engineering intuition* is necessary to quantify the susceptibility of AC mixes to cracking. A group of mixes was selected for comparison of fatigue performance using results from the Texas overlay and IL-SCB fracture tests. The results indicated that there was a good correlation between intermediate-temperature (25°C [77°F]) IL-SCB fracture tests and Texas overlay tests in identifying materials that had the best and worst performances.
3. *Correlation to field performance* should be considered when selecting the test method. The IL-SCB test and the FI showed very good correlation to the FHWA accelerated pavement testing results and field performance of pavement sections in different IDOT districts.
4. *Applicability and seamless implementation* of the proposed test method was the final consideration in the study. An objective was to develop a practical test method and make it available for agencies and contractors at a low cost. Two prototypes for streamlined and low-cost IL-SCB testing equipment are already in the market (developed by two different companies).

The following is a summary of the experimental findings from this study:

- Complex modulus was used for comprehensive viscoelastic characterization of AC mixtures and can trace significant changes in the AC mix design such as ABR, binder grade, and content. However, the cost and testing complexity make it less appealing for widespread implementation and use as a performance indicator or a quality control test.
- The Texas overlay test was able to qualitatively distinguish AC mixes' performance with changing recycled content. However, the test suffered from issues with repeatability and time-consuming specimen preparation and testing.
- The low-temperature cracking tests (semi-circular bending and disc compact tension) could not distinguish between AC mixes when there were distinct changes in mix design characteristics.
- The fracture behavior of AC mixtures was shown to be strongly dependent on test temperature and displacement rate. Fracture energy values reached a plateau at low temperatures, with marginal differences between AC mixes. Fracture energy had peak values at the intermediate temperature and displacement rates between approximately 0.167 and 50 mm/min (0.00656 and 2 in/min).
- Fundamental cracking mechanisms were investigated using the digital image correlation technique. The mechanisms of crack front damage varied with temperature, displacement rate, and RAP/RAS content level. When damage distribution became more localized, as in the case of low-temperature testing, an AC mixture's fracture behavior became more brittle. The same brittleness effect with localization of the crack front mechanism was observed in the AC mixes with increasing RAS levels.
- The proposed IL-SCB testing method showed consistent and repeatable trends for changes in AC mix design properties.
- The developed FI showed a consistent trend with approximate crack growth rate. The FI is a simple parameter that may also be correlated to fundamental crack growth mechanisms through the process zone. The parameter has the ability to distinguish AC mixes with distinct mix design properties that influence cracking resistance.
- The developed FI provided greater separation between AC mixes to capture some of the changes that could not be captured by fracture energy alone. The effects of binder grade bumping and ABR levels as low as 10% were captured by the index. A consistent reduction in FI values with increasing ABR was observed, whereby FI values were greater than 10 for the control AC mix and reduced to as low as 2 with high ABR mixes (30% to 60% ABR).
- The correlation between field performance and the FI for the cores obtained from nine IDOT districts was good. The FI values obtained for the field cores showed the effects of aging, with a clear reduction in FI values for the sections constructed more than 10 years ago compared with relatively new construction. In general, the FI values were consistent with field performance data provided by the districts.
- The data obtained from FHWA's accelerated pavement test sections indicated very good agreement between the FI and performance ranking based on number of loading repetitions to failure. The three poor-performing sections had FI values less than 2, whereas the control section (among the best performing in the accelerated testing) had an FI value of 10.
- A conceptual implementation plan was proposed for a balanced mix design approach. An interaction plot was introduced that combined the FI and Hamburg rut depth results. Preliminary threshold values and corresponding AC mixture classifications were proposed. This is a simple concept toward development of a balanced mix design combining volumetric mixture design principles with two critical performance indicators.

REFERENCES

AASHTO M 323-04. 2004. *Standard Specification for Superpave Volumetric Mix Design.* American Association of State Highway and Transportation Officials, Washington, DC.

AASHTO T 283-14. 2014. *Standard Method of Test for Resistance of Compacted Asphalt Mixtures to Moisture-Induced Damage.* American Association of State Highway and Transportation Officials, Washington, DC.

AASHTO T 316-13. 2013. *Standard Method of Test for Viscosity Determination of Asphalt Binder Using Rotational Viscometer* American Association of State Highway and Transportation Officials, Washington, DC.

AASHTO TP 79-15. 2015. *Standard Method of Test for Determining the Dynamic Modulus and Flow Number for Hot Mix Asphalt (HMA) Using the Asphalt Mixture Performance Tester (AMPT).* American Association of State Highway and Transportation Officials, Washington, DC.

AASHTO TP 105-13. 2013. *Standard Method for Determining the Fracture Energy of Asphalt Mixtures Using the Semi Circular Bend Geometry (SCB*). American Association of State Highway and Transportation Officials, Washington, DC.

Abanto-Bueno, J., and J. Lambros. 2002. "Investigation of crack growth in functionally graded materials using digital image correlation." *Engineering Fracture Mechanics*, Vol. 69, No. 14–16, pp. 1695–1711.

Al-Qadi, I. L., Q. Aurangzeb, and S. H. Carpenter. 2012. *Impact of High RAP Contents on Structural and Performance Properties of Asphalt Mixtures*. Report No. FHWA-ICT-12-002. Illinois Center for Transportation, Rantoul, IL.

Al-Qadi, I. L., S. H. Carpenter, G. Roberts, H. Ozer, Q. Aurangzeb, M. Elseifi, and J. Trepanier. 2009. *Determination of Usable Residual Asphalt Binder in RAP*. Report No. FHWA-ICT-09-031. Illinois Center for Transportation, Rantoul, IL.

Apeagyei, A., B. Diefenderfer, and S. Diefenderfer. 2011. "Rutting resistance of asphalt concrete mixtures that contain recycled asphalt pavement." *Transportation Research Record: Journal of the Transportation Research Board*, Vol. 2208, pp. 9–16.

Aurangzeb, Q. *Impact of Reclaimed Asphalt Pavements on Pavement Sustainability*. Ph.D. dissertation. University of Illinois at Urbana-Champaign, Urbana, IL, 2012.

Bazant, Z. P., and Y. N. Li. 1997. "Cohesive crack model with rate-dependent opening and viscoelasticity: I. mathematical model and scaling." *International Journal of Fracture*, Vol. 86, No. 3, pp. 247–265.

Bazant, Z. P., and Y. N. Li. 1997. "Cohesive crack model with rate-dependent opening and viscoelasticity: II. Numerical algorithm, behavior and size effect." *International Journal of Fracture*, Vol. 86, No. 3, pp. 267–288.

Bazant, Z. P., and J. Planas. 1997. *Fracture and Size Effect in Concrete and Other Quasibrittle Materials*. CRC Press, Boca Raton, FL.

Bazant, Z. P., and P. C. Prat. 1988. "Effect of temperature and humidity on fracture energy of concrete." *ACI Materials Journal*, Vol. 85, No. 4, pp. 262–271.

Behnia, B., E. Dave, S. Ahmed, W. Buttlar, and H. Reis. 2011. “Effects of recycled asphalt pavement amounts on low-temperature cracking performance of asphalt mixtures using acoustic emissions.”*Transportation Research Record: Journal of the Transportation Research Board*, Vol. 2208, pp. 64–71.

Braham, A., A. Zofka, X. Li, and F. Ni. 2012. “Exploring the reduction of laboratory testing for the cohesive zone model for asphalt concrete.” *International Journal of Pavement Engineering*, Vol. 13, No. 4, pp. 350–359.

Buttlar, W. G., C. N. Chiangmai, I. L. Al-Qadi, T. R. Murphy, and W. Pine. 2015. *Designing, Producing, and Constructing Fine-Graded Hot Mix Asphalt On Illinois Roadways*. FHWA-ICT-15-009. Illinois Center for Transportation, Rantoul, IL.

Carpenter, S. H. 2007. *Dynamic Modulus Performance of IDOT Mixtures*. Report No. FHWA-ICT-07-008. Illinois Center for Transportation, Rantoul, IL.

Carroll, J. D., W. Abuzaid, J. Lambros, and H. Sehitoglu. 2013. “High resolution digital image correlation measurements of strain accumulation in fatigue crack growth.” *International Journal of Fatigue*, Vol. 57, pp. 140–150.

Carvalho, R., N. Gibson, X. Li, and A. Andriescu. 2015. “Fatigue cracking of recycled and warm mix asphalts: Predicted performance considering structural variability influences.” *Journal of the Association of Asphalt Paving Technologists* (submitted for publication).

Daniel, J., and A. Lachance. 2005. “Mechanistic and volumetric properties of asphalt mixtures with recycled asphalt pavement.” *Transportation Research Record: Journal of the Transportation Research Board*, Vol. 1929, pp. 28–36.

Duan, K., X.-Z. Hu, and F. H. Wittman. 2003. “Thickness effect on fracture energy of cementitious materials.” *Cement and Concrete Research*, Vol. 33, 499–507.

Ghuzlan, K. A., and S. H Carpenter. 2000. “Energy-derived damage-based failure criterion for fatigue testing.” *Transportation Research Record: Journal of the Transportation Research Board*, No. 1723, pp. 141–149.

Goh, S. W., and Z. You. 2011. “Evaluation of recycled asphalt shingles in hot mix asphalt.” In *Proceedings of the 1st Congress of the Transportation and Development Institute of ASCE,* pp. 638–645. Washington, DC: American Society of Civil Engineers.

Hansen, K. R., and A. Copeland. 2014. *Annual Asphalt Pavement Industry Survey on Recycled Materials and Warm-Mix Asphalt Usage: 2009–2013*. Information Series 138, National Asphalt Pavement Association, Lanham.

Huang, B., G. Li, D. Vukosavljevic, X. Shu, and B. K. Egan. 2005. “Laboratory investigation of mixing HMA with reclaimed asphalt pavement.” *Transportation Research Record: Journal of the Transportation Research Board*, Vol. 1929, pp. 37–45.

Khan, T. *Displacement Rate and Temperature Effect on Asphalt Concrete Cracking*. 2015. M.S. thesis. University of Illinois at Urbana-Champaign, Urbana, IL.

Kim, M., W. Buttlar, J. Baek, and I. Al-Qadi. 2009. “Field and laboratory evaluation of fracture resistance of Illinois hot-mix asphalt overlay mixtures.” *Transportation Research Record: Journal of the Transportation Research Board*, Vol. 2127, pp. 146–154.

Kim, Y. R., H. J., Lee, and D. N. Little. 1997. “Fatigue characterization of asphalt concrete using viscoelasticity and continuum damage theory.” *Journal of the Association of Asphalt Paving Technologists*, Vol. 66, pp. 520–569.

Krishna Swamy, A., L. F. Mitchell, S. J. Hall, and J. S. Daniel. 2011. “Impact of RAP on the volumetric, stiffness, strength, and low-temperature properties of HMA.” *Journal of Materials in Civil Engineering*, Vol. 23, No. 11, pp. 1490–1497.

Leclerc, H., J.-N. Périé, S. Roux, and F. Hild. 2009. “Integrated digital image correlation for the identification of mechanical properties.” *Computer Vision/Computer Graphics Collaboration Techniques/Lecture Notes in Computer Science*, pp. 61–171.

Li, X., M. Marasteanu, R. Williams, and T. Clyne. 2008. “Effect of reclaimed asphalt pavement (proportion and type) and binder grade on asphalt mixtures.” *Transportation Research Record: Journal of the Transportation Research Board*, Vol. 2051, pp. 90–97.

Li, Y. N., and Z. P. Bazant. 1997. “Cohesive crack model with rate-dependent opening and viscoelasticity: II. Numerical algorithm, behavior and size effect.” *International Journal of Fracture*, Vol. 86, No. 3, pp. 267–288.

Lippert, D., H. Ozer, I. L. Al-Qadi, J. Meister, and G. Renshaw. 2015. *Construction and Performance Monitoring of Various Asphalt Mixes in Illinois 2015*. Interim Report. Illinois Center for Transportation, Rantoul, IL.

Lippert, D., S. Hang, and H. Ozer. 2015. *Illinois Highway Materials Sustainability Efforts of 2014*. Report No. FHWA-ICT-15-014, Rantoul, IL, Illinois Center for Transportation.

Marasteanu, M., W. Buttlar, H. Bahia, and C. Williams. 2012. *Investigation of Low Temperature Cracking in Asphalt Pavements*. Report No. MN/RC-2012-23,National Pooled Fund Study, Phase II. Minnesota Department of Transportation, St. Paul, MN.

McDaniel, R. S., A. Shah, and G. Huber. 2012. *Investigation of Low and High Temperature Properties of Plant Produced RAP Mixtures*. Report No. FHWA-HRT-11-058. Purdue University, West Lafayette, IN.

Mogawer, W., A. Austerman, R. Bonaquist, and M. Roussel. 2011. “Performance characteristics of thin-lift overlay mixtures.” *Transportation Research Record: Journal of the Transportation Research Board,* No. 2208, pp. 17–25.

Nguyen, Q. T., H. Di Benedetto, C. Sauzéat, and N. Tapsoba. 2013. “Time–temperature superposition principle validation for bituminous mixes in the linear and nonlinear domains.” *Journal of Materials in Civil Engineering*, Vol. 25, No. 9, pp. 1181–1188.

Ozer, H., I. L. Al-Qadi, and A. Kanaan. 2012. *Laboratory Evaluation of High Asphalt Binder Replacement with Recycled Asphalt Shingles (RAS) for a Low N-Design Asphalt Mixture*. Report No. FHWA-ICT-12-018. Illinois Center for Transportation, Rantoul, IL,.

Roque, R., B. Birgisson, C. Drakos, and B. Dietrich. 2004. “Development and Field Evaluation of Energy-Based Criteria for Top-Down Cracking Performance of Hot Mix Asphalt.” *Journal of the Association of Asphalt Paving Technologists*, Vol. 73, pp. 229–260.

Seo, Y., Y. Kim, M. Witczak, and R. Bonaquist. 2002. “Application of Digital image correlation method to mechanical testing of asphalt–aggregate mixtures.” *Transportation Research Record: Journal of the Transportation Research Board*, Vol. 1789, pp. 162–172.

Son, S. 2014. *Development of a Phenomenological Constitutive Model for Fracture Resistance Degradation of Asphalt Concrete with Damage Growth due to Repeated Loading*. Ph.D. dissertation. University of Illinois at Urbana-Champaign, Urbana, IL.

Shah, A., R. McDaniel, G. Huber, and V. Gallivan. 2007. “Investigation of properties of plant-produced reclaimed asphalt pavement mixtures.” *Transportation Research Record: Journal of the Transportation Research Board*, Vol. 1998, pp. 103–111.

Skarżyński, Ł., J. Kozicki, and J. Tejchman. 2013. “Application of DIC technique to concrete—Study on objectivity of measured surface displacements.” *Experimental Mechanics*, Vol. 53, No. 9, pp. 1545–1559.

Stroup-Gardiner, M., and C. Wagner. 1989. “Use of Reclaimed Asphalt Pavement in Superpave Hot-Mix Asphalt Applications.” *Transportation Research Record: Journal of the Transportation Research Board*, Vol. 1681, pp. 1–9.

Sutton, M. A., J.-J. Orteu, and H. W. Schreier. 2009. *Image Correlation for Shape, Motion and Deformation Measurements: Basic Concepts, Theory and Applications*. Springer, New York, NY.

Tabaković, A., A. Gibney, C. McNally, and M. Gilchrist. 2010. “Influence of recycled asphalt pavement on fatigue performance of asphalt concrete base courses*.” Journal of Materials in Civil Engineering*, Vol. 22, No. 6, pp. 643–650.

Underwood, B., C. Baek, and Y. Kim. 2012. “Simplified viscoelastic continuum damage model as platform for asphalt concrete fatigue analysis.” *Transportation Research Record: Journal of the Transportation Research Board*, Vol. 2298, pp. 36–45.

Vavrik, W. R., S. H. Carpenter, S. Gillen, J. Behnke, and F. Garrott. 2008. *Evaluation of Field-Produced Hot Mix Asphalt (HMA) Mixtures with Fractionated Recycled Asphalt Pavement (RAP): 2007 Illinois Tollway Field Mix Trials*. Report No. ICT-08-030. Illinois Center for Transportation, Rantoul, IL.

Wagoner, M. P. 2006. *Fracture Tests for Bituminous-Aggregate Mixtures: Laboratory and Field Investigations*. Ph.D. dissertation. University of Illinois at Urbana-Champaign, Urbana, IL.

Wagoner, M., W. Buttlar, G. Paulino, and P. Blankenship. 2005. “Investigation of the fracture resistance of hot-mix asphalt concrete using a disk-shaped compact tension test.” *Transportation Research Record: Journal of the Transportation Research Board*, Vol. 1929, pp. 183–192.

Walubita, L., X. Hu, B. Jamison, F. Zhou, T. Scullion, A. E. Martin, and S. Dessouky. 2010. *New Generation Mix-Designs: Laboratory Testing and Construction of the APT Test Sections*. Report No. FHWA/TX-10/0-6132-1. Federal Highway Administration, Washington, DC.

Williams, R. C. 2010. *Performance of Recycled Asphalt Shingles in Hot Mix Asphalt.* Report No. TPS-5(213), Pooled Fund Study. Institute for Transportation, Iowa State University, Ames, IA.

Williams, R. C., A. Cascione, D. S. Haugen, W. G. Buttlar, R. A. Bentsen, and J. Behnke. 2011. *Characterization of Hot Mix Asphalt Containing Post-Consumer Recycled Asphalt Shingles and Fractionated Reclaimed Asphalt Pavement*. Final Report Submitted to the Illinois State Toll Highway Authority. Iowa State University, Ames IA.

Williams, M. L., R. F. Landel, and J. D. Ferry. 1955. “The temperature dependence of relaxation mechanisms in amorphous polymers and other glass-forming liquids.” *Journal of the American Chemical Society*, Vol. 77, No. 14, pp. 3701–3707.

Witczak, M. W., K. Kaloush, T. Pellinen, M. Basyouny, and Q. H. Von. 2002. *Simple Performance Test for Superpave Mix Design*. Transportation Research Board, National Research Council, Washington, DC.

Wu, Z., H. Rong, J. Zheng, F. Xu, and W. Dong. 2011. “An experimental investigation on the FPZ properties in concrete using digital image correlation technique.” *Engineering Fracture Mechanics*, Vol. 78, No. 17, pp. 2978–2990.

Xiao, F., S. Amirkhanian, and C. H. Juang. 2007. “Rutting resistance of rubberized asphalt concrete pavements containing reclaimed asphalt pavement mixtures.” *Journal of Materials in Civil Engineering*, Vol. 19, No. 6, pp. 475–483.

Ye, Q., S. Wu, and N. Li. 2009. “Investigation of the dynamic and fatigue properties of fiber-modified asphalt mixtures” *International Journal of Fatigue,* Vol. 31, No. 10, pp. 1598–1602.

Zhou, F., and T. Scullion. 2005. *Overlay Tester: A Rapid Performance Related to Crack Resistance Test*. Report No. FHWA/TX-05/0/4467-2. Texas Transportation Institute, College Station, TX.

APPENDIX A: AGGREGATE GRADATIONS OF LABORATORY MIXES

Table A-1 Aggregate Gradations of Laboratory Mixes

Sieve	CM16	FM20	FM22	Mineral Filler	RAP* (3/8 in)	RAP* (–3/8 in)	RAS* Source 1	RAS* Source 2
1 in	100	100	100	100	100	100	100	100
3/4 in	100	100	100	100	99.3	100	100	100
1/2 in	100	100	100	100	90.8	100	100	100
3/8 in	97	100	100	100	78.6	99.3	100	100
No. 4	32	97	100	100	39	71.7	98.5	96.1
8	9	68	94.5	100	26.5	48.6	95.4	93.3
16	7	40	72	100	19.1	32.6	75.9	77.1
30	6	24	49	100	14.8	24.2	50.8	57.1
50	6	15	19.9	100	10.7	17.2	42.9	49.4
100	5	9	4.1	95	7.7	12.7	37.2	43.0
200	4.6	6.7	1.5	90	6	10.1	30.6	34.2
Binder Content	%	—	—	—	4.2	5.1	26.7	27.4

*Extracted gradation

APPENDIX B: SUMMARY OF MIXES AND LABORATORY MIX DESIGNS

Table B-1 Mix Design Characteristics of Plant- and Laboratory-Produced Mixes and Testing Program Applied to Each Mix.

Mix ID	Mix Name	Mixture Source	Binder Grade	RAP %	RAS %	ABR %	AC %	VMA %	E*	TOL	–12°C SCB	25°C SCB
P1[1]	N50 SC[3]	**TOL Study**	52-28	50	3.5	60	6.7	15		X	X	X
P2[1]	N50 SC[3]		58-28	27	—	29	5.8	14.7		X	X	X
P3	N70 BC[4]		58-28	26	—	29	4.8	13.4		X	X	X
P4	N30 BC[4]		58-28	46.5	—	37	4.8	13.6		X	X	X
P5	N70 SC[3]		64-22	10	—	6	6.1	15.8		X	X	X
P6	N90 SC[3]		76-22	10	—	6	5.6	14.1		X	X	X
P7	N50 SC[3]		64-22	—	—	—	5.9	16.7		X	X	X
P8	N50-50	**Designs by S.T.A.T.E. Testing**	58-28	42	4	49	5.5	13	X		X	X
P9	N50-60		52-28	42	6	59	5.6	13	X		X	X
P10	N70-25		58-28	29	—	25	6	14.5	X		X	X
P11	N70-50		58-28	30	5	48	6	14.5	X		X	X
P12	N80-25		70-28	8	5	26	6.1	16.1	X		X	X
P13	N80-50		70-28	10	8	50	6	15.8	X		X	X
P14[1]	N50-Joliet	**Total Recycle Mixes**	58-28	30	—	34	5.39	15.3	X		X	X
P15[1,2]	N50-Sandeno		52-28	52	4	60	6.72	15.1	X		X	X
P16[1,2]	N50-K5		52-28	53	5	57	6.5	14.9			X	X
L3	N90 0 CG	**Laboratory Design Mixtures**	**70-22**	—	—	—	6	15.3	X		X	X
L4	N90 0 CG		**64-22**	—	—	—	6	15.3	X		X	X
L5	N90 30 CG S1[7]		**70-22**	—	7	29.8	6	15.3			X	X
L6	N90 30 CG S1[7]		**58-28**	—	7	29.8	6	15.3			X	X
L7	N90 20 CG S1[7]		**58-28**	—	5	21.2	6	15.3			X	X
L8	N90 10 CG S1[7]		**64-22**	—	2.5	10.5	6	15.3	X		X	X
L9	N90 30 CG S2[8] AS[5]		**58-28**	11	5	30.5	6	15.2	X		X	X
L10	N90 60 CG S2[8] AS[5]		**52-34**	40	7	60.8	6.1	15.2			X	X
L11	N90 0 CG AS[5]		**64-22**	—	—	—	6	15.3			X	X
L12	N90 30 CG[6] S2[8] AS[5]		**58-28**	—	7	30.6	6	15.2			X	X
L13	N90 30 CG[6] S1[7] AS[5]		**58-28**	—	7	29.8	6	15.3			X	X

X = Test was performed for this mix.
[1] AC containing steel slag.
[2] AC containing recycled concrete aggregate (RCA)
[3] Surface course AC, placed at the topmost layer of the pavement and exposed to traffic.
[4] Base course AC, placed directly below the surface course.
[5] AS mixture with 1% anti-strip added to virgin binder.
[7] RAS source (S1)
[6] These mixtures have different RAS sources but similar mix design.
[8] RAS source (S2).

Table B-2 Laboratory Mix Design L3

AGGREGATE DETAILS						
Agg. Blending %	CM16	FM20	FM02	RAS	MF	Target
	61.5	26.9	11.3	0.0	0.3	100.0
	% Passing Sieve					
1" (25.0 mm)	100.0	100.0	100.0	100.0	100.0	*100.0*
3/4" (19.0 mm)	100.0	100.0	100.0	100.0	100.0	*100.0*
1/2" (12.5 mm)	100.0	100.0	100.0	100.0	100.0	*100.0*
3/8" (9.5 mm)	97.0	100.0	100.0	99.8	100.0	*98.2*
No. 4 (4.75 mm)	32.0	97.0	100.0	98.8	100.0	*57.4*
No. 8 (2.36 mm)	9.0	68.0	94.5	95.4	100.0	*34.8*
No. 16 (1.18 mm)	7.0	40.0	72.0	75.9	100.0	*23.5*
No. 30 (600 µm)	6.0	24.0	49.0	50.8	100.0	*16.0*
No. 50 (300 µm)	6.0	15.0	19.9	42.9	100.0	*10.3*
No. 100 (150 µm)	5.0	9.0	4.1	37.2	95.0	*6.2*
No. 200 (75 µm)	4.6	6.7	1.5	30.6	90.0	*5.1*
Bulk Spec Gravity (Gsb)	2.644	2.691	2.619	2.500	2.900	*2.654*
Apparent Spec Gravity (Gsa)	2.792	2.796	2.719		2.900	*#DIV/0!*
Absorption (%)	2.0	1.4	1.4	1.0		*1.723*

Notes:

BINDER DETAILS	
Binder Type	PG 70 - 22
Specific Gravity, G_b	1.03

MIXING CONDITIONS	
Mixing Temperature	*160 C*
Compaction Temperature	*150 C*
G_{mm}	2.491

VOLUMETRICS										
Binder%	Gmb @ N90	Ht @N90 (mm)	VTM	VMA	DP	VFA	% Gmm @ Nini	Gse	Absorbed Asphalt	Effective Asphalt
6%	2.394	115.36	3.9%	15.2%	0.85	74.4%		2.739	1.20%	4.87%
6%	2.399	114.89	3.7%	15.0%	0.85	75.4%		2.739	1.20%	4.87%
6%	2.387	115.78	4.2%	15.5%	0.85	73.0%		2.739	1.20%	4.87%

Table B-3 Laboratory Mix Design L4

AGGREGATE DETAILS						
Agg. Blending %	CM16	FM20	FM02	RAS	MF	Target
	61.5	26.9	11.3	0.0	0.3	100.0
	% Passing Sieve					
1" (25.0 mm)	100.0	100.0	100.0	100.0	100.0	*100.0*
3/4" (19.0 mm)	100.0	100.0	100.0	100.0	100.0	*100.0*
1/2" (12.5 mm)	100.0	100.0	100.0	100.0	100.0	*100.0*
3/8" (9.5 mm)	97.0	100.0	100.0	99.8	100.0	*98.2*
No. 4 (4.75 mm)	32.0	97.0	100.0	98.8	100.0	*57.4*
No. 8 (2.36 mm)	9.0	68.0	94.5	95.4	100.0	*34.8*
No. 16 (1.18 mm)	7.0	40.0	72.0	75.9	100.0	*23.5*
No. 30 (600 µm)	6.0	24.0	49.0	50.8	100.0	*16.0*
No. 50 (300 µm)	6.0	15.0	19.9	42.9	100.0	*10.3*
No. 100 (150 µm)	5.0	9.0	4.1	37.2	95.0	*6.2*
No. 200 (75 µm)	4.6	6.7	1.5	30.6	90.0	*5.1*
Bulk Spec Gravity (Gsb)	2.644	2.691	2.619	2.500	2.900	*2.654*
Apparent Spec Gravity (Gsa)	2.792	2.796	2.719		2.900	*#DIV/0!*
Absorption (%)	2.0	1.4	1.4	1.0		*1.723*

Notes:

BINDER DETAILS	
Binder Type	PG 64-22
Specific Gravity, G_b	1.03

MIXING CONDITIONS	
Mixing Temperature	*150 C*
Compaction Temperature	*150 C*
G_{mm}	2.496

VOLUMETRICS										
Binder%	Gmb @ N90	Ht @N90 (mm)	VTM	VMA	DP	VFA	% Gmm @ Nini	Gse	Absorbed Asphalt	Effective Asphalt
6%	2.392	115.36	4.2%	15.3%	0.85	72.7%		2.745	1.29%	4.79%
6%	2.393	114.89	4.1%	15.3%	0.85	72.9%		2.745	1.29%	4.79%

Table B-4 Laboratory Mix Design L5

AGGREGATE DETAILS						
Agg. Blending %	CM16	FM20	FM02	RAS	MF	Target
	63.5	16.0	12.5	7.0	1.0	100.0
	% Passing Sieve					
1" (25.0 mm)	100.0	100.0	100.0	100.0	100.0	*100.0*
3/4" (19.0 mm)	100.0	100.0	100.0	100.0	100.0	*100.0*
1/2" (12.5 mm)	100.0	100.0	100.0	100.0	100.0	*100.0*
3/8" (9.5 mm)	97.0	100.0	100.0	99.8	100.0	*98.1*
No. 4 (4.75 mm)	32.0	97.0	100.0	98.8	100.0	*56.3*
No. 8 (2.36 mm)	9.0	68.0	94.5	95.4	100.0	*36.1*
No. 16 (1.18 mm)	7.0	40.0	72.0	75.9	100.0	*26.2*
No. 30 (600 µm)	6.0	24.0	49.0	50.8	100.0	*18.3*
No. 50 (300 µm)	6.0	15.0	19.9	42.9	100.0	*12.7*
No. 100 (150 µm)	5.0	9.0	4.1	37.2	95.0	*8.7*
No. 200 (75 µm)	4.6	6.7	1.5	30.6	90.0	*7.2*
Bulk Spec Gravity (Gsb)	2.644	2.691	2.619	2.500	2.900	*2.640*
Apparent Spec Gravity (Gsa)	2.792	2.796	2.719		2.900	*#DIV/0!*
Absorption (%)	2.0	1.4	1.4	1.0		*1.692*

Notes:

BINDER DETAILS	
Binder Type	PG 70 - 22
Specific Gravity, G_b	1.03

MIXING CONDITIONS	
Mixing Temperature	*160 C*
Compaction Temperature	*150 C*
G_{mm}	2.476

VOLUMETRICS										
Binder%	Gmb @ N90	Ht @N90 (mm)	VTM	VMA	DP	VFA	% Gmm @ Nini	Gse	Absorbed Asphalt	Effective Asphalt
6%	2.381	113.83	3.8%	15.2%	1.20	74.8%		2.720	1.14%	4.92%
6%	2.362	114.65	4.6%	15.9%	1.20	71.0%		2.720	1.14%	4.92%
6%	2.377	113.68	4.0%	15.4%	1.20	74.0%		2.720	1.14%	4.92%

Table B-5 Laboratory Mix Design L6

AGGREGATE DETAILS						
Agg. Blending %	CM16	FM20	FM02	RAS	MF	Target
	63.5	16.0	12.5	7.0	1.0	100.0
% Passing Sieve						
1" (25.0 mm)	100.0	100.0	100.0	100.0	100.0	*100.0*
3/4" (19.0 mm)	100.0	100.0	100.0	100.0	100.0	*100.0*
1/2" (12.5 mm)	100.0	100.0	100.0	100.0	100.0	*100.0*
3/8" (9.5 mm)	97.0	100.0	100.0	99.8	100.0	*98.1*
No. 4 (4.75 mm)	32.0	97.0	100.0	98.8	100.0	*56.3*
No. 8 (2.36 mm)	9.0	68.0	94.5	95.4	100.0	*36.1*
No. 16 (1.18 mm)	7.0	40.0	72.0	75.9	100.0	*26.2*
No. 30 (600 µm)	6.0	24.0	49.0	50.8	100.0	*18.3*
No. 50 (300 µm)	6.0	15.0	19.9	42.9	100.0	*12.7*
No. 100 (150 µm)	5.0	9.0	4.1	37.2	95.0	*8.7*
No. 200 (75 µm)	4.6	6.7	1.5	30.6	90.0	*7.2*
Bulk Spec Gravity (Gsb)	2.644	2.691	2.619	2.500	2.900	*2.640*
Apparent Spec Gravity (Gsa)	2.792	2.796	2.719		2.900	*#DIV/0!*
Absorption (%)	2.0	1.4	1.4	1.0		*1.692*

Notes:

BINDER DETAILS	
Binder Type	PG 58 - 28
Specific Gravity, G_b	1.03

MIXING CONDITIONS	
Mixing Temperature	*153C*
Compaction Temperature	*147C*
G_{mm}	2.485

VOLUMETRICS										
Binder%	Gmb @ N90	Ht @N90 (mm)	VTM	VMA	DP	VFA	% Gmm @ Nini	Gse	Absorbed Asphalt	Effective Asphalt
6%	2.370	113.88	4.6%	15.6%	1.20	70.4%		2.731	1.31%	4.77%
6%	2.370	113.75	4.6%	15.6%	1.20	70.4%		2.731	1.31%	4.77%

Table B-6 Laboratory Mix Design L7

AGGREGATE DETAILS						
Agg. Blending %	CM16	FM20	FM02	RAS	MF	Target
	63.5	18.0	13.1	5.0	0.4	100.0
% Passing Sieve						
1" (25.0 mm)	100.0	100.0	100.0	100.0	100.0	*100.0*
3/4" (19.0 mm)	100.0	100.0	100.0	100.0	100.0	*100.0*
1/2" (12.5 mm)	100.0	100.0	100.0	100.0	100.0	*100.0*
3/8" (9.5 mm)	97.0	100.0	100.0	99.8	100.0	*98.1*
No. 4 (4.75 mm)	32.0	97.0	100.0	98.8	100.0	*56.2*
No. 8 (2.36 mm)	9.0	68.0	94.5	95.4	100.0	*35.5*
No. 16 (1.18 mm)	7.0	40.0	72.0	75.9	100.0	*25.3*
No. 30 (600 µm)	6.0	24.0	49.0	50.8	100.0	*17.5*
No. 50 (300 µm)	6.0	15.0	19.9	42.9	100.0	*11.7*
No. 100 (150 µm)	5.0	9.0	4.1	37.2	95.0	*7.6*
No. 200 (75 µm)	4.6	6.7	1.5	30.6	90.0	*6.2*
Bulk Spec Gravity (Gsb)	2.644	2.691	2.619	2.500	2.900	*2.642*
Apparent Spec Gravity (Gsa)	2.792	2.796	2.719		2.900	*#DIV/0!*
Absorption (%)	2.0	1.4	1.4	1.0		*1.696*

Notes:

BINDER DETAILS	
Binder Type	PG 58-28
Specific Gravity, G_b	1.03

MIXING CONDITIONS	
Mixing Temperature	*153C*
Compaction Temperature	*147C*
G_{mm}	2.484

VOLUMETRICS										
Binder%	Gmb @ N90	Ht @N90 (mm)	VTM	VMA	DP	VFA	% Gmm @ Nini	Gse	Absorbed Asphalt	Effective Asphalt
6%	2.388	113.7	3.9%	15.0%	1.04	74.3%		2.730	1.25%	4.82%
6%	2.383	114.18	4.1%	15.2%	1.04	73.3%		2.730	1.25%	4.82%

Table B-7 Laboratory Mix Design L8

AGGREGATE DETAILS						
Agg. Blending %	CM16	FM20	FM02	RAS	MF	Target
	63.5	18.5	15.5	2.5	0.0	100.0
	% Passing Sieve					
1" (25.0 mm)	100.0	100.0	100.0	100.0	100.0	*100.0*
3/4" (19.0 mm)	100.0	100.0	100.0	100.0	100.0	*100.0*
1/2" (12.5 mm)	100.0	100.0	100.0	100.0	100.0	*100.0*
3/8" (9.5 mm)	97.0	100.0	100.0	99.8	100.0	*98.1*
No. 4 (4.75 mm)	32.0	97.0	100.0	98.8	100.0	*56.2*
No. 8 (2.36 mm)	9.0	68.0	94.5	95.4	100.0	*35.3*
No. 16 (1.18 mm)	7.0	40.0	72.0	75.9	100.0	*24.9*
No. 30 (600 µm)	6.0	24.0	49.0	50.8	100.0	*17.1*
No. 50 (300 µm)	6.0	15.0	19.9	42.9	100.0	*10.7*
No. 100 (150 µm)	5.0	9.0	4.1	37.2	95.0	*6.4*
No. 200 (75 µm)	4.6	6.7	1.5	30.6	90.0	*5.2*
Bulk Spec Gravity (Gsb)	2.644	2.691	2.619	2.500	2.900	*2.645*
Apparent Spec Gravity (Gsa)	2.792	2.796	2.719		2.900	*#DIV/0!*
Absorption (%)	2.0	1.4	1.4	1.0		*1.708*

Notes:

BINDER DETAILS	
Binder Type	PG 64-22
Specific Gravity, G_b	1.03

MIXING CONDITIONS	
Mixing Temperature	*157C*
Compaction Temperature	*150C*
G_{mm}	2.488

VOLUMETRICS										
Binder%	Gmb @ N90	Ht @N90 (mm)	VTM	VMA	DP	VFA	% Gmm @ Nini	Gse	Absorbed Asphalt	Effective Asphalt
6%	2.385	114.93	4.1%	15.2%	0.86	72.8%		2.735	1.29%	4.79%
6%	2.380	115.18	4.3%	15.4%	0.86	71.8%		2.735	1.29%	4.79%

Table B-8 Laboratory Mix Design L9

AGGREGATE DETAILS								
Agg. Blending %	CM16	FM20	FM02	RAP(-3/8	RAP(+3/8	RAS	MF	Target
	56.0	17.8	9.9	7.0	4.0	5.0	0.3	100.0
	% Passing Sieve							
1" (25.0 mm)	100.0	100.0	100.0	100.0	100.0	100.0	100.0	*100.0*
3/4" (19.0 mm)	100.0	100.0	100.0	100.0	99.3	100.0	100.0	*100.0*
1/2" (12.5 mm)	100.0	100.0	100.0	100.0	90.8	100.0	100.0	*99.6*
3/8" (9.5 mm)	97.0	100.0	100.0	99.3	78.6	100.0	100.0	*97.4*
No. 4 (4.75 mm)	32.0	97.0	100.0	71.7	39.0	97.2	100.0	*56.8*
No. 8 (2.36 mm)	9.0	68.0	94.5	48.6	26.5	93.4	100.0	*35.9*
No. 16 (1.18 mm)	7.0	40.0	72.0	32.6	19.1	77.1	100.0	*25.4*
No. 30 (600 µm)	6.0	24.0	49.0	24.2	14.8	57.2	100.0	*17.9*
No. 50 (300 µm)	6.0	15.0	19.9	17.2	10.7	49.7	100.0	*12.4*
No. 100 (150 µm)	5.0	9.0	4.1	12.7	7.7	43.2	95.0	*8.5*
No. 200 (75 µm)	4.6	6.7	1.5	10.1	6.0	34.4	90.0	*6.9*
Bulk Spec Gravity (Gsb)	2.644	2.691	2.619	2.641	2.627	2.500	2.900	*2.642*
Apparent Spec Gravity (Gsa)	2.792	2.796	2.719		2.900			*#DIV/0!*
Absorption (%)	2.0	1.4	1.4	1.0				*1.825*

Pavegrip Antistrip was added to the binder. (1% of total binder weight)

BINDER DETAILS	
Binder Type	PG 58-28
Specific Gravity, G_b	1.03

MIXING CONDITIONS	
Mixing Temperature	*147C*
Compaction Temperature	*143C*
G_{mm}	2.492

VOLUMETRICS

Binder%	Gmb @ N90	Ht @N90 (mm)	VTM	VMA	DP	gmm		VFA	Gse	Absorbed Asphalt	Effective Asphalt
6.00%	2.384	112.93	4.4%	15.2%	1.14	2.493		71.3%	2.740	1.40%	4.68%
6.00%	2.383	113.25	4.4%	15.2%	1.14	2.492		71.3%	2.740	1.40%	4.68%

Table B-9 Laboratory Mix Design L10

AGGREGATE DETAILS								
Agg. Blending %	CM16	FM20	FM02	RAP(-3/8	RAP(+3/8	RAS	MF	Target
	38.0	11.4	3.4	20.0	20.0	7.0	0.2	100.0
				% Passing Sieve				
1" (25.0 mm)	100.0	100.0	100.0	100.0	100.0	100.0	100.0	*100.0*
3/4" (19.0 mm)	100.0	100.0	100.0	100.0	99.3	100.0	100.0	*99.9*
1/2" (12.5 mm)	100.0	100.0	100.0	100.0	90.8	100.0	100.0	*98.2*
3/8" (9.5 mm)	97.0	100.0	100.0	99.3	78.6	100.0	100.0	*94.4*
No. 4 (4.75 mm)	32.0	97.0	100.0	71.7	39.0	97.2	100.0	*55.8*
No. 8 (2.36 mm)	9.0	68.0	94.5	48.6	26.5	93.4	100.0	*36.1*
No. 16 (1.18 mm)	7.0	40.0	72.0	32.6	19.1	77.1	100.0	*25.6*
No. 30 (600 µm)	6.0	24.0	49.0	24.2	14.8	57.2	100.0	*18.7*
No. 50 (300 µm)	6.0	15.0	19.9	17.2	10.7	49.7	100.0	*13.9*
No. 100 (150 µm)	5.0	9.0	4.1	12.7	7.7	43.2	95.0	*10.4*
No. 200 (75 µm)	4.6	6.7	1.5	10.1	6.0	34.4	90.0	*8.4*
Bulk Spec Gravity (Gsb)	2.644	2.691	2.619	2.641	2.627	2.500	2.900	*2.634*
Apparent Spec Gravity (Gsa)	2.792	2.796	2.719		2.900			*#DIV/0!*
Absorption (%)	2.0	1.4	1.4	1.0				*2.017*

Pavegrip Antistrip was added to the binder. (1% of total binder weight)

BINDER DETAILS	
Binder Type	PG 52-34
Specific Gravity, G_b	1.03

MIXING CONDITIONS	
Mixing Temperature	*150C*
Compaction Temperature	*144C*
G_{mm}	

VOLUMETRICS

Binder%	Gmb @ N90	Ht @N90 (mm)	VTM	VMA	DP	Gmm		VFA	Gse	Absorbed Asphalt	Effective Asphalt
6.10%	2.379	111.46	4.5%	15.2%	1.37	2.492		70.2%	2.745	1.58%	4.61%
6.10%	2.386	111.07	4.0%	14.9%	1.37	2.487		72.9%	2.745	1.58%	4.61%
6.10%	2.379	111.6	4.6%	15.2%	1.37	2.494		69.7%	2.745	1.58%	4.61%

Table B-10 Laboratory Mix Design L11

AGGREGATE DETAILS						
Agg. Blending %	CM16	FM20	FM02	RAS	MF	Target
	61.5	26.9	11.3	0.0	0.3	100.0
% Passing Sieve						
1" (25.0 mm)	100.0	100.0	100.0	100.0	100.0	*100.0*
3/4" (19.0 mm)	100.0	100.0	100.0	100.0	100.0	*100.0*
1/2" (12.5 mm)	100.0	100.0	100.0	100.0	100.0	*100.0*
3/8" (9.5 mm)	97.0	100.0	100.0	99.8	100.0	*98.2*
No. 4 (4.75 mm)	32.0	97.0	100.0	98.8	100.0	*57.4*
No. 8 (2.36 mm)	9.0	68.0	94.5	95.4	100.0	*34.8*
No. 16 (1.18 mm)	7.0	40.0	72.0	75.9	100.0	*23.5*
No. 30 (600 µm)	6.0	24.0	49.0	50.8	100.0	*16.0*
No. 50 (300 µm)	6.0	15.0	19.9	42.9	100.0	*10.3*
No. 100 (150 µm)	5.0	9.0	4.1	37.2	95.0	*6.2*
No. 200 (75 µm)	4.6	6.7	1.5	30.6	90.0	*5.1*
Bulk Spec Gravity (Gsb)	2.644	2.691	2.619	2.500	2.900	*2.654*
Apparent Spec Gravity (Gsa)	2.792	2.796	2.719		2.900	*#DIV/0!*
Absorption (%)	2.0	1.4	1.4	1.0		*1.723*

Notes:
Pavegrip Antistrip was added to the binder. (1% of total binder weight)

BINDER DETAILS	
Binder Type	PG 64-22
Specific Gravity, G_b	1.03

MIXING CONDITIONS	
Mixing Temperature	*150 C*
Compaction Temperature	*150 C*
G_{mm}	2.496

VOLUMETRICS										
Binder%	Gmb @ N90	Ht @N90 (mm)	VTM	VMA	DP	VFA	% Gmm @ Nini	Gse	Absorbed Asphalt	Effective Asphalt
6%	2.392	115.36	4.2%	15.3%	0.85	72.7%		2.745	1.29%	4.79%
6%	2.393	114.89	4.1%	15.3%	0.85	72.9%		2.745	1.29%	4.79%

Table B-11 Laboratory Mix Design L12

AGGREGATE DETAILS							
Agg. Blending %	CM16	FM20	FM02	RAS	MF	Target	
	64.0	15.5	12.5	7.0	1.0	100.0	
	% Passing Sieve						
1" (25.0 mm)	100.0	100.0	100.0	100.0	100.0	*100.0*	Pavegrip Antistrip was added to the binder. (1% of total binder weight)
3/4" (19.0 mm)	100.0	100.0	100.0	100.0	100.0	*100.0*	
1/2" (12.5 mm)	100.0	100.0	100.0	100.0	100.0	*100.0*	
3/8" (9.5 mm)	97.0	100.0	100.0	100.0	100.0	*98.1*	
No. 4 (4.75 mm)	32.0	97.0	100.0	97.2	100.0	*55.8*	
No. 8 (2.36 mm)	9.0	68.0	94.5	93.4	100.0	*35.6*	
No. 16 (1.18 mm)	7.0	40.0	72.0	77.1	100.0	*26.1*	*BINDER DETAILS*
No. 30 (600 µm)	6.0	24.0	49.0	57.2	100.0	*18.7*	Binder Type: PG 64-22
No. 50 (300 µm)	6.0	15.0	19.9	49.7	100.0	*13.1*	Specific Gravity, G_b: 1.03
No. 100 (150 µm)	5.0	9.0	4.1	43.2	95.0	*9.1*	
No. 200 (75 µm)	4.6	6.7	1.5	34.4	90.0	*7.5*	
Bulk Spec Gravity (Gsb)	2.644	2.691	2.619	2.500	2.900	*2.640*	*MIXING CONDITIONS*
Apparent Spec Gravity (Gsa)	2.792	2.796	2.719		2.900	*#DIV/0!*	Mixing Temperature: *153*
Absorption (%)	2.0	1.4	1.4	1.0		*1.695*	Compaction Temperature: *145*
							G_{mm}: 2.484

VOLUMETRICS

Binder%	Gmb @ N90	Ht @N90 (mm)	VTM	VMA	DP	VFA	Gse	Absorbed Asphalt	Effective Asphalt
6%	2.380	113.58	4.2%	15.3%	1.25	72.4%	2.730	1.29%	4.78%
6%	2.382	113.53	4.1%	15.2%	1.25	72.9%	2.730	1.29%	4.78%

Table B-12 Laboratory Mix Design L13

AGGREGATE DETAILS						
Agg. Blending %	CM16	FM20	FM02	RAS	MF	Target
	63.5	16.0	12.5	7.0	1.0	100.0
	% Passing Sieve					
1" (25.0 mm)	100.0	100.0	100.0	100.0	100.0	*100.0*
3/4" (19.0 mm)	100.0	100.0	100.0	100.0	100.0	*100.0*
1/2" (12.5 mm)	100.0	100.0	100.0	100.0	100.0	*100.0*
3/8" (9.5 mm)	97.0	100.0	100.0	99.8	100.0	*98.1*
No. 4 (4.75 mm)	32.0	97.0	100.0	98.8	100.0	*56.3*
No. 8 (2.36 mm)	9.0	68.0	94.5	95.4	100.0	*36.1*
No. 16 (1.18 mm)	7.0	40.0	72.0	75.9	100.0	*26.2*
No. 30 (600 µm)	6.0	24.0	49.0	50.8	100.0	*18.3*
No. 50 (300 µm)	6.0	15.0	19.9	42.9	100.0	*12.7*
No. 100 (150 µm)	5.0	9.0	4.1	37.2	95.0	*8.7*
No. 200 (75 µm)	4.6	6.7	1.5	30.6	90.0	*7.2*
Bulk Spec Gravity (Gsb)	2.644	2.691	2.619	2.500	2.900	*2.640*
Apparent Spec Gravity (Gsa)	2.792	2.796	2.719		2.900	*#DIV/0!*
Absorption (%)	2.0	1.4	1.4	1.0		*1.692*

Notes:
Pavegrip Antistrip was added to the binder. (1% of total binder weight)

BINDER DETAILS	
Binder Type	PG 58 - 28
Specific Gravity, G_b	1.03

MIXING CONDITIONS	
Mixing Temperature	*153C*
Compaction Temperature	*147C*
G_{mm}	2.485

VOLUMETRICS										
Binder%	Gmb @ N90	Ht @N90 (mm)	VTM	VMA	DP	VFA	% Gmm @ Nini	Gse	Absorbed Asphalt	Effective Asphalt
6%	2.370	113.88	4.6%	15.6%	1.20	70.4%		2.731	1.31%	4.77%
6%	2.370	113.75	4.6%	15.6%	1.20	70.4%		2.731	1.31%	4.77%

APPENDIX C: FIELD CORE INVENTORY AND TEST RESULTS SUMMARY

SECTION C-1. FIELD CORE MIX DESIGN, STRUCTURE, AND PERFORMANCE DATA

Table C-1.1 Field Cores Mixture Design and Volumetrics

Core ID			Mixture Design and Volumetrics													
District	Section	Lab Name	Mix Type	N-design	NMAS	Year of Construction	VMA	Design Air Voids	AC Grade	AC %	RAP	RAS	% ABR	TSR	Dry Strength (psi)	Hamburg
1	1	1-1	SMA-SC	80	12.5	2008	17.87	3.5	PG 76-22	5.8	0	0	0	0.91	NA	NA
	2	1-2	SMA-SC	80	12.5	2008	17.5	3.5	PG 76-22	5.7	0	0	0	0.96	99.5	NA
	3	1-3	SMA-SC	80	12.5	2009	17.6	3.5	NA	6	0	0	0	0.99	97.6	NA
	4	1-4	SMA-SC	80	12.5	2013	17.4	3.5	PG 70-28	5.8	14.2	3	28.2	0.95	148.0	2.81 mm at 20000
	5	1-5	F-SC	90	9.5	2013	15.8	4.0	PG 70-28	5.5	8	5	29.6	0.97	179.2	1.74 mm at 20000
	6	1-6	F-SC	90	9.5	2013	16.4	4.0	PG 76-22	5.2	14	2.5	30.4	0.93	194.7	1.89 mm at 20000
	7	1-7	F-SC	90	9.5	2009	14.8	4.0	NA	5.3	10	0	10	0.93	162.3	NA
	8	1-8	D-SC	70	9.5	2010	14.9	4.0	NA	5.8	20	0	14.4	0.97	107.1	NA
	9	1-9	D-SC	70	9.5	2013	14.9	4.0	PG 58-28	5.9	30	0	20.2	0.99	115.3	8.95 mm at 10000
	10	1-10	D-SC	50	9.5	2013	14.9	3.0	PG 52-28	6.5	53	6	67.1	0.88	141.0	1.7 mm at 10000
	11	1-11	D-SC	70	NA	2009	14.6	4.0	PG 64-22	5.9	10	0	7.5	0.90	505.9	NA
	12	1-12	D-SC	70	9.5	2013	15.5	4.0	PG 58-28	5.7	17.5	2.5	30.3	0.89	172.2	2.74 mm at 10000
	13	1-13	F-SC	90	9.5	2013	15.1	4.0	PG 70-22	5.8	10	0	10.2	0.88	148.9	2.87 mm at 20000
2	1	2RT26	SMA-SC	NA	NA	2004	NA	4.0	PG 76-28	6.2	0	0	0	0.87	NA	NA
	2	22RT2	D-SC	50	NA	2003	NA	4.2	PG 70-22	5.3	0	0	0	0.86	NA	NA
	3	22SRT2	C-SC	70	NA	2004	NA	3.0	PG 58-28	5.2	15	0	0	0.85	NA	NA
3	1	3-6E	D-SC	70	9.5	2012	14.9	4.0	PG 64-22	6.2	10	0	7	0.93	133.6	6.7 mm at 10,000 passes
	2	3-6W	F-SC	50	9.5	2013	15	4.0	PG 64-22	6	40	0	27	0.88	104.0	Passed at 10,000 passes
	3	3-LB-E	LB	50	4.75	2012	19.8	4.0	PG 64-28	8.1	20	0	16.3	0.91	146.2	3.2 mm at 10,000 passes
	4	3-LB-W	LB	50	4.75	2013	NA	NA	PG 64-22	5.7	40	0	—	0.98	137.0	Passed at 10,000 passes
4	1	D4-IL78	E-SC	90	9.5	2012	NA	4.0	10128	5.8	10	5	—	NA	NA	
	2	D4-IL9	D-SC	50	9.5	2013	NA	4.0	10125	5.8	16	3.2	33.5	NA	99.0	3.8 mm at 10,000 passes 4.9 mm at 20,000 passes
	3	D4-IL55	E-SC	90	9.5	2012	15.1	4.0	10131	6	10	0	10.3	NA	128.1	NA

Core ID			Mixture Design and Volumetrics													
District	Section	Lab Name	Mix Type	N-design	NMAS	Year of Construction	VMA	Design Air Voids	AC Grade	AC %	RAP	RAS	% ABR	TSR	Dry Strength (psi)	Hamburg
5	1	5-US136-1	C-SC	50	NA	2013	15.2	4.0	PG 58-28	5.9	30	0	22	0.88	122.0	6.54 mm at 10,000 passes
	2	5-US136-2	D-SC	90	NA	2014	14.8	4.0	PG 70-22	5.9	10	0	9	0.93	152.0	1.59 mm at 15,000 passes
	3	5-I39	D-SC	90	NA	2013	NA	4.0	PG 70-28	6.2	12	0	10	0.98	104.0	3.41 mm at 15,000 passes
	4	5-I57	D-SC	90	NA	2013	NA	4.0	PG 70-28	5.9	10	0	9	0.88	102.0	4.76 mm at 15,000 passes
	5	5-IL47	D-SC	70	NA	2012	NA	4.0	PG 64-22	6.1	10	0	8	0.91	152.0	NA
	6	5-IL6		50	NA	2012	NA	4.0	PG 64-22	5.7	14	0	13	0.91	86.0	NA
6	1	6G2	D-SC	70	9.5	2013	18.3	4.0		6	Y	0	8.5	0.92	132.0	Passed for PG 70-XX
	2	6P	D-SC	70	9.5	2013	17.4	4.0		6	Y	0	16	0.95	107.0	Passed for PG 70-XX
7	1	7-I130	—	—	—	—	NA	—	—	—	—	—	—	—	—	—
	2	7-I121	—	—	—	—	NA	—	—	—	—	—	—	—	—	—
8	1	8JVS2	C-SC	70	9.5	2013	14.9	4.0	PG 64-22	5.6	15	0		0.88	123.1	4.3 mm at 7500 12.5 mm at 16500
	2	867S1	D-SC	70	9.5	2013	14.7	4.0	PG 64-22	6.2	15	0	14.5	0.95	130.1	5.0 mm at 7500 12.5 mm at 11,000
9	1	9-I4	D-SC	90	NA	2013	NA	N/A	PG 64-22	5.3	0	0	0	0.84	108.2	11.93 mm at 10,000 8.95 mm at 7500
	2	9-I54	C-SC	90	NA	2013	14.5	4.0	PG 64-22	N/A	20	0	—	0.89	104.3	8.7 mm at 7500

Table C-1.2 Field Volumetrics and Pavement Structure

Core ID			Field Volumetrics						Pavement Structure				
District	Sec.	Lab Name	Normalized Rutting	Prod. Voids	Prod. VMA	Production Density	Prod. AC %	Prod. Hamburg	Pavement Type	Thickness (Surface)	Thickness (All AC)	Base Type	Base Thickness
1	1	1-1	NA	NA	19.39	NA	NA	NA	NA	NA	NA	NA	NA
	2	1-2	NA	NA	19.13	NA	NA	NA	NA	NA	NA	NA	NA
	3	1-3	NA	NA	NA	NA	NA	NA	NA	NA	NA	NA	NA
	4	1-4	NA	NA	NA	NA	NA	NA	NA	NA	NA	NA	NA
	5	1-5	NA	NA	NA	NA	NA	NA	NA	NA	NA	NA	NA
	6	1-6	NA	NA	NA	NA	NA	NA	NA	NA	NA	NA	NA
	7	1-7	NA	NA	NA	NA	NA	NA	NA	NA	NA	NA	NA
	8	1-8	NA	NA	NA	NA	NA	NA	NA	NA	NA	NA	NA
	9	1-9	NA	NA	NA	NA	NA	NA	NA	NA	NA	NA	NA
	10	1-10	NA	NA	NA	NA	NA	NA	NA	NA	NA	NA	NA
	11	1-11	NA	NA	NA	NA	NA	NA	NA	NA	NA	NA	NA
	12	1-12	NA	NA	NA	NA	NA	NA	NA	NA	NA	NA	NA
	13	1-13	NA	NA	NA	NA	NA	NA	NA	NA	NA	NA	NA
2	1	2RT26	NA	NA	NA	NA	NA	NA	AC/Subgrade	2	13.25	Various, See Comments	11.25
	2	22RT2	NA	NA	NA	NA	NA	NA	AC/Subgrade	2	13	Asphalt Type 1 BC	11
	3	22SRT2	NA	NA	NA	NA	NA	NA	AC/Subgrade	8	8	NA	0
3	1	3-6E	4.2	2.30%	17.7	92.20%	6.10%	4.1 mm at 10,000 passes	AC/Brick	1.5	11.5	Brick	20
	2	3-6W	PASS	4%	14.3	92.90%	5.60%	Passed at 7,500 passes	AC/PCC	1.5	7.5	PCC	9
	3	3-LB-E	2	2.90%	19.1	96.90%	8.40%	11.9 mm at 10,000 passes		0.75	11.5	NA	NA
	4	3-LB-W	Pass	4.3	15.2	92.10%	6.10%	Passed at 7,500 passes		0.75	7.5	NA	NA
4	1	D4-IL78	2	4.9	16.7	93.40%	NA	2.2 mm at 20,000 passes 1.58 mm at 15000 passes	AC/PCC	2	NA	PCC	9
	2	D4-IL9	NA	3.4	15	96.20%	NA	3.3 mm at 10,000 passes 4.0 mm at 20,000 passes	AC/PCC	1.5	4.5	9-6-9 PCC	9
	3	D4-IL55	0.8	4.3	16.7	94.80%		4.5 mm at 20,000 passes	AC/Subgrade	3.75	16	NA	

Core ID			Field Volumetrics						Pavement Structure				
District	Sec.	Lab Name	Normalized Rutting	Prod. Voids	Prod. VMA	Production Density	Prod. AC %	Prod. Hamburg	Pavement Type	Thickness (Surface)	Thickness (All AC)	Base Type	Base Thickness
5	1	5-US136-1	6.7	4.6	15.7	94.10%	6.2	11.31 mm at 10,000 passes	AC/PCC	1.5	5.25	9-6-9 PCC	9
	2	5-US136-2	2.1	3.9	14.2	92.40%	5.6	4.28 mm at 15,000 passes	AC/PCCP	1.75	NA	PCCP	10
	3	5-I39	2.1	3.8	15.2	94.70%	6.1	4.29 mm at 15,000 passes	AC/Subgrade	8	12	NA	NA
	4	5-I57	1.48	4.3	14.4	93.50%	5.8	3.05 mm at 15,000 passes	AC/Subgrade	11.25	11.25	NA	NA
	5	5-IL47	NA	2.9	14.6	NA	6.1	NA	AC/Subgrade	1.5	17.5	9-6-9 PCC	9
	6	5-IL6	NA	4.1	14.6	NA	5.8	NA	AC/Base	1.5	6.5	Soil Cement Base Course	7
6	1	6G2	NA	3.9	15	94.2	6.1	NA	AC/Subgrade	2.25	17	NA	NA
	2	6P	4.2	3.9	14.2	94.1	5.9	4.2 mm at 7500 passes	AC/Subgrade	2.25	17	NA	NA
7	1	7-I130			NA								
	2	7-I121			NA								
8	1	8JVS2	4.3		NA				AC/PCC	2.25	10	9-6-9 PCC	9
	2	867S1	7	NA	NA	NA	NA	7.0 mm at 7500 12.5 mm at 10750	AC/PCC	1.5	5	PCC	7
9	1	9-I4	8.95	Acceptable	NA	Acceptable		NA	AC/PCC	1.5	3	PCC	9
	2	9-I54	7500	4.4	14.3	92.4		8.2 mm at 7500	AC/PCC	1.5	7.5	PCC	9

Table C-1.3 Traffic, Laboratory, and Pavement Performance

Core ID			Laboratory Performance			Pavement Performance	Traffic		
District	Sec.	Lab Name	Fracture Energy (SCB at 25°C, 50 mm/min)	FI (SCB at 25°C, 50 mm/min)	CRS	Distress Type	PV	Trucks	Comments
1	1	1-1	2527.92	4.96	NA	D1 Good	NA	NA	
	2	1-2	2302.83	3.06	NA	D1 Bad	NA	NA	
	3	1-3	2262.11	4.86	NA	BMPR Good	NA	NA	
	4	1-4	2284.52	1.76	NA	BMPR Bad	NA	NA	
	5	1-5	1230.72	1.29	NA	BMPR Bad	NA	NA	
	6	1-6	1710.81	2.93	NA	BMPR Bad	NA	NA	
	7	1-7	1555.91	2.25	NA	Good	NA	NA	
	8	1-8	2515.18	6.02	NA	Good	NA	NA	
	9	1-9	2937.24	10.88	NA	Good	NA	NA	
	10	1-10	1797.81	1.37	NA	Bad	NA	NA	
	11	1-11	1851.98	3.39	NA	Good	NA	NA	
	12	1-12	2713.77	3.88	NA	BMPR Bad	NA	NA	
	13	1-13	2607.86	10.41	NA	Bad	NA	NA	
2	1	2RT26	1236.78	1.22	5.1	An example of HMA pavement that has withstood weathering and traffic in good condition	8920	1435	4" AC base, 3.25" asphalt binder course, 4" poly. asphalt binder course
	2	22RT2	1536.10	1.30	6.2	Close-spaced cracking and cracking from gear box segregation	17900	540	
	3	22SRT2	1155.66	0.65	NA	Thermal cracking	NA	NA	Shoulder mix, up to 15% RAP was allowed
3	1	3-6E	2526.84	10.12	8.8	Bad	8950	942	
	2	3-6W	1721.26	2.39	8.9	Good	4800	600	
	3	3-LB-E			8.8		8950	942	
	4	3-LB-W			8.9		4800	600	
4	1	D4-IL78	1842.98	4.00	7.7	Subjective to the viewer; it has transvers cracking (reflective?) of a pavement rehab of similar age	10200	479	
	2	D4-IL9	2663.94	11.09	7.1	Subjective to the viewer; it has transvers cracking (reflective?) of a pavement rehab of similar age.	5800	452	
	3	D4-IL55	808.39	1.30	8.4		13400	2130	
5	1	5-US136-1	2267.30	3.69	8.4	Good – no visible distress	3000	750	
	2	5-US136-2	2958.57	23.59	9	Very good condition – new construction – no visible distress	12000	780	
	3	5-I39	3394.44	19.79	9	Very good condition – new construction – no visible distress	18500	5920	
	4	5-I57	1997.10	5.97	8.4	Good – no visible distress	23100	5567	
	5	5-IL47	2096.01	4.77	7.3	Good – reflective cracks have appeared	3550	695	
	6	5-IL6	2089.95	3.70	NA	Good – no visible distress	650	NA	
6	1	6G2	3067.90	25.15	NA	No cracking was observed within the project limits	NA	NA	
	2	6P	2029.31	2.07	NA	Transverse cracking observed at approximately 100 to 500 ft intervals	NA	NA	
7	1	7-I130	1050.82	1.31			NA	NA	
	2	7-I121	2219.71	6.12			NA	NA	

Core ID			Laboratory Performance			Pavement Performance	Traffic		
District	Sec.	Lab Name	Fracture Energy (SCB at 25°C, 50 mm/min)	FI (SCB at 25°C, 50 mm/min)	CRS	Distress Type	PV	Trucks	Comments
8	1	8JVS2	2987.16	15.00	8.1		2700	280	
	2	867S1	2384.85	11.32	6.5	Longitudinal cracking exists at centerline, edges and wheel paths along with transverse cracking periodically throughout project. Cracking developed the year following construction immediately after winter	8700	461	

SECTION C-2: FIELD CORES TEST RESULT SUMMARY

C-2.1 District 1

Cores from 13 sections from this district were collected and tested for fracture energy and FI using IL-SCB. The details of core locations for the sections tested are provided in Table C-2.1. The AC mixture properties for these sections covered a wide spectrum that included SMA, fine graded, and dense graded. The majority of the sections were constructed in 2013, with a few constructed in 2007 and 2009 (Table C-2.1). Polymer-modified binders were used in most of the sections. Sections with high ABR content used relatively softer binders. The fracture energy and FI results of the tested sections are summarized in Figure C-2.1.

Table C-2.1 Details of Sections with Core Locations for District 1

Lab Name	Core Label	Core Location	Contract	Section	Route	City	County
1-1	57	Interstate 94 (Edens Expressway)	62636	—	Lake Cook Rd. to Old Orchard Rd.		
1-2	104	Northbound Interstate 55	62895	—	US Route 52 to US Route 30		
1-3	176	Northbound Interstate 94 (Bishop Ford Expressway)	60D21	—	US Route 6 (159th St.) to Sibley Boulevard (147th St.)		
1-4	118	Illinois Route 83	60V54	—	Illinois Route 64 (North Ave.) to Illinois Route 19 (Irving Park Rd.)		
1-5	3	US Route 6 (159th St.)	60K98	—	Illinois Route 50 (Cicero Ave.) to Pulaski Rd.)		
1-6	121	US Route 52 (Jefferson St.)	60V93	—	Illinois Route 7 (Larkin Ave.) to Raynor Ave.		
1-7	23	Illinois Route 58 (Dempster St.)	60F26	—	Illinois Route 21 (Milwaukee Ave.) to Illinois Route 43 (Waukegan Rd.)		
1-8	238	Green Bay Road	60J73	—	South of Tower Rd. in Winnetka		
1-9	9	Northbound Wolf Rd.	60M30	—	1/4 mile north of Illinois Route 38 (Roosevelt Rd.)		
1-10	28	Southbound Harrison St.	60N67	—	1/4 mile north of Illinois Route 38 (Roosevelt Rd.)		
1-11	137	Eastbound Jefferson St.	60E66	—	Silver Cross Field		
1-12	11	State Street	60M43	—	US Route 6 (162nd St./State St.) to Marion St.		
1-13	172	Southbound US Route 12 / Illinois Route 59	60N25	—	South of Illinois Route 120 (Belvidere Rd.)		

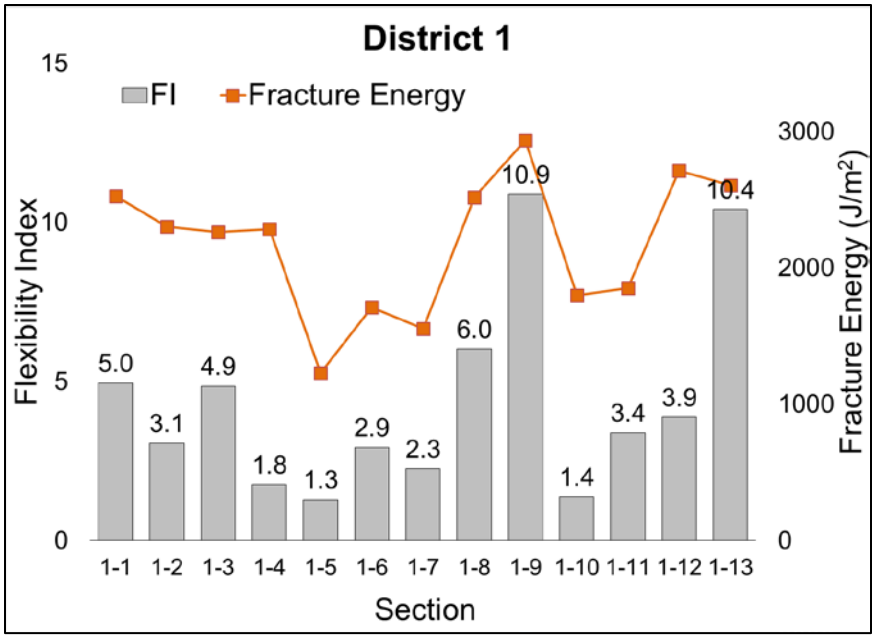

Figure C-2.1 FI and fracture energy for District 1.

C-2.2 District 2

Cores from three sections in this district were collected and tested for fracture energy and FI using IL-SCB. The cores were obtained from the city of Dixon along various routes, as presented in Table C-2.2. The sections were constructed in 2003 and 2004. The field condition of the sections shows that the sections withstood weathering and traffic; however, the current condition of the section shows weathering and cracks. The fracture energy and FI results of the tested sections are summarized in Figure C-2.2.

Table C-2.2 Details of Sections and Core Locations for District 2

Lab Name	Core Label	Core Location	Contract	Section	Route	City	County
2RT26	101RS-3	Northbound passing lane	64362	Mainline	Illinois 26 south of Dixon	Dixon	
22RT2	31-3	Westbound driving lane, approx. Station 396+00	84981	Mainline	Illinois 2 west of Dixon, River Rd. to Plock Rd.	Dixon	
22SRT2	31-3	Westbound shoulder lane, approx. Station 396+00	84981	Shoulder	Illinois 3 West of Dixon, River Rd. to Plock Rd.	Dixon	

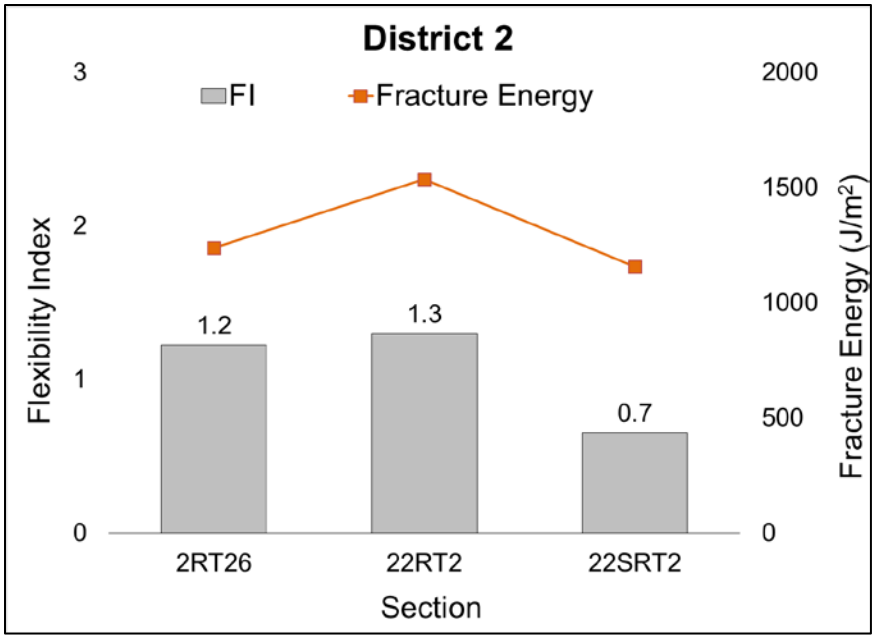

Figure C-2.2 FI and fracture energy for District 2.

C-2.3 District 3

Cores from four sections in this district were collected, and cores from only two sections were tested using IL-SCB. The details of cores from the two sections were provided by IDOT. The cores were obtained from Grundy County (identified as 6 East) and LaSalle County (identified as 6 West), as shown in Table C-2.3. The sections were newly built in 2012 and 2013. Section 6 East has good field performance, but 6 West is distressed. Table C-2.3 shows the surface course mixture details for each section. The fracture energy and FI results of the tested sections are summarized in Figure C-2.3.

Table C-2.3 Details of Sections and Core Location for District 3

Lab Name	Core Label	Core Location	Contract	Section	Route	City	County
3-6E	6 East	Center of WB lane, Route 6 west of Morris	66A75	Mainline	US 6 west of Morris		Grundy
3-6W	6 West	Center of WB lane, Route 6 west of Marseilles	66947	Mainline	US 6 between Ottawa and Marseilles		LaSalle

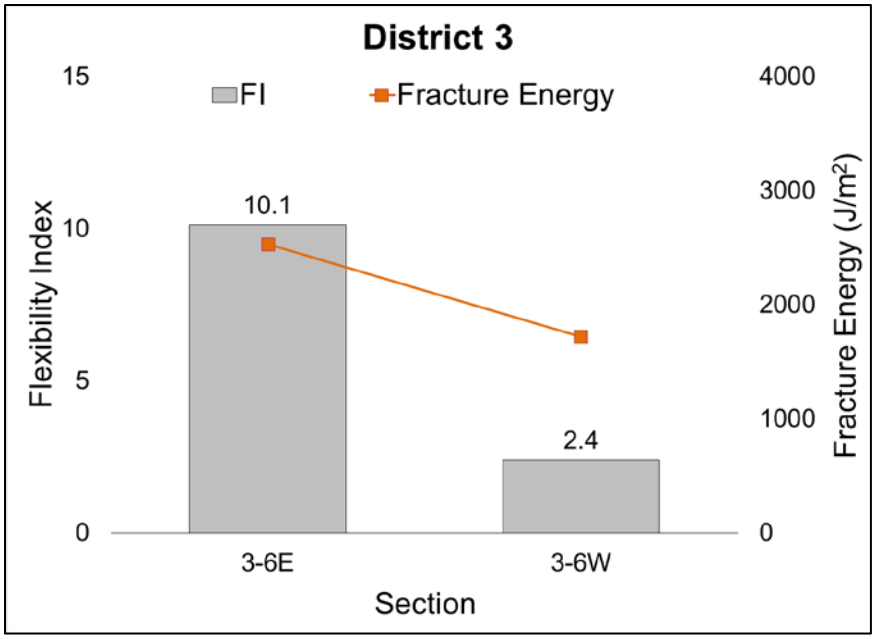

Figure C-2.3 FI and fracture energy for District 3.

C-2.4 District 4

Cores from three sections from this district were collected and tested for fracture energy and FI using IL-SCB. The details of core locations were provided by the IDOT. Two sections were on Routes IL-78 and IL-9 in Canton. The third section was on I-155 near Morton. The sections were observed to have cracking in the transverse direction, which could be either reflective cracking or transverse cracking. The surface course mixture details are provided in Table C-2.4. The fracture energy and FI results of the tested sections are summarized in Figure C-2.4.

Table C-2.4 Details of Sections and Core Locations for District 4

Lab Name	Core Label	Core Location	Contract	Section	Route	City	County
D4-IL78	IL78	Ash St. to Big Creek Park	68A20	Mainline	IL-78	Canton	
D4-IL9	IL9	Canton to US 24 in Banner	68811	Mainline	IL-9 to IL-78	Canton	
D4-IL55	I155	Hopedale to Birchwood Ave.	68914	Cores taken in SB lane just south of Townline Rd. interchange	I-155	Morton	

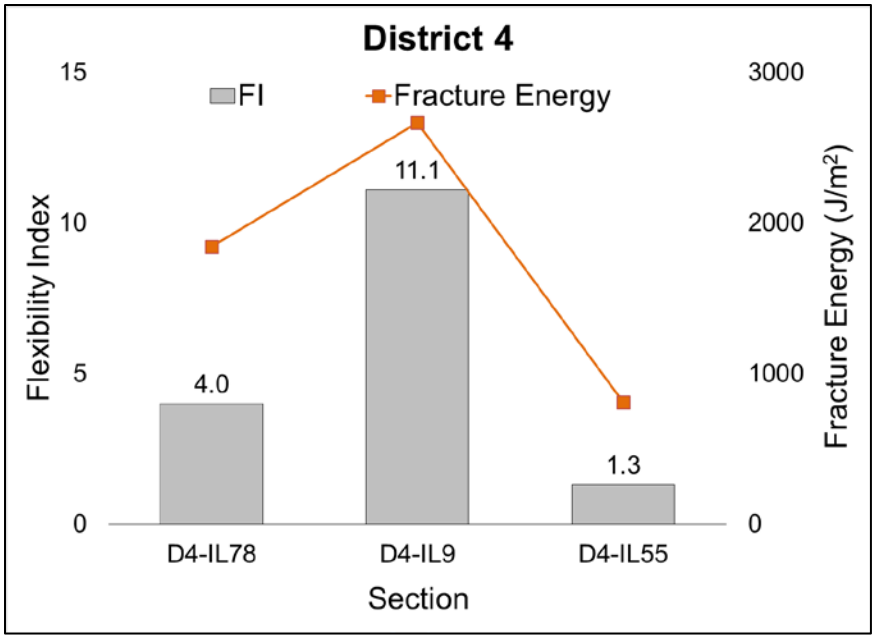

Figure C-2.4 FI and fracture energy for District 4.

C-2.5 District 5

Cores from six sections from this district were collected and tested for fracture energy and FI using IL-SCB. Two sections were from US-136, while one section each from I-39, I-57, IL-47, and CH-6 was collected. The sections were newly built (2012 to 2014). All the sections from this district showed good field performance, but it is clear that 5-US-136-2 and 5-39 are very high performance, while 5-US-136 and 5-IL6 would be more vulnerable to early deterioration. Table C-2.5 shows the surface course mixture details for each section. The fracture energy and FI results of the tested sections are summarized in Figure C-2.5.

Table C-2.5 Details of Sections and Core Locations for District 5

Lab Name	Core Label	Core Location	Contract	Section	Route	City	County
5-US136-1		US 136 Station 450+00 WB	70783	US Route 136 from Logan County line to McLean	US 136		
5-US136-2		US 136 Station 94+700 WB	90939	US 136 from National Ave. to west of Lick Creek	US 136	Danville	
5-I39		FAI 39 Station 225+00 SBDL	70634	FAI 39 from 2 miles north of Normal to FAI 55	I-39		
5-I57		FAI 57 Station 830+00 NBDL	70716	NB FAI 57 from Olympian Dr. to 2 miles south of Thomasboro	I-57		
5-IL47		IL-47 Station 556+00 NB	70706	IL-47 from Ford County line to US-136	IL-47		
5-IL6		CH-6 at 0.5 miles east of 2050E WB	91462	Douglas County Highway 6 from Hansen Rd. to county line	CH-6		

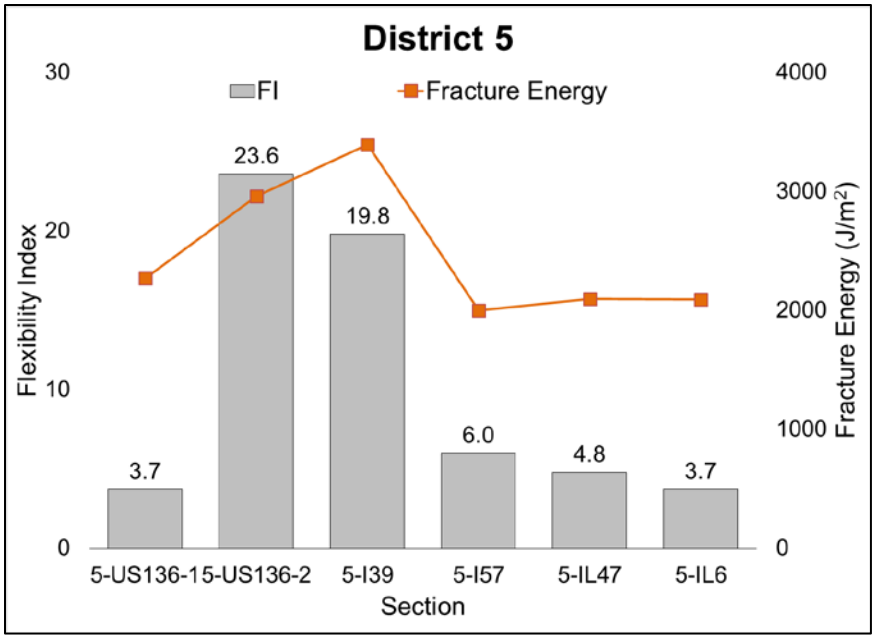

Figure C-2.5 FI and fracture energy for District 5.

C-2.6 District 6

Cores from two sections from this district were collected and tested for fracture energy and FI using IL-SCB. Both sections were in Cass County. The section labeled 6G had good performance, whereas 6P had poor performance, per the field evaluation data provided by IDOT. Both sections were from Route IL-125 and were constructed in 2013. Table C-2.6 shows the surface course mixture details for each section. The fracture energy and FI results of the tested sections are summarized in Figure C-2.6.

Table C-2.6 Details of Sections and Core Locations for District 6

Lab Name	Core Label	Core Location	Contract	Section	Route	City	County
6G	G	Ashland Bypass (eastbound lane)	72D75	Mainline	IL-125		Cass
6P	P	Ashland Bypass (westbound lane)	72F69	Mainline	IL-125		Cass

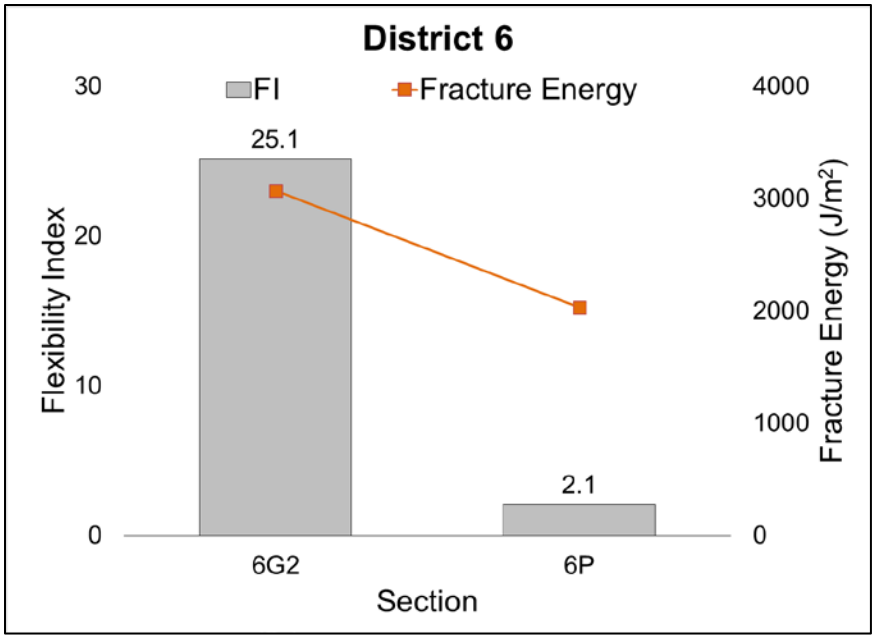

Figure C-2.6 FI and fracture energy for District 6.

C-2.7 District 7

Cores from two sections from this district were collected and tested for fracture energy and FI using IL-SCB. No information is available for these sections. The fracture energy and FI results of the tested sections are summarized in Figure C-2.7.

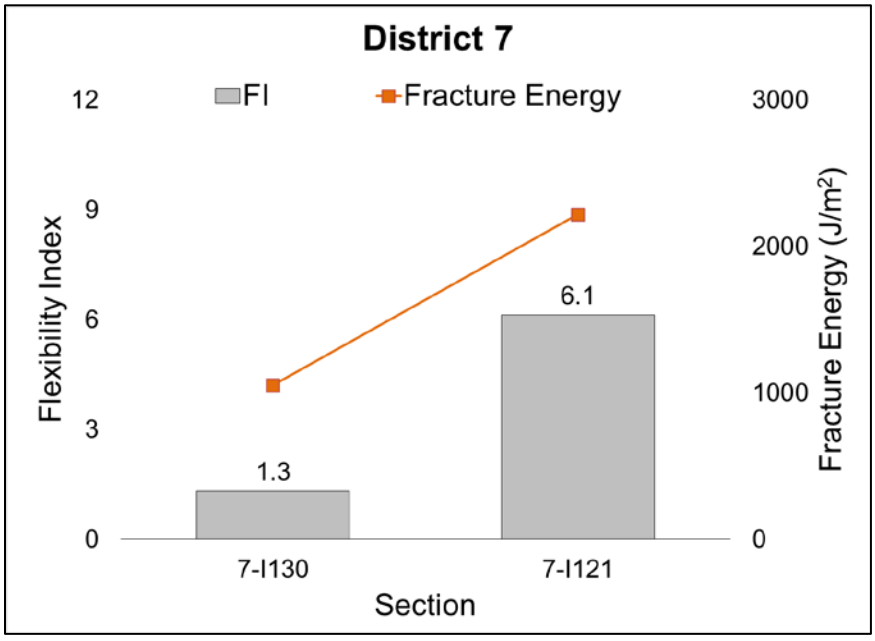

Figure C-2.7 FI and fracture energy for District 7.

C-2.8 District 8

Cores from two sections from this district were collected and tested for fracture energy and FI using IL-SCB. One was from IL-100 (Jersey County) and the other from US 67 (Greene County). The sections were constructed in 2013. The section on US 67 showed cracking throughout the project within a year of construction. Table C-2.7 presents the wearing surface AC details for each section. The fracture energy and FI results of the tested sections are summarized in Figure C-2.8. Soil swelling has been reported in those sections.

Table C-2.7 Details of Sections and Core Locations for District 8

Lab Name	Core Label	Core Location	Contract	Section	Route	City	County
8JVS2	2A-2J	Northbound station 594+00 (0.2 mile south of Nutwood near Waterworks Rd.)	76F24	Mainline	IL-100 from 0.1 mile east of TR35 to 0.2 miles east of Ski Lift Rd.		Jersey
867S1	1A-1J	Northbound lane at mile marker #24 (0.9 mile north of Roodhouse city limit)	76F25	Mainline	US-67 from TR-13 to 0.1 mile north of McCarthy Ave. in Whitehall		Greene

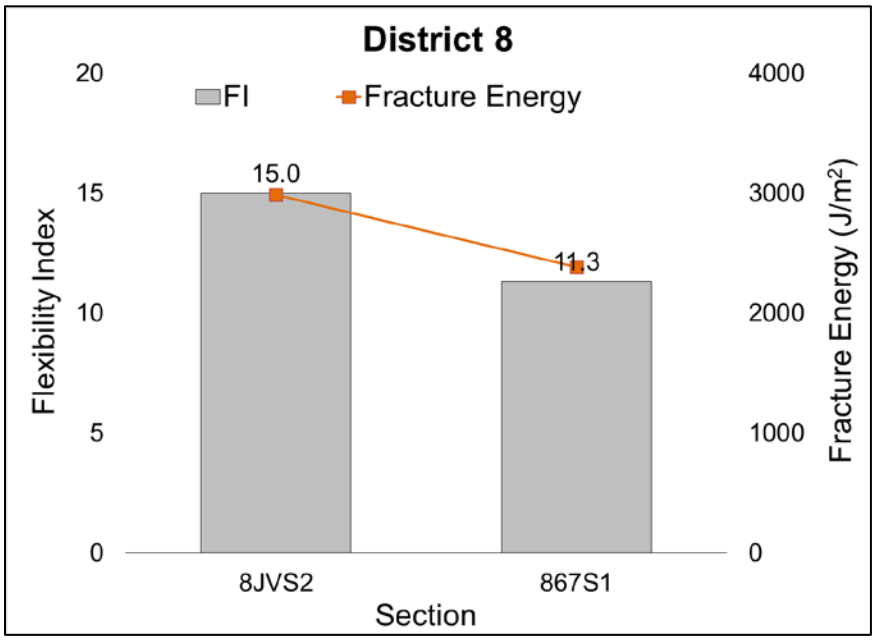

Figure C-2.8 FI and fracture energy for District 8.

C-2.9 District 9

Cores from two sections from this district, on IL-14 and IL-154 in Perry County, were collected and tested for fracture energy and FI using IL-SCB. The sections were newly constructed in 2013. Minor transverse and centerline cracking was observed on IL-14, and IL-154 had alligator, block, and centerline cracking with minor longitudinal cracking. Table C-2.8 shows the surface course mixture details for each section. The fracture energy and FI results of the tested sections are summarized in Figure C-2.9.

Table C-2.8 Details of Sections and Core Locations for District 9

Lab Name	Core Label	Core Location	Contract	Section	Route	City	County
9-I4	I14	±Sta. 200+00	98797	Mainline	IL-14		Near Perry/Franklin County line
9-I54	I154	55+00±	78351	Mainline	IL-154		Perry

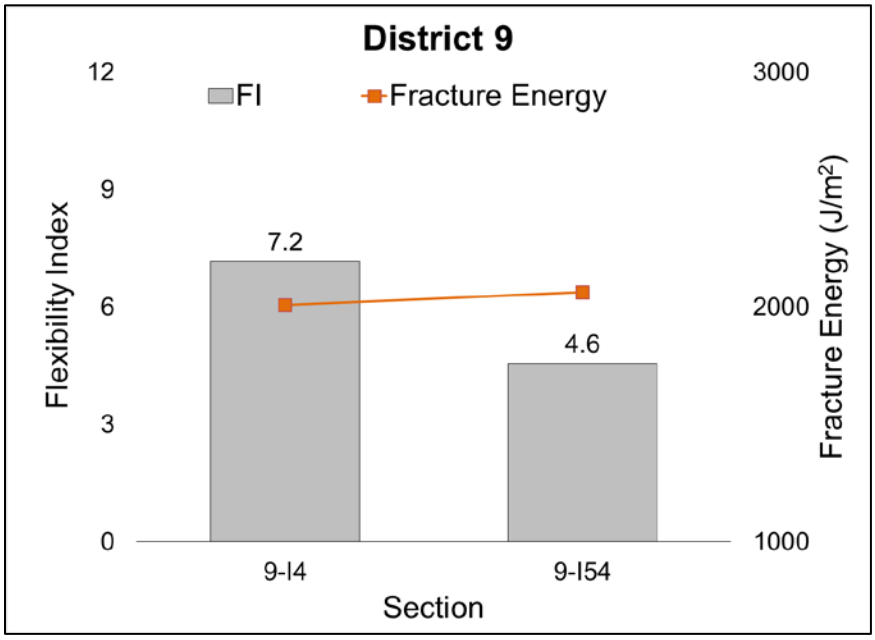

Figure C-2.9 FI and fracture energy for District 9.

APPENDIX D: PLANT MIX DESIGNS

Table D-1 Plant Mix 8 (P8)

IDOT Lab Verification No.: ---> | Ver. 9.01-06.15.12 | DATE: October 15 2012

Producer Number & Name --> 4066-06 | Rock Road | Rockford <--- Plant Location | RR12003

Material Code Number ---> 19512R | HMA N50 19.0 REC BIND

Plant Bin #	#5	#4	#3	#2	#1	MF	FRAP #3	FRAP #2	RAS #1	ASPHALT
Size	042CM11	032CM16			037FM01		017CM1294		017FM99	10126
Source (PROD #)	50072-01	50072-01			52010-07		4066-06		6616-04	5627-13
(NAME)	WCC	WCC			WCC		Rock Road		Southwind	BP Amoco
(LOC)	Irene	Irene			Airport		Irene		So. Beloit	Bartlett
(ADD. INFO)							Catergory 2			58-28
							3.7	0.0	28.7	< AC in RAP
	Aggregate Blend:								Plan PG Grade >	PG 58-28
	27.5	12.5	0.0	0.0	14.0	0.0	42.0	0.0	4.0	100.0

Lab Preparing Design: IL
Designing Lab Mix#: RR12003
Designing Lab Name: S.T.A.T.E.

Agg No. / Sieve Size	#5	#4	#3	#2	#1	MF	FRAP #3	FRAP #2	RAS #1	Aggregate Blend	Mixture Comp Spec
1" (25.0mm)	100.0	100.0	100.0	100.0	100.0	100.0	100.0	100.0	100.0	100	100
3/4"(19.0mm)	89.0	100.0	100.0	100.0	100.0	100.0	100.0	100.0	100.0	97	82-100
1/2" (12.5mm)	34.0	100.0	100.0	100.0	100.0	100.0	100.0	100.0	100.0	82	50-85
3/8" (9.5mm)	7.0	94.0	100.0	100.0	100.0	100.0	96.5	100.0	100.0	72	
No.4 (4.75mm)	2.0	32.0	100.0	100.0	96.0	100.0	48.9	100.0	97.3	42	24-50
No.8 (2.36mm)	2.0	5.0	100.0	100.0	80.0	100.0	25.7	100.0	92.3	27	20-36
No.16 (1.18mm)	2.0	4.0	100.0	100.0	62.0	100.0	20.2	100.0	79.4	21	10-25
No.30 (600µm)	2.0	4.0	100.0	100.0	40.0	100.0	16.7	100.0	61.7	16	
No.50 (300µm)	2.0	4.0	100.0	100.0	11.0	100.0	13.0	100.0	52.3	10	4-12
No.100 (150µm)	2.0	4.0	100.0	100.0	1.0	100.0	9.3	100.0	44.7	7	3-9
No.200(75µm)	1.7	3.2	100.0	100.0	0.3	100.0	6.1	100.0	34.0	4.8	3-6

AMOUNT OF AGED RCY AC: 2.7

AC REPLACEMENT (ABR): 49.1

VIRGIN AC: 2.8

Bulk Sp Gr	2.626	2.612	1.000	1.000	2.626	1.000	2.660	1.000	2.500	2.633	Dust/AC
Absorption, %	2.10	2.60	1.00	1.00	1.30	1.00	1.00	1.00	1.00	1.34	Ratio
									SP GR AC	1.040	0.88

SUMMARY OF SUPERPAVE GYRATORY DESIGN DATA

BITUMINOUS MIXTURE AGED: 1 HOURS @: 295

DATA for N-int. 6

	AC, %MIX	(Gmb)	(Gmm)	(Pa)	VMA	VFA	Vbe	Pbe	Pba
MIX 1	4.5	2.173	2.539	14.4	21.2	32.0	6.76	3.24	1.32
MIX 2	5.0	2.177	2.518	13.5	21.4	36.9	7.90	3.77	1.29
MIX 3	5.5	2.201	2.499	11.9	21.0	43.2	9.09	4.29	1.28
MIX 4	6.0	2.202	2.479	11.2	21.4	47.8	10.23	4.83	1.24

DATA for N-des. 50

		(Gmb)	(Gmm)	(Pa)	VMA	VFA	Vbe	Pbe	Gse	Pba
MIX 1	4.5	2.387	2.539	6.0	13.4	55.4	7.43	3.24	2.724	1.32
MIX 2	5.0	2.406	2.518	4.5	13.2	66.1	8.73	3.77	2.722	1.29
MIX 3	5.5	2.424	2.499	3.0	13.0	77.0	10.01	4.29	2.721	1.28
MIX 4	6.0	2.434	2.479	1.8	13.1	86.3	11.31	4.83	2.719	1.24

Hamburg Wheel Information

Sample No. Passes	20000
Sample Wheel Depth	4.57

TSR Information

Conditioned	136.4
Unconditioned	144.6
TSR	0.94
CA Strip Rating	2
FA Strip Rating	1
Additive Prod #	
Additive Product Name	
Additive %	

	NUMBER OF GYRATIONS	%AC	Gmb	Gmm	%VOIDS (Pa) Target	VMA	VFA	Gse	Gsb	TSR
		5.50								
OPTIMUM DESIGN DATA @Ndes: --->	50	5.5	2.424	2.499	3.0	13.0	76.9	2.721	2.633	0.94

REMARKS LINE 1: Hamburgs & TSR made with warm mix.
REMARKS LINE 2: MeadwestVaco M1 @ 0.4%

RR12003

Tested by : [signature]

Reviewed by : [signature]

Verified by: _____

Final Approval : _____

Table D-2 Plant Mix 9 (P9)

IDOT Lab Verification No.: ---> | Ver. 9.01-06.15.12 | DATE: September 28 2012

Producer Number & Name --> 4066-06 | Rock Road | Rockford <-- Plant Location | RR12002

Material Code Number ----> 19512R | HMA N50 19.0 REC BIND

Plant Bin #	#5	#4	#3	#2	#1	MF	FRAP #3	FRAP #2	RAS #1	ASPHALT
Size	042CM11	032CM16			037FM01		017CM1204		017FM06	10122
Source (PROD #)	56072-01	56072-01			52010-07		4066-06		6016-04	5627-13
(NAME)	WCC	WCC			WCC		Rock Road		Southwind	BP Amoco
(LOC)	Irene	Irene			Airport		Irene		So. Beloit	Bartlett
(ADD. INFO)							Catergory 2			46-34
							3.7	0.0	28.7	< AC in RAP
	Aggregate Blend:								Plan PG Grade >	PG 58-28
	29.5	14.5	0.0	0.0	8.0	0.0	42.0	0.0	6.0	100.0

Lab Preparing Design: IL
Designing Lab Mix#: RR12002
Designing Lab Name: S.T.A.T.E.

Agg No. / Sieve Size	#5	#4	#3	#2	#1	MF	FRAP #3	FRAP #2	RAS #1	Aggregate Blend	Mixture Comp Spec
1" (25.0mm)	100.0	100.0	100.0	100.0	100.0	100.0	100.0	100.0	100.0	100	100
3/4"(19.0mm)	86.0	100.0	100.0	100.0	100.0	100.0	100.0	100.0	100.0	97	82-100
1/2" (12.5mm)	34.0	100.0	100.0	100.0	100.0	100.0	100.0	100.0	100.0	81	50-85
3/8" (9.5mm)	7.0	94.0	100.0	100.0	100.0	100.0	96.5	100.0	100.0	76	
No.4 (4.75mm)	2.0	32.0	100.0	100.0	96.0	100.0	48.9	100.0	97.3	39	24-50
No.8 (2.36mm)	2.0	5.0	100.0	100.0	80.0	100.0	25.7	100.0	92.3	24	20-36
No.16 (1.18mm)	2.0	4.0	100.0	100.0	62.0	100.0	20.2	100.0	79.4	19	10-25
No.30 (600µm)	2.0	4.0	100.0	100.0	40.0	100.0	16.7	100.0	61.7	15	
No.50 (300µm)	2.0	4.0	100.0	100.0	11.0	100.0	13.0	100.0	52.3	11	4-12
No.100 (150µm)	2.0	4.0	100.0	100.0	1.0	100.0	9.3	100.0	44.7	8	3-9
No.200(75µm)	1.7	3.2	100.0	100.0	0.3	100.0	6.1	100.0	34.6	5.6	3-8
Bulk Sp Gr	2.626	2.612	1.000	1.000	2.626	1.000	2.660	1.000	2.500	2.630	Dust/AC
Absorption, %	2.10	2.60	1.00	1.00	1.30	1.00	1.00	1.00	1.00	1.36	Ratio
									SP GR AC	1.040	1.01

AMOUNT OF AGED RCY AC: 3.3

AC REPLACEMENT (ABR): 59.1

VIRGIN AC: 2.3

SUMMARY OF SUPERPAVE GYRATORY DESIGN DATA

BITUMINOUS MIXTURE AGED: 1 HOURS @: 295

DATA for N-Int. 6

	AC, %MIX	(Gmb)	(Gmm)	(Pa)	VMA	VFA	Vbe	Pbe	Pba
MIX 1	5.0	2.180	2.525	13.6	21.2	35.8	7.61	3.83	1.44
MIX 2	5.5	2.191	2.509	12.4	21.3	41.9	8.92	4.24	1.34
MIX 3	6.0	2.209	2.486	11.2	21.1	47.0	9.91	4.66	1.42
MIX 4	6.5	2.215	2.468	10.3	21.3	51.7	11.00	5.18	1.43

DATA for N-des. 50

		(Gmb)	(Gmm)	(Pa)	VMA	VFA	Vbe	Pbe	Gse	Pba
MIX 1	5.0	2.404	2.525	4.8	13.2	63.7	8.39	3.83	2.730	1.44
MIX 2	5.5	2.423	2.509	3.1	13.0	76.3	9.87	4.24	2.722	1.34
MIX 3	6.0	2.436	2.486	2.0	12.9	84.4	10.92	4.66	2.728	1.42
MIX 4	6.5	2.445	2.468	0.9	13.1	92.9	12.14	5.18	2.729	1.43

Hamburg Wheel Information	
Sample No. Passes	20000
Sample Wheel Depth	1.81

TSR Information	
Conditioned	133.6
Unconditioned	155.6
TSR	0.86
CA Strip Rating	2
FA Strip Rating	1
Additive Prod #	
Additive Product Name	
Additive %	

	NUMBER OF GYRATIONS	%AC	Gmb	Gmm	%VOIDS (Pa)	VMA	VFA	Gse	Gsb	TSR
		5.54								
OPTIMUM DESIGN DATA @Ndes: ---->	50	5.5	2.424	2.499	3.0	13.0	76.8	2.723	2.638	0.86
					Target					

REMARKS LINE 1: Hamburgs & TSR made with warm mix.
REMARKS LINE 2: MeadwestVaco M1 @ 0.4%

RR12002

Tested by : Matthew Duffy

Reviewed by :

Verified by: Scott

Final Approval :

Table D-3 Plant Mix 10 (P10)

IDOT Lab Verification No.: ---> | Ver. 9.01-06.15.12 | DATE: October 18 2012

Producer Number & Name --> 4066-06 | Rock Road | Rockford <--- Plant Location | RR12006

Material Code Number ----> 19524R | HMA N70 D REC SURF 9.5mm

Plant Bin #	#5	#4	#3	#2	#1	MF	FRAP #3	FRAP #2	RAS #1	ASPHALT
Size		032CM16			037FM01	004MF02	017CM1204	017FM0400		10129
Source (PROD #)		50072-01			52010-07	4066-06	4066-06	4066-06		6220-61
(NAME)		WCC			WCC	Rock Road	Rock Road	Rock Road		Flint Hills
(LOC)		Irene			Airport	Rockford	Rockford	Rockford		Dubuque,IA
(ADD. INFO)										PG 58-28
							3.7	6.0	0.9	< AC in RAP
	Aggregate Blend:								Plan PG Grade >	PG 58-28
	0.0	58.0	0.0	0.0	12.5	0.5	12.0	17.0	0.0	100.0

Lab Preparing Design: IL
Designing Lab Mix#: RR12006
Designing Lab Name: S.T.A.T.E.

Agg No. / Sieve Size	#5	#4	#3	#2	#1	MF	FRAP #3	FRAP #2	RAS #1	Aggregate Blend	Mixture Comp Spec
1" (25.0mm)	100.0	100.0	100.0	100.0	100.0	100.0	100.0	100.0	100.0	100	
3/4"(19.0mm)	100.0	100.0	100.0	100.0	100.0	100.0	100.0	100.0	100.0	100	
1/2" (12.5mm)	100.0	100.0	100.0	100.0	100.0	100.0	100.0	100.0	100.0	100	100
3/8" (9.5mm)	100.0	94.0	100.0	100.0	100.0	100.0	96.5	100.0	100.0	96	90-100
No.4 (4.75mm)	100.0	32.0	100.0	100.0	96.0	100.0	48.9	98.6	100.0	54	28-65
No.8 (2.36mm)	100.0	5.0	100.0	100.0	80.0	100.0	25.7	74.2	100.0	28	28-48
No.16 (1.18mm)	100.0	4.0	100.0	100.0	62.0	100.0	20.2	51.2	100.0	22	10-32
No.30 (600µm)	100.0	4.0	100.0	100.0	40.0	100.0	16.7	36.8	100.0	16	
No.50 (300µm)	100.0	4.0	100.0	100.0	11.0	100.0	13.0	25.9	100.0	10	4-15
No.100 (150µm)	100.0	4.0	100.0	100.0	1.0	95.0	9.3	17.4	100.0	7	3-10
No.200(75µm)	100.0	3.2	100.0	100.0	0.3	90.0	6.1	10.9	100.0	4.9	4-6
Bulk Sp Gr	1.000	2.612	1.000	1.000	2.626	2.900	2.660	2.660	1.000	2.629	Dust/AC
Absorption, %	1.00	2.60	1.00	1.00	1.30	1.00	1.00	1.00	1.00	1.83	Ratio
									SP GR AC	1.040	0.93

AMOUNT OF AGED RCY AC: 1.5

AC REPLACEMENT (ABR): 24.6

VIRGIN AC: 4.5

SUMMARY OF SUPERPAVE GYRATORY DESIGN DATA

BITUMINOUS MIXTURE AGED: 1 HOURS @: 295

DATA for N-Int. 7

	AC, %MIX	(Gmb)	(Gmm)	(Pa)	VMA	VFA	Vbe	Pbe	Pba
MIX 1	5.0	2.110	2.523	16.4	23.8	31.1	7.30	3.64	1.43
MIX 2	5.5	2.122	2.503	15.2	23.7	35.8	8.49	4.16	1.42
MIX 3	6.0	2.136	2.487	14.1	23.6	40.3	9.53	4.64	1.45
MIX 4	6.5	2.142	2.464	13.1	23.8	45.1	10.75	5.22	1.37

DATA for N-des. 70

		(Gmb)	(Gmm)	(Pa)	VMA	VFA	Vbe	Pbe	Gse	Pba
MIX 1	5.0	2.364	2.523	6.3	14.6	56.9	8.28	3.64	2.727	1.43
MIX 2	5.5	2.375	2.503	5.1	14.6	64.9	9.50	4.16	2.727	1.42
MIX 3	6.0	2.391	2.487	3.8	14.5	73.5	10.66	4.64	2.729	1.45
MIX 4	6.5	2.398	2.464	2.7	14.7	81.7	12.03	5.22	2.723	1.37

Hamburg Wheel Information	
Sample No. Passes	20000
Sample Wheel Depth	8.62

TSR Information	
Conditioned	81.2
Unconditioned	84.5
TSR	0.96
CA Strip Rating	1
FA Strip Rating	1
Additive Prod #	
Additive Product Name	
Additive %	

	NUMBER OF GYRATIONS	%AC	Gmb	Gmm	%VOIDS (Pa) Target	VMA	VFA	Gse	Gsb	TSR
		5.94								
OPTIMUM DESIGN DATA @Ndes: ---->	70	5.9	2.389	2.489	4.0	14.5	72.5	2.728	2.629	0.96

REMARKS LINE 1: Hamburgs & TSR Made With Warm Mix
REMARKS LINE 2: MeadwestVaco M1 @ 0.4%

Tested by: _____ Verified by: _____

Reviewed by: _____ Final Approval: _____

RR12006

Table D-4 Plant Mix 11 (P11)

IDOT Lab Verification No.: ---> | Ver. 9.01-06.15.12 | DATE: October 3 2012

Producer Number & Name --> 4066-06 | Rock Road | Rockford <--- Plant Location | RRRO12002

Material Code Number ----> 19524R | HMA N70 D REC SURF 9.5mm

Plant Bin #	#5	#4	#3	#2	#1	MF	FRAP #3	FRAP #2	RAS #1	ASPHALT
Size		632CM16			937FM01		017CM1204	017FM0400	017FM98	10126
Source (PROD #)		58072-01			52010-07		4066-06	4066-06	6616-04	6226-01
(NAME)		WCC			WCC		Rock Road	Rock Road	Southwind	Flint Hills
(LOC)		Irene			Airport		Rockford	Rockford	So.Beloit	Dubuque,IA
(ADD. INFO)							Catergory 2	Catergory 2		PG 58-28
							3.7	6.0	28.7	< AC in RAP
	Aggregate Blend:								Plan PG Grade >	PG 58-28
	0.0	57.0	0.0	0.0	8.0	0.0	16.0	14.0	5.0	100.0

Lab Preparing Design: IL
Designing Lab Mix#: RRR012002
Designing Lab Name: S.T.A.T.E.

Agg No. / Sieve Size	#5	#4	#3	#2	#1	MF	FRAP #3	FRAP #2	RAS #1	Aggregate Blend	Mixture Comp Spec
1" (25.0mm)	100.0	100.0	100.0	100.0	100.0	100.0	100.0	100.0	100.0	100	
3/4"(19.0mm)	100.0	100.0	100.0	100.0	100.0	100.0	100.0	100.0	100.0	100	
1/2" (12.5mm)	100.0	100.0	100.0	100.0	100.0	100.0	100.0	100.0	100.0	100	100
3/8" (9.5mm)	100.0	94.0	100.0	100.0	100.0	100.0	96.5	100.0	100.0	96	90-100
No.4 (4.75mm)	100.0	32.0	100.0	100.0	98.0	100.0	48.9	98.6	97.3	52	28-65
No.8 (2.36mm)	100.0	5.0	100.0	100.0	80.0	100.0	25.7	74.2	92.3	28	28-48
No.16 (1.18mm)	100.0	4.0	100.0	100.0	62.0	100.0	20.2	51.2	79.4	22	16-32
No.30 (600µm)	100.0	4.0	100.0	100.0	40.0	100.0	16.7	36.8	61.7	16	
No.50 (300µm)	100.0	4.0	100.0	100.0	11.0	100.0	13.0	25.9	52.3	11	4-15
No.100 (150µm)	100.0	4.0	100.0	100.0	1.0	100.0	9.3	17.4	44.7	9	3-16
No.200(75µm)	100.0	3.2	100.0	100.0	0.3	100.0	6.1	10.9	34.8	6.1	4-8
Bulk Sp Gr	1.000	2.612	1.000	1.000	2.626	1.000	2.660	2.660	2.500	2.621	Dust/AC
Absorption, %	1.00	2.80	1.00	1.00	1.30	1.00	1.80	1.00	1.00	1.59	Ratio
									SP GR AC	1.040	1.02

AMOUNT OF AGED RCY AC: 2.0
AC REPLACEMENT (ABR): 48.3
VIRGIN AC: 3.1

SUMMARY OF SUPERPAVE GYRATORY DESIGN DATA

BITUMINOUS MIXTURE AGED: 1 HOURS @: 295

DATA for N-int. 7

	AC, %MIX	(Gmb)	(Gmm)	(Pa)	VMA	VFA	Vbe	Pbe	Pba
MIX 1	5.0	2.122	2.522	15.9	23.1	31.4	7.25	3.55	1.52
MIX 2	5.5	2.126	2.501	15.0	23.3	35.9	8.37	4.09	1.49
MIX 3	6.0	2.138	2.480	13.8	23.3	40.9	9.55	4.65	1.44
MIX 4	6.5	2.146	2.464	12.9	23.4	45.0	10.55	5.11	1.48

DATA for N-des. 70

		(Gmb)	(Gmm)	(Pa)	VMA	VFA	Vbe	Pbe	Gse	Pba
MIX 1	5.0	2.355	2.522	6.6	14.7	55.0	8.04	3.55	2.726	1.52
MIX 2	5.5	2.370	2.501	5.2	14.6	64.1	9.33	4.09	2.724	1.49
MIX 3	6.0	2.385	2.480	3.8	14.5	73.6	10.68	4.65	2.720	1.44
MIX 4	6.5	2.392	2.464	2.9	14.7	80.1	11.76	5.11	2.723	1.48

Hamburg Wheel Information	
Sample No. Passes	20000
Sample Wheel Depth	2.87

TSR Information	
Conditioned	126.8
Unconditioned	131.1
TSR	0.97
CA Strip Rating	1
FA Strip Rating	1
Additive Prod #	
Additive Product Name	
Additive %	

	NUMBER OF GYRATIONS	%AC	Gmb	Gmm	%VOIDS (Pa)	VMA	VFA	Gse	Gsb	TSR
		5.94			Target					
OPTIMUM DESIGN DATA @Ndes: ---->	70	5.9	2.383	2.462	4.0	14.5	72.4	2.721	2.621	0.97

REMARKS LINE 1: Hamburgs & TSR Made With Warm Mix
REMARKS LINE 2: MeadwestVaco M1 @ 0.4%

Tested by : _____ Verified by: _____

Reviewed by : _____ Final Approval : _____

RRRO12002

Table D-5 Plant Mix 12 (P12)

IDOT Lab Verification No.: ---> | Ver. 9.01-06.15.12 | DATE: October 22 2012

Producer Number & Name --> 4066-06 | Rock Road | Rockford <--- Plant Location

Material Code Number ---> 18435R | HMA Polymer SMA 12.5 REC BIND N80 | RRR12007

Plant Bin #	#5	#4	#3	#2	#1	MF	FRAP #3	FRAP #2	RAS #1	ASPHALT
Size	031CM14	031CM13		038FM20		004MF02	017CM1204		017FM98	10130
Source (PROD #)	52400-29	52400-29		59072-01		4066-06	4066-06		6818-04	1757-95
(NAME)	Rock Road	Rock Road		WCC		Rock Road	Rock Road		Southwind	Seneca
(LOC)	Lathers	Lathers		Irene		Rockford	Rockford		So.Beloit	Lamont
(ADD. INFO)										SBS PG 70-28
	Aggregate Blend:						3.5	0.0	28.7	< AC in RAP
	50.0	24.5	0.0	8.0	0.0	5.0	8.0	0.0	Plan PG Grade > 4.5	PG 70-28 / 100.0

Lab Preparing Design: IL
Designing Lab Mix#: RRR12007
Designing Lab Name: S.T.A.T.E.

Agg No. / Sieve Size	#5	#4	#3	#2	#1	MF	FRAP #3	FRAP #2	RAS #1	Aggregate Blend	Mixture Comp Spec
1" (25.0mm)	100.0	100.0	100.0	100.0	100.0	100.0	100.0	100.0	100.0	100	
3/4"(19.0mm)	100.0	100.0	100.0	100.0	100.0	100.0	100.0	100.0	100.0	100	100
1/2" (12.5mm)	87.1	98.8	100.0	100.0	100.0	100.0	100.0	100.0	100.0	93	82-100
3/8" (9.5mm)	33.0	73.2	100.0	100.0	100.0	100.0	86.8	100.0	100.0	60	65 max
No.4 (4.75mm)	1.3	25.0	100.0	100.0	100.0	100.0	44.3	100.0	97.3	28	20-30
No.8 (2.36mm)	1.2	1.9	100.0	88.0	100.0	100.0	21.6	100.0	92.3	19	16-24
No.16 (1.18mm)	1.1	1.7	100.0	53.0	100.0	100.0	15.1	100.0	79.4	15	
No.30 (600µm)	1.1	1.6	100.0	30.0	100.0	100.0	12.0	100.0	61.7	12	12-16
No.50 (300µm)	1.1	1.6	100.0	15.0	100.0	100.0	9.5	100.0	52.3	10	10-15
No.100 (150µm)	1.0	1.5	100.0	7.0	100.0	95.0	7.0	100.0	44.7	9	
No.200(75µm)	1.0	1.3	100.0	4.3	100.0	90.0	5.3	100.0	34.0	7.6	6-10
Bulk Sp Gr	2.710	2.696	1.000	2.641	1.000	2.900	2.660	1.000	2.500	2.696	Dust/AC
Absorption, %	1.30	1.50	1.00	1.90	1.00	1.00	1.00	1.00	1.00	1.31	Ratio
									SP GR AC	1.040	1.26

AMOUNT OF AGED RCY AC: 1.6

AC REPLACEMENT (ABR): 28.1

VIRGIN AC: 4.5

SUMMARY OF SUPERPAVE GYRATORY DESIGN DATA

BITUMINOUS MIXTURE AGED: 1 HOURS @ 305

DATA for N-int. 7

	AC, %MIX	(Gmb)	(Gmm)	(Pa)	VMA	VFA	Vbe	Pbe	Pba
MIX 1	5.5	2.096	2.512	16.6	28.7	37.1	9.93	4.94	0.59
MIX 2	6.0	2.104	2.494	15.6	29.6	41.3	11.00	5.44	0.60
MIX 3	6.5	2.114	2.474	14.5	28.7	45.5	12.13	5.97	0.57
MIX 4	7.0	2.116	2.455	13.8	27.0	48.8	13.18	6.48	0.56

DATA for N-des. 80

		(Gmb)	(Gmm)	(Pa)	VMA	VFA	Vbe	Pbe	Gse	Pba
MIX 1	5.5	2.383	2.512	5.1	18.5	68.9	11.33	4.94	2.737	0.59
MIX 2	6.0	2.405	2.494	3.6	18.1	77.8	12.57	5.44	2.736	0.60
MIX 3	6.5	2.413	2.474	2.5	18.3	84.8	13.84	5.97	2.736	0.57
MIX 4	7.0	2.421	2.455	1.4	18.5	91.8	15.09	6.48	2.735	0.56

Hamburg Wheel Information
Sample No. Passes:
Sample Wheel Depth:

TSR Information
Conditioned: 0.0
Unconditioned: 0.0
TSR: 0.00
CA Strip Rating:
FA Strip Rating:
Additive Prod #:
Additive Product Name:
Additive %:

	NUMBER OF GYRATIONS	%AC	Gmb	Gmm	%VOIDS (Pa) Target	VMA	VFA	Gse	Gsb	TSR
OPTIMUM DESIGN DATA @Ndes: --->	80	6.03 6.0	2.405	2.483	3.5	18.1	78.3	2.738	2.696	0.00

REMARKS LINE 1: Hamburge & TSR Made With Warm Mix
REMARKS LINE 2: MeadwestVaco M1 @ 0.4%

Tested by:
Reviewed by:
Verified by:
Final Approval:

RRR12007

Table D-6 Plant Mix 13 (P13)

IDOT Lab Verification No.: ---> | Ver. 9.01-06.15.12 | DATE: October 15 2012

Producer Number & Name --> 4066-06 | Rock Road | Rockford <--- Plant Location | RRR12004

Material Code Number ---> 18435R | HMA Polymer SMA 12.5 REC BIND N80

Plant Bin #	#5	#4	#3	#2	#1	MF	FRAP #3	FRAP #2	RAS #1	ASPHALT
Size	031CM14	031CM13				004MF02	017CM1264	017FM0409	017FM98	10130
Source (PROD #)	52400-29	52400-29				4066-06	4066-06	4066-06	6616-04	1757-05
(NAME)	Rock Road	Rock Road				Rock Road	Rock Road	Rock Road	Southwind	Seneca
(LOC)	Lathers	Lathers				Rockford	Rockford	Rockford	So.Beloit	Lemont
(ADD. INFO)										SBS PG 70-28
							3.5	6.2	28.7	< AC in RAP
	Aggregate Blend:								Plan PG Grade >	PG 70-28
	49.0	22.5	0.0	0.0	0.0	3.0	10.0	8.0	7.5	100.0

Lab Preparing Design: IL
Designing Lab Mix#: RRR12004
Designing Lab Name: S.T.A.T.E.

Agg No. / Sieve Size	#5	#4	#3	#2	#1	MF	FRAP #3	FRAP #2	RAS #1	Aggregate Blend	Mixture Comp Spec
1" (25.0mm)	100.0	100.0	100.0	100.0	100.0	100.0	100.0	100.0	100.0	100	
3/4"(19.0mm)	100.0	100.0	100.0	100.0	100.0	100.0	100.0	100.0	100.0	100	100
1/2" (12.5mm)	87.1	96.5	100.0	100.0	100.0	100.0	100.0	100.0	100.0	93	82-100
3/8" (9.5mm)	33.0	73.2	100.0	100.0	100.0	100.0	96.8	100.0	100.0	61	65 max
No.4 (4.75mm)	1.3	25.0	100.0	100.0	100.0	100.0	44.3	97.9	97.3	29	28-30
No.8 (2.36mm)	1.2	1.9	100.0	100.0	100.0	100.0	21.6	69.8	92.3	19	16-24
No.16 (1.18mm)	1.1	1.7	100.0	100.0	100.0	100.0	15.1	46.5	79.4	15	
No.30 (600µm)	1.1	1.6	100.0	100.0	100.0	100.0	12.0	33.5	61.7	12	12-16
No.50 (300µm)	1.1	1.6	100.0	100.0	100.0	100.0	9.5	24.4	52.3	11	10-15
No.100 (150µm)	1.0	1.5	100.0	100.0	100.0	95.0	7.0	15.7	44.7	9	
No.200(75µm)	1.0	1.3	100.0	100.0	100.0	90.0	5.3	11.4	34.0	7.5	8-10

Bulk Sp Gr	2.710	2.686	1.000	1.000	1.000	2.900	2.660	2.660	2.580	2.686	Dust/AC
Absorption, %	1.30	1.50	1.00	1.00	1.00	1.00	1.00	1.00	1.00	1.23	Ratio
									SP GR AC	1.040	1.25

AMOUNT OF AGED RCY AC: 3.0

AC REPLACEMENT (ABR): 50.1

VIRGIN AC: 3.0

SUMMARY OF SUPERPAVE GYRATORY DESIGN DATA

BITUMINOUS MIXTURE AGED: 1 HOURS @ 305

DATA for N-int. 7

	AC, %MIX	(Gmb)	(Gmm)	(Pa)	VMA	VFA	Vbe	Pbe	Pba
MIX 1	5.5	2.092	2.507	16.5	26.4	37.3	9.85	4.90	0.64
MIX 2	6.0	2.166	2.492	15.4	26.2	41.3	10.83	5.34	0.70
MIX 3	6.5	2.115	2.471	14.4	26.4	45.4	11.98	5.89	0.85
MIX 4	7.0	2.134	2.454	13.1	26.1	50.0	13.06	6.37	0.88

DATA for N-des. 80

		(Gmb)	(Gmm)	(Pa)	VMA	VFA	Vbe	Pbe	Gse	Pba
MIX 1	5.5	2.379	2.507	5.1	16.3	68.6	11.20	4.90	2.731	0.64
MIX 2	6.0	2.465	2.492	3.5	15.8	78.1	12.36	5.34	2.735	0.70
MIX 3	6.5	2.418	2.471	2.1	15.8	86.6	13.69	5.89	2.732	0.85
MIX 4	7.0	2.430	2.454	1.0	15.9	93.7	14.57	6.37	2.734	0.88

Hamburg Wheel Information

Sample No. Passes	20000
Sample Wheel Depth	3.61

TSR Information

Conditioned	121.3
Unconditioned	135.0
TSR	0.90
CA Strip Rating	2
FA Strip Rating	1
Additive Prod #	
Additive Product Name	
Additive %	

	NUMBER OF GYRATIONS	%AC	Gmb	Gmm	%VOIDS (Pa)	VMA	VFA	Gse	Gsb	TSR
		5.99			Target					
OPTIMUM DESIGN DATA @Ndes: ---->	80	6.0	2.465	2.492	3.5	15.8	77.9	2.735	2.686	0.90

REMARKS LINE 1: Hamburgs & TSR Made With Warm Mix
REMARKS LINE 2: MeadwestVaco M1 @ 0.4%

RRR12004

Tested by: Matt Valley
Reviewed by:
Verified by:
Final Approval :

Table D-7 Plant Mix 14 (P14) (Joliet)

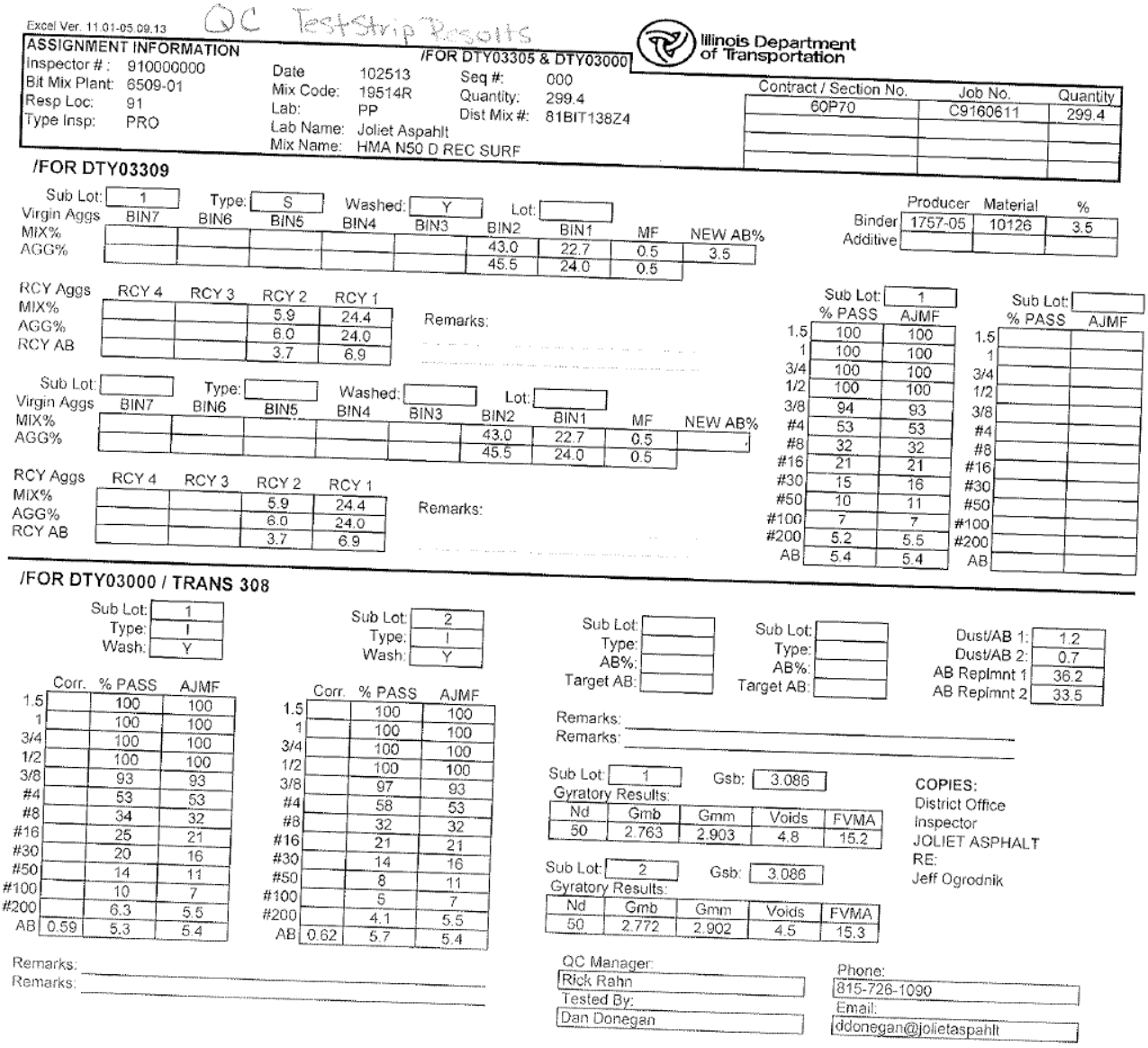

Excel Ver. 11.01-05.09.13 — QC Test Strip Results

Illinois Department of Transportation

ASSIGNMENT INFORMATION — /FOR DTY03305 & DTY03000

Inspector # :	910000000	Date	102513	Seq #:	000
Bit Mix Plant:	6509-01	Mix Code:	19514R	Quantity:	299.4
Resp Loc:	91	Lab:	PP	Dist Mix #:	81BIT138Z4
Type Insp:	PRO	Lab Name:	Joliet Aspahlt		
		Mix Name:	HMA N50 D REC SURF		

Contract / Section No.	Job No.	Quantity
60P70	C9160611	299.4

/FOR DTY03309

Sub Lot: 1 — Type: S — Washed: Y — Lot:

	BIN7	BIN6	BIN5	BIN4	BIN3	BIN2	BIN1	MF	NEW AB%
Virgin Aggs MIX%						43.0	22.7	0.5	3.5
AGG%						45.5	24.0	0.5	

	Producer	Material	%
Binder	1757-05	10126	3.5
Additive			

	RCY 4	RCY 3	RCY 2	RCY 1
RCY Aggs MIX%			5.9	24.4
AGG%			6.0	24.0
RCY AB			3.7	6.9

Remarks:

Sub Lot: 1

	% PASS	AJMF
1.5	100	100
1	100	100
3/4	100	100
1/2	100	100
3/8	94	93
#4	53	53
#8	32	32
#16	21	21
#30	15	16
#50	10	11
#100	7	7
#200	5.2	5.5
AB	5.4	5.4

Sub Lot: — Type: — Washed: — Lot:

	BIN7	BIN6	BIN5	BIN4	BIN3	BIN2	BIN1	MF	NEW AB%
Virgin Aggs MIX%						43.0	22.7	0.5	
AGG%						45.5	24.0	0.5	

	RCY 4	RCY 3	RCY 2	RCY 1
RCY Aggs MIX%			5.9	24.4
AGG%			6.0	24.0
RCY AB			3.7	6.9

Remarks:

Sub Lot: — % PASS — AJMF

	% PASS	AJMF
1.5		
1		
3/4		
1/2		
3/8		
#4		
#8		
#16		
#30		
#50		
#100		
#200		
AB		

/FOR DTY03000 / TRANS 308

Sub Lot: 1 — Type: I — Wash: Y

	Corr.	% PASS	AJMF
1.5		100	100
1		100	100
3/4		100	100
1/2		100	100
3/8		93	93
#4		53	53
#8		34	32
#16		25	21
#30		20	16
#50		14	11
#100		10	7
#200		6.3	5.5
AB	0.59	5.3	5.4

Sub Lot: 2 — Type: I — Wash: Y

	Corr.	% PASS	AJMF
1.5		100	100
1		100	100
3/4		100	100
1/2		100	100
3/8		97	93
#4		58	53
#8		32	32
#16		21	21
#30		14	16
#50		8	11
#100		5	7
#200		4.1	5.5
AB	0.62	5.7	5.4

Remarks:
Remarks:

Sub Lot: — Type: — AB%: — Target AB:

Sub Lot: — Type: — AB%: — Target AB:

Dust/AB 1:	1.2
Dust/AB 2:	0.7
AB Replmnt 1	36.2
AB Replmnt 2	33.5

Remarks:
Remarks:

Sub Lot: 1 — Gsb: 3.086

Gyratory Results:

Nd	Gmb	Gmm	Voids	FVMA
50	2.763	2.903	4.8	15.2

Sub Lot: 2 — Gsb: 3.086

Gyratory Results:

Nd	Gmb	Gmm	Voids	FVMA
50	2.772	2.902	4.5	15.3

COPIES:
District Office
Inspector
JOLIET ASPHALT
RE:
Jeff Ogrodnik

QC Manager: Rick Rahn — Phone: 815-726-1090
Tested By: Dan Donegan — Email: ddonegan@jolietaspahlt

Table D-8 Plant Mix 15 (P15) (Sandeno)

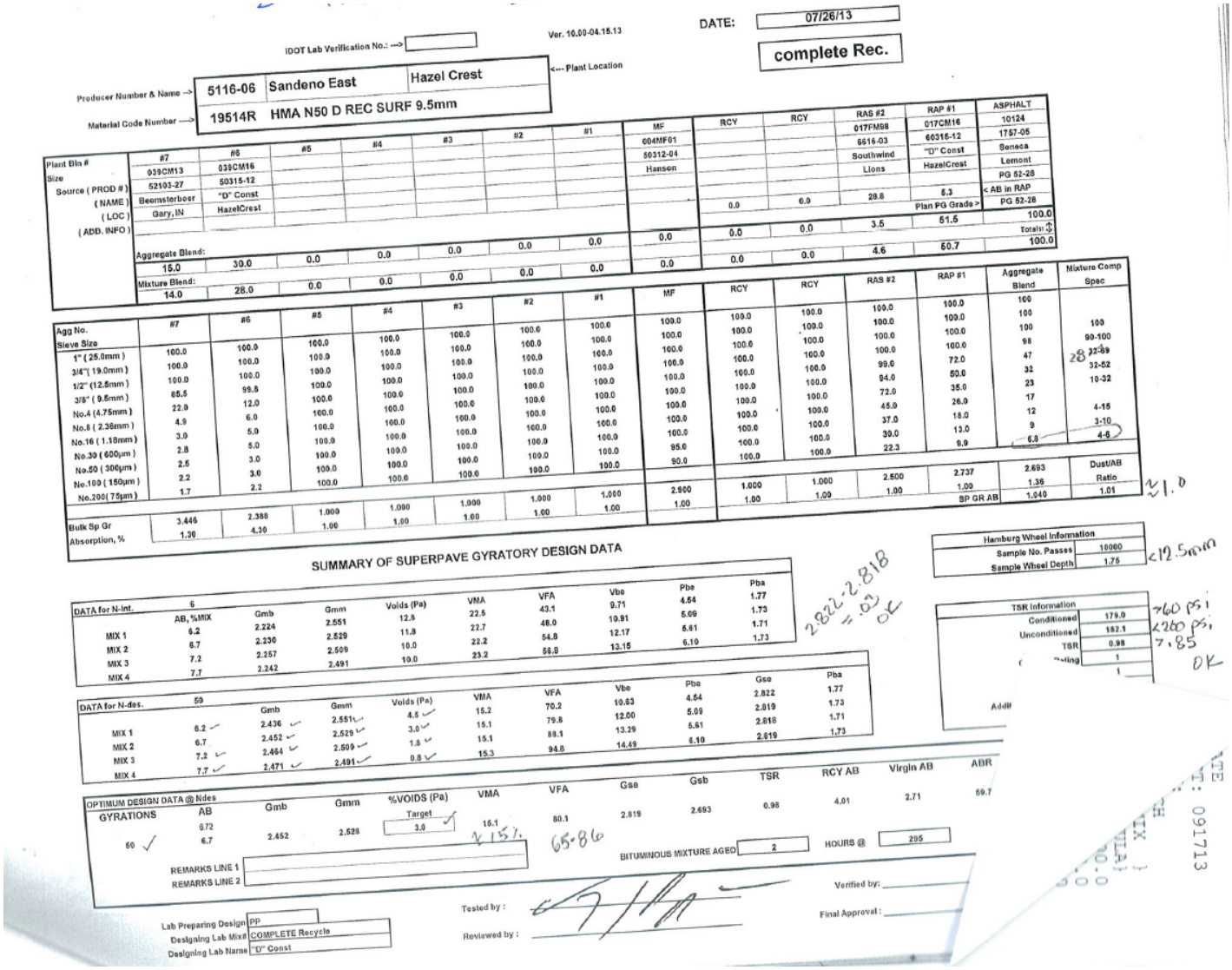

IDOT Lab Verification No.: ---> Ver. 10.00-04.15.13

DATE: 07/26/13

complete Rec.

Producer Number & Name --> 5116-06 | Sandeno East | Hazel Crest <--- Plant Location

Material Code Number --> 19514R HMA N50 D REC SURF 9.5mm

Plant Bin #	#7	#6	#5	#4	#3	#2	#1	MF	RCY	RCY	RAS #2	RAP #1	ASPHALT
Size	039CM13	039CM16						604MF01			017FM98	017CM16	10124
Source (PROD #)	52103-27	50315-12						50312-04			6616-03	60315-12	1757-05
(NAME)	Beemsterboer	"D" Const						Hanson			Southwind	"D" Const	Seneca
(LOC)	Gary, IN	HazelCrest									Lions	HazelCrest	Lemont
(ADD. INFO)													PG 52-28
									0.0	0.0	28.8	5.3	< AB in RAP
												Plan PG Grade >	PG 52-28
Aggregate Blend:								0.0	0.0	0.0	3.5	51.5	100.0
	15.0	30.0	0.0	0.0	0.0	0.0	0.0						Totals:
Mixture Blend:								0.0	0.0	0.0	4.6	50.7	100.0
	14.0	28.0	0.0	0.0	0.0	0.0	0.0						

Agg No.	#7	#6	#5	#4	#3	#2	#1	MF	RCY	RCY	RAS #2	RAP #1	Aggregate Blend	Mixture Comp Spec
Sieve Size														
1" (25.0mm)	100.0	100.0	100.0	100.0	100.0	100.0	100.0	100.0	100.0	100.0	100.0	100.0	100	
3/4"(19.0mm)	100.0	100.0	100.0	100.0	100.0	100.0	100.0	100.0	100.0	100.0	100.0	100.0	100	100
1/2" (12.5mm)	100.0	100.0	100.0	100.0	100.0	100.0	100.0	100.0	100.0	100.0	100.0	100.0	100	90-100
3/8" (9.5mm)	85.5	99.8	100.0	100.0	100.0	100.0	100.0	100.0	100.0	100.0	100.0	100.0	98	28 32-59
No.4 (4.75mm)	22.9	12.0	100.0	100.0	100.0	100.0	100.0	100.0	100.0	100.0	99.0	72.0	47	32-52
No.8 (2.36mm)	4.9	6.0	100.0	100.0	100.0	100.0	100.0	100.0	100.0	100.0	84.0	50.0	32	10-32
No.16 (1.18mm)	3.0	5.0	100.0	100.0	100.0	100.0	100.0	100.0	100.0	100.0	72.0	35.0	23	
No.30 (600µm)	2.8	5.0	100.0	100.0	100.0	100.0	100.0	100.0	100.0	100.0	45.0	26.0	17	
No.50 (300µm)	2.5	3.0	100.0	100.0	100.0	100.0	100.0	100.0	100.0	100.0	37.0	18.0	12	4-15
No.100 (150µm)	2.2	3.0	100.0	100.0	100.0	100.0	100.0	100.0	100.0	100.0	30.0	13.0	9	3-10
No.200(75µm)	1.7	2.2						95.0	100.0	100.0	22.3	9.9	6.8	4-8
Bulk Sp Gr	3.445	2.388	1.000	1.000	1.000	1.000	1.000	2.900	1.000	1.000	2.500	2.737	2.693	Dust/AB
Absorption, %	1.30	4.30	1.00	1.00	1.00	1.00	1.00	1.00	1.00	1.00	1.00	1.00	1.36	Ratio
												SP GR AB	1.040	1.01

SUMMARY OF SUPERPAVE GYRATORY DESIGN DATA

DATA for N-Int.	6								
	AB, %MIX	Gmb	Gmm	Voids (Pa)	VMA	VFA	Vbe	Pbe	Pba
MIX 1	6.2	2.224	2.551	12.8	22.5	43.1	9.71	4.54	1.77
MIX 2	6.7	2.230	2.529	11.8	22.7	48.0	10.91	5.09	1.73
MIX 3	7.2	2.257	2.509	10.0	22.2	54.8	12.17	5.61	1.71
MIX 4	7.7	2.242	2.491	10.0	23.2	56.8	13.15	6.10	1.73

DATA for N-des.	50									
		Gmb	Gmm	Voids (Pa)	VMA	VFA	Vbe	Pbe	Gse	Pba
MIX 1	6.2	2.436	2.551	4.5	15.2	70.2	10.63	4.54	2.822	1.77
MIX 2	6.7	2.452	2.529	3.0	15.1	79.8	12.00	5.09	2.819	1.73
MIX 3	7.2	2.464	2.509	1.8	15.1	88.1	13.29	5.61	2.818	1.71
MIX 4	7.7	2.471	2.491	0.8	15.3	94.8	14.49	6.10	2.819	1.73

OPTIMUM DESIGN DATA @ Ndes												
GYRATIONS	AB	Gmb	Gmm	%VOIDS (Pa)	VMA	VFA	Gse	Gsb	TSR	RCY AB	Virgin AB	ABR
				Target								
	6.72			3.0	15.1	80.1	2.819	2.693	0.98	4.01	2.71	59.7
50	6.7	2.452	2.529									

REMARKS LINE 1

REMARKS LINE 2

BITUMINOUS MIXTURE AGED 2 HOURS @ 295

Lab Preparing Design PP

Designing Lab Mix# COMPLETE Recycle

Designing Lab Name "D" Const

Tested by :

Reviewed by :

Verified by:

Final Approval :

Hamburg Wheel Information	
Sample No. Passes	10000
Sample Wheel Depth	1.75

TSR Information	
Conditioned	179.0
Unconditioned	182.1
TSR	0.98
Rating	1
	1

Table D-9 Plant Mix 16 (P16) (K5)

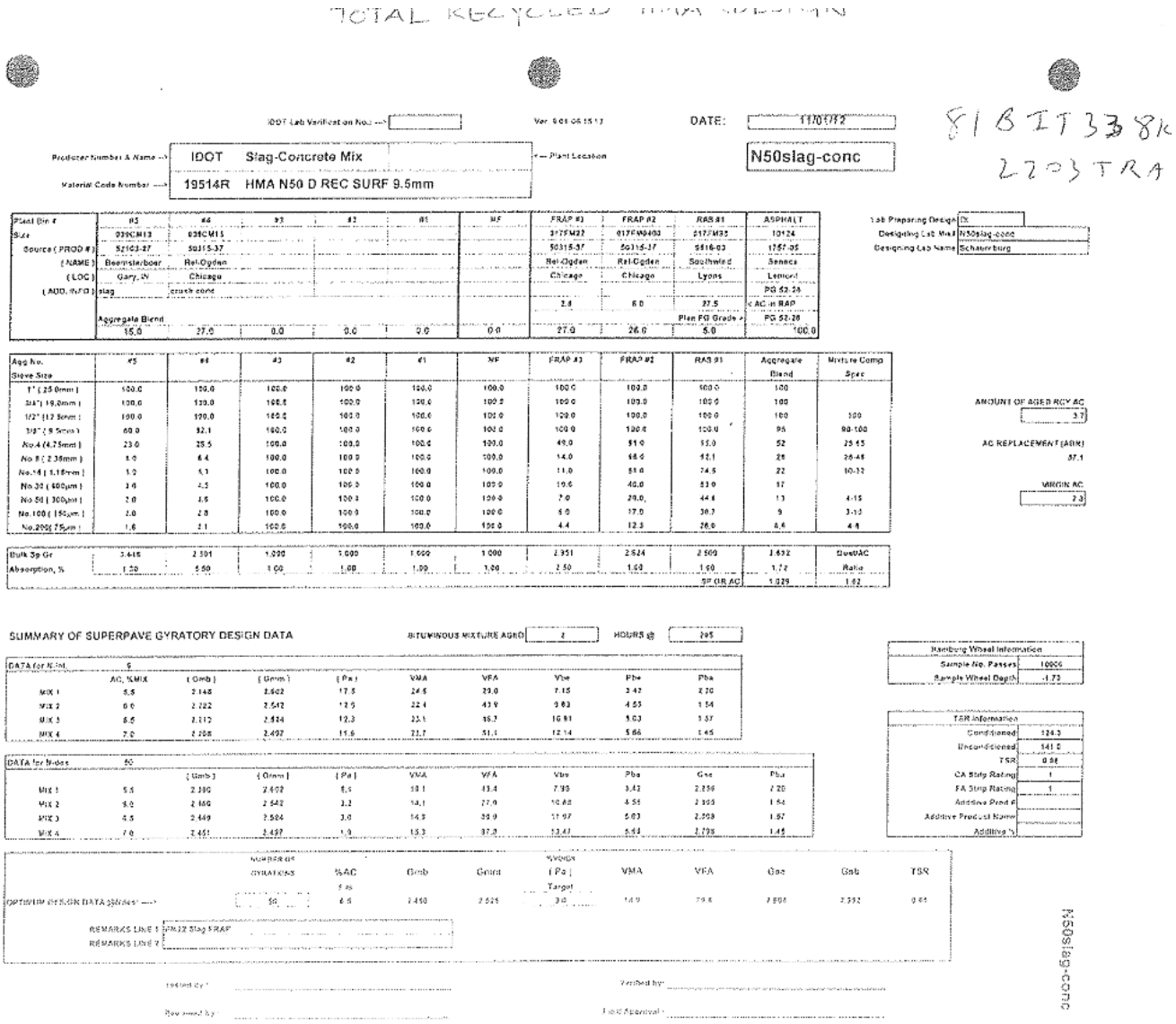

TOTAL RECYCLED [illegible]

IDOT Lab Verification No.: --- Ver. 9.01.06.15.1.3 DATE: 11/10/12

Producer Number & Name --> IDOT Slag-Concrete Mix <-- Plant Location: N50slag-conc

Material Code Number --> 19514R HMA N50 D REC SURF 9.5mm

81BIT3398K
2203TRA

Plant Bin #	#5	#4	#3	#2	#1	MF	FRAP #3	FRAP #2	RAS #1	ASPHALT
Size	939CM13	939CM15					3175M27	6175M3400	5175M35	10124
Source (PROD #)	52103-37	50315-37					50315-37	50315-37	5516-03	1757-05
(NAME)	Beamsterboer	Rel-Ogden					Rel-Ogden	Rel-Ogden	Southwind	Seneca
(LOC)	Gary, IN	Chicago					Chicago	Chicago	Lyons	Lemont
(ADD. INFO)	slag	crush conc								PG 52-28
							2.8	5.0	27.5	< AC in RAP
	Aggregate Blend								Plan PG Grade >	PG 52-28
	15.0	27.0	0.0	0.0	0.0	0.0	27.0	26.0	5.0	100.0

Lab Preparing Design: IL
Designing Lab Mix#: N50slag-conc
Designing Lab Name: Schaumburg

Agg No. / Sieve Size	#5	#4	#3	#2	#1	MF	FRAP #3	FRAP #2	RAS #1	Aggregate Blend	Mixture Comp Spec
1" (25.0mm)	100.0	100.0	100.0	100.0	100.0	100.0	100.0	100.0	100.0	100	
3/4" (19.0mm)	100.0	100.0	100.0	100.0	100.0	100.0	100.0	100.0	100.0	100	
1/2" (12.5mm)	100.0	100.0	100.0	100.0	100.0	100.0	100.0	100.0	100.0	100	100
3/8" (9.5mm)	60.0	92.1	100.0	100.0	100.0	100.0	100.0	100.0	100.0	95	90-100
No.4 (4.75mm)	23.0	25.5	100.0	100.0	100.0	100.0	49.0	91.0	55.0	52	25-55
No.8 (2.36mm)	5.0	6.4	100.0	100.0	100.0	100.0	14.0	68.0	42.1	28	28-48
No.16 (1.18mm)	3.0	5.1	100.0	100.0	100.0	100.0	11.0	51.0	24.5	22	10-32
No.30 (600µm)	3.0	4.5	100.0	100.0	100.0	100.0	10.0	40.0	13.0	17	
No.50 (300µm)	2.0	3.5	100.0	100.0	100.0	100.0	7.0	29.0	44.8	13	4-15
No.100 (150µm)	2.0	2.8	100.0	100.0	100.0	100.0	5.0	17.0	30.7	9	3-10
No.200(75µm)	1.6	2.1	100.0	100.0	100.0	100.0	4.4	12.3	26.0	8.6	4-8
Bulk Sp Gr	2.445	2.591	1.000	1.000	1.000	1.000	2.951	2.624	2.509	2.632	SlurDAC
Absorption, %	1.20	5.50	1.00	1.00	1.00	1.00	2.50	1.60	1.60	1.72	Rate
									SP OR AC	1.029	1.62

AMOUNT OF AGED RCY AC: 3.7
AC REPLACEMENT (ARR): 87.1
VIRGIN AC: 2.3

SUMMARY OF SUPERPAVE GYRATORY DESIGN DATA

BITUMINOUS MIXTURE AGED: 2 HOURS @ 295

DATA for N-ini: 6

	AC, %MIX	(Gmb)	(Gmm)	(Pa)	VMA	VFA	Vbe	Pbe	Pba
MIX 1	5.5	2.146	2.502	17.5	24.5	29.0	7.15	3.42	2.20
MIX 2	6.0	2.222	2.542	12.5	22.4	43.9	9.83	4.53	1.54
MIX 3	6.5	2.213	2.524	12.3	23.1	46.7	10.81	5.03	1.57
MIX 4	7.0	2.208	2.492	11.6	23.7	51.1	12.14	5.66	1.45

DATA for N-des: 50

		(Gmb)	(Gmm)	(Pa)	VMA	VFA	Vbe	Pbe	Gse	Pba
Mix 1	5.5	2.380	2.402	6.5	16.1	43.4	7.93	3.42	2.656	2.20
Mix 2	6.0	2.460	2.542	3.2	16.1	77.9	10.88	4.55	2.925	1.54
MIX 3	6.5	2.449	2.524	3.0	16.5	59.9	11.97	5.03	2.908	1.57
MIX 4	7.0	2.451	2.497	1.9	16.3	87.3	13.47	5.64	2.798	1.45

Hamburg Wheel Information
Sample No. Passes: 10000
Sample Wheel Depth: 4.73

TSR Information
Conditioned: 124.3
Unconditioned: 141.0
TSR: 0.88
CA Strip Rating: 1
FA Strip Rating: 1
Additive Prod #:
Additive Product Name:
Additive %:

	NUMBER OF GYRATIONS	%AC	Gmb	Gmm	%VOIDS (Pa) Target	VMA	VFA	Gse	Gsb	TSR
		Lbs								
OPTIMUM DESIGN DATA (Mix#) -->	50	6.5	2.460	2.525	3.0	16.0	79.6	2.898	2.582	0.88

REMARKS LINE 1: 25% IZ Slag 5 RAP
REMARKS LINE 2:

Tested by: Verified by:
Reviewed by: IDOT Approval:

N50slag-conc

APPENDIX E: COMPLEX MODULUS TEST RESULTS

Table E.1 Prony Series and Shift Factors of N50 Mixtures

N50-50%ABR		N50-60%ABR		N50-34%TR-R		N50-60%-TRA-26	
E_α		E_α		E_α		E_α	
80.94		130.98		132.29		157.64	
Taus	**E_n**	**Taus**	**E_n**	**Taus**	**E_n**	**Taus**	**E_n**
1.05E+05	60.26	1.05E+05	81.43	1.05E+06	159.37	3.33E+05	169.11
1.71E+04	100.89	2.15E+04	108.82	1.86E+05	238.35	4.59E+04	258.67
2.78E+03	210.94	4.38E+03	195.69	3.29E+04	425.23	6.33E+03	465.37
4.52E+02	427.9	8.94E+02	340.2	5.81E+03	697.3	8.74E+02	766.02
7.36E+01	824.47	1.82E+02	581.35	1.03E+03	1076.76	1.21E+02	1177.72
1.20E+01	1430.56	3.72E+01	945.44	1.81E+02	1547.36	1.66E+01	1663.13
1.94E+00	2152.67	7.60E+00	1430.34	3.20E+01	2070.27	2.29E+00	2155.95
3.16E-01	2763.6	1.55E+00	1975.01	5.66E+00	2581.16	3.16E-01	2571.32
5.14E-02	3051.68	3.16E-01	2466.62	1.00E+00	3011.1	4.36E-02	2840.61
8.36E-03	2970.15	1.32E-02	2878.51	1.77E-01	3305.7	6.02E-03	2934.09
1.36E-03	2621.98	2.69E-03	2749.45	5.52E-03	3413.4	8.30E-04	2859.01
2.21E-04	2157.5	1.12E-04	2103.5	9.75E-04	3255.14	1.14E-04	2659.38
3.59E-05	1684.58	2.28E-05	1727.23	1.72E-04	3007.56	1.58E-05	2369.07
5.84E-06	1277.45	4.66E-06	1378.76	3.04E-05	2695.03	2.18E-06	2066.53
9.50E-07	927.1	9.50E-07	1083.37	5.38E-06	2380.98	3.00E-07	1698.45
C_1	**C_2**	**C_1**	**C_2**	**C_1**	**C_2**	**C_1**	**C_2**
35.6649	294.2	35.9295	294.2	40.2545	294.2	40.2056	294.2

Taus: Relaxation time in seconds, $\mathbf{E_\alpha}$ is long-term modulus [MPa], E_n is Prony series modulus term [MPa], C1 and C2 are Williams-Landel-Ferry equation shift factor coefficients.

Table E.2 Prony Series and Shift Factors of N70 Mixtures

N70-25%ABR		N70-50%ABR	
E_α		E_α	
69.24		173.3	
Taus	**E_n**	**Taus**	**E_n**
3.33E+05	8.35	3.33E+05	40.42
4.46E+04	18.39	4.64E+04	87.23
4.17E+03	39.49	4.17E+03	174.24
5.55E+02	102.42	5.37E+02	362.34
5.23E+01	241.38	5.23E+01	696.75
1.22E+01	457.2	1.22E+01	1036.83
2.82E+00	832.18	2.82E+00	1457.05
6.56E-01	1393.99	6.56E-01	1916.1
1.52E-01	2081.87	1.52E-01	2348.02
3.54E-02	2740.83	3.54E-02	2685.68
8.23E-03	3194.32	8.23E-03	2878.34
1.91E-03	3348.19	1.91E-03	2914.19
4.44E-04	3208.23	2.79E-04	2706
1.03E-04	2872	2.40E-05	2288.22
2.40E-05	2415.49	3.38E-06	1821.43
C_1	**C_2**	**C_1**	**C_2**
36.2367	294.2	37.697	294.2

Taus: Relaxation time in seconds, E_α is long-term modulus [MPa], E_n is Prony series modulus term [MPa], C1 and C2 are Williams-Landel-Ferry equation shift factor coefficients.

Table E.3 Prony Series and Shift Factors of N80 Mixtures

N80-25%ABR		N80-50%ABR	
E_α		E_α	
188.98		180.13	
Taus	**E_n**	**Taus**	**E_n**
1.05E+05	80.55	1.05E+06	93.52
2.76E+04	82.09	1.45E+05	132.59
4.37E+03	171.21	2.00E+04	237.5
3.16E+02	411.37	2.76E+03	408.54
3.42E+01	736.44	3.81E+02	684.19
8.98E+00	1051.86	5.26E+01	1074.97
2.35E+00	1421.94	7.25E+00	1546.01
6.18E-01	1800.79	1.00E+00	1996.68
1.62E-01	2124.38	1.38E-01	2301.67
4.25E-02	2335.44	1.90E-02	2384.1
1.11E-02	2402.55	2.62E-03	2251.43
2.92E-03	2334.23	3.62E-04	1976.95
4.56E-04	2041.79	4.99E-05	1636.5
3.23E-05	1518.65	6.89E-06	1309.54
3.62E-06	1127.67	9.50E-07	989.92
C_1	**C_2**	**C_1**	**C_2**
36.4378	294.2	36.021	294.2

Taus: Relaxation time in seconds, $\mathbf{E_\alpha}$ is long-term modulus [MPa], E_n is Prony series modulus term [MPa], C1 and C2 are Williams-Landel-Ferry equation shift factor coefficients.

Table E.4 Prony Series and Shift Factors of N90 Mixtures

N90-0%ABR		N90-30%ABR		N90-20%ABR	
E_α		E_α		E_α	
63.39		48.61		63.05	
Taus	**E_n**	**Taus**	**E_n**	**Taus**	**E_n**
1.05E+05	24.22	1.05E+05	49.45	1.05E+05	27.75
1.71E+04	39.67	1.71E+04	83.49	1.71E+04	45.77
2.78E+03	85.64	2.78E+03	171.66	2.78E+03	98.49
4.52E+02	193.26	4.52E+02	337.04	4.52E+02	217.43
7.36E+01	452.33	7.36E+01	627.22	7.36E+01	482.03
1.20E+01	1019.08	1.20E+01	1070.15	1.20E+01	990.19
1.94E+00	2013.43	1.94E+00	1641.6	1.94E+00	1732.19
3.16E-01	3212.43	3.16E-01	2243.43	3.16E-01	2435.38
5.14E-02	4010.34	5.14E-02	2736.42	5.14E-02	2733.58
8.36E-03	4011.34	8.36E-03	3011.11	8.36E-03	2537.6
1.36E-03	3389.49	1.36E-03	3030.78	1.36E-03	2049.7
2.21E-04	2555.12	2.21E-04	2840.85	2.21E-04	1508.89
3.59E-05	1787.98	3.59E-05	2505.59	3.59E-05	1045.19
5.84E-06	1200.05	5.84E-06	2130.93	5.84E-06	700.11
9.50E-07	772.68	9.50E-07	1708.29	9.50E-07	451.92
C_1	**C_2**	**C_1**	**C_2**	**C_1**	**C_2**
33.3993	294.2	37.3109	294.2	37.3109	294.2

Taus: Relaxation time in seconds, $\mathbf{E_\alpha}$ is long-term modulus [MPa], E_n is Prony series modulus term [MPa], C1 and C2 are Williams-Landel-Ferry equation shift factor coefficients.

APPENDIX F: HAMBURG TEST RESULTS SUMMARY

Hamburg Wheel Test Report

Project Name:	ABR	**Project Number:**	R27-128	**Date Tested:**	03/13/15
Mix ID:	L4				
Mix Type:	N90-0 CG	**Sampling:**	Stockpile agg, prepared binder		
Binder:	PG64-22	**Specimen Prep:**	Lab batched, mixed, compacted		
Ndesign:	N90	**Compaction Type:**	SGC		

Specimen Information:

Compacted Thickness: 130 mm
Fabrication: Saw cut into 2 specimens, saw cut mating faces

Test Tempurature: 50°C

Test Results:

Maximum Displacement	6.8	**mm,**	**at**	7,500	**passes**
End Maximum Displacement	20.1	**mm,**	**at**	12,000	**passes**

Pass/Fail: Pass < 12.5 mm (0.5 in.) at 7,500 passes

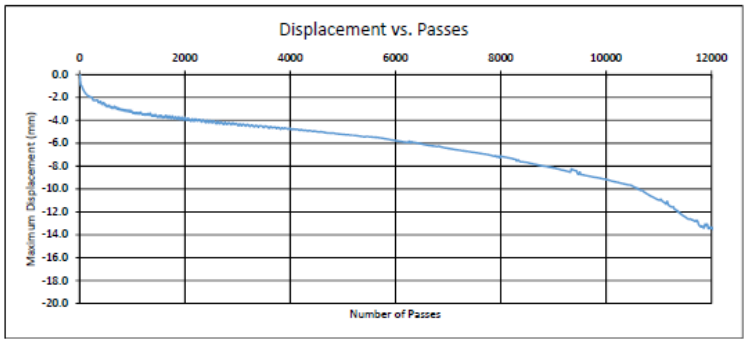

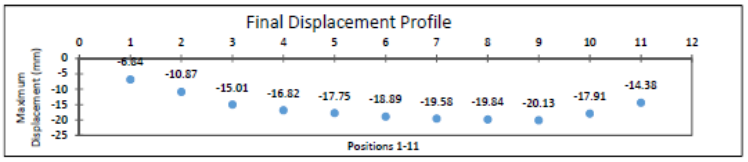

Hamburg Wheel Test Report

Project Name:	ABR	**Project Number:**	R27-128	**Date Tested:**	04/08/15

Mix ID: L7
Mix Type: N90-20 CG S1
Binder: PG58-28
Ndesign: N90

Sampling: Stockpile agg, prepared binder
Specimen Prep: Lab batched, mixed, compacted
Compaction Type: SGC

Specimen Information:

Compacted Thickness: 130 mm
Fabrication: Saw cut into 2 specimens, saw cut mating faces

Test Tempurature: 50°C

Test Results:

Maximum Displacement	7.2	**mm, at**	5,000	**passes**	
End Maximum Displacement	20.3	**mm, at**	20,000	**passes**	

Pass/Fail: Pass < 12.5 mm (0.5 in.) at 5,000 passes

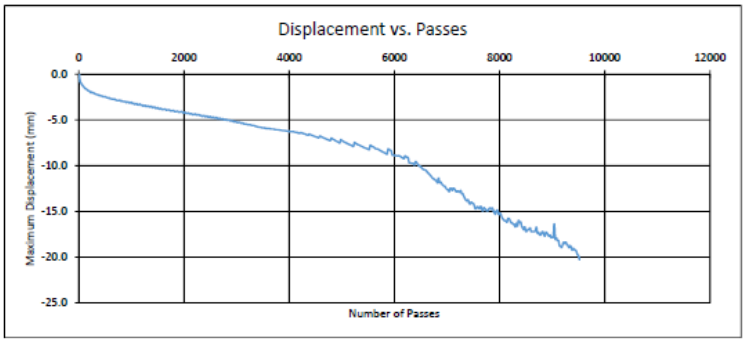

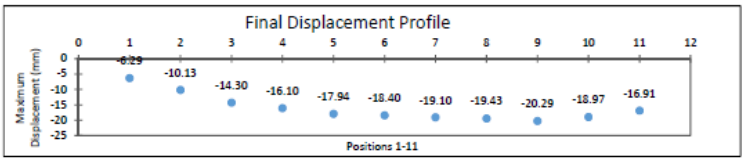

Hamburg Wheel Test Report

Project Name:	ABR	**Project Number:**	R27-128	**Date Tested:**	07/15/15
Mix ID:	L9				
Mix Type:	N90-30 CG $S2^4$ AS^5	**Sampling:**	Stockpile agg, prepared binder		
Binder:	PG58-28	**Specimen Prep:**	Lab batched, mixed, compacted		
Ndesign:	N90	**Compaction Type**	SGC		

Specimen Information:

Compacted Thickness:	130 mm
Fabrication:	Saw cut into 2 specimens, saw cut mating faces

Test Tempurature: 50°C

Test Results:

Maximum Displacement	3.9	**mm,**	**at**	5,000	**passes**
End Maximum Displacement	6.1	**mm,**	**at**	20,000	**passes**

Pass/Fail: Pass < 12.5 mm (0.5 in.) at 5,000 passes

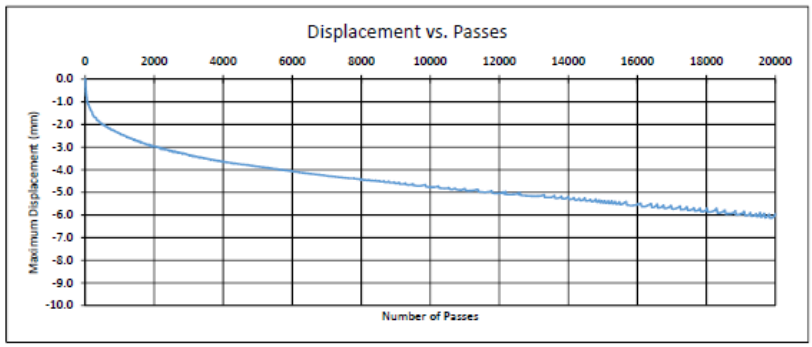

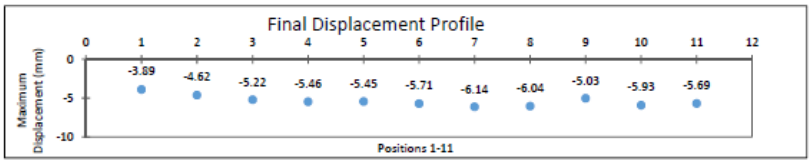

Hamburg Wheel Test Report

Project Name:	ABR	**Project Number:**	R27-128	**Date Tested:**	07/16/15

Mix ID:	L10		
Mix Type:	N90-60 CG S2 AS	**Sampling:**	Stockpile agg, prepared binder
Binder:	PG52-34	**Specimen Prep:**	Lab batched, mixed, compacted
Ndesign:	N90	**Compaction Type:**	SGC

Specimen Information:

Compacted Thickness:	130 mm
Fabrication:	Saw cut into 2 specimens, saw cut mating faces

Test Tempurature: 50°C

Test Results:

Maximum Displacement	2.3	**mm,**	**at**	5,000	**passes**
End Maximum Displacement	3.2	**mm,**	**at**	20,000	**passes**

Pass/Fail: Pass < 12.5 mm (0.5 in.) at 5,000 passes

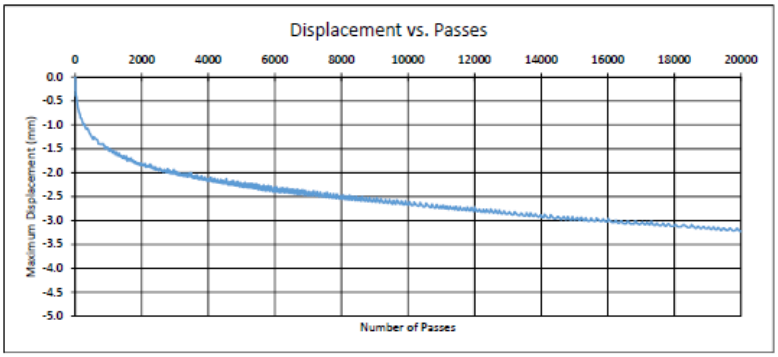

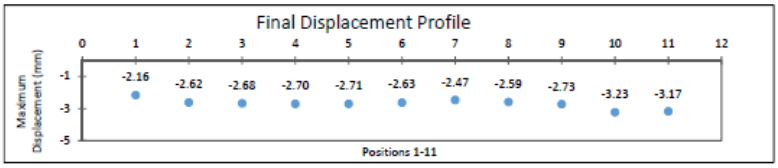

Hamburg Wheel Test Report

Project Name: ABR **Project Number:** R27-128 **Date Tested:** 07/26/15

Mix ID: L12
Mix Type: N90-30 CG S2[4] AS[1]
Binder: PG58-28
Ndesign: N90

Sampling: Stockpile agg, prepared binder
Specimen Prep: Lab batched, mixed, compacted
Compaction Type SGC

Specimen Information:

Compacted Thickness: 130 mm
Fabrication: Saw cut into 2 specimens, saw cut mating faces

Test Tempurature 50°C

Test Results:

Maximum Displacement	3.5	**mm,**	**at**	5,000	**passes**
End Maximum Displacement	5.0	**mm,**	**at**	20,000	**passes**

Pass/Fail: Pass < 12.5 mm (0.5 in.) at 5,000 passes

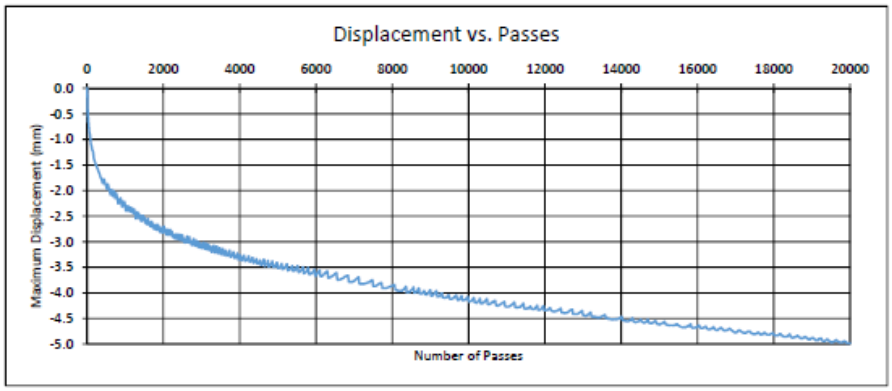

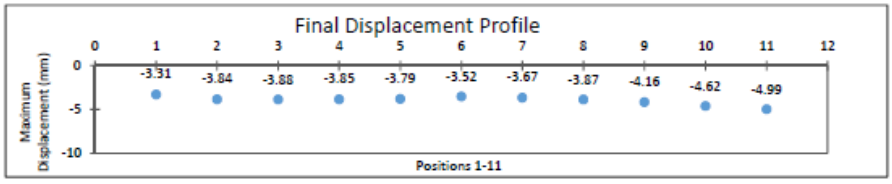

APPENDIX G: IL-SCB DETAILED TEST RESULTS SUMMARY

Table G-1 Plant Mixtures

Table G-1.1 P1-P15 IL-SCB (25ºC at 50 mm/min)

Mix ID	Mix Name	Energy (LLD) (J/m^2)	Avg	Std Dev	COV	Flexibility Index	Avg	Std Dev	COV	Peak Load (KN)	Avg	Std Dev	COV
P1	TOL MIX 1	1510.4 1784.9 1381.4	1558.9	168.3	10.8	2.6 2.7 1.9	2.4	0.4	15.4	3.7 3.9 3.6	3.7	0.1	3.2
P2	TOL MIX 2	1648.6 1856.5 1391.4	1752.6	103.9	5.9	2.8 3.7 1.6	3.3	0.5	14.4	4.1 4.0 3.9	4.0	0.0	0.9
P3	TOL MIX 3	1276.3 1029.1 1527.2	1277.5	203.3	15.9	2.1 1.2 1.7	1.7	0.4	23.8	3.6 3.4 3.9	3.6	0.2	5.7
P4	TOL MIX 4	1484.7 1304.2 1370.8	1337.5	33.3	2.5	2.9 1.1 1.4	1.3	0.2	13.9	3.5 4.2 4.0	4.1	0.1	2.9
P5	TOL MIX 5	1095.0 986.6	1040.8	54.2	5.2	0.3 0.3	0.3	0.0	7.1	4.9 4.8	4.9	0.1	1.5
P6	TOL MIX 6	2089.7 1742.8 2039.7	1957.4	153.1	7.8	2.8 2.0 3.2	2.7	0.5	18.7	5.1 4.6 4.6	4.8	0.3	5.2
P7	TOL MIX 7	2120.5 2141.1 1890.6	2015.8	125.3	6.2	9.7 5.9 4.7	5.3	0.6	11.8	3.2 3.8 3.5	3.6	0.1	3.2
P8	N50-50	1040.4 1337.6 1175.8	1184.6	121.5	10.3	1.5 2.5 1.5	1.8	0.5	26.3	3.4 3.4 4.1	3.6	0.3	9.3

Mix ID	Mix Name	Energy (LLD) (J/m^2)	Avg	Std Dev	COV	Flexibility Index	Avg	Std Dev	COV	Peak Load (KN)	Avg	Std Dev	COV
P9	N50-60	1059.7	967.2	92.4	9.6	2.2	1.6	0.6	37.1	3.0	2.8	0.2	7.3
		874.8				1.0				2.6			
P10	N70-25	2024.1	1969.4	127.7	6.5	9.1	8.9	1.7	19.2	3.1	3.0	0.1	4.3
		2091.1				10.9				2.8			
		1793.0				6.8				3.0			
P11	N70-50	1141.6	1366.7	159.2	11.7	1.2	2.0	0.6	28.3	4.8	4.3	0.4	8.6
		1473.9				2.5				3.9			
		1484.7				2.4				4.1			
		1145.4				1.1				3.8			
P12	N80-25	1581.3	1828.9	271.8	14.9	2.6	8.2	1.4	17.6	3.6	2.8	0.1	4.6
		1119.5				1.5				3.5			
		1557.1				6.8				2.7			
		2100.7				9.7				3.0			
P13	N80-50	1603.4	1338.5	270.5	20.2	1.9	2.8	1.4	49.2	4.6	3.6	0.7	19.2
		1444.9				4.7				3.0			
		556.8				0.3				3.5			
		646.2				0.4				3.9			
		967.1				1.7				3.3			
P14	TR-JOLIET	2161.3	2225.5	131.7	5.9	5.2	6.9	1.1	16.7	3.8	3.8	0.1	2.3
		2441.7				8.4				3.8			
		2208.3				7.2				4.0			
		2090.6				6.7				3.7			
P15	TR-SANDENO	1537.1	1444.8	61.5	4.3	2.6	2.1	0.3	14.5	4.0	3.8	0.2	5.8
		1434.3				1.9				4.0			
		1443.5				1.8				3.6			
		1364.1				2.2				3.5			

Table G-1.2 P17-P22 IL-SCB (25ºC at 50 mm/min)

Mix	Replicate ID	Energy (LLD) (J/m^2)	Average	Std Dev	COV	Peak Load (kN)	Average Peak Load	Std Dev	COV	FI	Average	Std Dev	COV
P17	147M-B1.dat	2110.8	2167.9	53.0	2.4	4.2	4.1	0.1	1.3	4.3	4.5	0.2	5.4
	147M-B2.dat	2215.5				4.0				4.8			
	147M-T2.dat	2177.3				4.1				4.6			
P18	156M-B2.dat	2024.8	2048.7	126.9	6.2	4.0	4.0	0.1	2.2	4.4	4.5	0.2	4.2
	156M-T1.dat	2185.8				4.0				4.7			
	156M-T2.dat	1935.4				4.1				4.4			
P19	157M-B1.dat	1687.6	1884.7	159.5	8.5	4.1	4.2	0.1	2.6	3.2	3.5	0.4	10.9
	157M-B2.dat	1942.5				4.2				4.0			
	157M-T1.dat	2065.0				4.4				3.7			
	157M-T2.dat	1843.9				4.1				3.2			
P20	141M-B1.dat	2095.5	2015.7	98.5	4.9	3.7	3.8	0.1	3.2	5.3	5.1	0.3	6.4
	141M-B2.dat	2093.1				3.7				5.3			
	141M-T1.dat	1983.8				3.9				5.3			
	141M-T2.dat	1890.3				3.8				4.6			
P21	140M-B1.dat	1779.4	1817.9	125.5	6.9	3.1	3.0	0.1	4.7	6.7	6.9	0.3	4.6
	140M-B2.dat	1958.1				3.2				6.6			
	140M-T2.dat	1716.2				2.9				7.2			
P22	159M-B1.dat	2008.9	1963.6	98.4	5.0	3.0	3.1	0.1	4.0	9.0	8.8	1.9	21.3
	159M-B2.dat	2031.3				3.1				10.5			
	159M-T1.dat	1850.7				3.3				6.8			

Table G-1.3 P1-P15 IL-SCB (25°C at 25 mm/min)

Mix	Replicate ID	Energy (LLD) (J/m^2)	Average	Std Dev	COV	Peak Load (kN)	Average Peak Load	Std Dev	COV
P1	MIX1-SCB-3-T-1.dat	1291.3	1296.6	15.6	1.2	3.2	3.1	0.1	4.3
	MIX1-SCB-4-B-1.dat	1314.1				2.9			
	MIX1-SCB-3-T-1.dat	1284.4				3.2			
P2	MIX2-SCB-3-B-1.dat	1349.0	1383.6	31.1	2.2	4.5	4.5	0.1	2.4
	MIX2-SCB-3-B-2.dat	1393.1				4.6			
	MIX2-SCB-3-T-2.dat	1408.9				4.4			
P3	MIX3-SCB-4-B-1.dat	1043.6	1073.8	44.5	4.1	4.1	4.0	0.1	3.4
	MIX3-SCB-4-B-2.dat	1124.9				3.9			
	MIX3-SCB-4-T-1.dat	1053.0				4.1			
P4	MIX4-SCB-3-B-2.dat	1054.6	1112.2	64.4	5.8	4.3	4.2	0.2	4.3
	MIX4-SCB-3-T-1.dat	1181.7				4.0			
	MIX4-SCB-4-B-1.dat	1100.2				4.4			
P5	MIX5-SCB-3-B-1.dat	1194.9	1203.5	12.1	1.0	4.4	4.7	0.4	7.9
	MIX5-SCB-3-T-1.dat	1212.0				5.0			
P6	MIX6-SCB-4-B-1.dat	1738.1	1879.7	149.5	8.0	4.8	4.8	0.3	5.3
	MIX6-SCB-4-B-2.dat	1865.1				4.5			
	MIX6-SCB-4-T-1.dat	2035.9				5.0			
P7	MIX7-SCB-3-B-1.dat	1839.1	2040.0	204.1	10.0	3.0	3.0	0.1	4.7
	MIX7-SCB-3-T-1.dat	2247.1				3.2			
	MIX7-SCB-3-T-2.dat	2033.8				2.9			
P8	N50-50-SCBII-1-T-2 HI.dat	1392.8	1161.9	229.4	19.7	2.4	3.3	0.9	26.4
	N50-50-SCBIII-B-1-1 HI.dat	934.1				3.5			
	N50-50-SCBIII-T-2-2 HI.dat	1158.8				4.1			
P9	N50-60-SCB4-B-1 HI.dat	548.5	644.0	82.8	12.9	3.2	3.1	0.3	10.4
	N50-60-SCB4-T-2 HI.dat	690.6				3.4			
	N50-60-SCBII-2-B-2 HI.dat	693.0				2.8			
P10	N70-25-SCBII-3-2 HI.dat	1224.1	1269.9	64.8	5.1	2.1	2.2	0.1	5.2
	N70-25-SCBIII-T-2-2 HI.dat	1315.7				2.3			

Mix	Replicate ID	Energy (LLD) (J/m^2)	Average	Std Dev	COV	Peak Load (kN)	Average Peak Load	Std Dev	COV
P11	N70-50-SCBII-2-T-1 HI.dat	1115.4	1260.4	126.7	10.1	3.5	3.4	0.1	3.9
	N70-50-SCBIII-T-2-1 HI.dat	1350.0				3.3			
	N70-50-SCBIII-T-2-1 HI.dat	1315.8				3.4			
P12	N80-25-SCBII-2-B-1 HI.dat	1100.4	1316.6	226.1	17.2	2.3	2.5	0.2	7.6
	N80-25-SCBIII-T-2-1 HI.dat	1297.9				2.5			
	N80-25-SCBIII-T-3-1 HI.dat	1551.5				2.7			
P13	N80-50-SCBII-2-B-2 HI.dat	705.6	745.2	141.6	19.0	3.5	3.3	0.2	5.5
	N80-50-SCBIII-B-1-1 HI.dat	902.5				3.1			
	N80-50-SCBIII-T-2-1 HI.dat	627.6				3.3			
P14	TR-J-4-B-1.dat	1388.5	1387.0	57.3	4.1	2.0	2.2	0.2	7.3
	TR-J-4-T-1.dat	1434.3				2.1			
	TR-J-6-B-2.dat	1419.1				2.4			
	TR-J-6-T-1.dat	1305.9				2.3			
P15	TR-S-3-B-2.dat	970.2	1039.1	89.0	8.6	2.7	2.6	0.2	5.9
	TR-S-3-T-2.dat	960.1				2.7			
	TR-S-5-B-2.dat	1082.7				2.4			
	TR-S-5-T-2.dat	1143.3				2.5			

Table G-1.4 P1-P15 IL-SCB (25°C at 6.25 mm/min)

Mix	Replicate ID	Energy (LLD) (J/m^2)	Average	Std Dev	COV	Peak Load (kN)	Average Peak Load	Std Dev	COV
P1	MIX1-SCB-1-B-1.dat	1145.3	1073.3	65.1	6.1	1.9	2.1	0.2	8.2
	MIX1-SCB-1-B-2.dat	1055.7				2.2			
	MIX1-SCB-2-T-2.dat	1018.8				2.3			
P2	MIX2-SCB-1-B-2.dat	1071.5	1131.4	208.7	18.4	2.1	2.2	0.4	16.8
	MIX2-SCB-1-T-1.dat	1363.5				2.6			
	MIX2-SCB-1-T-2.dat	959.3				1.9			
P3	MIX3-SCB-2-B-2.dat	855.9	827.3	165.9	20.0	1.6	1.5	0.2	14.8
	MIX3-SCB-2-T-1.dat	977.1				1.6			
	MIX3-SCB-2-T-2.dat	649.0				1.2			
P4	MIX4-SCB-1-B-1.dat	976.1	946.4	133.6	14.1	2.5	2.4	0.1	4.3
	MIX4-SCB-1-B-2.dat	855.2				2.3			
	MIX4-SCB-1-T-1.dat	1007.9				2.5			
P5	MIX5-SCB-1-B-2.dat	879.9	933.4	80.6	8.6	1.4	1.5	0.1	6.7
	MIX5-SCB-2-B-1.dat	933.2				1.5			
	MIX5-SCB-2-T-2.dat	987.1				1.6			
P6	MIX6-SCB-1-B-1.dat	879.9	933.4	53.6	5.7	2.2	2.1	0.1	3.4
	MIX-6-SCB-1-T-1.dat	933.2				2.0			
	MIX6-SCB-1-T-2.dat	987.1				2.1			
P7	MIX7-SCB-1-T-2.dat	1369.1	1358.9	212.4	15.6	2.8	3.1	0.4	11.2
	MIX7-SCB-2-B-1.dat	1141.5				3.1			
	MIX7-SCB-2-B-2.dat	1565.9				3.5			
P12	N80-25-5-B.dat	680.3	786.9	133.3	16.9	1.7	1.7	0.0	0.7
	N80-25-9-B.dat	744.0				1.7			
	N80-25-9-T.dat	936.3				1.7			
P13	N80-50-8-T.dat	724.0	729.4	95.9	13.1	2.2	2.3	0.1	5.6
	N80-50-9-B.dat	827.8				2.5			
	N80-50-9-T.dat	636.3				2.3			
P14	JOLIET-12-T-2.dat	1286.2	1201.9	108.8	9.0	2.0	2.2	0.2	8.0
	JOLIET-13-T-1.dat	1079.1				2.2			
	JOLIET-16-T-2.dat	1240.3				2.4			
P15	SANDENO 13-T-1.dat	867.4	904.0	51.7	5.7	1.6	1.7	0.1	4.6
	SANDENO 17-B-1.dat	940.5				1.7			

Table G-2 Laboratory Mixtures

Table G-2.1 L3-L13

Mix ID	Mix Name	Replicate	Energy (LLD) (J/m^2)	Avg	Std Dev	COV	SCB Strength (MPa)	Avg	Std Dev	COV	FI	Avg	Std Dev	COV
L3	L3 N90-0 (PG 70-22)	1	2273.7	2306.9	72.5	3.1	0.36	0.37	0.01	1.79	16.1	15.7	0.77	4.9
		2	2407.6				0.38				16.4			
		3	2239.6				0.37				14.6			
L4	L4 N90-0 (PG 64-22)	1	1715.2	1943.5	161.9	8.3	0.45	0.37	0.06	16.4	10.9	12.8	1.75	13.7
		2	2043.9				0.31				12.2			
		3	2071.5				0.34				15.1			
L5	L5 N90-30 (PG 70-22)	1	1450.6	1417.6	54.4	3.8	0.53	0.48	0.03	7.2	2.1	2.3	0.26	11.5
		2	1462.0				0.47				2.6			
		3	1341.3				0.45				2.0			
L6	L6 N90-30 (PG 58-28)	1	1391.0	1503.5	71.24	4.7	0.42	0.51	0.10	18.9	4.4	4.6	0.94	20.3
		2	1588.0				0.46				4.6			
		3	1510.0				0.64				3.5			
		4	1525.0								6.1			
L7	L7 N90-20 (PG 58-28)	1	1747.4	1718.2	75.9	4.4	0.37	0.36	0.02	4.6	9.0	9.2	0.39	4.27
		2	1793.1				0.36				9.7			
		3	1614.2				0.33				8.9			
L8	L8 N90-10 (PG 64-22)	1	1964.8	2019.4	111.1	5.5	0.5	0.50	0.01	1.4	4.8	5.9	1.14	19.6
		2	2174.3				0.5				7.5			
		3	1919.1				0.49				5.3			
L9	L9 N90-30 (PG 58-28)-AS	1	1643.3	1642.1	58.2	3.6	0.45	0.44	0.02	4.3	3.5	4.0	0.59	15.0
		2	1570.3				0.42				4.8			
		3	1712.9				0.46				3.6			
L10	L10 N90-60 (PG 58-28)-AS	1	1140.3	1374.1	218.4	15.9	0.50	0.56	0.07	12.0	1.3	1.8	0.32	18.1
		2	1235.1				0.52				1.7			
		3	1408.6				0.56				2.1			
		4	1714.0				0.67				2.0			

Mix ID	Mix Name	Replicate	Energy (LLD) (J/m^2)	Avg	Std Dev	COV	SCB Strength (MPa)	Avg	Std Dev	COV	FI	Avg	Std Dev	COV
L11	L11 N90-0 (PG 64-22)-AS			1464.9	164.9	11.2	0.46	0.33	0.09	27.3		12.9	0.61	4.8
		1	1651.5				0.34				13.8			
		2	1490.3				0.31				12.4			
		3	1250.7				0.21				12.5			
L12	L12 N90-30-7% IDOT (PG 58-28)-AS	1	1510.4	1442.5	67.9	4.7	0.38	0.39	0.01	3.9	5.7	4.7	0.58	12.4
		2	1444.8				0.42				4.8			
		3	1322.2				0.40				4.3			
		4	1430.4				0.38				4.6			
		5	1504.5				0.39				3.9			
L13	L13 N90-30-7% SW (PG 58-28)-AS	1	1631.6	1540.8	232.3	15.1	0.55	0.50	0.04	7.6	2.6	2.6	0.20	7.6
		2	1833.8				0.47				2.7			
		3	1604.4				0.55				2.8			
		4	1506.3				0.49				2.5			
		5	1127.8				0.46				2.2			

Table G-3 Field Cores

District	Mix ID	Replicate ID	Energy (LLD) (J/m^2)	Average	Std Dev	COV	Peak Load (kN)	Average Peak Load	Std Dev	COV	FI	Average	Std Dev	COV
District 1	1	B-T1	2993.6	2527.9	323.0	12.8	3.6	3.6	0.4	11.6	10.3	6.6	3.0	46.0
		B-T2	2353.1				3.3				6.1			
		C-T1	2274.7				3.4				7.2			
		C-T2	2490.3				4.2				2.9			
	2	D-T1	2978.0	2302.8	465.8	20.2	4.8	4.4	0.5	11.1	5.5	4.1	1.0	24.7
		D-T2	2232.3				4.7				3.2			
		E-T1	1940.1				4.1				3.6			
		E-T2	2060.9				3.8				3.9			
	3	A-T1	2917.3	2262.1	460.0	20.3	4.2	4.1	0.6	14.4	8.7	6.0	2.4	39.5
		A-T2	2120.2				4.0				7.1			
		E-T1	1841.9				3.3				4.7			
		E-T2	2169.0				4.8				3.4			
	4	A-T1	2237.7	2284.5	292.0	12.8	5.2	6.0	0.7	11.8	3.2	2.1	0.9	42.4
		A-T2	2601.0				6.5				2.5			
		D-T1	1907.7				5.6				1.1			
		D-T2	2391.7				6.7				1.8			
	5	D-T1	1163.0	1230.7	164.0	13.3	3.4	3.6	0.2	4.5	1.7	1.6	0.2	13.2
		D-T2	1111.4				3.5				1.4			
		F-T2	1417.7				3.7				1.8			
	6	A-T1	1821.2	1710.8	164.9	9.6	3.4	3.4	0.1	3.9	5.3	3.9	1.0	26.5
		A-T2	1877.8				3.4				3.6			
		C-T1	1532.9				3.4				2.9			
		C-T2	1611.5				3.2				3.8			
	7	A-T1	1772.4	1555.9	210.1	13.5	3.0	3.3	0.3	9.8	3.8	2.9	1.0	34.9
		A-T2	1542.5				3.4				3.2			
		F-T2	1352.9				3.7				1.8			
	8	A-T1	2843.8	2515.2	357.6	14.2	2.6	2.5	0.1	3.9	16.3	11.8	4.7	39.8
		A-T2	2658.9				2.4				13.0			
		B-T1	2011.2				2.6				5.2			
		B-T2	2546.7				2.4				12.9			
	9	B-T1	2919.2	2937.2	174.1	5.9	2.5	2.2	0.2	9.5	16.7	21.2	4.2	20.0
		B-T2	2710.9				2.1				19.5			
		C-T1	3128.3				2.2				21.9			
		C-T2	2990.5				2.1				26.7			

District	Mix ID	Replicate ID	Energy (LLD) (J/m^2)	Average	Std Dev	COV	Peak Load (kN)	Average Peak Load	Std Dev	COV	FI	Average	Std Dev	COV
	10	D-T1	1641.0	1797.8	203.0	11.3	4.9	4.8	0.2	3.5	1.4	1.7	0.4	26.7
		D-T2	2089.5				4.9				2.3			
		F-T1	1681.0				4.6				1.2			
		F-T2	1779.7				4.9				1.8			
	11	D-T1	1687.3	1852.0	283.7	15.3	2.5	2.5	0.1	5.3	5.4	6.6	1.2	17.6
		D-T2	1554.6				2.5				6.3			
		F-T1	1985.2				2.4				6.5			
		F-T2	2180.9				2.7				8.1			
	12	D-T1	3177.6	2713.8	463.3	17.1	4.6	4.8	0.3	6.8	6.9	5.1	1.5	29.0
		D-T2	2836.0				5.3				4.9			
		F-T1	2072.7				4.6				3.3			
		F-T2	2768.8				4.8				5.2			
	13	E-T1	3024.5	2607.9	287.8	11.0	3.1	3.1	0.1	1.8	17.6	12.8	3.3	25.5
		E-T2	2569.3				3.0				12.1			
		G-T1	2387.9				3.0				11.0			
		G-T2	2449.8				3.1				10.5			
District 2	2RT26	1-1	1494.9	1236.8	278.5	22.5	4.0	3.9	0.4	11.0	1.7	1.3	0.4	28.1
		2-2	1273.8				4.3				1.3			
		2-1	941.7				3.4				1.0			
	22RT2	1-2	1618.3	1536.1	255.0	16.6	3.9	3.6	0.5	14.8	2.1	2.0	0.1	7.1
		1-1	1739.9				3.9				1.9			
		2-2	1250.1				3.0				2.1			
	22SRT 2	7-1	1226.4	1155.7	157.0	13.6	3.6	3.7	0.2	6.2	1.0	0.8	0.3	41.8
		7-2	972.9				4.0				0.5			
		8-1	1332.6				3.9				1.2			
		8-2	1090.8				3.5				0.6			
District 3	6E	2-1	2681.3	2526.8	306.6	12.1	2.3	2.3	0.0	1.6	16.8	16.5	1.9	11.3
		2-2	2725.4				2.4				18.2			
		8-2	2173.8				2.3				14.5			
	6W	2-2	1703.8	1721.3	62.4	3.6	2.8	3.0	0.2	6.8	5.7	3.9	1.8	47.1
		3-1	1790.5				3.1				4.0			
		3-2	1669.5				3.1				2.0			
District 4	4I9-1	A-1	1946.1	1801.3	105.0	5.8	2.7	2.5	0.2	7.8	6.3	7.2	1.4	18.7
		A-2	1774.3				2.3				9.1			
		B-1	1789.8				2.6				7.2			

District	Mix ID	Replicate ID	Energy (LLD) (J/m^2)	Average	Std Dev	COV	Peak Load (kN)	Average Peak Load	Std Dev	COV	FI	Average	Std Dev	COV
		B-2	1695.1				2.4				6.3			
	4I9-2	C-1	1627.4	1884.7	310.4	16.5	3.6	2.9	0.7	23.9	3.1	4.6	1.6	35.0
		C-2	1696.6				3.5				3.6			
		D-1	2317.4				2.4				6.6			
		D-2	1897.3				2.3				5.1			
	4I55-1	A-1	2575.4	2720.0	329.4	12.1	2.1	2.3	0.1	6.4	21.3	18.5	2.5	13.5
		A-2	2659.0				2.3				19.3			
		B-1	3196.7				2.5				18.1			
		B-2	2448.8				2.4				15.3			
	4I55-2	A-1	2686.2	2607.9	321.0	12.3	2.7	2.5	0.2	8.8	16.8	16.4	6.3	38.4
		A-2	2675.3				2.2				24.5			
		B-1	2155.7				2.4				9.4			
		B-2	2914.3				2.7				14.8			
	4I78-1	A-1	771.8	803.3	64.8	8.1	2.2	2.5	0.3	10.7	1.8	1.3	0.3	25.8
		A-2	869.7				2.9				1.3			
		C-1	728.4				2.4				0.9			
		C-2	843.3				2.4				1.3			
	4I78-2	A-1	658.0	813.5	144.6	17.8	2.2	2.2	0.1	6.6	1.2	1.8	0.7	35.7
		A-2	878.5				2.4				2.0			
		B-1	735.7				2.1				1.4			
		B-2	981.8				2.1				2.7			
District 5	1	1-1	2146.2	2267.3	173.0	7.6	2.5	3.1	0.6	19.1	6.6	5.8	1.6	27.7
		7-1	2201.8				3.4				4.4			
		8-2	2197.2				3.8				4.5			
		2-1	2524.0				2.8				7.6			
	2	1-1	2905.2	2958.6	73.8	2.5	2.9	2.8	0.1	3.9	21.2	23.3	3.6	15.4
		1-2	2927.7				2.8				21.2			
		2-2	3042.8				2.7				27.4			
	3	1-2	3489.0	3394.4	356.4	10.5	3.7	3.5	0.3	8.7	17.4	20.6	5.5	26.7
		2-1	3439.7				3.7				20.4			
		7-1	3748.9				3.4				28.4			
		8-2	2900.1				3.1				16.2			
	4	1-1	2110.5	1997.1	316.7	15.9	3.0	3.0	0.3	8.8	7.8	7.5	0.7	9.0
		7-2	2359.6				3.4				8.2			
		8-2	1906.3				3.0				7.1			

District	Mix ID	Replicate ID	Energy (LLD) (J/m^2)	Average	Std Dev	COV	Peak Load (kN)	Average Peak Load	Std Dev	COV	FI	Average	Std Dev	COV
		2-1	1612.0				2.7				6.7			
	5	1-1	2533.6	2096.0	346.6	16.5	2.8	3.2	0.3	9.6	12.1	7.1	3.5	49.0
		2-1	2191.8				3.5				5.7			
		7-1	1735.7				3.2				4.1			
		8-1	1923.0				3.2				6.6			
	6	2-1	1722.2	2090.0	315.8	15.1	1.9	2.0	0.1	4.9	6.2	7.7	1.6	20.8
		2-2	2474.6				2.0				9.6			
		3-1	2170.7				2.0				8.4			
		3-2	1992.3				2.1				6.6			
District 6	6G2	A-1	3325.9	3067.9	231.1	7.5	3.4	3.2	0.2	5.4	30.0	25.1	5.7	22.7
		C-2	2880.0				3.1				18.8			
		C-1	2997.8				3.1				26.5			
	6P	A-1	1860.7	2029.3	267.4	13.2	3.4	3.7	0.5	14.0	1.9	3.0	1.9	63.4
		A-2	2337.6				3.4				5.2			
		C-1	1889.7				4.3				1.9			
District 7	D7-1-I130	2-1	892.9	1050.8	142.0	13.5	2.8	2.9	0.3	10.3	1.8	1.6	0.4	28.1
		2-2	1195.5				3.4				1.1			
		6-1	972.2				2.7				1.4			
		6-2	1142.7				2.7				2.1			
	D7-2-I121	1-1	2376.2	2219.7	173.2	7.8	4.2	3.6	0.6	18.1	4.6	7.4	3.2	42.7
		1-2	2310.9				4.1				4.9			
		4-1	2211.2				3.2				10.8			
		4-2	1980.6				2.9				9.5			
District 8	8JVS2	B-2	3141.3	2987.2	157.1	5.3	3.7	3.9	0.2	4.7	18.6	14.7	3.4	23.2
		C-1	2992.9				4.0				13.1			
		C-2	2827.2				4.1				12.3			
	867S1	A-1	2430.7	2384.9	378.0	15.9	2.7	2.8	0.2	8.5	15.3	13.9	1.7	12.4
		A-2	2056.4				2.7				11.4			
		B-1	2899.6				3.1				14.3			
		B-2	2152.8				2.6				14.5			
District 9	9I4	5-1	2010.6	2007.9	3.8	0.2	2.0	2.0	0.0	0.0	11.7	11.7	0.0	0.2
		6-2	2005.2				2.0				11.7			
	9I54	1-1	2335.0	2062.0	236.5	11.5	2.8	2.8	0.5	18.5	9.2	7.5	1.9	24.7
		2-1	1931.9				2.3				7.9			
		2-2	1919.3				3.4				5.5			

Table G-4 ALF Mixtures

Lane	Replicate	Energy (LLD) (J/m^2)	Average	Std Dev	COV	SCB Strength (MPa)	Average	Std Dev	COV	Flexibility Index	Average	Std Dev	COV
1	1	2231.0	2394.4	97.8	4.1	0.40	0.44	0.05	10.76	11.0	9.9	1.8	18.0
	2	2456.5				0.39				12.3			
	3	2409.5				0.50				8.2			
	4	2480.6				0.49				8.2			
3	1	2259.8	1861.3	230.6	12.4	0.80	0.68	0.07	10.98	1.2	1.53	0.3	18.8
	2	1751.1				0.63				1.9			
	3	1706.1				0.70				1.4			
	4	1728.2				0.60				1.8			
4	1	2264.8	2284.3	159.7	7.0	0.54	0.55	0.04	7.93	7.0	6.7	1.2	17.7
	2	2288.6				0.62				4.9			
	3	2517.1				0.51				8.2			
	4	2066.6				0.53				6.6			
5	1	1980.9	1967.2	158.1	8.0	0.86	0.80	0.04	5.31	1.3	1.4	0.1	7.5
	2	1767.1				0.74				1.3			
	3	2153.7				0.81				1.5			
7	1	1309.7	1518.0	147.3	9.7	0.56	0.59	0.02	3.55	1.5	1.9	0.3	14.1
	2	1623.3				0.59				1.8			
	3	1621.1				0.61				1.8			
	4	1337.9				0.55				2.2			
	5	1235.2				0.45				2.1			
8	1	2128.4	2279.6	107.1	4.7	0.48	0.50	0.03	5.46	6.3	6.5	0.8	12.2
	2	2360.8				0.48				7.5			
	3	2349.7				0.54				5.6			

Lane	Replicate	Energy (LLD) (J/m^2)	Average	Std Dev	COV	SCB Strength (MPa)	Average	Std Dev	COV	Flexibility Index	Average	Std Dev	COV
9	1	2863.0	2434.9	277.3	11.4	0.62	0.58	0.06	11.28	8.0	7.3	0.5	6.24
	2	2327.2				0.61				7.3			
	3	2450.1				0.61				7.1			
	4	2099.4				0.46				6.7			
11	1	2618.8	2300.9	224.8	9.8	0.63	0.60	0.07	11.21	5.4	5.27	1.1	20.8
	2	2319.0				0.68				3.3			
	3	2137.6				0.56				5.1			
	4	2280.5				0.62				4.9			
	5	1939.1				0.47				6.7			
	6	2510.3				0.60				6.2			

APPENDIX H: DIC AND FINITE ELEMENT SIMULATION RESULTS

H.1 BACKGROUND FOR DIGITAL IMAGE CORRELATION TECHNIQUE

DIC is an imaging technique that enables measurement of displacements, strains, and stresses (the latter through appropriate constitutive equations) on the entire surface of a specimen, for the time instant corresponding to each picture taken (Sutton et al. 2009). DIC has the advantage of being a non-contact full-field measurement technique and has been used for fracture or material characterization in many situations. For example, DIC has been used to study the mechanical and fracture properties of composites (Leclerc et al. 2009), metals (Carroll et al. 2013), functionally graded materials (Abanto-Bueno and Lambros 2002), concrete (Wu et al. 2011; Skarżyński et al. 2013), and asphalt (Seo et al. 2002; Buttlar et al. 2014).

To obtain the displacement field on the surface of a specimen, a reference picture is taken (usually at the unloaded state) of a random speckle pattern on the surface, and the pixels in a zone of interest are selected. Then, subsets of pixels are compared to a deformed picture (taken at a loaded state) to find a best match and thus compute the deformation of the subset (i.e., the displacement and the displacement gradients corresponding to the center of the subset). The main assumptions of DIC are the following: the deformation of each subset is assumed to be a homogeneous in-plane deformation and the specimen surface speckle pattern light intensity remains the same throughout deformation, which implies both light uniformity and no speckle deterioration. The light uniformity must be both spatial and temporal so that each point on the specimen maintains the same recorded grayscale value throughout the experiment, thus allowing correlation with the reference picture. With these assumptions, the equations governing the deformation at a point are the following (Chu et al. 1985; Bruck et al. 1989):

$$x' = x + u + \frac{\partial u}{\partial x}\Delta x + \frac{\partial u}{\partial y}\Delta y, \tag{H.1}$$

$$y' = y + v + \frac{\partial v}{\partial x}\Delta x + \frac{\partial v}{\partial y}\Delta y, \tag{H.2}$$

where *x* and *y* are Cartesian position coordinates, *u* and *v* are the corresponding displacements, and $'$ denotes the variables in the deformed frame.

Previous studies on asphalt concrete using DIC recommended cleaning the surface with sandpaper and an airbrush to smooth it, applying several light layers of white paint, and then spraying with black paint to obtain the speckle pattern. Although we did at first follow the procedure of Seo (2002) (referred to henceforth as the white pattern), problems resulted because the surface of asphalt was not perfectly flat; consequently, there were some irregularities and surface voids on the surface that could not be painted or that created shadows in the pictures, increasing the error in the measurements compared to experiments on flat surfaces. Because the surface voids created black zones in the otherwise white background, as an alternative we applied a black layer of paint and then created the speckle pattern by spraying white paint on top of it (i.e., in essence reversing the colors in the procedure of Seo (2002) (referred to henceforth as the black pattern).

Figure H.1 shows photos of a sample pattern using each method, along with the intensity histograms for each. The histograms showed a reasonable intensity spectrum for all three patterns, which was unimodal in nature and thus appropriate for DIC (Sutton et al. 2009). The noise level for the patternsobtained by correlating successive images of a the same undeformed surface was similar: displacements measured around ± 0.01 mm with a standard deviation around 0.006 mm, and they appear random, as seen in the arrow plots also shown in Figure H.1.

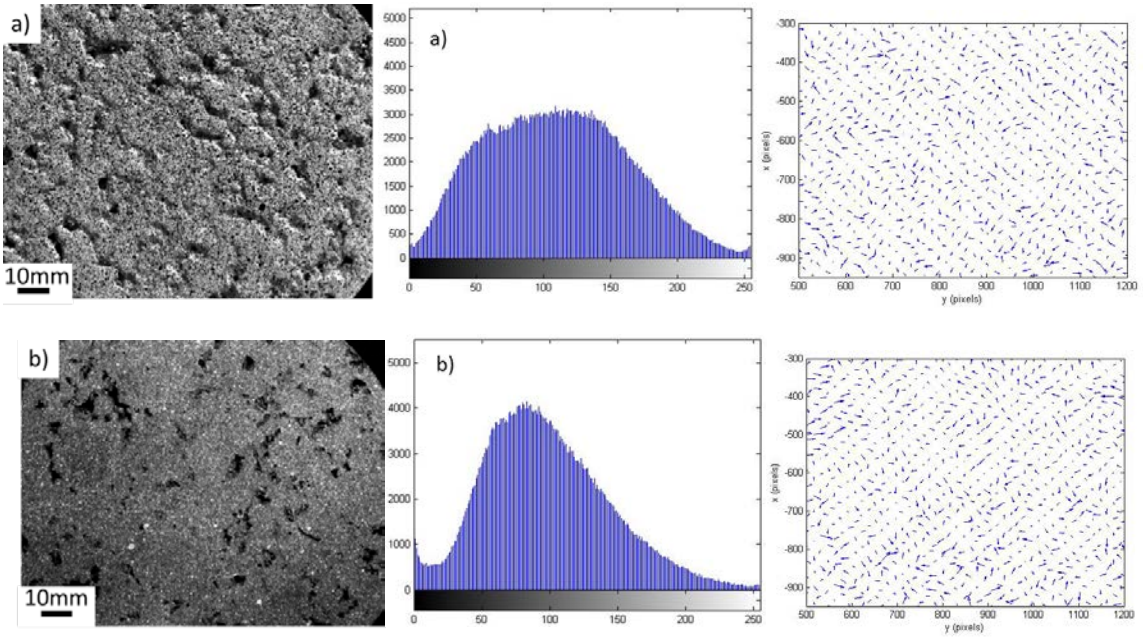

Figure H.1 Speckle pattern (left), grayscale intensity histogram (middle), and arrows plots denoting noise from correlation of two images without deformation for (a) white pattern and (b) black pattern. Note more shadows in the speckle pattern of the white pattern.

Typical SCB fracture test images with corresponding load-displacement curve are shown in Figure H.2 (on the following page) for a plant mix.

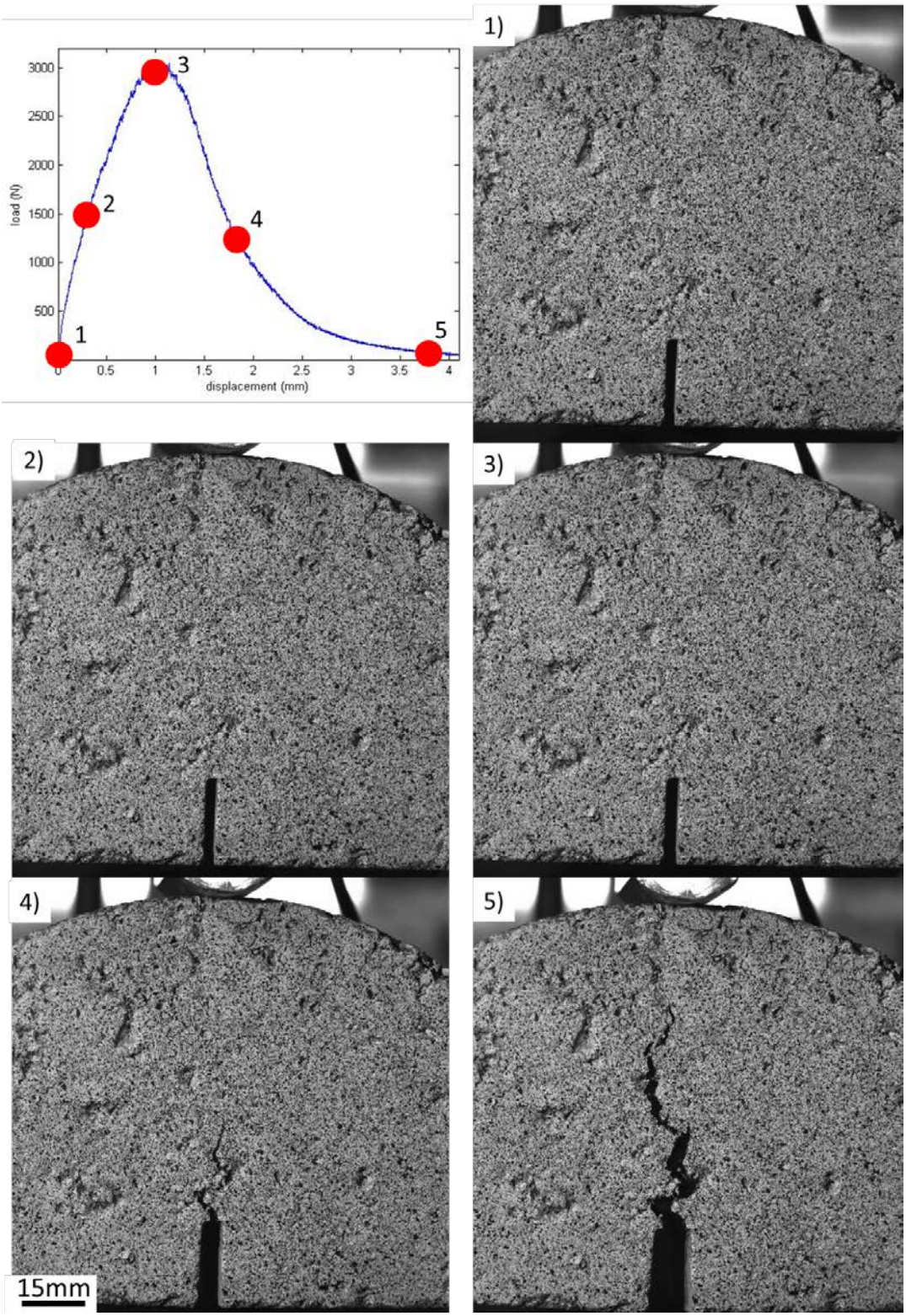

Figure H.2 Typical SCB fracture test images with corresponding load-displacement curve (Mix P6 at 6.25 mm/min and 25°C).

H.2 INVESTIGATION OF POSSIBLE LOAD POINT DAMAGE

This part of the investigation was conducted on the seven IDOT plant mixes at 6.25 and 50 mm/min. The progressive evolution of the compressive horizontal strain ε_{yy} measured in the zone directly under the loading head is shown in Figure H.3. The load-displacement curve for the experiment is shown with the load level corresponding to the five strain plots indicated as a red dot. The strain contours plotted are the negative (i.e., compressive) ones, and all the positive strains are plotted in the same dark red color.

The results did not show a strain field that could be interpreted as a crushing of the material. The area of the compressive zone was seen to develop as the load increased, reach a maximum after peak load and then shrink (though still remaining larger than at peak load) as the crack propagated. (The crack location as a function of time in each image is shown by the blue dots in Figure H.3.) However, the magnitude of the strains kept increasing (in absolute value) throughout the experiment.

We did not observe any noticeable impact of the mixture or the loading rate (6.25 vs. 50 mm/min) on this effect. The development of the compressive region at the load point primarily appears to be a specimen geometry effect: as the specimen bends, the lower part experienced tension, while the top was compressed. When the crack propagated, the neutral axis for the bending strains moved farther toward the top of the specimen, and the compressive zone became smaller in extent—although it increased in magnitude. It can be concluded that energy dissipated by possible crushing or plastic deformations at the load point is negligible due to a small region affected and magnitude of strains.

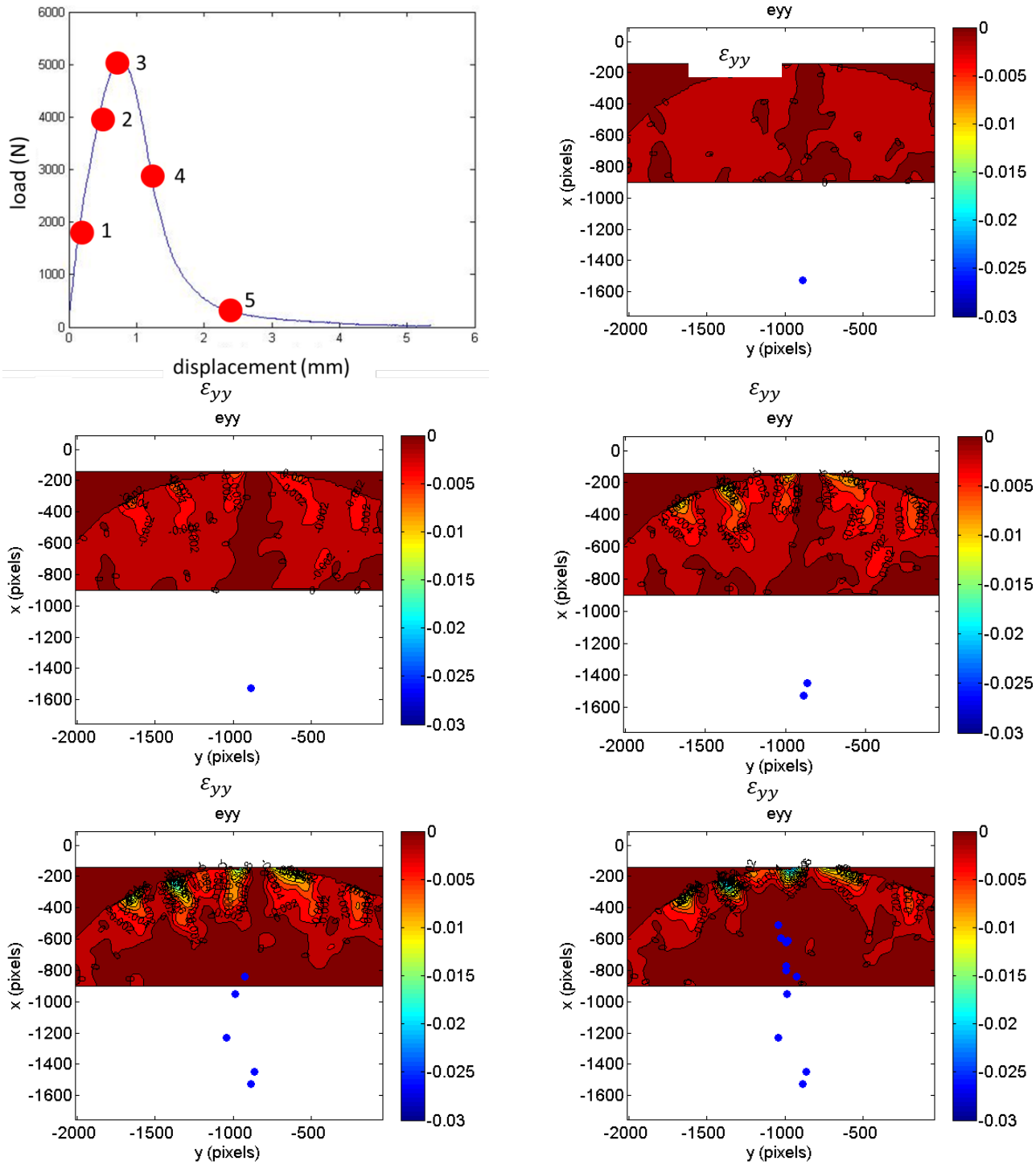

Figure H.3 Mix P6, 25°C, 50 mm/min: Evolution of compressive zone during a test. The scale shows only the compressive horizontal strains (tensile strains are in dark red). Blue dots = successive locations of the notch or crack tip.

H.3 BULK VISCOUS DISSIPATION

Asphalt concrete is considered a viscoelastic material, meaning that it exhibits some elastic characteristics, such as an instantaneous deformation behavior, and some viscous characteristics, such as a flow or time dependent behavior. In the elastic case, one state of stresses corresponds to a unique state of strains (and vice versa). In the viscoelastic case, there is a time dependency that leads to creep, relaxation, and recovery, among other phenomena, which are manifested as a hysteresis loop in the stress–strain response of a viscoelastic material. This implies two important points on this type of material: first there is some energy dissipation in the material when it is loaded (the area contained inside a loop path in stress–strain space) that must be differentiated from the energy dissipated by the fracture itself (i.e., the material toughness), and second, the modulus cannot be considered a constant, which complicates the computation of a stress field from the DIC-measured strain field.

As has been well developed in viscoelasticity theory, the integral representation for the constitutive response of viscoelastic media is based on the Boltzmann superposition principle (Chen and Tsai 1998), which states that a generalized viscoelastic stress–strain relationship for arbitrary stress–strain history can be obtained by linearly adding the responses to standard excitations. This principle gives the following convolution equations (summation implied when indices are repeated) (Wineman and Rajagopal 2000; Ozer 2011):

$$E(t) = E_e + \sum_{n=1}^{N} E_n \, e^{-t/\rho_n}, \tag{H.5}$$

where σ_{ij} and ε_{ij} are the stress and strain tensor components, E_{ijkl} and D_{ijkl} are the time- and temperature-dependent stiffness and compliance moduli, and ξ is a reduced time defined for thermo-rheologically simple materials as $\xi = \frac{t}{a_T}$, where a_T is a shift factor as defined by the William–Landel–Ferry (WLF) equation (Williams et al. 1955). To use these equations, it is still necessary to explicitly know the temperature- and time-dependent modulus function E (or compliance D). At the same time, asphalt concrete is often considered a thermo-rheologically simple material (Bai 2008; Christensen and Bonaquist 2012), obeying the time–temperature superposition rule (i.e., a long time response is similar to a high-temperature response). A master curve representing the modulus function over a wide range of temperatures and time can be obtained experimentally. The generalized Maxwell model (also known as Prony series) can be used to fit the master curve data obtained experimentally (AASHTO TP 62-03; Park and Kim 2001) at a variety of temperatures. Once the coefficients are determined, the modulus is an equation of the form:

$$E(t) = E_e + \sum_{n=1}^{N} E_n \, e^{-t/\rho_n}, \tag{H.5}$$

where E_e is the equilibrium modulus, the E_n are the Prony coefficients, and the ρ_n are the relaxation times. With these equations, it is then possible to obtain the stresses from strains and vice versa, depending on the loading history and temperature, for viscoelastic materials.

In a fracture test, as the crack is propagating, the material is unloading behind it and strains decrease in the far field (defined as the region outside any process zone). For an elastic material, the strains should return to their original unloaded state, except if some permanent deformation occurred, such as in the process zone or a zone of (small-scale) yielding. In viscoelastic materials, the far-field strains should recover also, but a complete recovery does not always happen or may take a significant amount of time rather than happening instantaneously. This may be another source of energy dissipation in the viscoelastic materials that is not related to fracture process itself.

Using the full-field DIC results, we looked at the far field of the crack to study the energy dissipated in the bulk material, which was computed as the area inside the stress–strain path experienced in a given region throughout the entire experiment (i.e., starting from the loading path as the crack approached the regions of interest and ending with the unloading and subsequent long-term relaxation). The regions selected for such far-field dissipation measurements are shown in Figure H.4a. This choice was made so that they represent areas larger than the aggregate size (to avoid local effects) but are sufficiently far away from the crack to be (primarily) outside the fracture process zone.

To obtain the total energy dissipated, both 3D stress and 3D strain data would be necessary, but the DIC technique allows measurement of only in-plane displacement and strain components on the surface. Assuming plane stress conditions on the surface, stresses were then computed from the DIC measurements using the viscoelastic constitutive equation (H.3). Note that this computation must be performed with the appropriate material Prony series properties for each specific mix. Therefore extensive constitutive testing had to be done to obtain relaxation moduli for each mix for which this viscoelastic computation is to be employed, and the appropriate properties must be used on a case-by-case basis.

Typical stress–strain paths obtained in this way for one mix, averaged over both regions of interest in Figure H.4a, from the three in-plane components (*xx*, *yy*, and *xy*) are shown in Figure H.4b. The figure shows that the area enclosed in the opening component (*yy*) is the dominant one, so this component is the one used for the remaining results shown in this section. This figure also demonstrates non-linearity of the response due to viscoelasticity of the material. Far-field regions experience loading as the crack approaches and unloading as the crack propagates. During the loading and unloading cycles, some of the energy may be dissipated, depending on the viscoelasticity of the material.

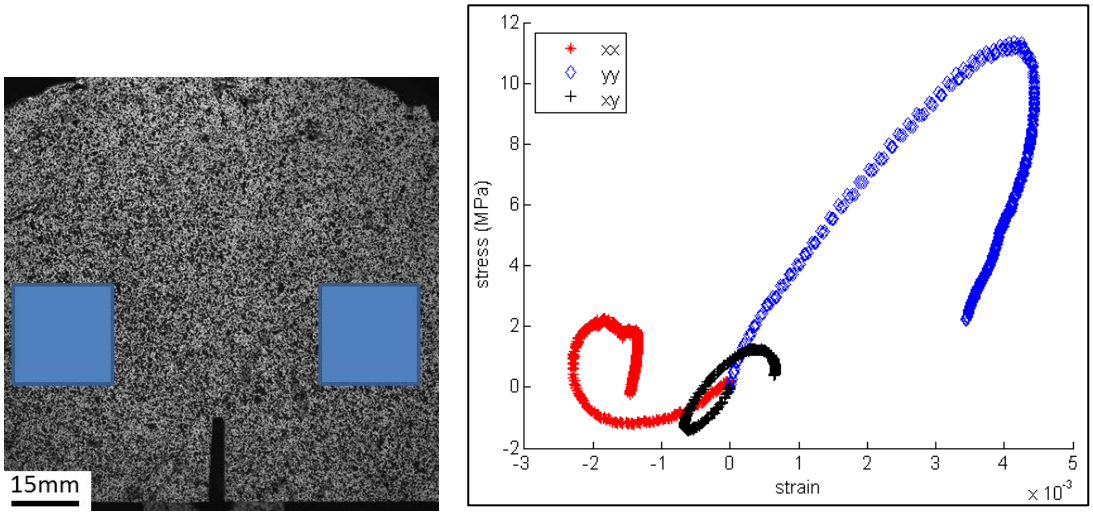

(a) (b)

Figure H.4 (a) Areas over which far-field viscoelastic energy dissipation was computed. (b) Stress-strain path experienced in the areas shown in (a) shown individually for each in-plane component as labeled. Note that the total energy dissipated would be the summed area within each loop with the *xy* area multiplied by 2.

To evaluate how much energy is dissipated in the far-field regions, several experiments were conducted at different rates with varying material viscoelastic characteristics. The average opening stress–strain paths in these regions were computed for Mixes L4 (0% RAS), L7 (5% RAS), and L6 (7% RAS) (L7 and L6 have the same binder). For reference with the subsequent results, Figure H.5 shows

the force-displacement results for each experiment at 6.25 and 50 mm/min, illustrating good repeatability and good separation between cases. Figure H.6a shows the effect of loading rate by comparing of the “loops” generated in the same mix (lab mix L4) at 25°C for 6.25 mm/min and 50 mm/min. The rate dependency is clearly highlighted here: at a higher rate, the strains decrease but the stresses increase. The opposite evolution of the variables compensated for the energy dissipated, and there was no obvious modification of the area under the curve.

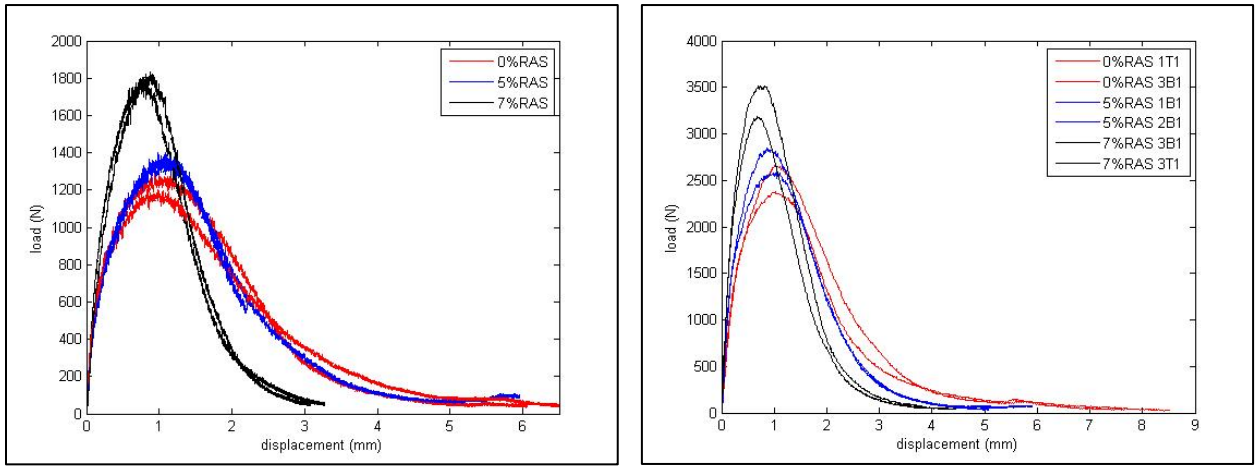

Figure H.5 Load-displacement curves for laboratory mixes at 6.25 mm/min and 50 mm/min.

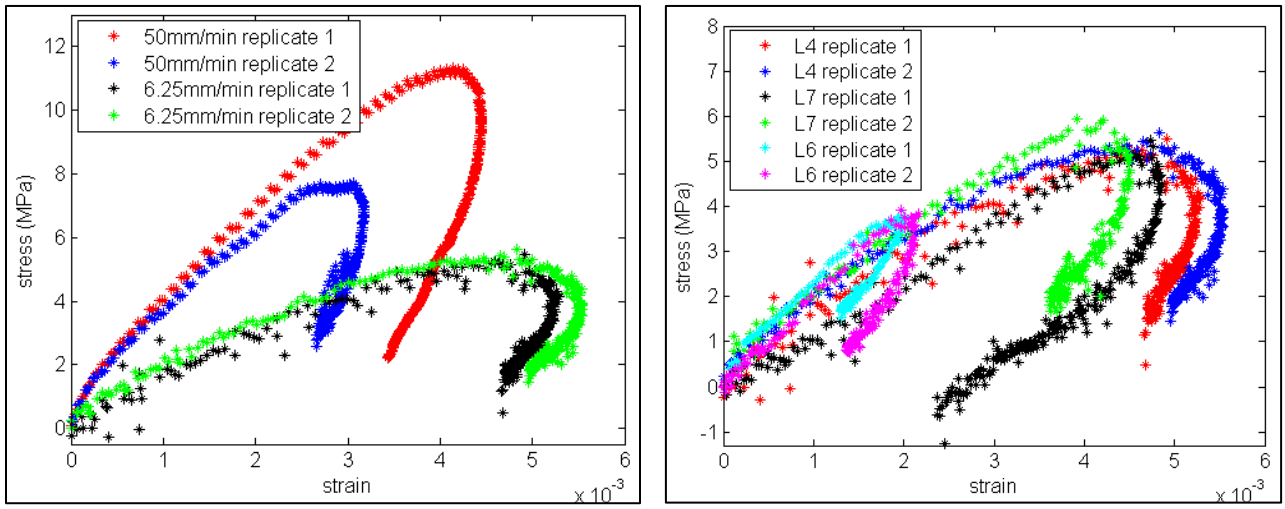

(a) (b)

Figure H.6 (a) Stress vs. strain, mix L4, 25°C, rate comparison for both replicates: red and blue = 50 mm/min, black and green = 6.25 mm/min. (b) Stress vs. strain, 25°C, 6.25 mm/min both replicates, effect of RAS: blue and red = L4 (0% RAS), black and green = L7 (5% RAS), cyan and magenta = L6 (7% RAS).

To provide a better understanding of the energy dissipated in the bulk of the material, the strain energy density W was computed as:

$$W = \int_0^{\varepsilon} \sigma_{ij} d\varepsilon_{ij}. \qquad \text{(H.6)}$$

This energy is computed from all three components measured at the surface of the specimen; the results are shown in Table H.1 for the three mixes. The comparison for different loading rates shows a small increase of the energy dissipated as the loading rate increases, which is not obvious in Figure H.6a. This finding shows that the increase of the stresses with loading rate was more significant than the change in strains and was the reason for equivalent amount or more energy dissipation with increasing loading rate.

Table H.1 Strain Energy Density *W* for Mixes L4, L7, and L6 at 6.25 and 50 mm/min

***W* (J/m³)**	**6.25 mm/min**		**50 mm/min**	
Replicate	**1**	**2**	**1**	**2**
L4 (0%RAS)	3.69E+04	3.42E+04	2.80E+04	4.70E+04
L7 (5%RAS)	2.04E+04	2.01E+04	2.65E+04	2.24E+04
L6 (7%RAS)	5.25E+03	5.9E+03	9.33E+03	7.79E+03

The same methodology was also used to compare the energy dissipation with increasing RAS content. Figure H.6b shows the stress–strain paths for the three mixes, two replicates each, at 6.25 mm/min. The curves corresponding to the same mix have a similar behavior; however, the comparison between mixes shows a decrease of the area under the curve for increasing RAS content (see also same trend in dissipated energy in Table H.1).

This difference is particularly noticeable for Mix L6, while the difference between Mixes L4 and Mix L7 is smaller. This is due to the modification of the binder: a more compliant one was used for Mixes L6 and L7 to compensate for the a priori expected embrittlement that would be introduced by RAS. It is still interesting to notice that the effects of increasing RAS content are counterbalanced by the composition of the binder when comparing Mixes L4 and L7. However, the decrease of energy dissipation with increasing RAS still shows a loss of viscosity of the material.

Figure H.6b shows another interesting phenomenon: the difference between mixes is mostly due to differences in the strain levels. Binder grade and presence of RAS played a great role on the stress and strain response. As RAS is added to the mix (L6 and L7), strains are reduced—indicating the development of greater stiffness or less viscous strains in the specimen.

H. 4 FRACTURE PROCESS ZONE ASSESSMENT

As discussed, the crack propagated primarily between the aggregates at room temperature and through aggregates at low temperature for the plant mixes. To understand more about the influence of the aggregate structure on the fracture mechanisms, however, we studied the development and evolution of the fracture process zone (FPZ) itself. The FPZ can be thought of as the zone near and around the crack tip where the material is experiencing damage even though it may not be fully cracked (i.e., it has not separated into new traction-free surfaces). This damage can appear in different forms such as microcracks or void formation, significant plastic flow, or large-scale shearing (shear bands).

The DIC technique has been used in the past to study the FPZ of many materials such as graphite (e.g., Mostafavi and Marrow 2012), concrete (e.g., Wu et al. 2011; Skarżyński et al. 2011, 2013), polymers (e.g., Abanto-Bueno and Lambros 2005; Lambros and Patel 2011), and metals (e.g., Carroll et al. 2013), but few such studies have been done for asphalt mixes (e.g., Romeo 2013).

To study damage at the crack tip, we used microscale experiments in which a higher resolution CCD camera is used to capture DIC images at a spatial resolution of 8 microns/pixel (as opposed to about 40 microns/pixel earlier), making it possible to capture with DIC the finer details around the crack tip, such as the differences in strain distribution within the aggregate and within the binder. The microscale experiments were run at 25°C (6.25 and 50 mm/min) and –12°C (0.7 and 0.1 mm/min) on Mixes L4 (0% RAS), L6 (7% RAS), L9 (7% RAS, same binder as L4), and P8 (which has larger aggregates). In this manner, we could investigate at the microscale level the effects of rate (6.25 vs. 50 mm/min), temperature (25°C vs. –12°C), recycled content (0% RAS vs. 7% RAS), and aggregate size.

To correlate specific regions of the microstructure with the measured FPZ strain field development, we must be able to precisely align the DIC results with microstructural features. To this end, a picture of the specimen without paint and the result of the DIC-measured strain field were superimposed as precisely as possible. By changing the transparency of the top picture, it was possible to have the strain field and aggregate structure on the same picture at the microscale.

The accuracy of aligning the optical microstructure image with the DIC results is still crucial to obtain reliable results in this comparison. Therefore, the first requirement was that the strain field be plotted on the reference frame and not on the deformed one. If the strain field was plotted on the deformed configuration, then it would be impossible to compare it with the aggregates picture because the latter had been taken for an undeformed specimen. The second requirement was positioning of the two pictures by using surface features visible in both datasets (DIC image and original microstructure image). Initial alignment was done by positioning the notch at the same location in both images. However, that alone was not sufficient to provide the accuracy needed for the desired comparison. Therefore, other markers were used in addition to the notch. There were always holes or voids on the surface of all specimens that were visible in both pictures (aggregate micrograph and DIC experimental pictures). The two pictures were aligned to have these features match up, thus ensuring the accurate alignment of both pictures. The alignment error was estimated by scaling and aligning the pictures several times independently, and it showed a maximum error of around 1% for the scale and positioning

Figure H.7 compares the DIC-measured strain field at peak load for Mixes L4 (0% RAS), L6 (7% RAS), and L9 (7% RAS, same binder as L4) under the combinations of loading rate and temperature used. These experimental results confirm that in the binder, strain is elevated but the aggregate strain is low, in fact almost zero, for virtually all rates and temperatures used here. This difference between strains in the aggregate and in the binder was also shown by Masad et al. (2001) using DIC and finite elements. This discrepancy in local response can be explained by the difference in mechanical properties of the individual elements: the aggregates are stiff while the binder is softer and more compliant, both at low and intermediate temperature; consequently, the binder strains the most. This local response difference highlights the impact of the aggregates on the strain field and is consistent with the macroscale results which showed that the crack mainly propagates in the binder. By looking at Figure H.7, it is clear that the material behavior is highly heterogeneous at this length scale and that the assumptions of homogeneity necessary for the theories for using continuum concepts such as stress intensity factor KI and J-integral do not apply at this scale.

Figure H.7 also offers a comparison of the extent of straining for different temperatures, rates, and RAS content—essentially a visualization of the extent of the process zone if defined as a certain level of straining. It should be noted that the experiments done at the same temperature have the same contour color bar scale, but the contour scale for –12°C is ten times smaller than for 25°C. Temperature had a very noticeable effect on strains: at low temperature, the strain level was about ten times smaller and the strains were much more localized at the notch tip. This is consistent with the embrittlement of asphalt at low temperature that is also seen in the load-displacement curves, which tend to have higher peak load but much less displacement at lower temperatures. The comparison between the two mixes also shows an embrittlement with an increase in RAS content. The strain level is smaller and the strains more localized for 7% RAS. This embrittlement is also shown with the plot for Mix L9 at 50 mm/min, where the crack had already propagated about 15 mm at peak load, while the crack was not visible or had propagated only a few millimeters in the other mixes.

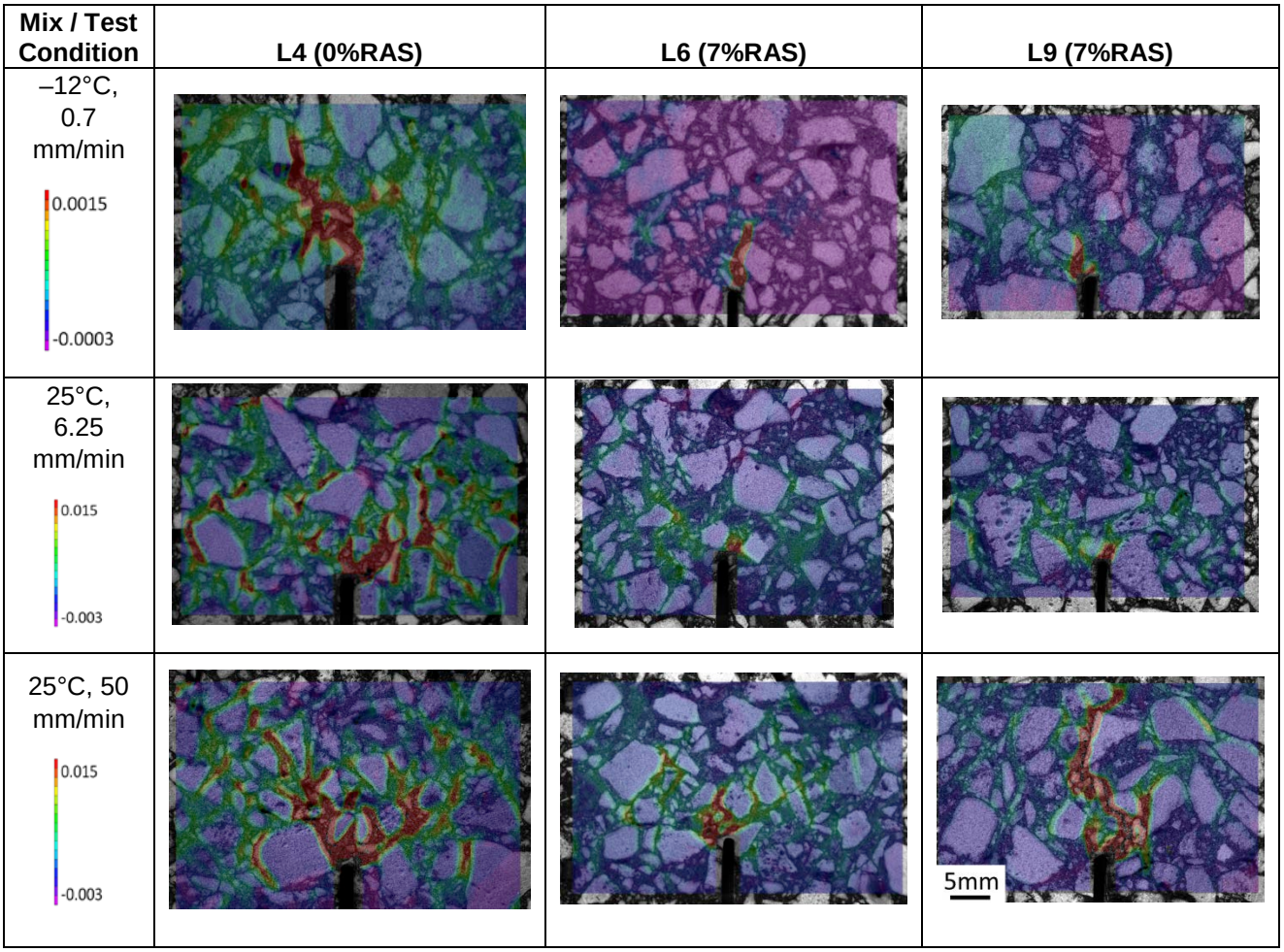

Figure H.7 Strain field superimposed on the aggregate structure for mixes L4 and L6 at –12°C (0.7 mm/min), 25°C (6.25 and 50 mm/min). The contour color scale is shown in the first column (note order of magnitude difference in low-temperature results), and the length scale is common to all pictures.

The strain contours in Figure H.7 for the different mixes L4, L6 and L9 is at peak load (and before crack initiation from the notch in all cases except for L9 at 50 mm/min), but in each case this corresponds to a

different peak load value because their load-displacement curves were different, as is shown in the collection of curves for different RAS contents in Figure H.8a. Therefore, it may also be instructive to compare the respective strain fields that formed at the same load. However, the comparison of the strain fields for the same load is made more complicated because of the slow acquisition rate of the camera used for the high magnifications studied (about four frames per second). Because the experiment, especially at lower temperatures and/or higher loading rates, is over in a few seconds, it was sometimes not possible to find pictures corresponding to exactly the same load between different experiments. However, it was possible to do so for the experiments at 6.25 mm/min because the loading rate was slower.

Figure H.8 shows the comparison of the strain field for Mixes L4, L6 and L9 at 1100 N—the level indicated by the three red dots in the load vs. displacement curves for the three experiments. The results at the same load emphasize the effect seen in Figure H.8 much more: the strain field developed was only significant for Mix L4 and was close to zero in the entire field of view for the two other mixes. For Mix L4, 1100 N is close to peak load, while it is smaller than half peak load for the two other mixes. This shows an embrittlement of the material with increasing RAS content: for the same load, the strains are much smaller in the mixes with a high RAS content, no matter which binder was used.

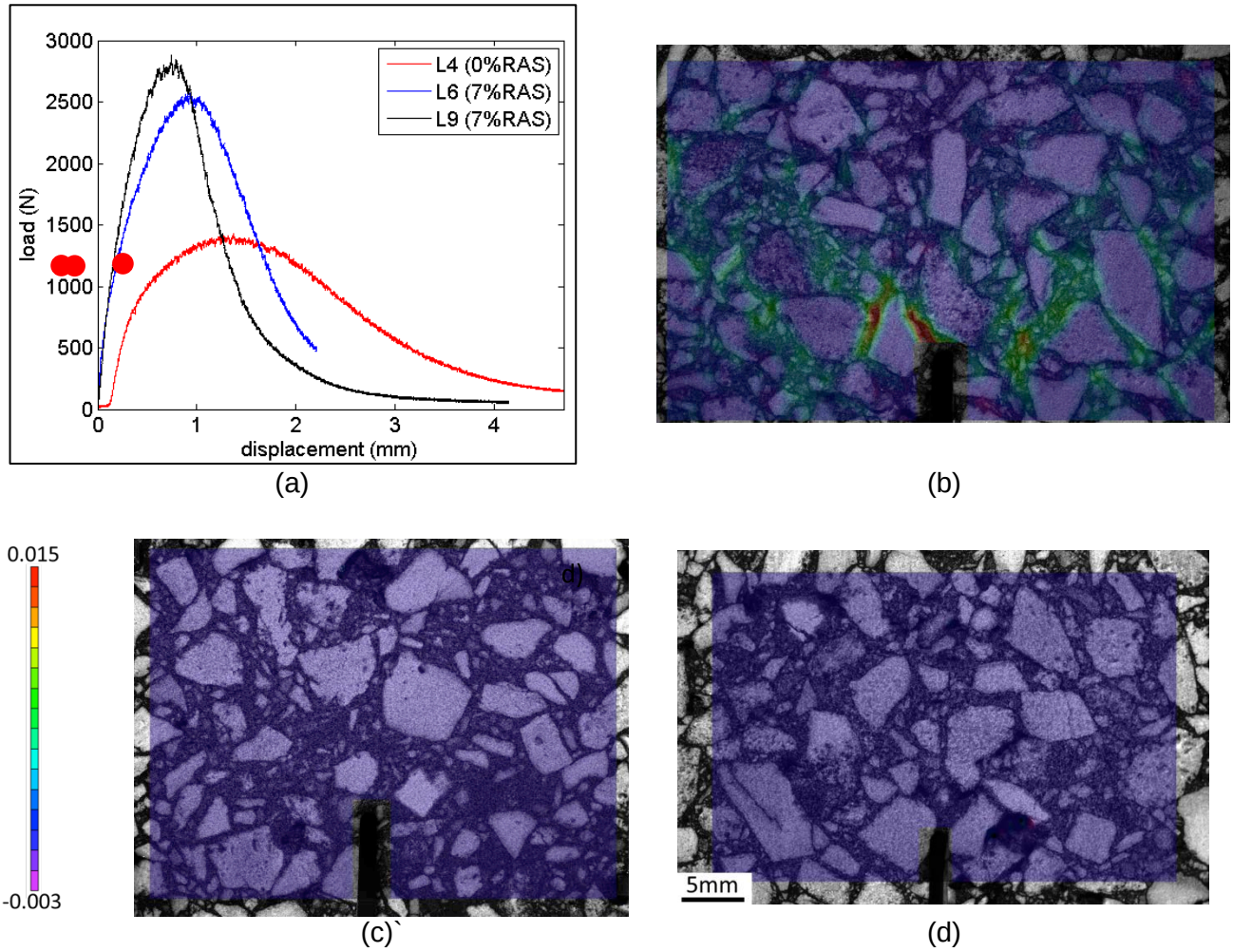

Figure H.8 Strain field superimposed on the aggregate structure for Mixes L4, L6, and L9 at 6.25 mm/min at the same load (1100 N). (a) Load vs. displacement curve for the three mixes; the red dot corresponds to the load for each picture; (b) Mix L4; (c) Mix L6; (d) Mix L9.

The pictures showing the strain field superimposed on the microstructure also enabled studying the crack path dependence on aggregate size. Mix P8 had larger aggregates than the other mixes, and some interesting phenomena were observed. As discussed, the crack propagated primarily around aggregates; however, in some cases, the crack cut through aggregates. In this mix, we observed that some of the largest aggregates were pre-cracked, a feature not present with the medium and small aggregates. When the large, pre-cracked aggregates were located near the crack path, the crack would advance by cutting through the larger pre-cracked aggregates, as shown in Figure H.9. This was the only case in which significant straining within an aggregate was observed across all mixes, and even then, straining was highly localized around the aggregate crack.

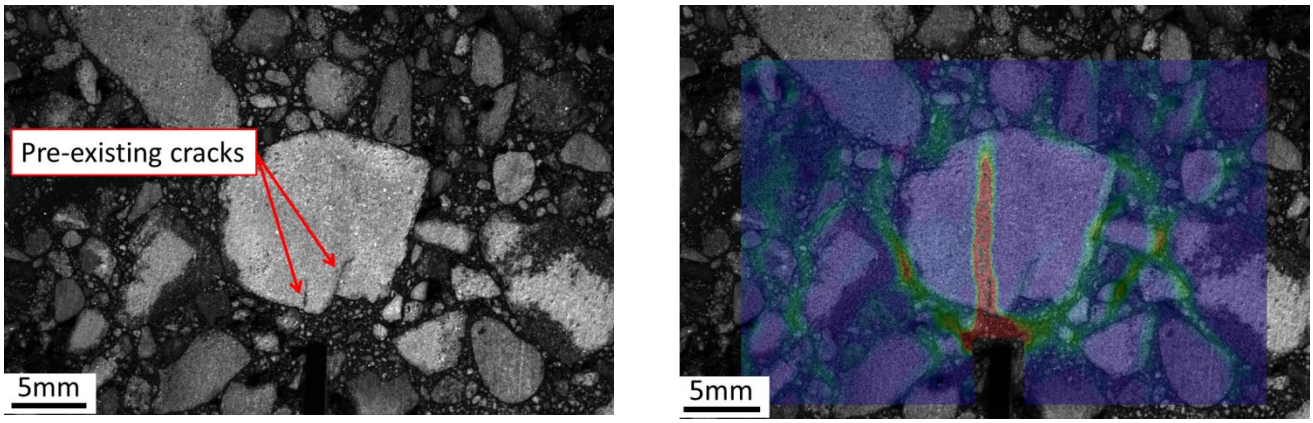

(a) (b)

**Figure H.9 Crack cutting through a pre-cracked aggregate for Mix P8 and 50 mm/min.
(a) Microstructure with location of pre-existing cracks;
(b) Strain field at peak load superimposed on the aggregate structure.**

To compare the mixes, rates, and temperatures, we tried to quantify the FPZ size. The method for doing so was based on the work of Wu et al. (2011) on concrete, where the FPZ was determined to be the zone where the strains exceed a threshold—the tensile strain capacity. which is the maximum strain that the material can reach without creation of a crack. When adopting this definition of the FPZ, we did not have values for the tensile strain capacity for each of our mixes and decided to use the threshold as a way to compare mixes rather than obtaining an absolute measurement of the FPZ extent in each mix. The threshold differed for 25°C (fixed at 3000 με) and –12°C (fixed at 1500 με). The value for 25°C was defined to be on the order of magnitude of the creep intercept values for asphalt at 60°C presented in Zelelew and Papagiannakis (2012) (between 2500 με and 10,000 με) and to highlight the zones of strain concentration shown in Figure H.7. The threshold at –12°C had to be lower because there is less strain at a lower temperature (see Figure H.7) and was therefore chosen as half the threshold at 25°C.

Figure H.10 shows the FPZ computed when thresholding the DIC-measured strain fields using the selected strain levels. The red area is the zone where the measured tensile strains exceed the threshold, the green area is where strains are below the threshold, and the blue area is the notch. The areas identified as part of the FPZ are consistent with the stain fields shown in Figure H.7, where strain was seen to concentrate in the binder. A comparison between Mixes L4, L6, and L9 clearly shows a decrease in the FPZ size as the RAS content increases, as it embrittles the material.

Mix / Test	L4 (0% RAS)	L6 (7% RAS)	L9 (7% RAS)
–12°C, 0.7 mm/min	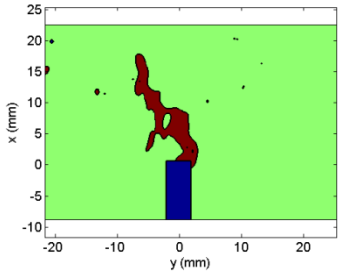	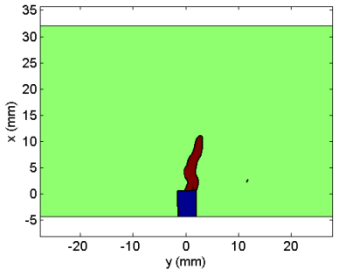	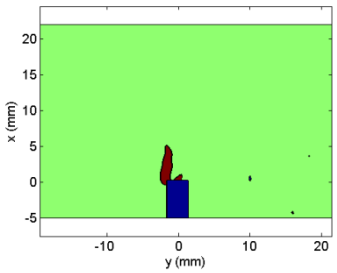
25°C, 6.25 mm/min	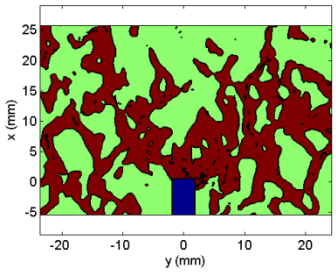	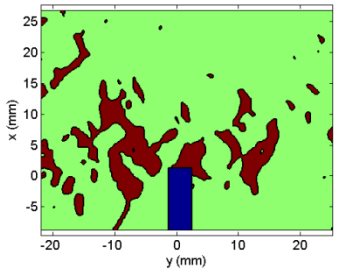	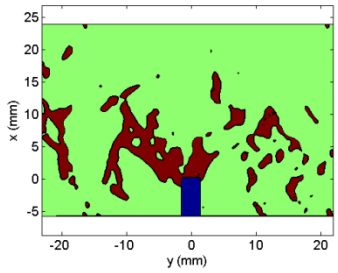
25°C, 50 mm/min	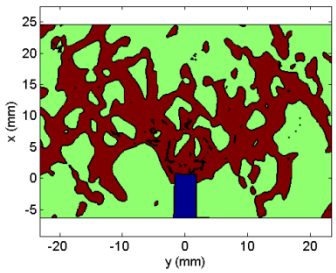	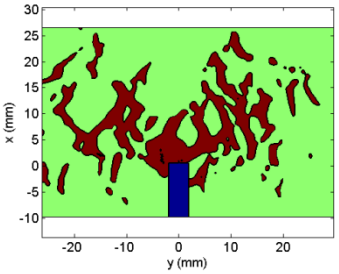	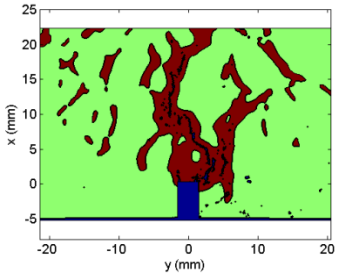

Figure H.10 FPZ quantification using a strain threshold. Peak load pictures for Mixes L4 and L6 at –12°C (0.7 mm/min) and 25°C (6.25 and 50 mm/min).

Table H.2 shows a summary of the area of the FPZ at peak load for all the mixes tested for 25°C, computed as the area where the strains exceed the threshold value (red areas in Figure H.10) and shown as an absolute area and as a percentage of the total area of the SCB specimen. For the lower temperature of –12°C, these measurements are about 10 to 15 times smaller. Although the average values show that at an increasing rate the FPZ area decreased for Mix L4, increased for Mix L6, and was unchanged for Mix L9, with only two replicates per case it is difficult to make a clear distinction between the rates. The rates, however, are somewhat close to each other, so a further study of rates—perhaps spanning orders of magnitudes of difference—would be needed. In contrast, the effect of RAS is clear, with a decrease of the FPZ area for an increasing RAS content.

Table H.2 FPZ Area Computation at Peak Load for Mixes L4 and L6 at 25°C (6.25 and 50 mm/min) Based on Strain Thresholding Shown in Figure H.10. (A + symbol means the FPZ was Wider than the field of view and therefore the area computed is likely an underestimate)

Mix	L4 (0% RAS)	L6 (7% RAS)	L9 (7% RAS)	L4 (0% RAS)	L6 (7% RAS)	L9 (7% RAS)
Rate	**6.25 mm/min**			**50 mm/min**		
Average Area of FPZ (mm²)	541 ± 120 (+)	150 ± 75	126 ± 48	439 ± 135 (+)	360 ± 36	133 ± 65
Area FPZ / Area SCB (%)	6.05 ± 2.5 (+)	1.9 ± 0.9	1.8 ± 0.8	5 ± 1.5 (+)	4.1 ± 0.4	1.5 ± 0.8

H.5 NUMERICAL SIMULATIONS INVESTIGATING BULK DISSIPATION

The fracture properties of any material are sensitive to the rate of loading and crack growth. In particular, AC materials exhibit creep behavior, which further increases the loading rate sensitivity of the fracture properties. This may not be the case at relatively low temperatures and high dynamic loading rates, where the AC response is quasi-elastic. But at slower loading rates and high temperatures, the contribution of creep becomes important, and the fracture response of the material cannot be characterized without taking into account creep effects.

At prolonged loading and high temperatures, creep begins to shape the response of AC. In particular, the fracture properties are dependent on the creep effects via two factors: (1) drop in fracture resistance, and (2) relaxation of the stress concentration at the crack tip with increasing creep.

The purpose of this study was to characterize the bulk creep response of bituminous composites in the vicinity of the crack tip and in the far field outside the fracture zone. This was achieved through an experimental testing approach coupled with a computational finite element framework where cohesive zone fracture models were integrated with viscoelastic constitutive bulk properties. The objectives were as follows: (1) develop dynamic fracture computational model of mode I SCB fracture at relatively intermediate temperatures and over a range of loading rates, (2) compare computational model results with experimental fracture tests, (3) characterize the creep response in the vicinity of the crack tip and in the far field outside the fracture zone, (4) characterize the contribution of bulk dissipation in the pre- and post-peak stages.

A numerical model of the SCB specimen was developed in the FE code Abaqus to examine mode I fracture. The FE mesh is shown in Figure H.11. A fine mesh was used in the plastic zone area where crack propagation occurs. The loading arm was modeled as an analytical rigid surface, with friction algorithm between the arm and the specimen. The dimensions of the loading head are shown in Figure H.11. Cohesive elements as small as 1 mm in size were inserted along the symmetry axis, as shown in Figure H.11. A small load was initially applied before the main step in order to make sure the specimen was in full contact with the rolling supports and the loading arm. Load-displacement curves obtained from numerical simulations were calibrated to match experimental results, as shown in Figure H.12 for a plant mix. The calibrated material properties were used in the study to evaluate the contribution of bulk dissipation to total fracture energy.

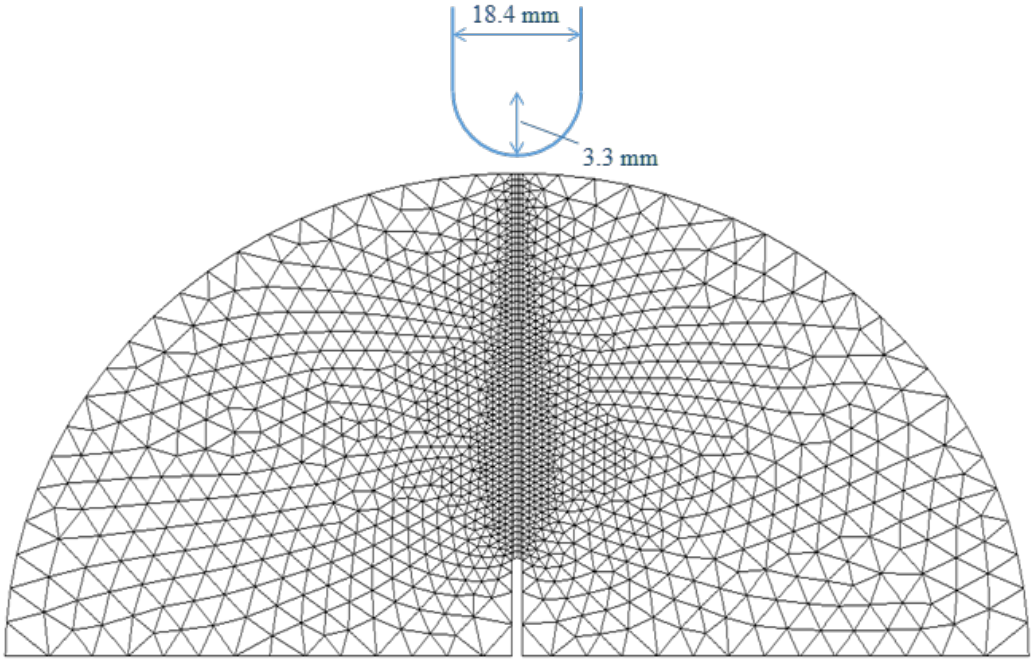

Figure H.11 Finite element model.

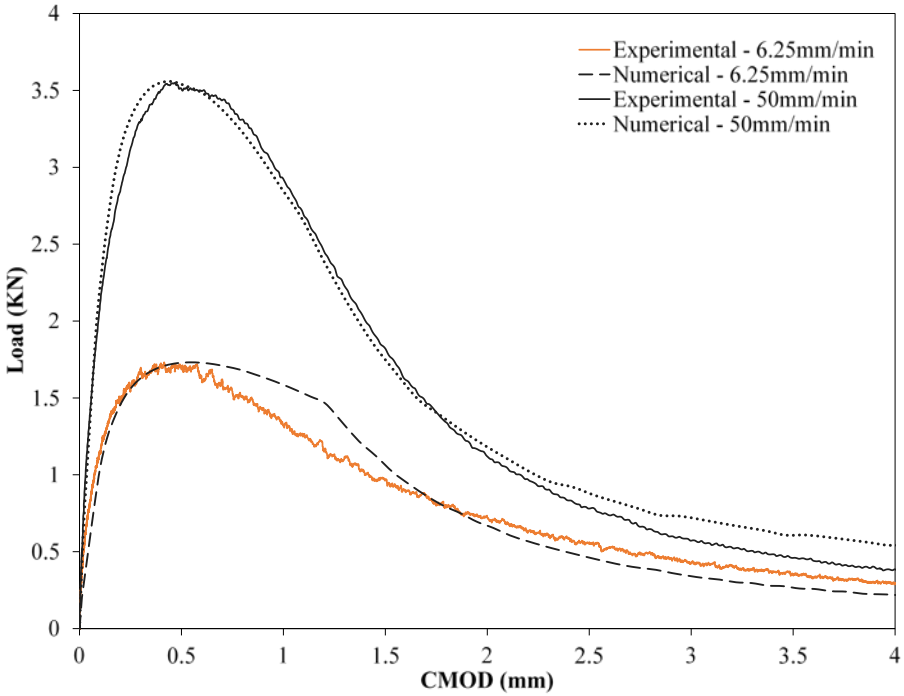

Figure H.12 Comparison of finite element simulation and experimental results of a plant mix (P12) for tests conducted at 25°C and at two different rates.

Figure H.13 shows a histogram plot of the energy dissipation terms of bulk, damage, and external work at different loading rates for the rate-dependent fracture scenario. The external work represents the area under the load-displacement curve, which directly reflects the measured fracture energy. The damage terms reflect all the energy dissipated in the cohesive fracture model as the crack initiates and propagates in the specimen. It can be observed from this figure that the bulk dissipation constitutes only a small portion of the measured fracture energy reflected through the external work term. This further implies that the increase in bulk dissipation with increasing loading rate does not account for the higher fracture energy (external work) with increasing rates.

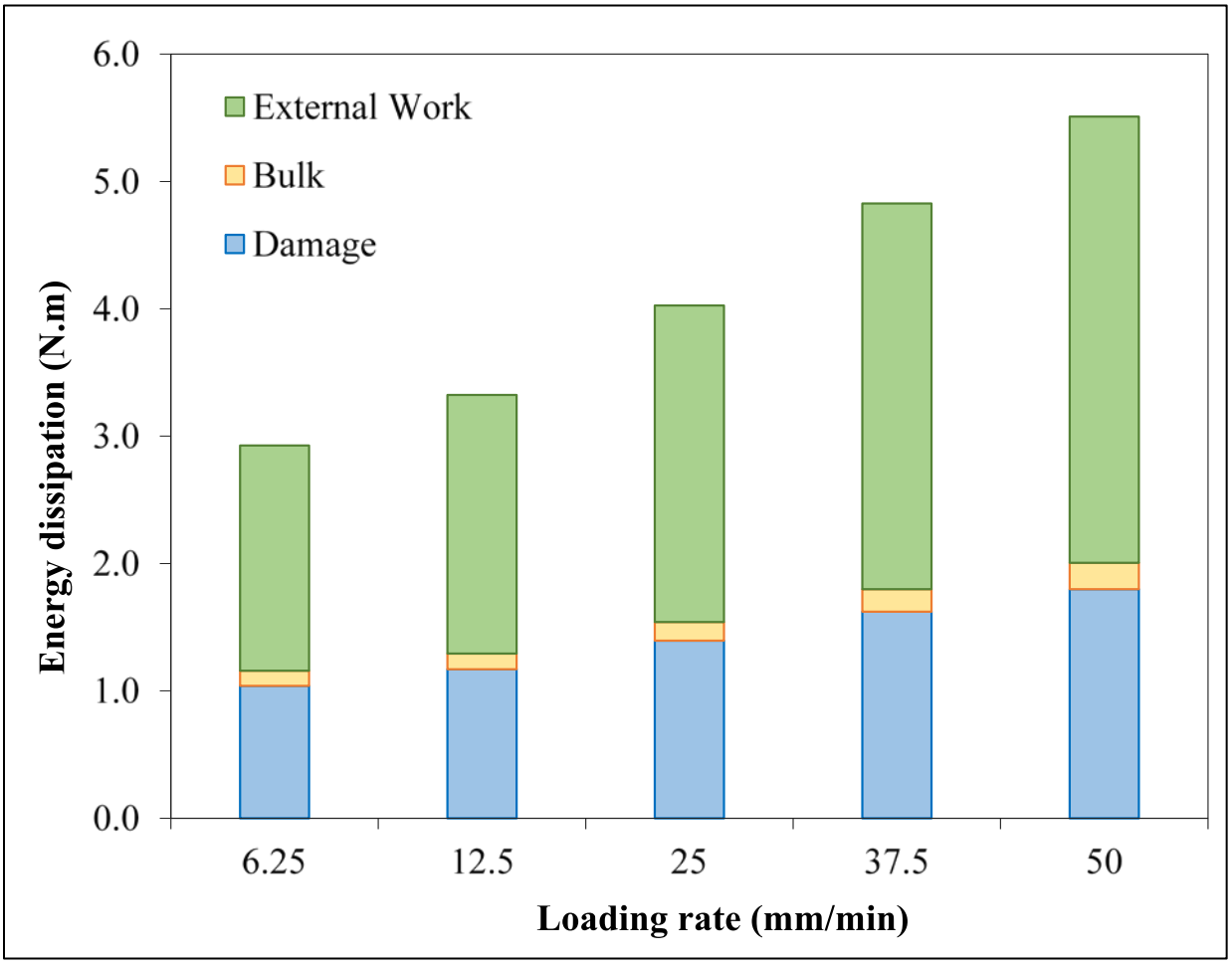

Figure H.13 Energy dissipation terms at various loading rates for rate-dependent fracture properties and T = 25°C.

REFERENCES FOR APPENDIX H

AASHTO TP 62-03. *Determining Dynamic Modulus of Hot Mix Asphalt Concrete Mixtures* American Association of State Highways and Transportation Officials, Washington, DC 2005.

Abanto-Bueno, J., and J. Lambros. "Experimental Determination of Cohesive Failure Properties of a Photodegradable Copolymer." *Experimental Mechanics*, Vol. 45, No. 2, 2005, pp. 114–152.

Abanto-Bueno, J., and J. Lambros. "Investigation of Crack Growth in Functionally Graded Materials Using Digital Image Correlation." *Engineering Fracture Mechanics*, Vol. 69, No. 14-16, 2002, pp. 1695–1711.

Ahmedzade P., and B. Sengoz. "Evaluation of Steel Slag Coarse Aggregate in Hot Mix Asphalt Concrete." *Journal of Hazardous Materials*, Vol. 165, 2009, pp. 300-305.

Bai, B.Q. "Shift Factor Model Evaluation using Tested Data from PMA at Low Temperatures and Data Reduction Methods for IDT and HT-BBR Testing." *Pavement Cracking – Mechanisms, Modeling, Detection, Testing and Case Histories, CRC Press*, 2008, pp. 617-626.

Bruck H.A., S.R. McNeil, M.A. Sutton, and W.H. Peters III. "Digital Image Correlation Using Newton-Raphson Method of Partial Differential Correction." *Experimental Mechanics,* Vol. 29, No. 3, 1989, pp. 261–267.

Buttlar, W.G., B.C. Hill, R. Kim, M.E. Kutay, A. Millien, A. Montepara, G.H. Paulino, C. Petit, I.O. Pop, E. Romeo, R. Roncella, S.A. Safavizadeh, G. Tebaldi, and A. Wargo. "Digital Image Correlation Techniques to Investigate Strain Fields and Cracking Phenomena in Asphalt Materials." *Materials and Structures*, Vol. 47, No. 8, 2014, pp.1373–1390.

Carroll J.D., W. Abuzaid, J. Lambros, and H. Sehitoglu, "High Resolution Digital Image Correlation Measurements of Strain Accumulation in Fatigue Crack Growth." *International Journal of Fatigue*, Vol. 57, 2013, pp. 140–150.

Chen J.S., and C.J Tsai. "Relating Tensile, Bending, and Shear Test Data of Asphalt Binders to Pavement Performance." *Journal of Materials Engineering and Performance*, Vol. 7, 1998, pp. 805–811.

Christensen D.W., and R. Bonaquist. "Modeling of Fatigue Damage Functions for Hot Mix Asphalt and Application to Surface Cracking." *Road Materials and Pavement Design*, Vol. 13, 2012, pp. 102-123

Chu T.C., Ranson W.F., Sutton M.A., Peters W.H. "Applications of Digital Image-Correlation Techniques to Experimental Mechanics." *Experimental Mechanics*, Vol. 25, No. 3. , 1985, pp. 232–244.

Doll, B., 2015 (May), *Evaluation of Viscous Effects In Crack Tip Fields In Recycled Asphalt Pavement Materials Using Digital Image Correlation*, MS thesis, University of Illinois, Urbana, IL.

Goh S.W., and Z. You Z. (2011) "Evaluation of Recycled Asphalt Shingles in Hot Mix Asphalt." pp. 638–645. In Proceedings *Transportation and Development Institute Congress 2011*.

Gorkem C., and B. Sengoz "Predicting Stripping and Moisture Induced Damage of Asphalt Concrete Prepared with Polymer Modified Bitumen and Hydrated Lime." *Construction and Building Materials*, Vol. 23, 2009, pp. 2227–2236.

Johnson E., G. Johnson, S. Dai, D. Linell, J. McGraw, and M. Watson. 2010 (Jan.), *Incorporation Of Recycled Asphalt Shingles in Hot Mixed Asphalt Pavement Mixtures,* Final Report #2010-08 Minnesota Department of Transportation, Office of Policy Analysis, Research and Innovation.

Kim K.W., M. El Hussein, "Variation of Fracture Toughness of Asphalt Concrete under Low Temperatures." *Construction and Building Material*, Vol. 11, No. 7-8, 1997, pp. 403–411.

Leclerc H., J.N. Périé, S. Roux, F. Hild. 2009 “Integrated Digital Image Correlation for the Identification of Mechanical Properties.” *Computer Vision/Computer Graphics Collaboration Techniques Lecture Notes in Computer Science*, Vol 5496, pp.161–171.

Lambros J., and J. Patel, “Microscale Digital Image Correlation Study of Irradiation Induced Ductile-to-Brittle Transition in Polyethylene.” *Journal of Strain Analysis for Engineering Design*, Vol. 46, 2011, pp. 347–350.

Lim I.L., I.W. Johnston, and S.K. Choi, “Stress Intensity Factors for Semi-Circular Specimens under Three-Point Bending.” *Engineering Fracture Mechanics* Vol. 44, No. 3, 1993.

M.O. Marasteanu, S. Dai, J.F. Labuz, and X. Li, “Determining the Low-Temperature Fracture Toughness of Asphalt Mixtures.” *Transportation Research Record*, Vol 1789, 2002.

Masad E., Somadevan N., Bahia H.U., Kose S., “Modeling and Experimental Measurements of Strain Distribution in Asphalt Mixes.” *Journal of Transportation Engineering*, Vol. 127, No. 6, 2001.

Newcomb D., M. Stroup-Gardiner, B. Weikle, A. Drescher, 1993 *Influence of Roofing Shingles on Asphalt Concrete Mixture Properties*, Report No. 93/09 Submitted to Minnesota Department of Transportation, Office of Research Administration. St. Paul, MN.

Mostafavi M., and T.J. Marrow. “Quantitative In-situ Study of Short Crack Propagation in Polygranular Graphite by Digital Image Correlation.” *Fatigue and Fracture of Engineering Materials and Structures*, Vol. 35, 2012.

Osman M.O. 2014. *Special Provision for Reclaimed Asphalt Pavement (RAP) and Reclaimed Asphalt Shingles (RAS),* Report No. 80306m. Illinois Department of Transportation, Bureau of Materials and Physical Research.

Ozer H., I.L. Al-Qadi, C.A. Duarte. “Effects of Non Uniform and Three-Dimensional Contact Stresses on Near-Surface Cracking.” *Transportation Research Record: Journal of the Transportation Research Board*, No. 2210, 2011.

Ozer H., I.L. Al-Qadi, and Kanaan A. (2012), *Laboratory Evaluation of High Asphalt Binder Replacement with Recycled Asphalt Shingles (RAS) for a Low N-Design Asphalt Mixture*, Report No. ICT-R27-SP19. Rantoul IL. Illinois Center for Transportation.

Park S.W., Kim Y.R. “Fitting Prony-Series Viscoelastic Models with Power-Law Presmoothing.” *Journal of Materials in Civil Engineering*, Vol. 13, No. 1, 2001.

Petersen J.C., and P.M. Harnsberger. “Asphalt Aging: Dual Oxidation Mechanism and its Interrelationships with Asphalt Composition and Oxidative Age Hardening.” *Transportation Research Record: Journal of the Transportation Research Board*, Vol. 1638, 2007.

E. Romeo “Two-Dimensional Digital Image Correlation for Asphalt Mixture Characterization: Interest and Limitations.” *Road Materials and Pavement Design*, Vol. 14, No. 4, 2013.

Schapery R.A. “Correspondence Principles and a Generalized J Integral for Large Deformation and Fracture Analysis of Viscoelastic Media.” *International Journal of Fracture*, Vol. 25, 1984.

Schapery R.A. “On the Mechanics of Crack Closing and Bonding in Linear Viscoelastic Media.” *International Journal of Fracture*, Vol. 39, 1989.

Seo Y., Y.R. Kim, M.W. Witczak, and R. Bonaquist “Application of Digital Image Correlation Method to Mechanical Testing of Asphalt–Aggregate Mixtures.” *Transportation Research Record: Journal of the Transportation Research Board*, Vol. 1789, 2002.

Skarżyński L., J. Kozicki , J. Tejchman. “Application of DIC Technique to Concrete —Study on Objectivity of Measured Surface Displacements.” *Experimental Mechanics*, Vol. 53, 2013.

Sutton M.A., J.J. Orteu, and H. Schreier, 2009. “Image Correlation for Shape, Motion and Deformation Measurements: Basic Concepts: Theory and Applications,” New York: Springer US, 2009.

Tabatabaee H.A., and H.U. Bahia. “Establishing use of asphalt binder cracking tests for prevention of pavement cracking.” *Road Materials and Pavement Design*, Vol. 15, No. 1, 2014.

H.M. Zelelew, and A.T. Papagiannakis, “Interpreting Asphalt Concrete Creep Behavior through Non-Newtonian Mastic Rheology.” *Road Materials and Pavement Design*, Vol. 13, No 2, 2012.

Williams M.L., R. Landel, J. Ferr “The Temperature Dependence of Relaxation Mechanisms in Amorphous Polymers and Other Glass-forming Liquids.” *Journal of American Chemical Society*, Vol. 77, No. 14, 1955.

Williams M.L. “On the stress distribution at the base of a stationary crack.” *Journal of Applied Mechanics*, Vol. 24, 1957, pp. 109–114.

Wineman A.S., and K.R. Rajagopal, 2000, *Mechanical Response of Polymers—An Introduction*. Cambridge: Cambridge University Press.

Wu Z.M., H. Rong, J.J. Zheng, F. Xu, and W. Dong. “An experimental investigation on the FPZ properties in concrete using digital image correlation technique.” *Engineering Fracture Mechanics*, Vol. 78, 2011.

Zhao S., B. Bowers, B. Huang, and X. Shu. “Characterizing Rheological Properties of Binder and Blending Efficiency of Asphalt Paving Mixtures Containing RAS through GPC.” *Journal of Materials in Civil Engineering*, Vol. 26, 2014.

APPENDIX I: THICKNESS EFFECT STUDY

Four different mixes, as shown in Table I.1, were tested for the thickness study. SCB specimens were prepared with five thicknesses (25, 37.5, 43.75, 50, and 62.5 mm). All of the SCB tests were conducted at a rate of 25 mm/min at a single temperature of 25°C.

Table I.1 General Identification of Mixtures Used

Mixture ID	NMAS (mm)	Asphalt Binder	Mix Type	Mix Prepared
N80-0%-SO	4.75	PG 70-22 (SBS)	SMA	Plant
N70-38%	9.5	PG 58-28	Course	Plant
N80-25%	12.5	PG 70-28	SMA	Plant
N90-0%-I	19	PG 64-22	Course	Lab

Figure I.1 Variation in thicknesses from 25 on the left to 62.5 mm on the right.

Fracture energy results with varying thickness are shown in Figure I.2. Based on the fracture theories, the expectation is an increase in fracture energy with increasing thickness due to higher confining stresses developing inside the specimen at the crack fronts. The data shown in the following figure do not follow a consistent trend. Therefore, a thickness correction for fracture energy was not developed. Further testing is required to investigate thickness effect on fracture energy.

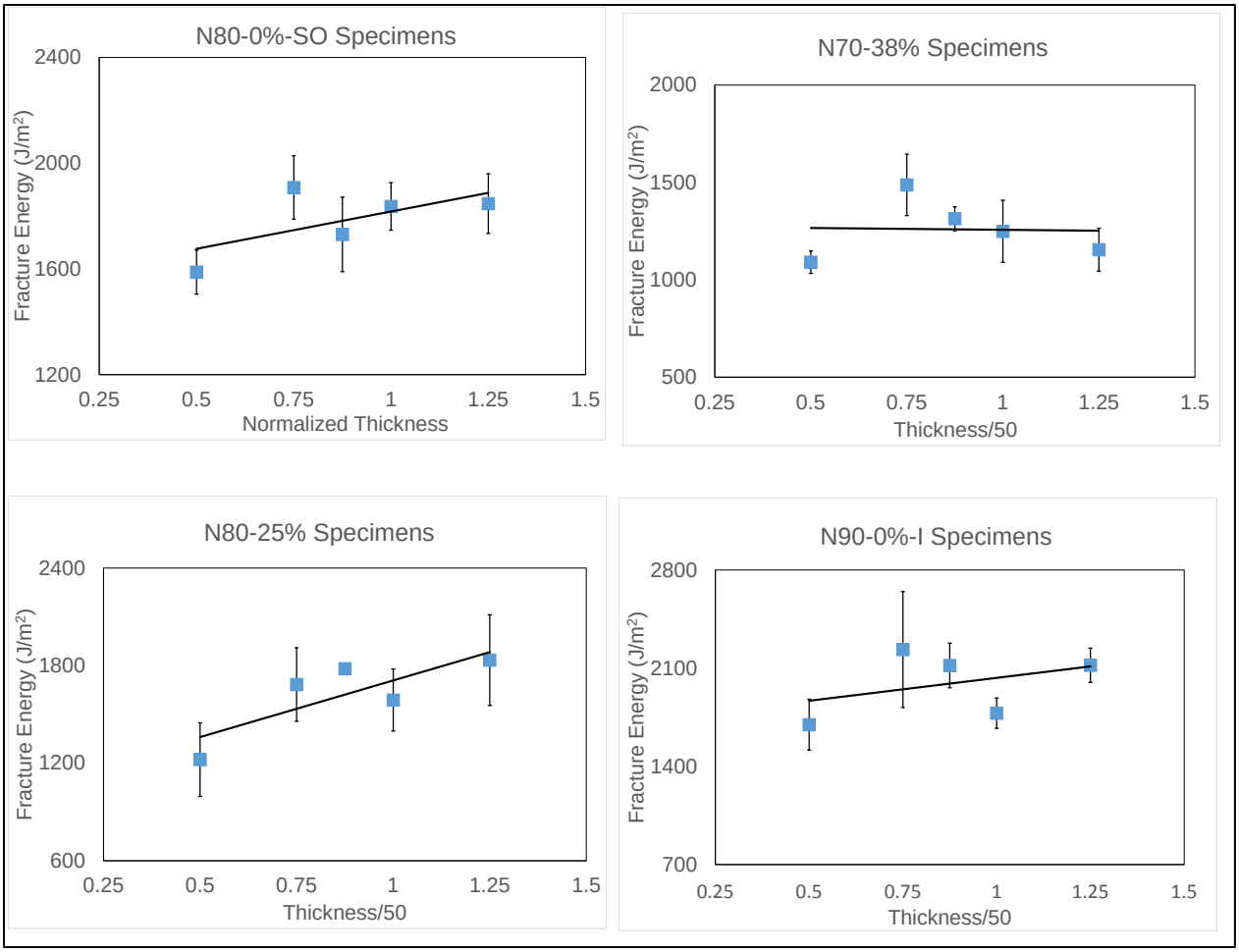

Figure I.2 Fracture energy (G_f) vs. normalized thickness.

Flexibility index values with varying thicknesses are shown in the following plot. The trend for the flexibility index is more evident. Therefore, a correction factor was developed only for the flexibility index at this point. The correction factor adjusts the flexibility index with respect to a reference thickness (50 mm). The corrected values of the flexibility index are found by multiplying the flexibility index by the ratio of experimental thickness and reference thickness (50 mm). A comparison of flexibility index values after correction is given in Figure I.4.

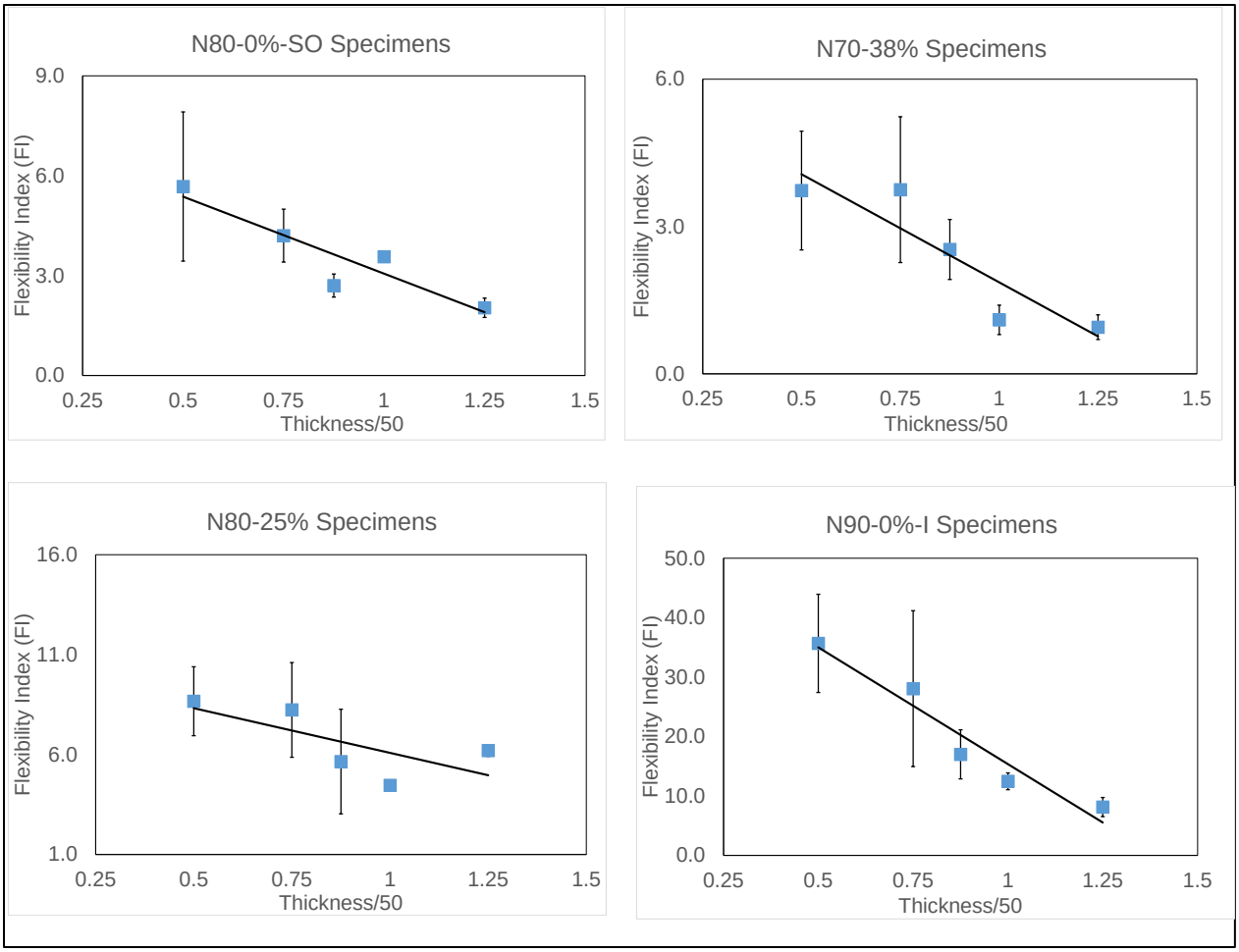

Figure I.3 Flexibility index vs. normalized thickness.

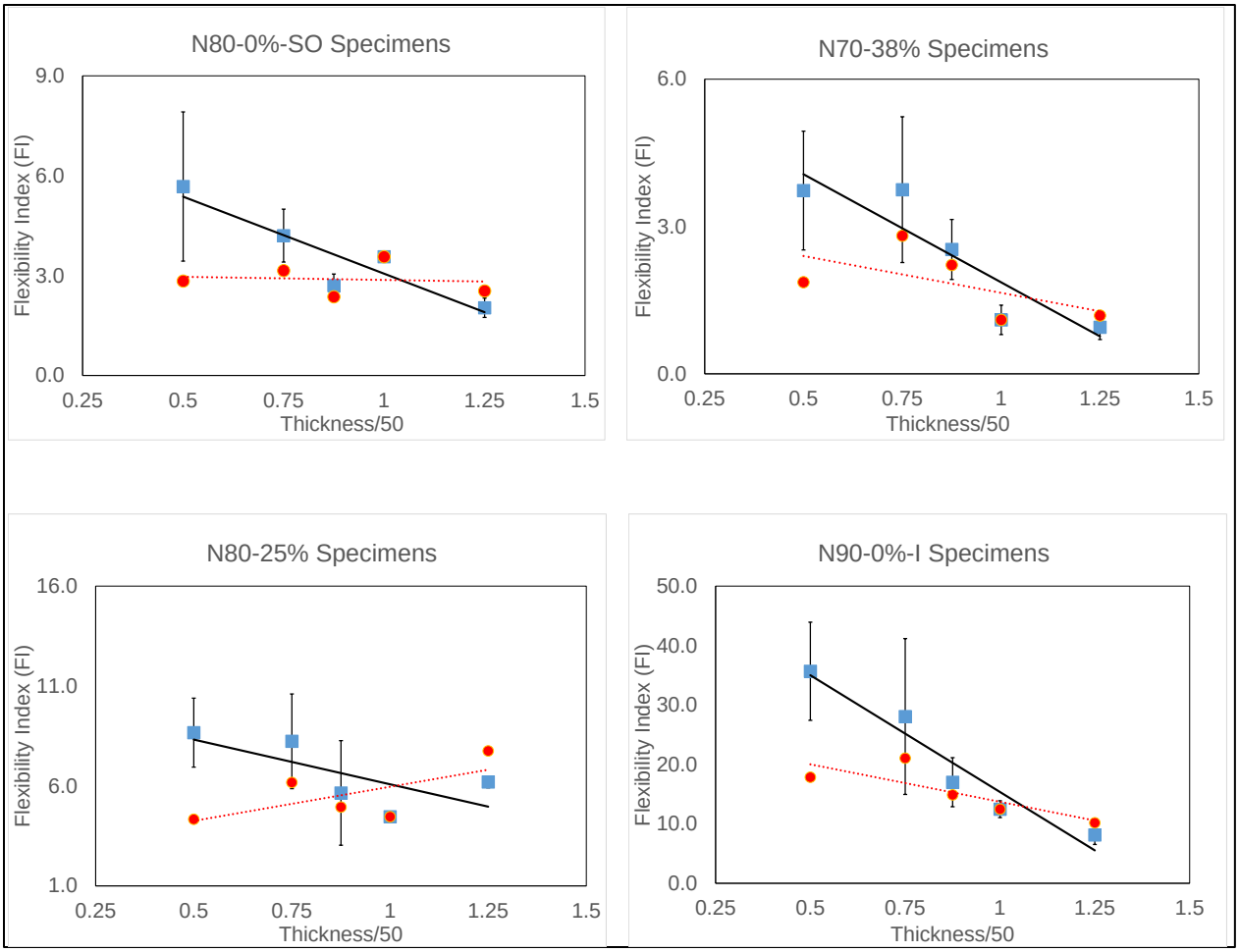

Figure I.4 A comparison of actual and corrected flexibility index vs. normalized thickness.

APPENDIX J: FINE AGGREGATE MIXTURE–LEVEL TESTING

J.1 INTRODUCTION AND OBJECTIVES

The objective of the study was to develop alternative testing protocols for preparing fine asphalt mixture (FAM) specimens and characterizing the inherent properties of RAS and its interaction with virgin aggregates and asphalt binder. The characteristics determined were linear viscoelastic modulus, shear strength, and fatigue resistance. A fine aggregate scale was selected for use based on its convenience in specimen preparation without the need for mix design. Fine asphalt mixture specimens with varying percentages of recycled shingles were prepared for modulus and shear strength testing to validate the developed test method. The test method was tailored for use with a conventional dynamic shear rheometer (DSR).

J.2 EXPERIMENTAL PROGRAM AND MATERIALS

Three FAM specimens were prepared with PG 46-34 asphalt binder, and two FAM specimens were prepared with PG 64-22 asphalt binder. Two asphalt binder types were considered in order to examine the effectiveness of binder grade bumping, which is a common practice when RAP and RAS are used in the mixes, as well as sensitivity of the DSR to binder grade. The three mixes with PG 46-34 were prepared with 0%, 2.5%, and 7.1% RAS, respectively, while the two mixes with PG 64-22 were prepared with 0% RAS and 7.1 % RAS, respectively. FAM specimens with two different binder grades were prepared only with virgin materials. All the mixes were prepared with the same aggregate gradation and type, known as FM-20 (a crushed fine aggregate) in Illinois. The gradation of FM-20 and RAS is shown in Figure J.1.

Gyratory-compacted samples were prepared from each mix. Samples were mixed and compacted at a temperature of 155°C (311°F). Aggregates were placed in the oven overnight, and the asphalt binder was heated for approximately 2 hr before mixing. To avoid extra aging and to simulate the RAS plant mixing procedure, RAS materials were placed in the oven only 20 min before mixing.

Samples were short-term aged until they reach compaction temperature (approximately 2 hr at compaction temperature), and each mixture was subjected to 150 gyrations, a number chosen in order to obtain mixes with consistent air void content. The DSR mixture samples were then cored from the gyratory-compacted samples to the desired diameter of 12.45 mm (0.492 in) and length of 50 to 60 mm (1.90 to 2.36 in). Samples were then glued at the top and the bottom to special circular steel caps to hold them in the DSR fixture. Figure J.2 illustrates the sample preparation process and testing fixture for holding solid samples. The solid-testing fixture was used to align the caps on the samples and glue them together.

Three specimens were selected from each gyratory-compacted sample in order to measure air void content. For most of the mixes, the air void content was found to be in the range of 8% to 10%. The lowest was for the mix with PG 46-34 and 0% RAS, and the highest was for the mix with PG 64-22 which contained approximately 9.8% air void content.

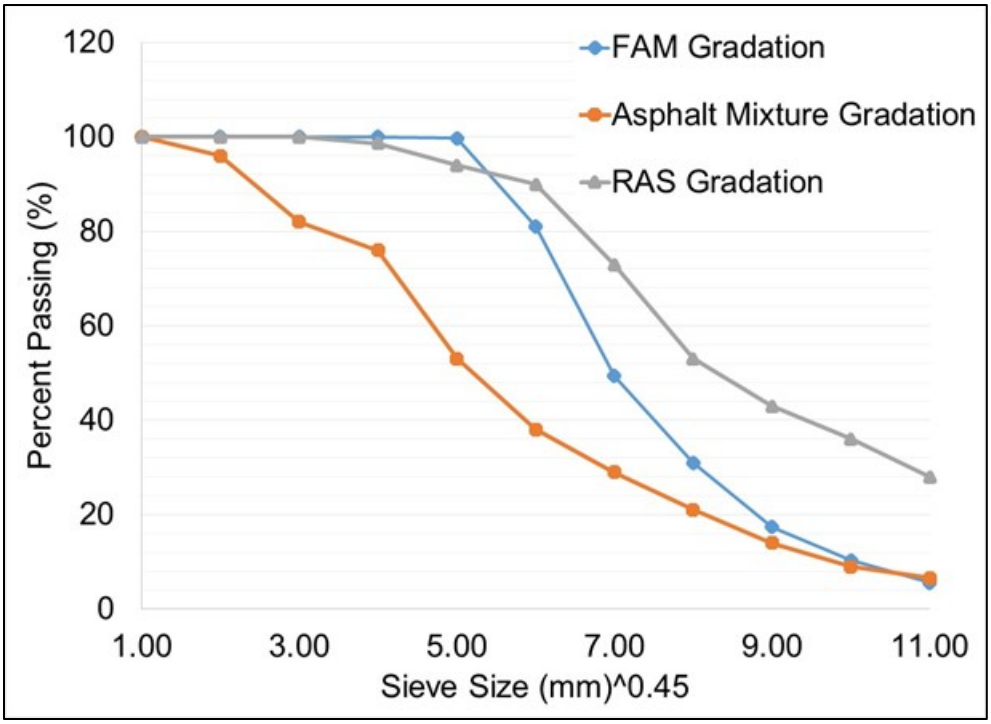

Figure J.1 Gradation curves of RAS, FAM specimen, and asphalt mixture previously used in Ozer et al. (2012) at the highest binder replacement level, 7.5% RAS.

Table J.1 Aggregates, RAS, and Air Content of Mastic Samples

	FM-20 Aggregates (% by Weight in Mix)	RAS (% by Weight in Mix)	Virgin Asphalt Binder (% by Weight in Mix	Total Air Void Content (%) (Virgin + RAS)	Asphalt Binder Replacement* (%)
Virgin Mix	94.33	0	5.67	5.66	0
LRAS Mix	92.5	2.47	5.03	5.70	11.32
HRAS Mix	88.9	7.11	3.99	5.87	31.66

*Asphalt binder replacement $= \frac{\text{Recycled Asphalt Binder (RAP and RAS)}}{\text{Total Asphalt Binder Content}} * 100$

Figure J.2 Specimen preparation process for FAM specimens including cutting, coring, and test setup.

J.3 EXPERIMENTAL PROGRAM

Three tests were performed on the FAM specimens using conventional DSR equipment with a modified feature to allow testing of solid samples. This setup was used to obtain the linear viscoelastic characterization, strength, and fatigue properties of FAM specimens. As a first step of linear viscoelastic characterization, specimens were tested to ensure linear viscoelastic range of the mixes. Most of the specimens were shown to have a linear viscoelastic range at a strain of about 0.005%. However, a complex shear modulus test was conducted on the FAM specimens at a strain rate of 0.01% because the tests conducted at lower strain levels yielded erratic results, especially at low temperatures, due to resolution of the equipment. In addition, some specimens were randomly selected and checked to determine whether any damage accumulated after the completion of the complex modulus test at 0.01% strain; no damage was noted. After the frequency sweep test was performed at all temperatures, the same specimen was subjected to modulus testing at the intermediate temperature. The results were compared with the initial results from the original test. Results showed very little difference between two repetitions of testing (and even a slight increase in modulus), indicating that the linear viscoelastic range was maintained during the tests conducted at 0.01% strain.

The frequency sweep test was then performed at different frequencies ranging from 0.1 to 10 Hz and at different temperatures—22°C (71.6°F), 28°C (82.4°F), 34°C (93.2°F), 46°C (114.8°F), and 54°C (129.2°F)—for all the mixes, in addition to 64°C (147.2°F) and 76°C (168.8°F) for some of the PG 64-22 specimens. After the frequency sweep test, the same specimens were used to test for shear strength and underwent limited fatigue testing as well.

A shear strength test was performed until 4% strain was reached at a temperature of 46°C (114.8°F). Samples were conditioned for 30 min before tests were run at each temperature. In addition, limited stress- and strain-controlled fatigue tests were conducted. The fatigue test was initially performed at a strain-

controlled mode of 0.15% strain rate; however, limited mixes were tested with this testing mode because of limitations related to the torque capacity of the DSR. In addition, a stress-controlled fatigue test was performed on the mixes with PG 46-34 at two different stress levels, 200,000 and 300,000 Pa.

J.4 RESULTS AND DISCUSSION

J.4.1 Complex Shear Modulus Test for FAM Specimens

The complex shear modulus tests were performed at different temperatures and frequencies ranging from 0.1 to 10 Hz. In general, a minimum four replicates were used for most of the mixes. The results obtained from the frequency sweep tests at different temperatures were used to build master curves at a reference temperature of 28°C (82.4°F). A sigmoidal fit was used to fit and average the data, as shown in Figure J.3a on the following page.

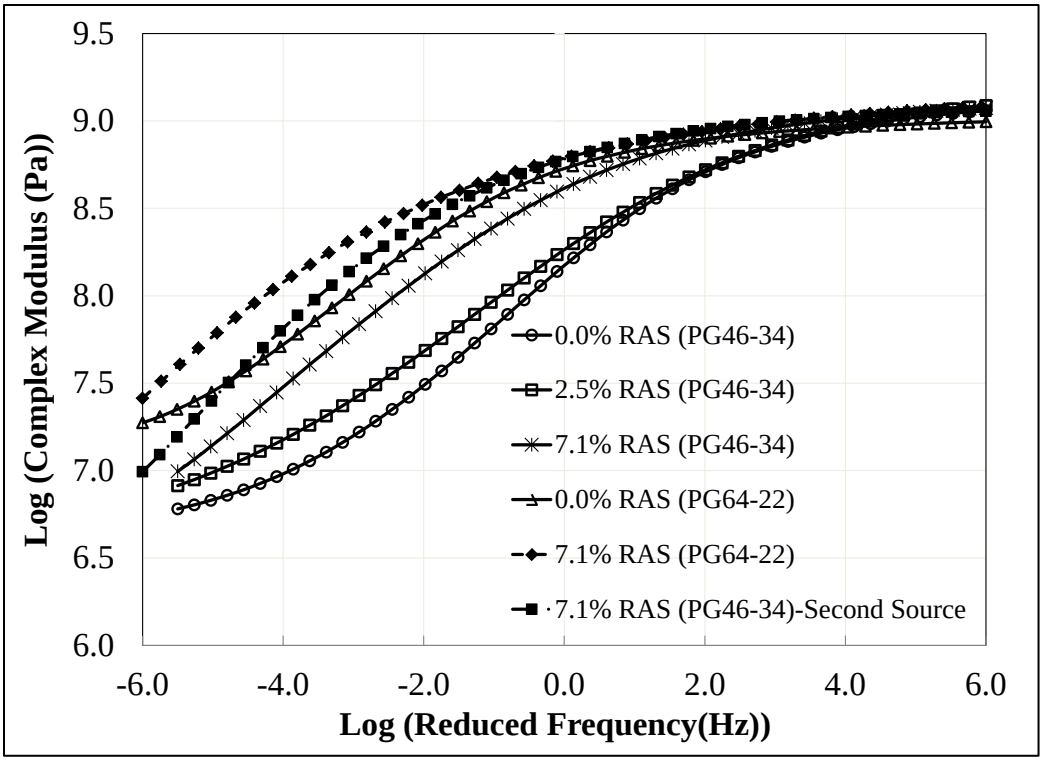

(a)

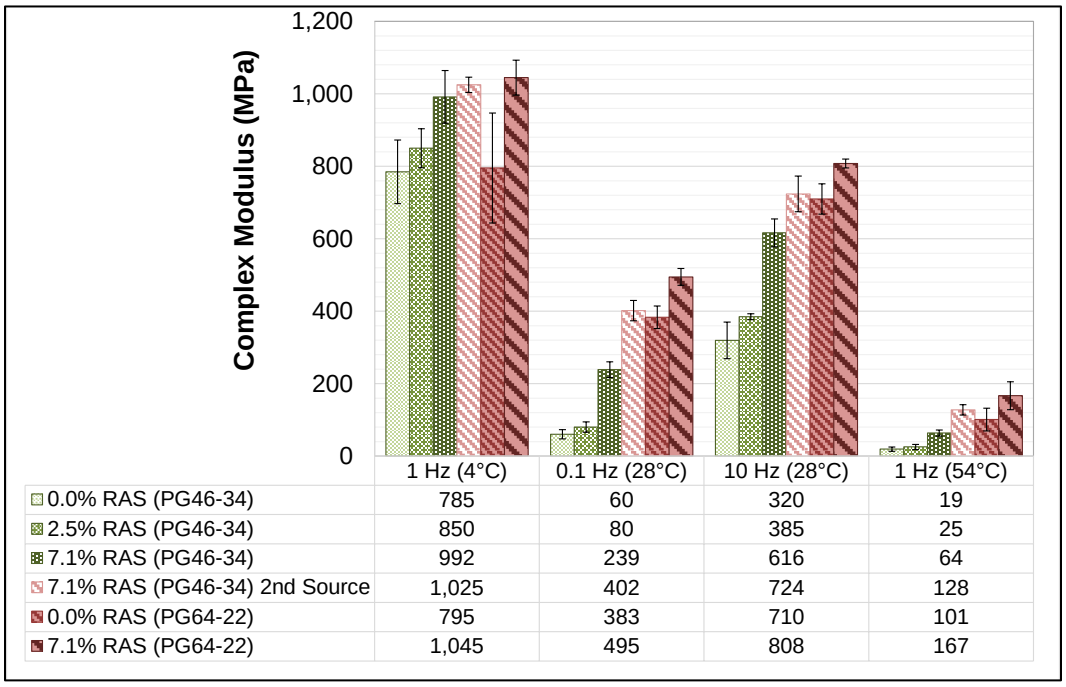

	1 Hz (4°C)	0.1 Hz (28°C)	10 Hz (28°C)	1 Hz (54°C)
0.0% RAS (PG46-34)	785	60	320	19
2.5% RAS (PG46-34)	850	80	385	25
7.1% RAS (PG46-34)	992	239	616	64
7.1% RAS (PG46-34) 2nd Source	1,025	402	724	128
0.0% RAS (PG64-22)	795	383	710	101
7.1% RAS (PG64-22)	1,045	495	808	167

(b)

Figure J.3 DSR complex modulus test results for FAM specimens at various RAS contents and with various asphalt binder types. (a) Master curves obtained using complex shear modulus tests; (b) Selected values of complex shear modulus at different temperature and frequency for comparison and repeatability illustration.

The influence of using RAS can be also seen in the phase angle response from the frequency sweep test, as shown in Figure J.4a and 4b on the following page. A shift of the phase angle curves to the left with increasing RAS is evident, which results in a higher phase angle at the same reduced frequency. Due to the differences in the time scale of relaxation, the mix with PG 64-22 and 7.1% RAS showed the lowest phase angle among all mixes, while the mix with PG 46-34 and 7.1% RAS had the lowest phase angle response among the mixes prepared with PG 46-34 at the same frequency.

It is also evident from the phase angle patterns that the mixes with RAS had not completed their relaxation in the range of testing temperatures and frequencies. Similar to the complex modulus curves, Figure 4b illustrates direct phase angle measurements at different temperatures and frequencies. It was observed that repeatability of phase angle measurements is higher than that of complex modulus measurements. However, a similar trend w clearly seen in the figure for samples with increasing RAS or different binder grade. Phase angle readings of the samples with the same amount of RAS from two sources are significantly different from each other.

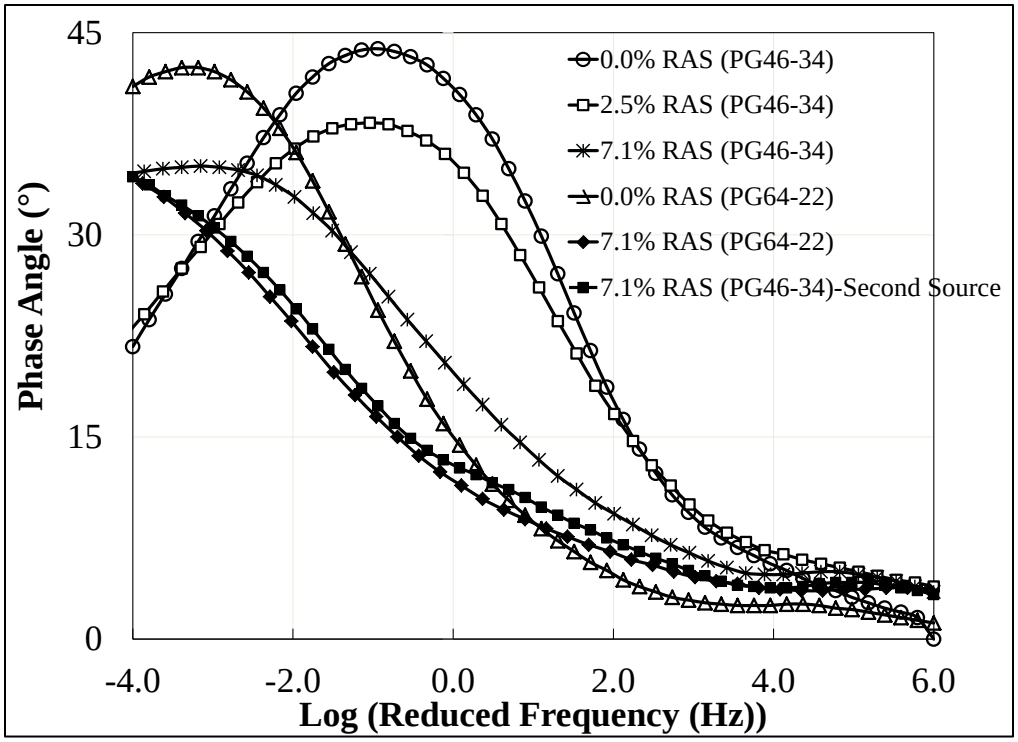

(a)

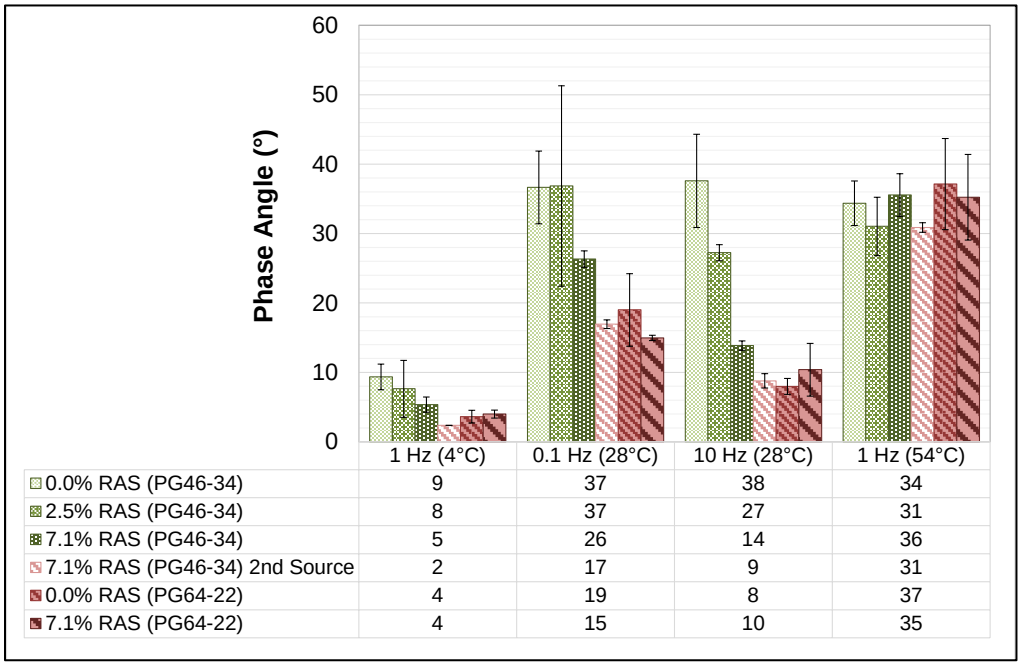

	1 Hz (4°C)	0.1 Hz (28°C)	10 Hz (28°C)	1 Hz (54°C)
0.0% RAS (PG46-34)	9	37	38	34
2.5% RAS (PG46-34)	8	37	27	31
7.1% RAS (PG46-34)	5	26	14	36
7.1% RAS (PG46-34) 2nd Source	2	17	9	31
0.0% RAS (PG64-22)	4	19	8	37
7.1% RAS (PG64-22)	4	15	10	35

(b)

Figure J.4 Phase angle measurements from the DSR complex shear modulus test (a) Phase angle master curve; (b) Selected values of phase angle at different temperature and frequency for comparison and repeatability illustration.

Statistical analysis was conducted to ensure repeatability of the test results. The results from the statistical tests are not shown here because of space limitations. According to the results, most of the replicates were shown to be repeatable and to reveal similar trends when they were statistically analyzed using SAS software. Results also showed that both RAS sources were significantly different from each other when evaluated using the complex shear modulus test. In general, it was shown with complex modulus and phase angle test results that the effect of RAS binder can clearly be identified in the results with reasonable repeatability, which has been a concern in mastic or fine asphalt mixture testing.

In addition to the FAM testing, RAS asphalt binder was extracted and tested using the DSR. RAS asphalt binder was blended to achieve a percentage that represents the percentage of ABR in the FAM with PG 46-34 and 7.1% RAS. The complex shear modulus results of extracted binders were used along with the results obtained from testing the virgin PG 46-34 asphalt binder, as well as the asphalt mixture complex modulus testing results obtained from our previous study (Ozer et al. 2012).

Complex modulus results for each mix were normalized by the instantaneous complex modulus value shown in Figure J.5 on the following page. The frequency corresponding to a 50% reduction in the complex modulus was used to identify the viscoelastic characteristics of RAS at different scales and to evaluate any similarities in the asphalt mixture and FAM specimens in terms of their viscoelastic characteristics. The delay in reaching 50% reduction in complex shear modulus is highest in the binder level. Mixture level showed an earlier reduction in the complex modulus, followed by the FAM, and then the binder level. The reduction in the complex modulus and when it occurs is an indication of the relaxation properties altered by the RAS material. Relaxation time shows that mixture- and FAM-level tests provide a comparable delay in viscoelastic properties when similar levels of RAS content are used.

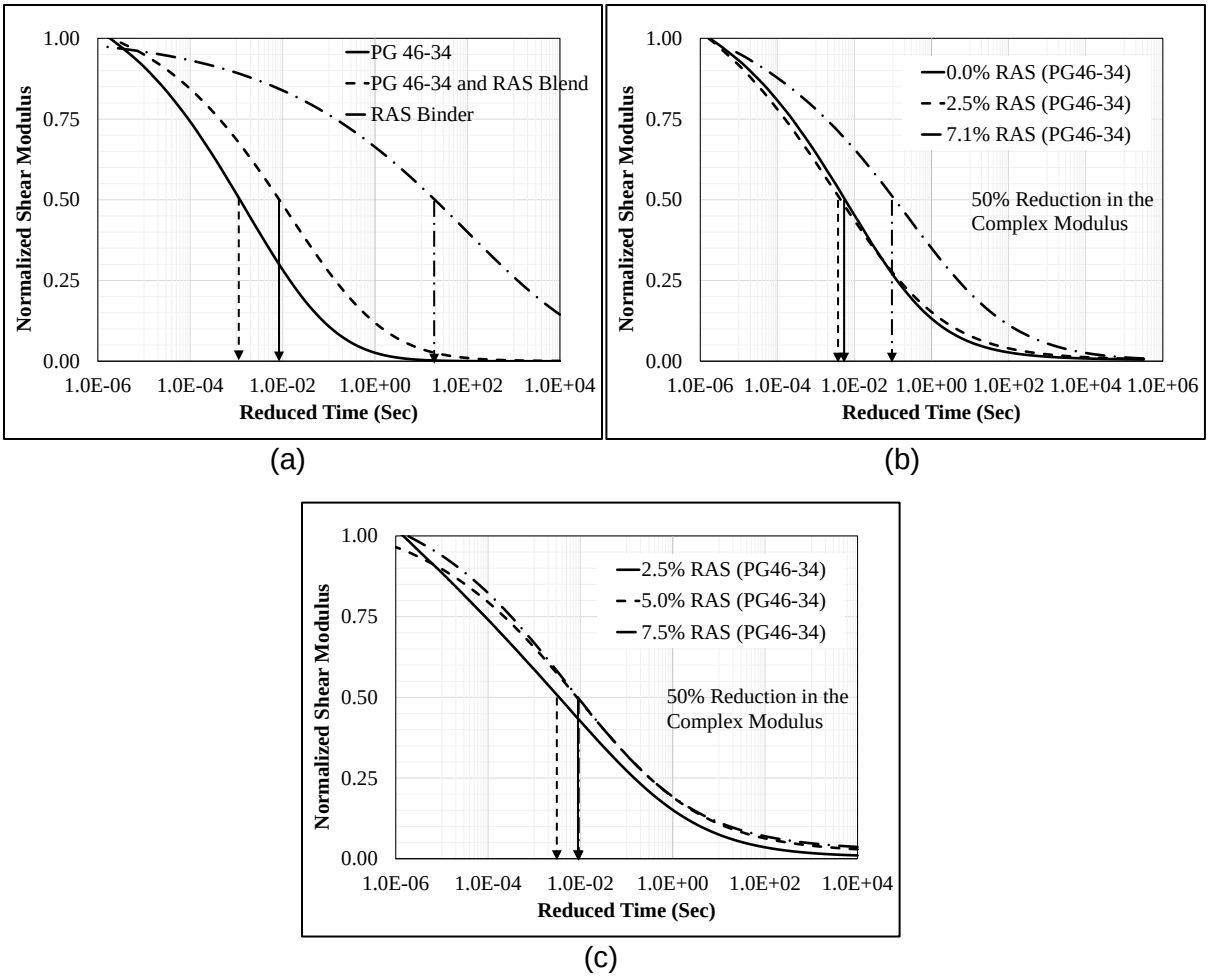

Figure J.5 Modulus relaxation with reduced time obtained from the master curves at the (a) Binder level (PG 46-34, blend of PG 46-34 and 7.1% RAS binder), (b) FAM level (at 0%, 2.5%, and 7.1% RAS), and (c) Mixture level (at 2.5%, 5%, and 7.5% RAS).

J.4.2 Shear Strength Test

Strength tests were also performed to evaluate the influence of RAS on FAM. Fresh and already tested specimens were used for strength testing. After the complex shear modulus test had been performed on the FAM specimens, some of the tested specimens were used to test for shear strength at 46°C (114.8°F). Because the modulus test was shown to be nondestructive, reusing the same specimen for strength testing was considered acceptable in the scope of this study. Specimens were conditioned for 30 min at 46°C (114.8°F) in the DSR temperature-control fixture before testing. The shear strength test was then conducted as stress growth using a shear rate of 0.0004 1/s until reaching a strain of 4%. As expected, most samples completely failed before this range was reached.

Figure J.6 shows the strength test results obtained for the various fine mixes. The influence of RAS and the effect of changing the asphalt binder grade as well as the effect of changing the RAS source can clearly be seen in the strength of the materials. The mix with PG 64-22 and 7.1% RAS showed the highest strength of all mixes, followed by the mix with PG 64-22 and 0% RAS. However, the mix with PG 46-34 and 7.1% RAS showed a strength and peak load similar to those of the mix with PG 64-22

and 0% RAS. It was also found that this mix failed before the PG 64-22 and 0% mix reached complete failure.

The peak stress and corresponding strain, along with the failure plane shape, are shown in Figure J.7. Two typical patterns were observed from the strength test results. The first was an increase in strength corresponding to an increase in RAS content, while corresponding strain at peak stress decreased with increasing RAS content. Second, this test clearly showed the influence of using RAS on the strength of the asphalt mixture. Typical failure patterns after the strength test are also shown in Figure J.7. The failure plane was usually at an angle at or around 45° to the loading plane, which indicates the critical plane with shear and tensile normal stresses.

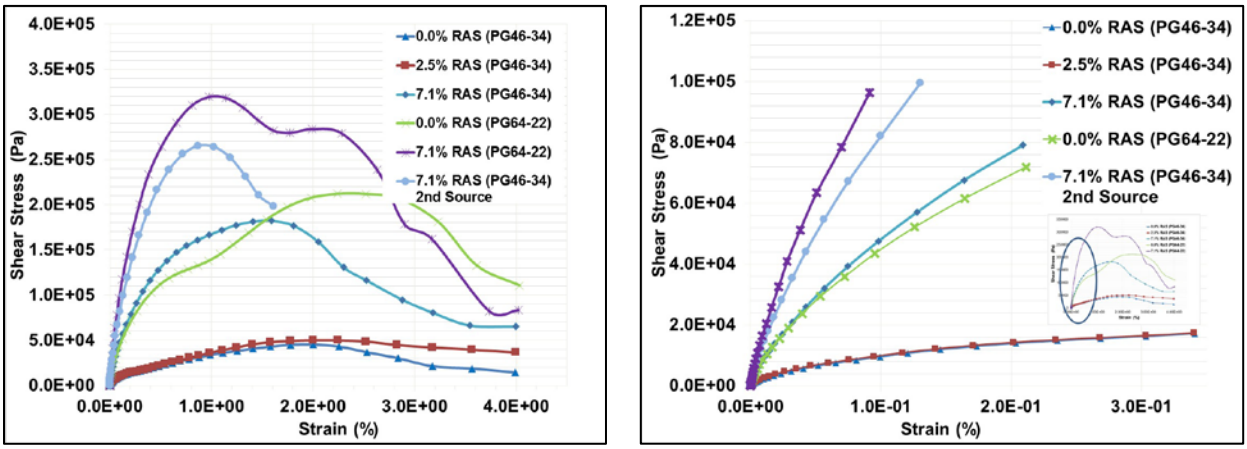

Figure J.6 Strength test results obtained at 46°C (114.8°F). (a) Complete experimental curve; (b) Vlose-up view of the test results at lower strain levels.

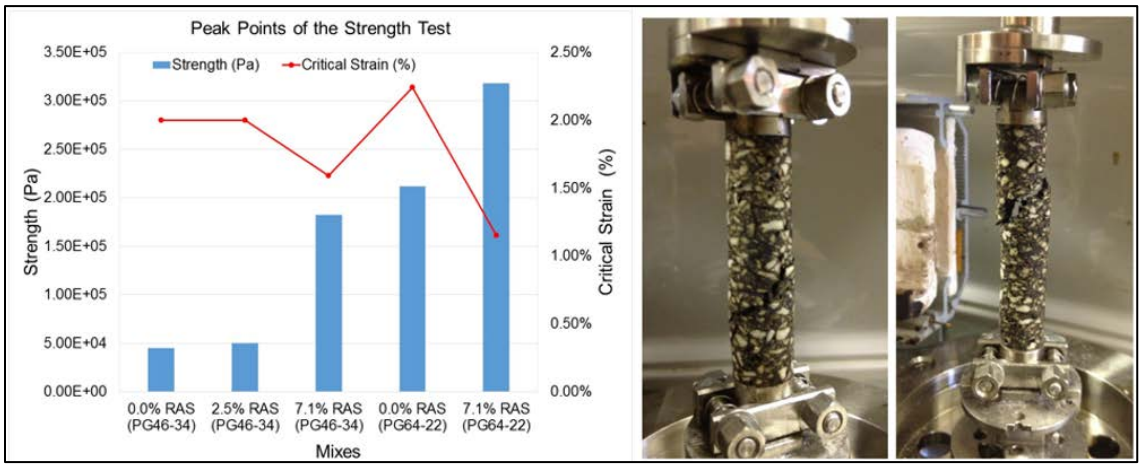

Figure J.7 Shear stress and strain at the failure point and typical failure pattern of the specimens.

J.4.3 Fatigue Test

Several fatigue tests were performed on the FAM. The torque capacity of the equipment limited the number of fatigue tests that could be performed. Most notably, the mixtures with PG 64-22 asphalt binder grade exceeded the DSR machine capacity at a loading frequency of 10 Hz. This effect was also observed for the mixtures with PG 46-34 and 7.1% RAS during the strain-controlled fatigue test.

Fatigue results were initially obtained from a strain-controlled fatigue test at 0.15% strain and 10 Hz and a temperature of 25°C (77°F) and 35°C (95°F). The number of cycles to failure for FAM specimen is shown in Figure J.8 along with the asphalt mixture test results obtained in our previous study (Ozer et al. 2012). Mixture fatigue testing was conducted using push-pull test at 25°C (68°F) and 250 microstrains. Number of cycles to failure is found at 50% reduction in the modulus. Fatigue test results under strain control at the mixture and fine aggregate level show the same trend (decreasing fatigue life) with increasing RAS content.

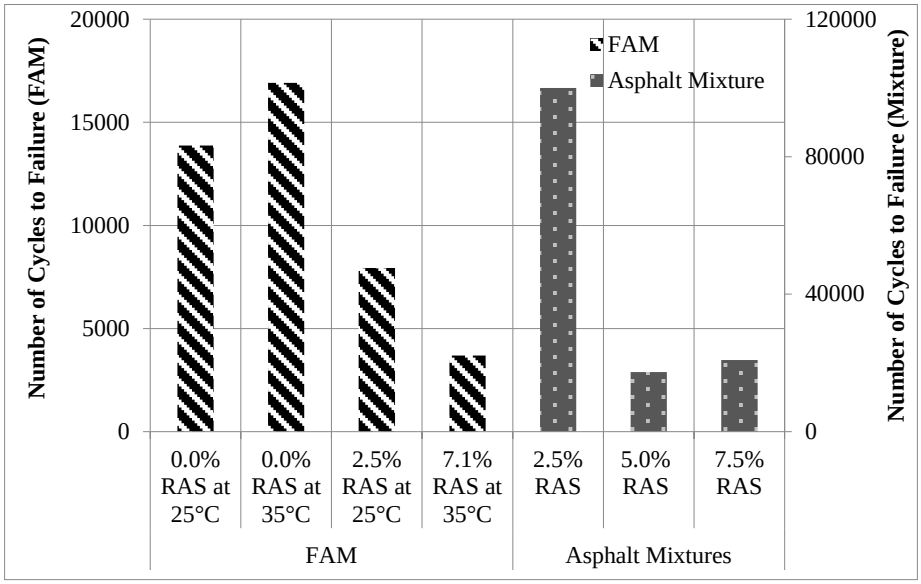

Figure J.8 Modulus degradation chart from strain-controlled fatigue tests for FAM and an asphalt mixture (Ozer et al. 2012). Fatigue testing on FAM specimens was conduced at 0.15% strain level and a temperature of 25°C (77°F) and 35°C (95°F).

Fatigue testing was continued using the stress-controlled mode. The stress levels (200,000 and 300,000 Pa) were chosen to obtain a reasonable number of cycles to failure for all the mixes. In the stress-controlled fatigue tests, the number of cycles to failure increased for materials with higher RAS. This result was due to smaller initial strains in mixes with higher RAS, which had higher stiffness. The number of cycles to failure for stress-controlled tests is shown in Figure J.9. As expected, failure occurred at much earlier cycles at higher stresses. In contrast to strain-controlled fatigue tests, stress-controlled fatigue tests resulted in higher fatigue life for mixes with increasing RAS content. This is due to lower initial strains applied to the specimens with higher modulus (in the case of mixes with higher contents of RAS).

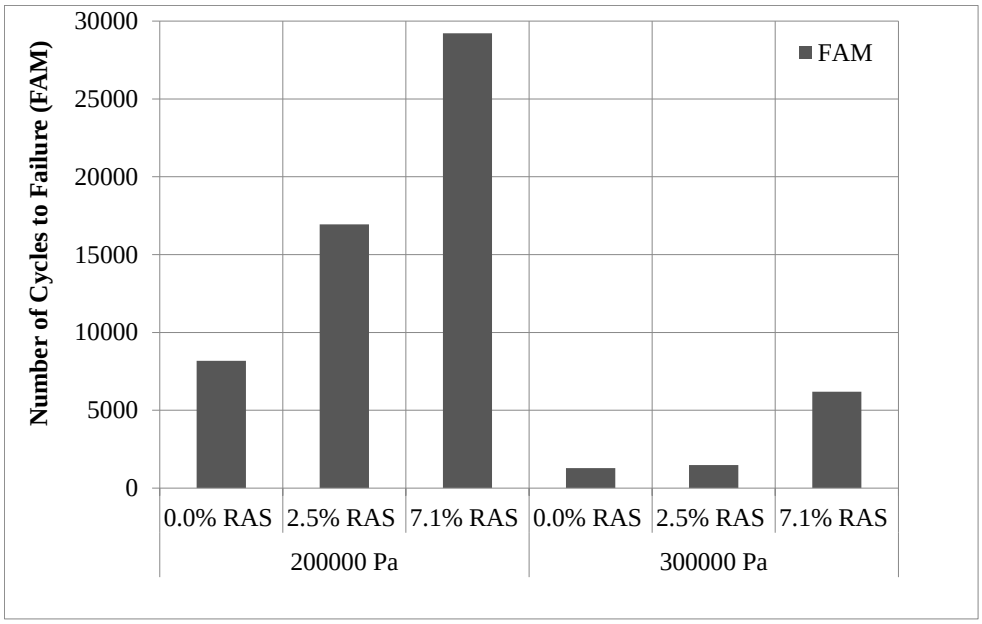

Figure J.9 Modulus degradation chart from the stress-controlled fatigue test (a) at 200,000 Pa, 10 Hz frequency, and a temperature of 25°C (77°F); (b) at 300,000 Pa, 10 Hz, and 25°C.

It can be argued that stress- and strain-controlled fatigue tests are used for different purposes. Strain-controlled tests are more appropriate for pavements under displacement boundary conditions (thermal stresses induced by thermal strains), whereas stress-controlled tests represent repeated application of traffic loading. Therefore, critical test conditions for asphalt mixtures may change depending on the mode of the fatigue test. The strain-controlled test may reveal weaknesses of stiffer mixes (in the case of mixes with recycled materials), whereas stress-controlled tests can be more damaging to softer mixes.

J.5 SUMMARY AND CONCLUSIONS

A test method was developed using Superpave DSR equipment and FAM to characterize the viscoelastic modulus, strength, and fatigue properties of mixes altered by the addition of RAS. The test method was successfully used to identify critical changes in mix performance with the addition of RAS. Specimen preparation protocols provided consistent volumetric and test results to statistically isolate the effect of RAS on the test outcome as well as the effect of changing the RAS source. FAM testing is a rapid way to evaluate a large array of test parameters and to narrow choices for mix-level testing. The proposed test can be used for characterization and screening of other recycled materials, by-products, binder additives, and rejuvenators.

REFERENCES FOR APPENDIX J

Ozer H., I. L. I.L. Al-Qadi, and A. I. Kanaan. 2012 Laboratory Evaluation of High Asphalt Binder Replacement with Recycled Asphalt Shingles (RAS) for a Low N-Design Asphalt Mixture. Report No. FHWA-ICT-12-018, Rantoul, IL. Illinois Center for Transportation.

Ozer H., I. L. I.L. Al-Qadi, A. I. Kanaan and D. L. Lippert. “Performance Characterization of High Asphalt Binder Replacement with Recycled Asphalt Shingles (RAS) for A low N-design Mixture.” In Transportation Research Record: Journal of Transportation Research Board, No. 13-4500, 2013.

APPENDIX K: IL-SCB AASHTO SPECIFICATIONS (SUBMITTED)

Standard Method of Test for Determining the Fracture Potential of Asphalt Mixtures Using Semicircular Bend Geometry (SCB) at Intermediate Temperature

AASHTO Designation: TP XX-XX (2015)

Revised Draft (05-17-2015)

American Association of State Highway and Transportation Officials
444 North Capitol Street N.W., Suite 249
Washington, D.C. 20001

Standard Method of Test for

Determining the Fracture Potential of Asphalt Mixtures Using the Semicircular Bend Geometry (SCB) at Intermediate Temperature

AASHTO Designation: TP XX-XX

1. SCOPE

This test method covers the determination of the fracture energy (G_f) of asphalt mixtures using the semicircular bend (SCB) geometry at an intermediate test temperature. The method also includes procedures for calculating other relevant parameters derived from the load-displacement curve. These parameters, in conjunction with field performance, can be used to develop a flexibility index (FI) to predict an asphalt mixtures' damage resistance. The index can be used as part of the asphalt mixture approval process.

These procedures apply to test specimens having a nominal maximum aggregate size (NMAS) of 19 mm or less. Lab compacted and field core specimens can be used. Lab compacted specimens shall be 150 ± 1 mm in diameter and 50 ± 1 mm thick. When field cores are used, specimens shall be 150 ± 8 mm in diameter and 25 to 50 mm thick. A thickness correction factor may be applied for field cores tested at thickness less than 45 mm.

A vertical notch parallel to the loading axis shall be cut on the SCB specimen. The SCB specimen is a half disc with a notch parallel to the loading and the vertical axis of the semicircular disc.

This standard does not purport to address all of the safety concerns, if any, associated with its use. It is the responsibility of the user of this standard to establish and follow appropriate health and safety practices and determine the applicability of regulatory limitations prior to use.

2. REFERENCED DOCUMENTS

AASHTO Standards:

T 166, Bulk Specific Gravity (Gmb) of Compacted Hot Mix Asphalt (HMA) Using Saturated Surface-Dry Specimens

T 209, Theoretical Maximum Specific Gravity (Gmm) and Density of Hot Mix Asphalt (HMA)

T 269, Percent Air Voids in Compacted Dense and Open Asphalt Mixtures

T 283, Resistance of Compacted Asphalt Mixtures to Moisture-Induced Damage

T 312, Preparing and Determining the Density of Asphalt Mixture Specimens by Means of the Superpave Gyratory Compactor

TP 105, Determining the Fracture Energy of Asphalt Mixtures using Semicircular Bend Geometry (SCB).

ASTM Standards:

D 8, Standard Terminology Relating to Materials for Roads and Pavements

D 3549/D 3549M, Standard Test Method for Thickness or Height of Compacted Bituminous Paving Mixture Specimens

D 5361/D 5361M, Standard Practice for Sampling Compacted Bituminous Mixtures for Laboratory Testing

3. TERMINOLOGY

Definitions:

3.1.1. *critical displacement, u_1,* the intersection of the post-peak slope with the displacement-axis yields.

3.1.2. *displacement at peak load, u_0,* recorded displacement at peak load.

3.1.3. *final displacement (u_{final}), the recorded displacement at the 0.1 kN cut-off load.*

3.1.4. *flexibility index, FI* — an index intended to characterize the damage resistance of asphalt mixtures.

3.1.5. *fracture energy, G_f* —the energy required to create a unit surface area of a crack.

3.1.6. *linear variable displacement transducer, LVDT*—sensor device for measuring linear displacement.

3.1.7. *ligament area, $Area_{lig}$*—cross-sectional area of specimen through which the crack propagates, calculated by multiplying ligament width (test specimen thickness) and ligament length.

3.1.8. *load-line displacement, LLD*—the displacement measured in the direction of the load application.

3.1.9. *post-peak slope, m,* slope at the first inflection point of the load-displacement curve after the peak.

3.1.10. *semicircular bend (SCB) geometry*—a geometry that utilizes a semicircular specimen.

3.1.11. *secant stiffness, S,* the secant slope is defined between the starting point of load vs. load-line displacement curve and point peak load is reached.

3.1.12. *work of fracture (W_f)—The work of fracture is calculated as the area under the load versus load-line displacement curve.*

4. SUMMARY OF METHOD

An asphalt pavement core or Superpave gyratory compactor (SGC) compacted asphalt mixture specimen is trimmed and cut in half to create a semicircular test specimen. A notch is sawn in the flat side of the semicircular specimen opposite the curved edge. The semicircular specimen is positioned in the fixture with the notched side down centered on two rollers. A load is applied along the vertical radius of the specimen and the load and load-line displacement (LLD) are measured during the entire duration of the test. The load is applied such that a constant LLD rate of 50 mm/min is obtained and maintained for the duration of the test. The SCB test fixture and SCB specimen geometry are shown in Figure 1.

Fracture energy (G_f), secant stiffness (S), post-peak slope (m), displacement at peak load (w_0), and critical displacement (w_1), and a flexibility index are calculated from the load and LLD results.

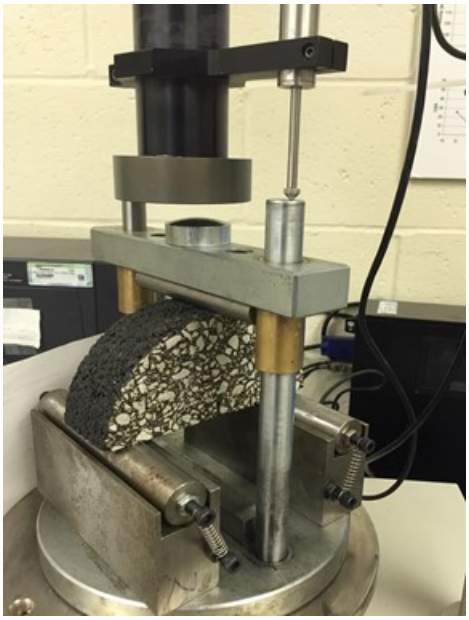

SCB Fixture

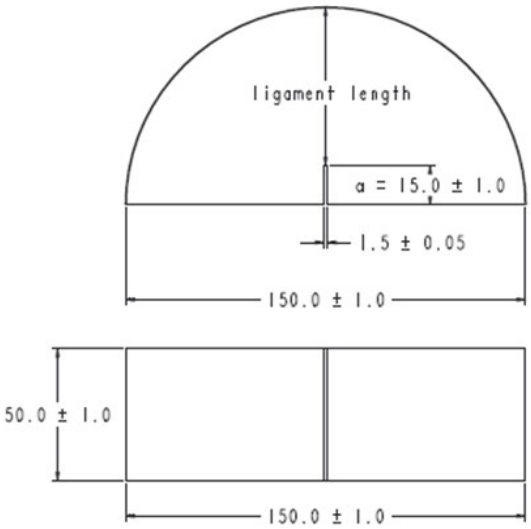

SCB Specimen

Figure 1— SCB test specimen and configuration (dimensions in millimeters)

5. SIGNIFICANCE AND USE

The SCB test is used to determine fracture resistance parameters of an asphalt mixture at an intermediate temperature. Low-temperature fracture parameters can be determined in accordance with TP 105-13. These parameters describe the fracture and fatigue resistance of asphalt mixtures. The calculated fracture energy indicates an asphalt mixture's overall capacity to resist cracking-related damage. Generally, a mixture with higher fracture energy can resist greater stresses with higher damage resistance. It should not be directly used in structural design and analysis of pavements. It also represents the main parameter used in more complex analyses based on a theoretical crack (cohesive zone) models. In order to be used as part of a cohesive zone model, fracture energy as calculated from the experiment shall be corrected to determine energy associated with crack propagation only. A correction factor may be used to eliminate other sources of inelastic energy contributing to the total fracture energy calculated directly from the experiment.

From the fracture parameters obtained at intermediate temperature, the flexibility index (FI) of an asphalt mixture is calculated. The flexibility index is calculated considering the fracture energy and slope of the load-displacement curve after the post-peak representing average crack growth rate. The FI provides a means to identify brittle mixes that are prone to premature cracking. Flexibility Index values obtained using this procedure are used in ranking cracking resistance of alternative mixes for a given layer in a structural design. The range for an acceptable FI will vary according to local environmental conditions, application of mixture and expectation of service life.

This test method and flexibility index can be used to rank the cracking resistance of asphalt mixtures containing various asphalt binders, modifiers of asphalt binders, aggregate blends, fibers, and recycled materials.

The specimens can be readily obtained from SGC compacted cylinders or from field cores with a diameter of 150 mm.

6. APPARATUS

Testing Machine—A semicircular bend (SCB) test system consisting of a closed-loop axial loading device, a load measuring device, a bend test fixture, specimen deformation measurement devices, and a control and data acquisition system. A constant displacement-rate device shall be used such as an electromechanical, screw-driven machine, or a closed loop, feedback-controlled servo-hydraulic load frame.

6.1.1. *Axial Loading Device*—The loading device shall be capable of delivering loads in compression with a resolution of 10 N and a minimum capacity of 10 kN.

6.1.2. *Bend Test Fixture*—The fixture is composed of a steel base plate, two U-shaped roller support steel blocks, two steel rollers with a diameter (D) of 25 mm and a U-shaped LVDT positioning frame (see Figure 2). The initial roller position is fixed by springs and backstops that establish the initial test spans dimension. The support rollers are allowed to rotate away from the backstops during the test; but remain in contact with the sample. The tip of the loading head has a contact curvature of 12.5 mm radius. Illustrations of the loading and supports are shown in Figures 2 and 3.

6.1.3. *Internal Displacement Measuring Device*— The displacement measurement can be performed using the machine's stroke (position) transducer if the resolution of the stroke is sufficient (0.01 mm or lower). The fracture test displacement data may be corrected for system compliance, loading-pin penetration and specimen compression by performing a calibration of the testing system.

6.1.4. *External Displacement Measuring Device*— If an internal displacement measuring device does not exist or has insufficient precision, an externally applied displacement measurement device such as a linear variable differential transducer (LVDT) can be used (Figure 2).

Front View

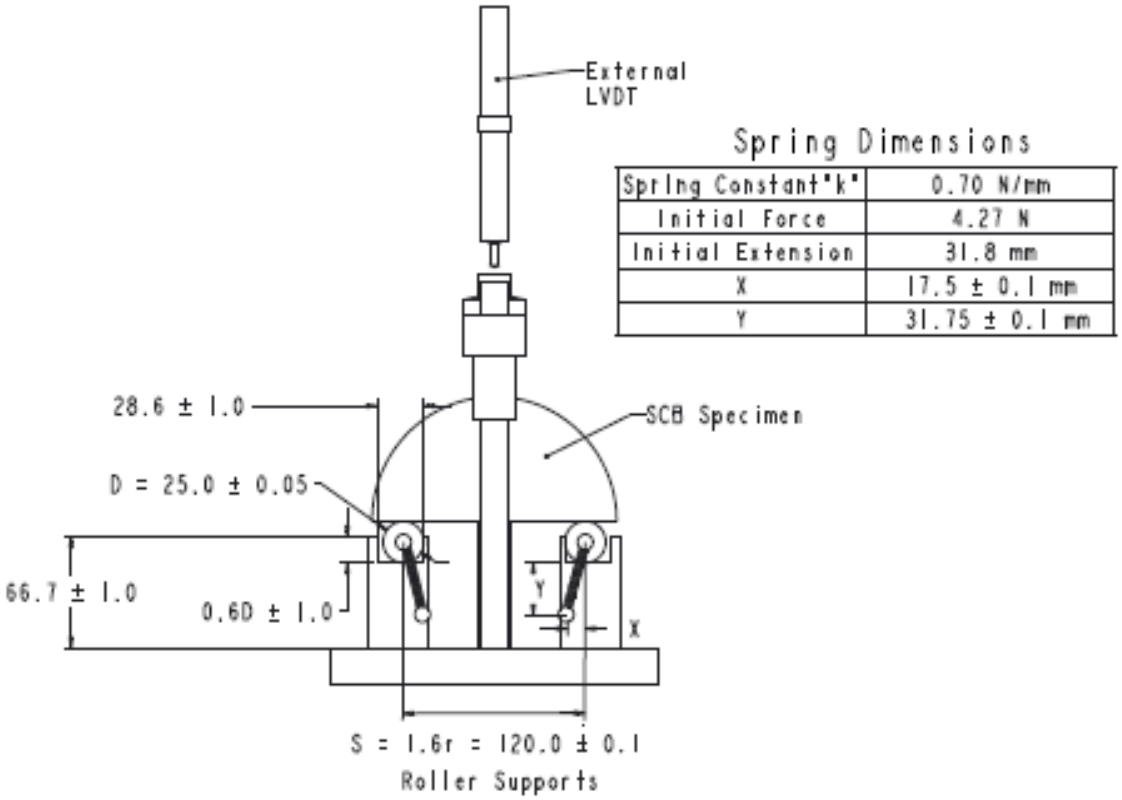

Side View

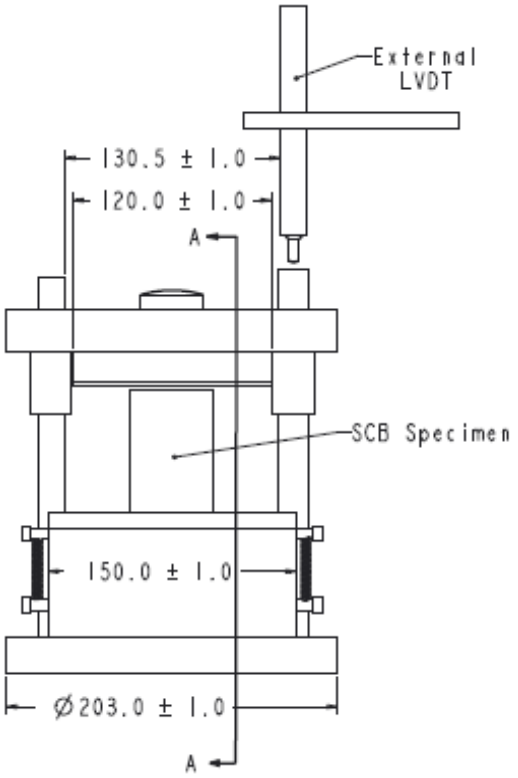

Figure 2— Front and side view of the SCB test fixture (dimension in millimeters)

Top View

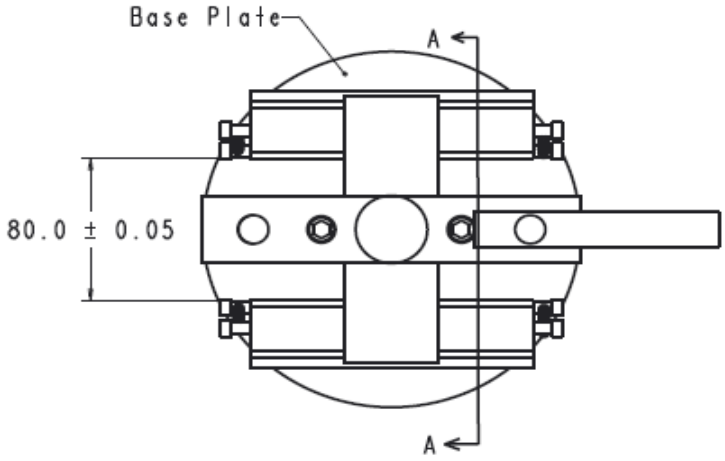

Cross-section (AA)

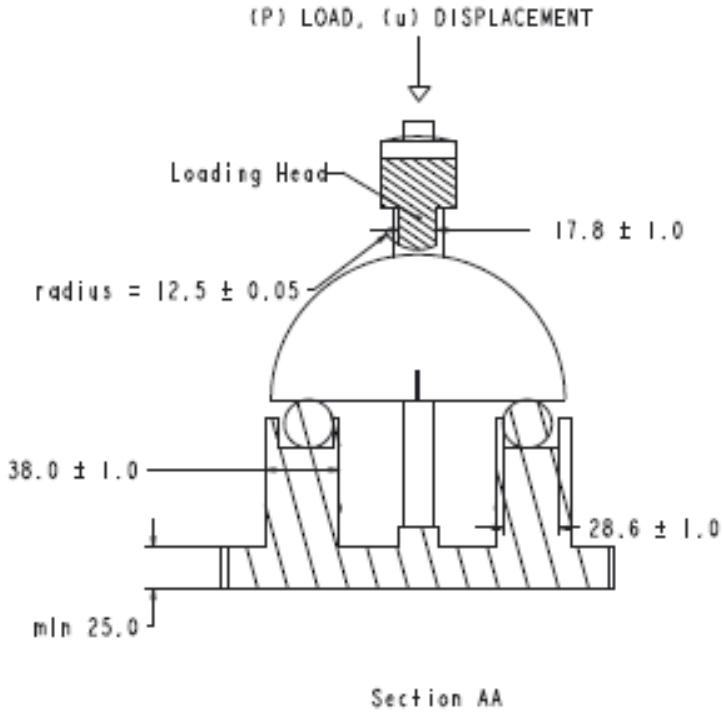

Loading Head

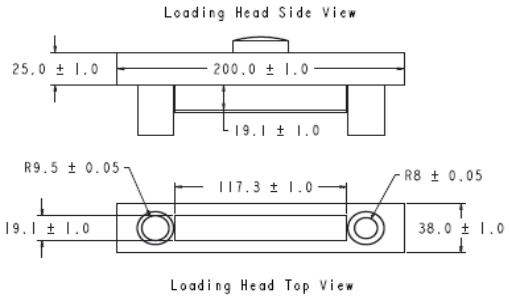

Figure 3—Top view, cross-section, and loading head of the SCB test fixture (dimensions in millimeters)

6.1.5. *Control and Data Acquisition System*—Time and load, and load-line displacement (using external or internal displacement measurement device) is recorded. The control data acquisition system is required to apply a constant load-line displacement rate at a precision of 50 ± 1 mm/min and collect data at a minimum sampling frequency of 20 Hz in order to obtain a smooth load- line displacement curve.

7. HAZARDS

Standard laboratory caution should be used in handling, compacting and fabricating asphalt mixtures test specimens in accordance with AASHTO T 312.

8. CALIBRATION AND STANDARDIZATION

Verify the capability of the environmental chamber to maintain a constant and uniform temperature. A water bath as used in AASHTO T 283 may be used in lieu of an environmental chamber.

Note 1— Caution should be used if an oven is selected for samples conditioning as this will likely result in variable sample conditioning.

Verify the calibration of all measurement components (such as load cells and LVDTs) of the testing system.

If any of the verifications yield data that does not comply with the accuracy specified, correct the problem prior to proceeding with testing. Appropriate action may include maintenance of system components, calibration of system components (using an independent calibration agency, service by the manufacturer, or in-house resources), or replacement of the system components.

9. PREPARATION OF TEST SPECIMENS AND PRELIMINARY DETERMINATIONS

Specimen Size—For mixtures with nominal maximum aggregate size of 19 mm or less, prepare the test specimens from a lab compacted SGC cylinder or from pavement cores. The final SGC test cylinders shall have smooth parallel faces with a thickness of 50 ± 1 mm and a diameter of 150 ± 1 mm (see Figure 4). If field specimens are used, the final test specimen dimensions shall be 150 ± 8 mm in diameter with smooth parallel faces 25 to 50 mm thick depending on available layer thickness.

Note 2—A typical laboratory saw for mixture specimen preparation can be used to obtain cylindrical slices with smooth parallel surfaces. Diamond-impregnated cutting faces and water cooling are recommended to minimize damage to the specimen. When cutting the SCB specimens, it is recommended not to push the two halves against each other because it may create an uneven base surface of the test specimen that will affect the results.

9.1.1. *SGC Specimens*—Prepare one laboratory SGC specimen according to T 312 in the SGC with a minimum compaction height of 160 mm. From the center of the SGC specimen, obtain two cylindrical 50 ± 1 mm thick slices (see Figure 4). Cut each slice into two identical “halves”. This results in four SCB test specimens with target 7.0 +/- 0.5% air voids in the top and bottom slices.

Note 3—For laboratory-compacted specimens, if target air voids cannot be achieved for each slice, specimen height can be increased. If specimen height cannot be increased to get 7% air voids in the slices, obtain a single slice from the middle of two SGC specimens.

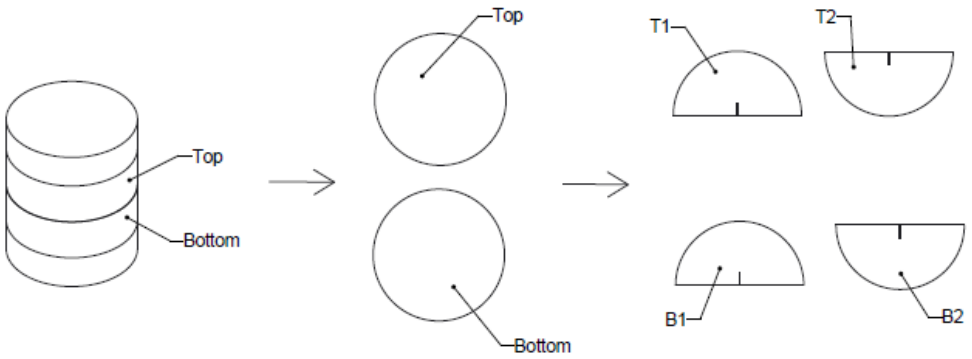

Figure 4— Specimen preparation from SGC specimens

9.1.2. *Field Cores*—Obtain field cores from the pavement in accordance with ASTM D 5361. Obtain one 150 mm diameter pavement cores if the lift thickness is greater than or equal to 100 mm or two 150 mm diameter cores if the lift thickness is less than 100 mm.

9.1.2.1. *Field Specimens*—Prepare four replicate SCB test specimens using pavement cores obtained from a pavement lift, with smooth, parallel surfaces that conform to the height and diameter requirements specified herein. The thickness of test specimens in most cases for field cores may vary from 25 to 50 mm. If the lift thickness is less than 50 mm, test specimens should be prepared as thick as possible but in no case be less than two times the nominal maximum aggregate size of the mixture or 25 mm whichever is greater. If lift thickness is greater than 50 mm, a 50 mm slice shall be prepared. Cores from pavements with lifts greater than 75 mm may be sliced to provide two cylindrical specimens of equal thickness. Cut each cylindrical specimen exactly in half to produce two identical, semicircular SCB specimens. Each slice of the field core shall have parallel smooth cut faces on the top and bottom.

Notch Cutting— Cut a notch along the axis of symmetry of each semicircular specimen to a depth of 15 ± 1 mm and 1.5 ± 0.1 mm in width (see Figure 1).

Note 4—If the notch terminates in an aggregate particle 9.5 mm or larger on both faces of the specimen, the specimen shall be discarded.

Determining Specimen Dimensions—Measure and record the ligament length (see Figure 1) and thickness of each specimen in accordance with ASTM D 3549/D 3549M, to the nearest 1 mm. Measure the notch depth on both faces of the specimen and record the average value to the nearest 0.5 mm.

Determining the Bulk Specific Gravity—Determine the bulk specific gravity directly on the test specimens obtained from SGC cylinders or field cores according to AASHTO T 166.

10. TEST PROCEDURE

Conditioning—Test specimens shall be conditioned in an environmental chamber or water bath at 25 ± 0.5 °C for 2 ± 0.5 h.

10.1.1. *Temperature Control* —The temperature of the specimen shall be maintained within 0.5 °C of the desired test temperature (25 °C) throughout the conditioning and testing periods. Testing shall be completed within 5 ± 1 minutes after removal from the environmental chamber or water bath.

Contact Load— First, impose a small contact load of 0.1 ± 0.01 kN in LLD control with a loading rate of 0.05 kN/s

10.1.2. *Record Contact Load*— Record the contact load to ensure it is achieved.

10.1.3. *Loading*—After the contact load of 0.1 kN is reached, the test is conducted using LLD control at a rate of 50 mm/min. The test stops when the load drops below 0.1 kN.

11. PARAMETERS

Determining Work of Fracture (W_f)—The work of fracture is calculated as the area under the load vs. load-line displacement curve. If test is stopped prior to reaching 0.1 kN, the remainder of the load vs. load-line displacement curve should be produced by extrapolation techniques.

The area under the load-displacement curve is calculated using a numerical integration technique. In order to apply the numerical integration, raw load-displacement data shall be divided into two curves described by an appropriate fitting equation. A polynomial equation with a degree of three is sufficient for the curve prior to peak load (Equation 1). An exponential-based function (Equation 2) is used for the post-peak load portion of the curve. Then, analytical integration shall be applied to calculate the area under each curve (Equation 3).

For displacements (u) prior to the peak load (P_{max}):

$$P_1(u) = c_1 \times u^3 + c_2 \times u^2 + c_3 \times u + c_4 \qquad \text{Equation 1}$$

where c's are polynomial coefficients.

For displacements (u) after the peak load (P_{max}) to the cut-off displacement (u_{final})

$$P_2(u) = \sum_{i=1}^{n} d_i \exp\left[-\left(\frac{u - e_i}{f_i}\right)^2\right] \qquad \text{Equation 2}$$

where d, e, and f's are polynomial coefficients, n is the number of exponential terms.

Work of fracture can be analytically or numerically calculated using the integral equation below and boundaries of displacement.

$$W_f = \int_0^{u_0} P_1(u)du + \int_{u_0}^{u_{final}} P_2(u)du \qquad \text{Equation 3}$$

where u_{final} is the displacement at the 0.1 kN cut-off load.

Note 5— Due to the relative difference between the compliance of testing frame and specimen, displacement recorded may vary. A correction factor may be considered to correct recorded displacements when applicable.

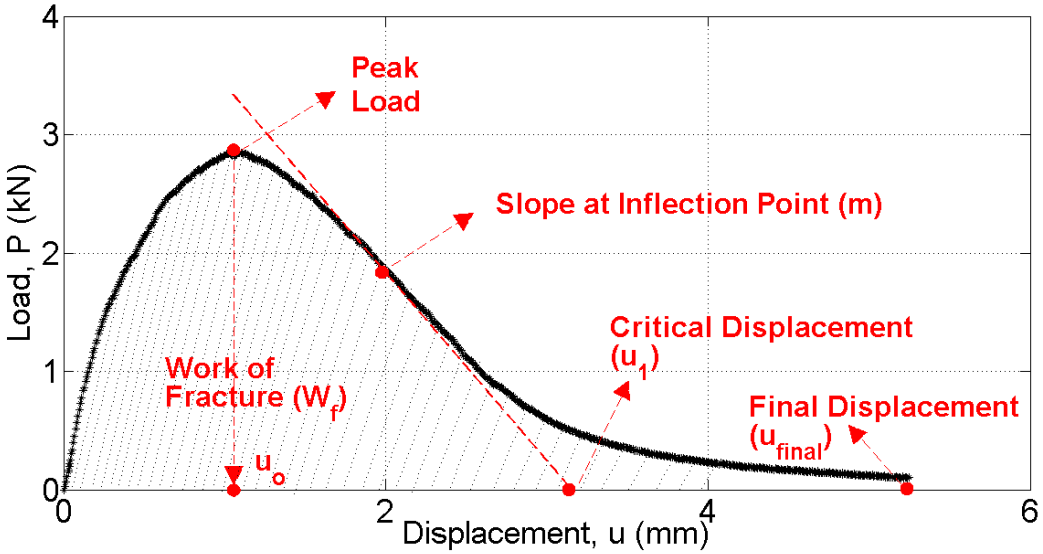

Figure 5—Recorded load (P) versus load-line displacement (u) curve

Fracture Energy (G_F)—The fracture energy G_F (RILEM TC 50-FMC) is calculated by dividing the work of fracture (the area under the load versus the average load-line displacement curve; see Figure 5) by the ligament area (the product of the ligament length and the thickness of the specimen) of the SCB specimen prior to testing:

$$G_f = \frac{W_f}{Area_{lig}} \times 10^6$$

where:

G_f = fracture energy (Joules/m^2);

W_f = work of fracture (Joules)

P = load (kN);

u = load-line displacement (mm);

$Area_{lig}$ = ligament area (mm^2), where

$Area_{lig}$ = ligament length *x t*

t = specimen thickness (mm)

Note 6—Fracture energy is a size-dependent property. This specification does not aim at calculating size independent fracture energy. Therefore, cracking resistance of asphalt mixes quantified with fracture energy may vary when the notch length to radius ratio changes.

Determining secant stiffness (S)—Secant stiffness is calculated by dividing the peak load by the displacement achieved at the same load.

Determining post-peak slope (m) — The inflection point is determined on the load-displacement curve (Figure 5) after the peak point. The slope of the tangential curve drawn at the inflection point represents post-peak slope.

Determining displacement at peak load (u_o) — The displacement when peak load is reached.

Determining critical displacement (u_1) — Intersection of the tangential post-peak slope with the displacement-axis yields the critical displacement value. A straight line is drawn connecting the inflection point and displacement axis with a slope m.

Flexibility Index (FI) — Flexibility index can be calculated from the parameters obtained using the load-displacement curve. The factor A is used for unit conversion and scaling. "A" is equal to 0.01.

$$FI = \frac{G_f}{|m|} \times A \qquad \text{Equation 4}$$

where:

$|m|$= absolute value of post-peak load slope m (kN/mm).

12. CORRECTION FACTORS

Specimen thickness correction for energy parameters—Thickness correction for energy and other load-displacement curve parameters may be needed. This correction factor will be applied to the flexibility index obtained from field specimens.

Shift factor from lab to field specimens—Apply a shift factor between SGC and pavement cores specimens based on the age of field specimens.

13. REPORT

Report the following information:

13.1.1. Bulk specific gravity of each specimen tested, to the nearest 0.001;

13.1.2. Air void content of each slice, to the nearest 0.1;

13.1.3. Thickness t and ligament length of each specimen tested, to the nearest 0.1 mm;

13.1.4. Initial notch length a, to the nearest 0.5 mm;

13.1.5. Average and coefficient of variation of peak load, to the nearest 0.1 kN;

13.1.6. Average and coefficient of variation of recorded time at peak load, to the nearest 0.1 s;

13.1.7. Average and coefficient of variation of load-line displacement at the peak load (u_0), to the nearest 0.1 mm

13.1.8. Average and coefficient of variation of critical displacement (u_1), to the nearest 0.1 mm;

13.1.9. Average and coefficient of variation of secant stiffness S, to the nearest 0.1 kN/mm

13.1.10. Average and coefficient of variation of post-peak slope (m), to the nearest 0.1 kN/mm

13.1.11. Average and coefficient of variation of fracture energy G_f to the nearest 1 J/m^2.

13.1.12. Average and coefficient of variation of flexibility index to the nearest 0.1.

14. PRECISION AND BIAS

Precision— The research required to develop precision estimates has not been conducted.

Bias— The research required to establish the bias of this method has not been conducted.

15. KEYWORDS

Fracture energy; asphalt mixture; semicircular bend (SCB); stiffness; work of fracture; flexibility index.

16. REFERENCES

RILEM Technical Committee 50-FMC. "Determination of the Fracture Energy of Mortar and Concrete by Means of Three-Point Bend Tests on Notched Beams." In Materials and Structures, No. 106. Springer Netherlands for International Union of Laboratories and Experts in Construction Materials, Systems and Structures (RILEM), Dordrecht, The Netherlands, July— August 1985, pp. 285-290

Guinea, G. V., Planas, J., & Elices, M. (1992). Measurement of the fracture energy using three-point bend tests: Part 1— Influence of experimental procedures. Materials and Structures, 25(4), 212-218

Planas, J., Elices, M., & Guinea, G. V. (1992). Measurement of the fracture energy using three-point bend tests: Part 2— Influence of bulk energy dissipation. Materials and Structures, 25(5), 305-312.

Li, Xue, and M. O. Marasteanu. "Evaluation of the Low Temperature Fracture Resistance of Asphalt Mixtures Using the Semi Circular Bend Test." In Journal of the Association of Asphalt Paving Technologists, Vol. 73. AAPT, Lino Lakes, MN, 2004, pp. 401-426.

Wu, Z., L.N. Mohammad, L.B. Wang, and M.A. Mull. 2005. Fracture Resistance Characterization of Superpave Mixtures Using the Semi-Circular Bending Test. Journal of ASTM International, 2(3), 1-15.